UNIVERSITY OF SOUTHAMPTON

GEOCHEMISTRY AND ORIGIN OF THE ASIMOTRYPES CARBONATE-HOSTED MESOTHERMAL GOLD DEPOSIT, PANGEON MOUNTAIN, NORTH GREECE

DEMETRIOS G. ELIOPOULOS, H. B.Sc., M.Sc.

SUBMITTED FOR Ph.D.

SCHOOL OF OCEAN AND EARTH SCIENCE

APRIL 2000

UNIVERSITY OF SOUTHAMPTON

ABSTRACT

FACULTY OF SCIENCE

SCHOOL OF OCEAN AND EARTH SCIENCE

Doctor of Philosophy

GEOCHEMISTRY AND ORIGIN OF THE ASIMOTRYPES CARBONATE-HOSTED MESOTHERMAL GOLD DEPOSIT, PANGEON Mt., N. GREECE

by Demetrios George Eliopoulos

The Asimotrypes mesothermal gold deposit located in the Pangeon Mt (E. Macedonia, N. Greece), is part of the Western Rhodope Massif (WRM), which represents the metamorphic core complex of an alpine collision orogen. Alpine metamorphism, of U. Cretaceous - M. Eocene age, reached upper greenschist to lower amphibolite conditions. A low-pressure greenshist facies retrograde overprint during uplift marked the end of Alpine metamorphism in the Miocene. Post-metamorphic Miocene uplift has been recognised in the Pangeon Mt and it was ascribed to Late Cainozoic extensional tectonics.

The Asimotrypes ore, of replacement and shear-zone style consists mainly of arsenopyrite, pyrite and gold, with subordinate sphalerite, galena, chalcopyrite, pyrrhotite, tetrahedrite-tennantite, marcasite, covellite and malachite. Gold is either refractory occurring mainly in arsenopyrite and to a lesser extent in As-pyrite, or free in the oxide minerals.

Three types of fluid inclusions (with subtypes) were recognised based on constituent phases at room temperature and microthermometric behaviour: (i) H_2O-CO_2 3-phase inclusions: L_1 (H_2O)+L_2 (CO_2)+V (CO_2); (ii) Aqueous 2-phase inclusions: L+V; and (iii) Naturally decrepitated and/or leaked inclusions: V or L+V. The fluids have low salinity (<5 wt % NaCl equiv.), but variable CO_2/H_2O ratios. Microthermometric studies in gangue quartz indicate early ore deposition at P-T conditions of 275^0-310^{0}C and 2.7-3.1 kb during unmixing of the mineralising fluids, followed by deposition at temperatures down to 130^{0}C and low near surface pressures.

$\delta^{34}S$ values of primary sulphide minerals suggest a magmatic source for the sulphur. $\delta^{13}C$ values in marble calcite are indicative of a marine environment of deposition, also supported by a plot of $\delta^{13}C$ versus $\delta^{18}O$ for the same samples. Calculated isotopic composition of ore fluids in quartz, sericite and whole rock at 275^{0}C and 340^{0}C are consistent with values of metamorphic fluids. Whole rock hydrogen isotopic composition of -117±7.5(1σ) indicates that the mineralising fluid was of meteoric origin. Sr isotope data implies seawater origin for strontium. Lead isotope data in ores from the Rhodope showed that Pb is derived from crustal rock types.

Sulphide species such as $Au(HS)^-_2$, were probably the most effective complexing agents for gold in the Asimotrypes fluids, which were typically low in salinity. A decrease of sulphur species activity and cooling are suggested to be the favoured depositional mechanism in a reducing environment. Combined with geological evidence, the fluid inclusion and stable data of the Asimotrypes gold ore, are consistent with genesis from deeply convecting meteoric waters driven by regional uplift through rocks undergoing retrogressive greenschist facies metamorphism.

DEDICATION

This Thesis is dedicated to my wife

Maria

for her continuous encouragement, support and patience and to our belovest

Triplet boys

Giorgos, Yannis and Thanos

ACKNOWLEDGEMENTS

I gratefully acknowledge the contributions made by Prof. R. W. Nesbitt, who accepted me in the School of Ocean and Earth Science, University of Southampton, to accomplish this Thesis. During the course of this work he provided valuable advice and ideas which greatly improved my insight of the geologic and metallogenetic processes in the studied area, and critically read, and contributed to, earlier drafts of this Thesis.

Special acknowledgement goes to Dr. T. J. Shepherd and Dr. J. Naden of the British Geological Survey, who taught me the methodology of studying fluid inclusions and introduced me to the fluid inclusion research and applications in the ore forming processes, in the frame of a Bilateral Agreement between our Institutes. Acknowledgement is extended to Dr. S. P. Kilias, Assistant Professor at the Athens University for stipulating discussions on fluid inclusion data and interpretation, and to Dr. A. J. Barker, School of Ocean and Earth Science, University of Southampton, for his constructive comments and recommendations.

Many thanks to my colleagues at the Institute of Geology and Mineral Exploration of Greece, Dr. M. Vartis-Matarangas, Dr. P. Tsombos and Dr. J. Chatzipanagis, who provided valuable support in the field and in the office in more ways than I can possibly acknowledge.

Special thanks are due to Dr. J. H. Baker of the University of Utrecht for climbing together up to the Asimotrypes mine several times, Dr. K. L. Ashworth for stipulating discussions, and Dr. P. de Groot for assistance in the O and C isotope analyses of calcitic marbles.

TABLE OF CONTENTS

LIST OF PHOTOGRAPHIC PLATES

CHAPTER 5

CHAPTER 7

LIST OF TABLES

CHAPTER 8

CHAPTER 9

APPENDIX II

APPENDIX III

LIST OF FIGURES

CHAPTER 1 **Page**

CHAPTER 2

CHAPTER 7

CHAPTER 8

APPENDIX I

APPENDIX II

INTRODUCTION

Mesothermal gold deposits constitute the principal source of lode and placer Au world-wide. In addition, these deposits are significant to the understanding of the genesis of gold deposits in general, since they are young analogues of the larger and more enigmatic Archean gold deposits.

Throughout earth history mesothermal gold deposits are found in structurally controlled sites within, and adjacent to, orogenic belts. These belts can be classified as peripheral or internal orogens, based on their spatial relationship to external and internal oceans during the supercontinent cycle. Peripheral orogens are zones of subduction and terrane accretion at the margins of oceans, which remain open during the break-up, dispersal, and re-aggregation of continental fragments to form supercontinents. The Paleozoic and Mesozoic margins of the Pacific are peripheral or external orogens. In contrast, internal orogens are zones of collision, which are formed where internal oceans close and continental fragments aggregate to form a supercontinent. The Appalachian/Caledonian orogen, which formed during the closure of the Iapetus Ocean, is an example of an internal orogen. Both types of orogen contain significant mesothermal gold provinces. However, if the interpretation that Late Archean and Paleoproterozoic granitoid-greenstone terranes represent peripheral orogens which formed during the breakup and dispersal stages of a supercontinent cycle is correct, then peripheral orogens host the majority of mesothermal gold deposits.

Mesothermal gold deposits are mostly gold-only deposits associated with carbonatised wall rocks. They occur in low- to medium-grade metamorphic terrains

of all ages, but only in those that have been intruded by granitoid batholiths. A numerically minor subgroup of these deposits occurs in high-grade terrains and calc-silicate mineral alteration zones. The deposits are characterised by a high gold/silver ratio, great vertical continuity with little vertical zonation, and a broadly syn-tectonic time of emplacement (Hodgson, 1993). Commonly associated minerals include pyrite, less commonly pyrrhotite, the common base-metal sulphides, arsenopyrite, tourmaline and molybdenite. Mineralisation may occur in any rock type and ranges in form from veins, to veinlet systems, to disseminated replacement zones. Most mineralised zones are hosted by and always related to steeply dipping reverse - or oblique-slip brittle-fracture to ductile-shear zones.

Mesothermal gold deposits irrespective of age, world-wide, share a range of similar characteristics which include:

- spatial association with major fault systems
- considerable depth extent
- deposition from deep metamorphic , low salinity, H_2O-CO_2 $\pm CH_4$ fluids which advent into zones of structural permeability
- similar element association and alteration assemblages

One of the enduring and least tractable problems in gold metallogeny remains the origin of these mesothermal lode deposits. Not only the nature of the fundamental processes involved in the generation of these deposits remains controversial, but also there are a diversity of hypotheses on the source of volatiles and solutes, especially gold. Mesothermal Au-Ag deposits have variously been attributed to lateral secretion (Boyle, 1979), magmatic (Carter, 1948; Ferguson et al., 1968; Mason and Melnik, 1986) exhalative (Fripp, 1976a; Ridler, 1976; Hutchinson and Burlington, 1984), structurally focussed metamorphic outgassing (Fyfe and Henley, 1973; Kerrich and Fryer, 1979; Kerrich, 1987; Groves and Phillips, 1987; Wall,

1987), and meteoric water circulation (Nesbitt and Muehlenbachs, 1989). Recently, mantle degassing-granulitization (Fyon et al., 1984; Colvine et al., 1984, 1988; Cameron, 1988) has been advocated as a new genetic scheme, and the possible direct orthomagmatic link of Au to felsic igneous rocks has been revived (Burrows et al., 1986; Wood et al., 1986a; Hattori, 1987; Cameron and Hatori, 1987; Burrows and Spooner, 1987).

The most generally accepted genetic models for the formation of Phanerozoic mesothermal gold deposits are:

- derivation from metamorphic processes and metamorphic fluids, and
- deep convection of meteoric water in the brittle continental crust

These two principal genetic models are similar in many respects, such as the importance of regional structure and the chemistry of the ore deposits, and differ in the source and migration paths of the fluids. Additional testing is required to resolve the conflicts over fluid source between the metamorphic and meteoric models and more detailed investigation on the structure and chemistry of the ore zones to determine the exact controls on gold deposition.

Under this concept the area of Asimotrypes in northern Greece, which has been intensively mined by the ancient Greeks for a long period of time, has been selected for further research focussed on the application and corroboration of the concepts briefly described above and amplification of many of these concepts in an area providing different lithologies and geological age compared to the ones studied so far world-wide. The concepts are particularly investigated from the standpoint of geological, geochemical, fluid inclusion and isotopic studies. Finally, the model is compared to other similar deposit types world-wide.

CHAPTER 1

REGIONAL GEOLOGY AND TECTONICS

1.1. The Rhodope Massif

The Rhodope Massif is located in northern Greece and it is bounded to the west by the Strymon River fracture zone, to the east by the Evros River, to the north it extends into Bulgaria, whereas to the south its border remains unclear since it is subducted underneath the northern Aegean sea (Fig. 1.1).

Three lithological units are distinguished in the Rhodope Massif: the metamorphic basement, the Circum Rhodope Belt and the Tertiary volcano-sedimentary basins. The Rhodope Massif is upthrusted by the Serbomacedonian Massif along a flat N-S trending thrust fault, the Strymon Fault. Both, the Rhodope and the Serbomacedonian Massifs form a continental fragment, which was extensively reworked during the Alpine Orogeny.

The metamorphic basement of the Rhodope Massif consists of para- and orthogneisses, mica schists, amphibolites and thin calcareous schists. Mineralogical and geochemical evidence suggest that the protoliths of the basement gneisses are mainly magmatites of Hercynian age 285 Ma in West Rhodope (Wawrzenitz et al., 1994) and 296 Ma in East Rhodope (Peicheva et al., 1992), whilst most of the amphibolites are MORB basalts (Liati, 1989). In the eastern Rhodope Massif a thick sequence of dismembered metamorphosed mafic and ultramafic ophiolites occur. Carbonate series dominant in the Western Rhodope Zone consists of marbles with intercalation of mica schist, chlorite schist and quartzite.

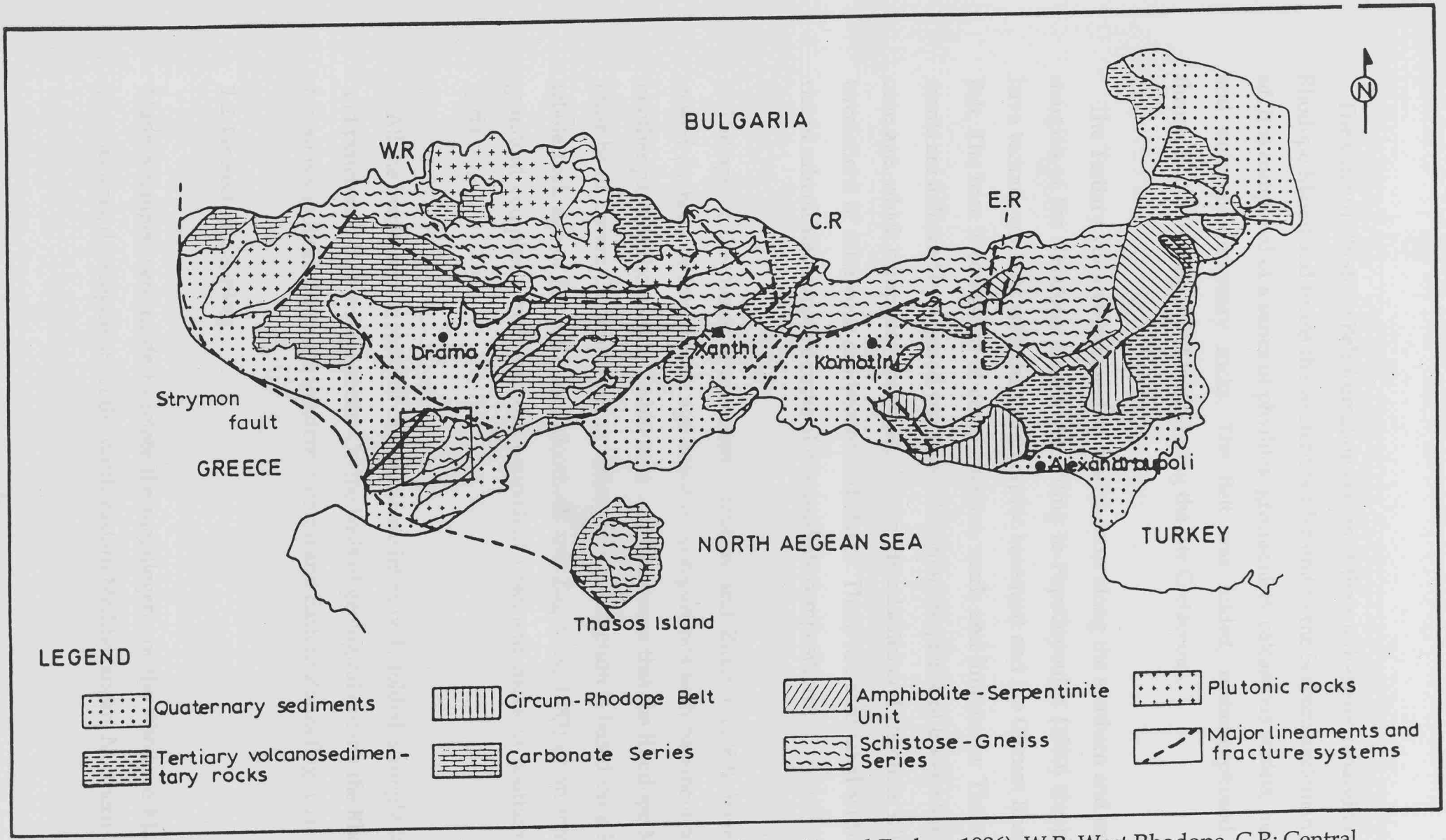

Figure 1.1: Geological map of the Rhodope Massif in 1:1000000 scale (Dimadis and Zachos, 1986). W.R: West Rhodope, C.R: Central Rhodope, E.R: East Rhodope, Square: Field Area.

The Circum Rhodope Belt formation occurs at the south-eastern margin of the Rhodope Massif and forms the western border unit to the Serbomacedonian Massif. It is composed of a series of phyllites, greenschists, calcareous schists, marbles and volcanosedimentary rocks. The Belt was folded, metamorphosed and thrusted onto the Rhodope Massif during the late Cretaceous.

The Tertiary volcano-sedimentary basins occur along the southern and eastern margins of the Rhodope massif. According to Papadopoulos (1980) the basins have tectonic contacts with the metamorphic basement and the Circum Rhodope Belt. The base is composed of conglomerates, marls and limestones. These sediments are followed by a mixed volcano-sedimentary sequence of Eocene to Oligocene age, which comprises andesites, dacites, rhyodacites and rhyolites with intercalations of calcareous sandstones and shales. These are associated with a series of subvolcanic intrusive rocks of intermediate compositions.

The age of the massif is uncertain. Dimitrov and Zidarov (1969), have suggested Archean or Proterozoic age based on comparisons with basement terrain in other parts of the world. Nesbitt et al., (1988) assume that the Rhodope Massif must be of Lower Carboniferous or older. This assumption is based on a Rb/Sr whole rock age of 342 ± 27 ma (Moorbath and Zagorcev, 1983) of an intrusive granitoid complex which intrudes equivalent basement rocks in southern Bulgaria.

All the metamorphic rocks of the massif are intensively folded, strongly faulted and penetrated by intrusive rocks. On the basis of geological criteria the Rhodope Massif is subdivided into the Western, Central and Eastern Zones (Fig. 1.1).

1.2 Geotectonic Setting

Many attempts were made to relate the metallogeny of the Rhodope Massif to plate tectonic developments in the north-eastern Mediterranean. Northern Greece

is located at the junction between the African and Eurasian plates and many geological features, including the styles and distribution of mineralisations, result from Permian to Tertiary plate movement. Basically, the African Plate was driven down below the Eurasian Plate, but the Rhodope and Serbomacedonian Massifs formed a rigid pivotal block causing sinistral rotation with the result that micro-plates developed through the whole Aegean region.

Several plate tectonic models have been proposed by various authors, mainly based on complex movements of distinct micro-plates in the Tethyan area since Jurassic times to address the geotectonic evolution of the Rhodope and Serbomacedonian Massifs. These models are summarised and comprehensively reviewed by Frei (1992).

Channel and Horvath (1976) suggest that during the Senonian a NNW-ward drift of the Serbomacedonian-Rhodopian micro-plate caused a partial subduction of the Tethys along the NE edge of the Serbomacedonian, which was active to the early Eocene. Subsequent rifting and northward convergence of Africa resulted inwestward movement and final arrangement of the Serbomacedonian-Rhodopian micro-continent during Palaeocene and Pliocene times, accompanied by subduction related magmatism and associated metallogenesis.

According to Dewey et al., (1973), in relation to the position of the Africa and European plates during the Eocene to Miocene, the Rhodope and Serbomacedonian Massifs formed a common micro-continent with Turkey and Iran between north and south facing subduction zones accompanied by extensive Eocene acid intermediate volcanism. From Miocene to present, in relation to the convergence of Africa to Europe, the Rhodope and Serbomacedonian Massifs were docked with Europe. The collision led to the formation of napes and ophiolite zones, which were completed during the Oligocene. The formation of the Hellenic subduction took place during the Upper Miocene or later, in relation to the welding of microplates with Europe. The convergence between Iran and Iraq, squeezed

Figure 1.2: Proposed plate boundary during the Miocene (after Dewey et al., 1973). Apulia, Moesia, and Rhodope were welded against Europe. Convergence of Africa against Europe continued along the sutures. At the very end of the Miocene - beginning of Pliocene the Hellenic subduction system formed. Turkey was pushed westward and the Anatolian Fault Zone was initiated, the extension of which can be traced into the North Aegean (in Frei, 1992).

Turkey westward and the Anatolian fault zone was developed. Continued convergence led to complex intraplate deformations and seismicity over wide zones (Fig. 1.2). The Rhodope and Serbomacedonian Massifs were affected by extensional deformation leading to graben structures and steep faults along which various subvolcanics were emplaced into shallower crust levels.

Hsu et al., (1977) suggested that the Rhodope and Serbomacedonian Massifs together with the Moesian platform formed a micro-continent during the Alpidic time, whilst the inner Balkanides root in an intracontinental basin. The rotation of the Rhodope and Serbomacedonian micro-continent caused the opening of the Vardar Ocean followed by the development of the Kimmerian orogeny. The rotation of the Italo-dinaric micro-continent to the west during the Upper Triassic - Lower Cretaceous initiated the subduction of the Vardar Ocean. The Rhodope and Serbomacedonian Massifs together with the North Anatolian Massif were part of an island arc, while back arc basins such as the Srednogorie and the Black Sea were developed to the east.

1. 3 Structural Geology and Regional Tectonics

The Rhodope and Serbomacedonian Massifs constitute major complex geotectonic elements of the internal Hellenides. Both Massifs have undergone repeated compression, extension and rotation during plate movements from the Jurassic to Quaternary. The result of the above activity is that the region is cut by major low angle thrusts and extension faults upon which are superimposed a network of large horst-graben structures (Fig.1.3 &1.4).

The massifs also show at least three periods of regional metamorphism and five separate phases of folding while all younger rocks are folded and faulted (Papanikolaou and Panagopoulos, 1981; Chatzipanagis et al., 1983; Tsombos and Karmis, 1988; Kilias and Mountrakis, 1989; Patras et al., 1989; Pavlides et al., 1989;

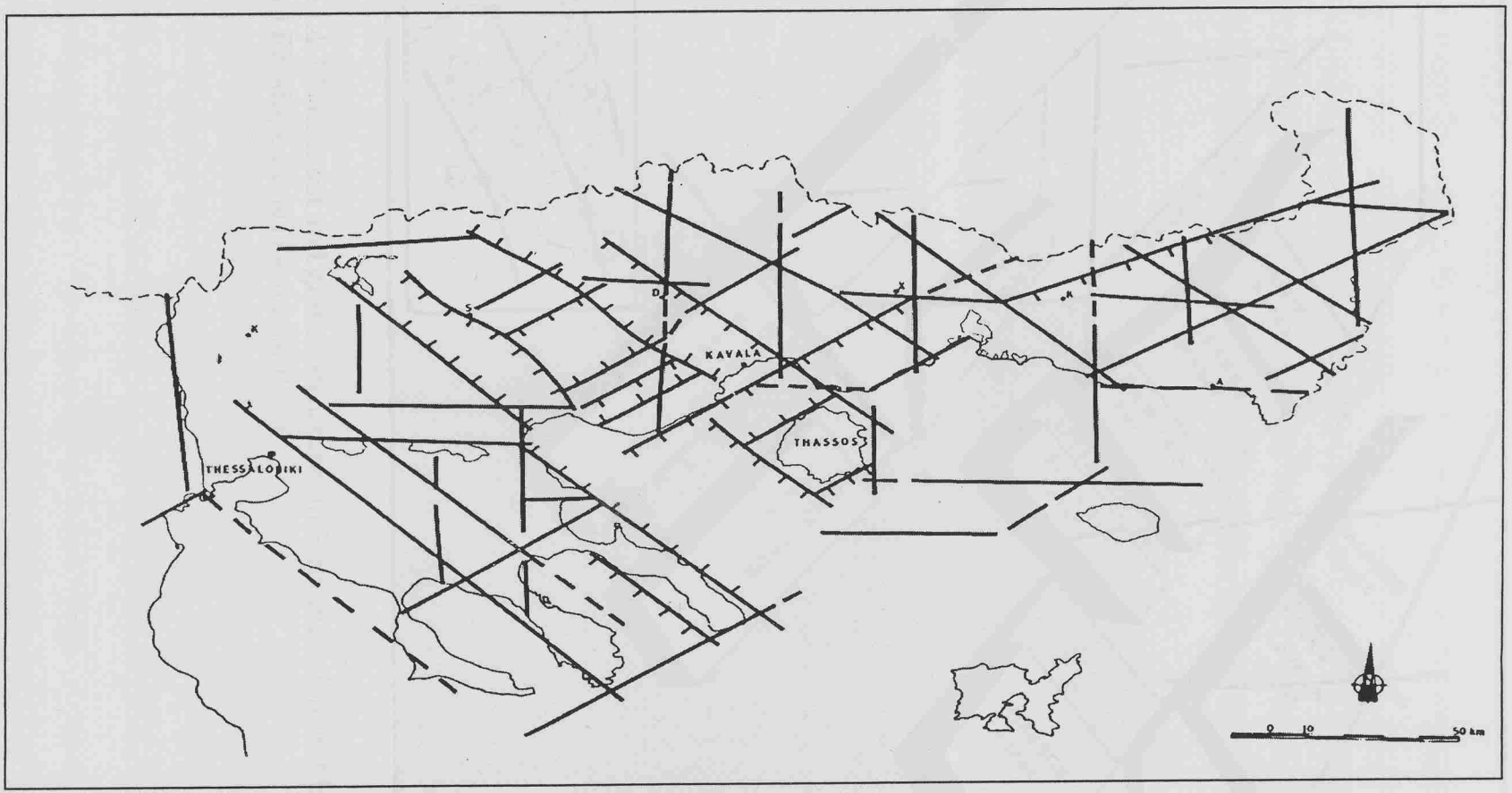

Figure 1.3: Simplified major linear structure map of northern Greece (Tsombos, 1993).

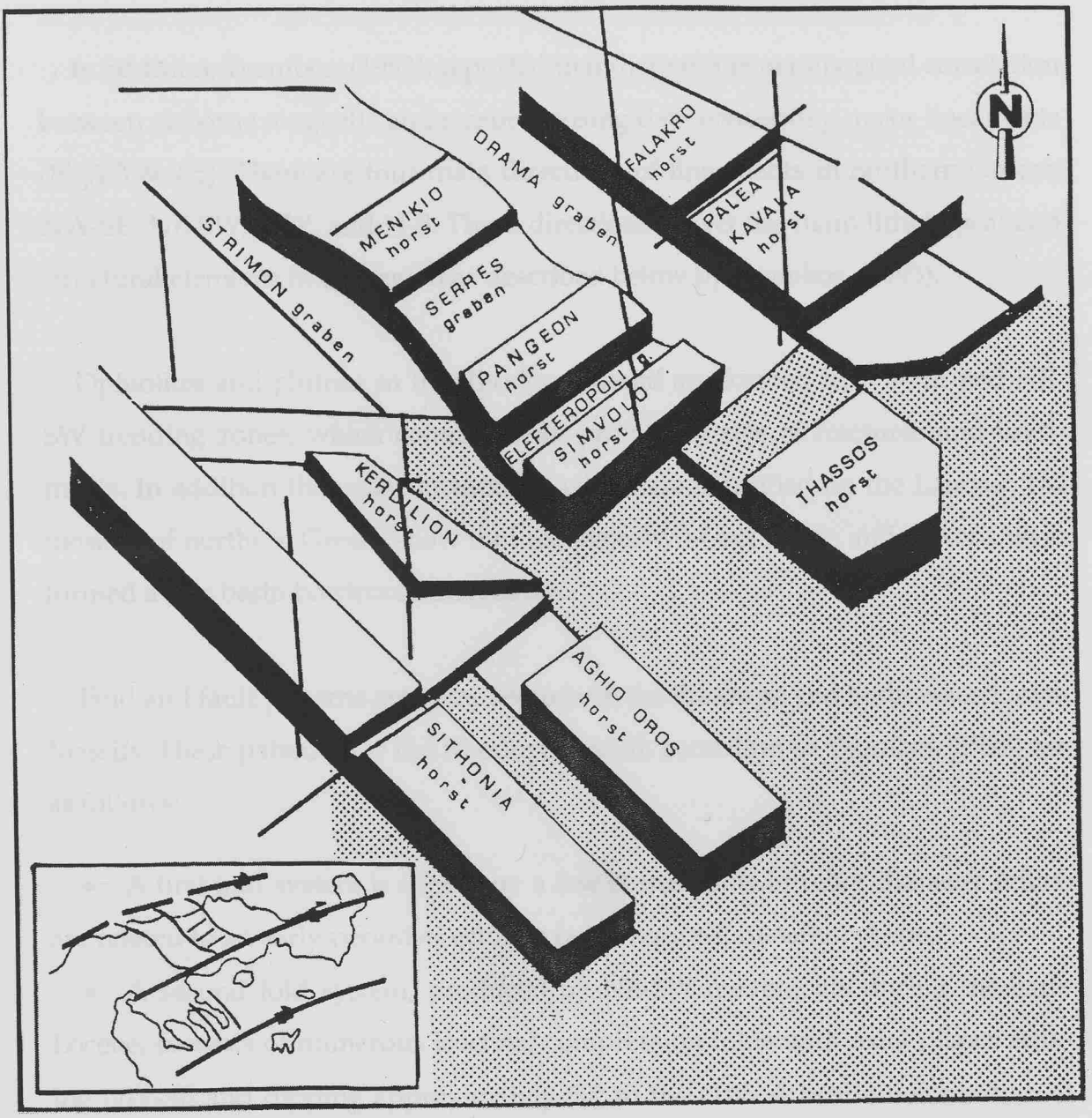

Figure 1.4: Major horst and graben structures in Serbomacedonian Massif and Western Rhodope Zone (Tsombos, 1993).

Zagorcev, 1989; Tsombos and Kalogeropoulos, 1990). Large acidic and smaller basic intrusives accompanied this tectonic activity.

In addition, Tsombos (1993), reported that there is a generally good correlation between airborne magnetic and remote sensing data concerning major lineaments (Fig.1.3 & 1.5). There are four main directions of lineaments in northern Greece: NW-SE, NE-SW, E-W, and N-S. These directions reflect the main lithological and structural elements in the region as described below by Tsombos, (1993).

Ophiolites and plutons in the Rhodope Massif are formed in NW-SE and NE-SW trending zones, which coincide with prominent sets of fractures and lineaments. In addition the major lineaments which are identified on the Landsat TM mosaics of northern Greece show that the majority of ophiolites and plutons were formed at the basin borders of this region.

Fold and fault patterns are complex in both the Rhodope and Serbomacedonian Massifs. These patterns for the Rhodope Massif, according to Tsombos (1993) are as follows:

- A first fold system is shown by a few closed folds of relict character which are related to an early period of eclogite facies regional metamorphism.
- A second fold system, produced by NE-SW movements during the early Eocene, consists of numerous isoclinal compression folds with axial planes striking NW-SE and dipping approximately 50° to the NW. A brittle deformation of early Eocene age also produced a NE-SW trending lineation system.
- A third fold system is comprised of open drag folds and dislocation cleavages as a result of decompressional forces during the uplift of the Rhodopian orogeny. Major horst-graben structures began to develop at this time and movement has continued to the present day (Fig.1.4).

Three main sets of low angle thrusts and shears are observed in northern Greece. The two earliest thrust sets are strike NE-SW and NW-SE respectively and

the latest approximately E-W (Chatzipanagis, 1991; Arvanitides and Ashworth, 1993; Tsombos, 1993). Most appear to be Tertiary, but some may be reactivated older structures. The character of these low angle structures is, however, based heavily on conjecture as illustrated by the case of the Strymon Valley Fault. This fault structure separates the Rhodope Massif from the Serbomacedonian Massif (Fig. 1.1) and is of particular interest because it influences debate on whether the two massifs were formed separately or are portions of a single massif dislocated by a major fault system. Many authors have interpreted the Strymon Valley fault as a flat lying thrust striking north-west and inclined gently to the south-west. The Serbomacedonian Massif rocks are considered to have moved northeastwards along the thrust and now rest upon the Rhodope Massif (Kockel and Walther, 1965; Omenneto, 1985; Zagorcev, 1989). Other authors, however, consider the fault to be part of a major graben structure or a block-dividing deep fault zone (Ryazkov and Dobrev, 1989; Pavlides et al. 1989). Shanov et al., 1989 and Ryazkov and Dobrev (1989) used geophysical data to postulate an internal block structure within the Rhodope Massif, flanked on the west by the Strymon Valley fault and on the east by the equally large Nestos fault. Recently, the Strymon Valley fault has been interpreted as a major south-west dipping detachment normal fault of late Cainozoic age, which emplaced the medium grade Rhodope metamorphic complex (Dinder and Royden, 1993; Sokoutis et al. 1993) and the mid-crustal rocks of the Pangeon complex.

Although the character, age and influence of major low angle fault structures is debatable, the presence of major horst-graben fault systems can be clearly demonstrated by remote sensing, and field mapping (Tsombos, 1993). The horst-graben structures extend throughout the whole Aegean region, and they appear to have controlled the distribution of the Tertiary volcanosedimentary basins to the south of the Rhodope Massif since the Miocene (Fig. 1.4 & 1.5). The major faults which bound the horst-grabens are essentially vertical wrench faults trending mainly NW-SE and NE-SW. The NW-SE faults are antithetic and the NE-SW faults are

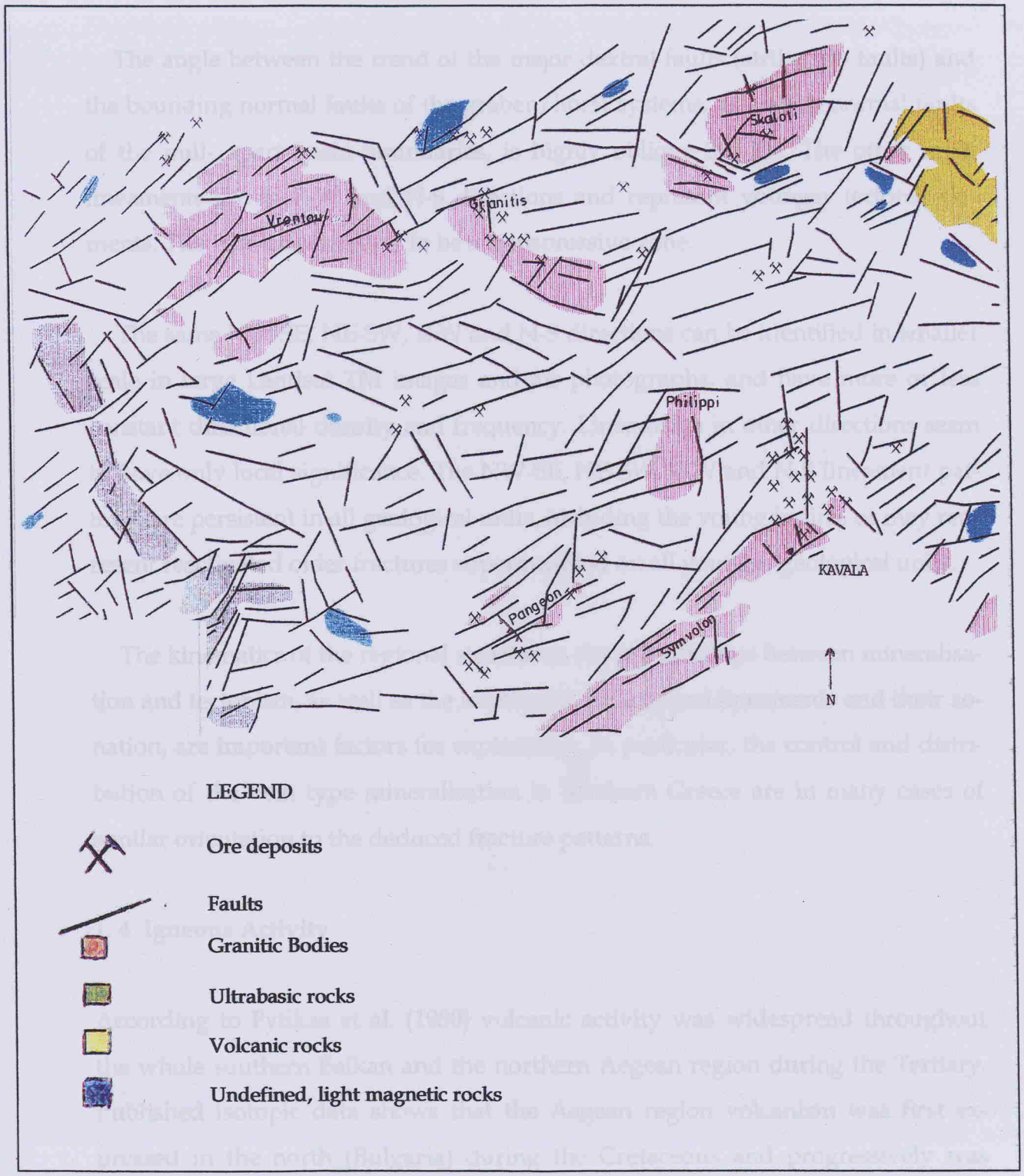

Figure 1.5: Major lineaments and airborne magnetics interpretation in the West Rhodope Zone (Tsombos and Skianis, 1993).

synthetic to the main dextral fault system of the north Aegean trough (Fig. 1.5). The system of dextral faults appears to be repeated north of the Aegean trough.

The angle between the trend of the major dextral faults (strike slip faults) and the bounding normal faults of the graben/horst systems, as well as normal faults of the pull- apart basin boundaries, is highly oblique 35°-45°. The other main lineaments are in E-W and N-S directions and represent younger tectonic elements. The whole area seems to be a transpressive zone.

The same NW-SE, NE-SW, E-W and N-S directions can be identified in smaller scale in large Landsat TM images and air photographs, and have more or less constant directional density and frequency. Lineaments in other directions seem to have only local significance. The NW-SE, NE-SW, E-W and N-S lineament patterns are persistent in all geological units, including the young basins, or may represent reactivated older fractures superimposed on all younger geological units.

The kinematics of the regional structures, the relationships between mineralisation and tectonism, as well as the location of the mapped lineaments and their zonation, are important factors for exploration. In particular, the control and distribution of the vein type mineralisation in northern Greece are in many cases of similar orientation to the deduced fracture patterns.

1. 4 Igneous Activity

According to Fytikas et al. (1980) volcanic activity was widespread throughout the whole southern Balkan and the northern Aegean region during the Tertiary. Published isotopic data shows that the Aegean region volcanism was first expressed in the north (Bulgaria) during the Cretaceous and progressively was spread to the south, through northern Greece, during the Oligocene to Lower Miocene, to develop the currently active south Aegean volcanic arc. The northern Aegean Tertiary calc-alkaline magmatism is documented in a belt, which extends

in an E-W to NE-SW direction from the NE continental Greece to the central Aegean and into the central Anatolia. There is a clear discrimination in the type of the north-eastern Greece magmatic activity, with volcanic and subvolcanic rocks dominating the eastern Rhodope Zone and co-magmatic plutons dominating the Western Rhodope Zone. This activity was accompanied by large acidic intrusives which penetrated both the Rhodope Massif and the Circum Rhodope Belt rocks. More specifically the Western Rhodope Zone itself contains only co-magmatic plutons.

The plutonic intrusives of the Rhodope Massif (Fig. 1.6) have Eocene to Miocene ages, Table 1.1, (Meyer, 1968; Theodorikas, 1983; Soldatos, 1985; Kyriakopoulos, 1987) with the exception of the Elatia granite which is Upper Cretaceous (Soldatos, 1985). The most intense period of magmatism was during the Oligocene and early Miocene (38 ma to 17 ma). The compositional trend was calc-alkaline monzodiorite-granodiorite-granite and some are accompanied by skarn mineralisation.

Table 1.1: Summary of age determinations of intrusions in the Rhodope Massif.

Location	Intrusion Type	Age (Ma)	Determination Method	Reference
Kavala	Granodiorite	13.9±0.06 to 15.9±0.1	Rb-Sr	Kyriakopoulos, 1987
Xanthi	Granite	26.3±1.0 to 28.8±0.7	Rb-Sr, K-Ar	Kyriakopoulos, 1987
Maronia	Monzodiorite	28.9±0.1 to 29.8±1.3	Rb-Sr	Kyriakopoulos, 1987
Kirki-Leptokaria	Monzodirite	31.8±0.6 to 31.9±0.5	Rb-Sr, K-Ar	Kyriakopoulos, 1987
Samothraki	Granite	18.5±0.3 to 18.9±0.4	Rb-Sr, K-Ar	Kyriakopoulos, 1987
Vrondou	Granitoid	29.1±1.0 to 33±2.0	K-Ar	Marakis, 1969
Pangeon	Granodiorite	13-15	K-Ar	Meyer,1968
Symvolon	Granodiorite	21	K-Ar	Dinter, 1995
Elatia	Granodiorite	87.7±27	K-Ar	Soldatos, 1985
Skaloti	Granitoid	Oligocene	K-Ar	Soldatos, 1985

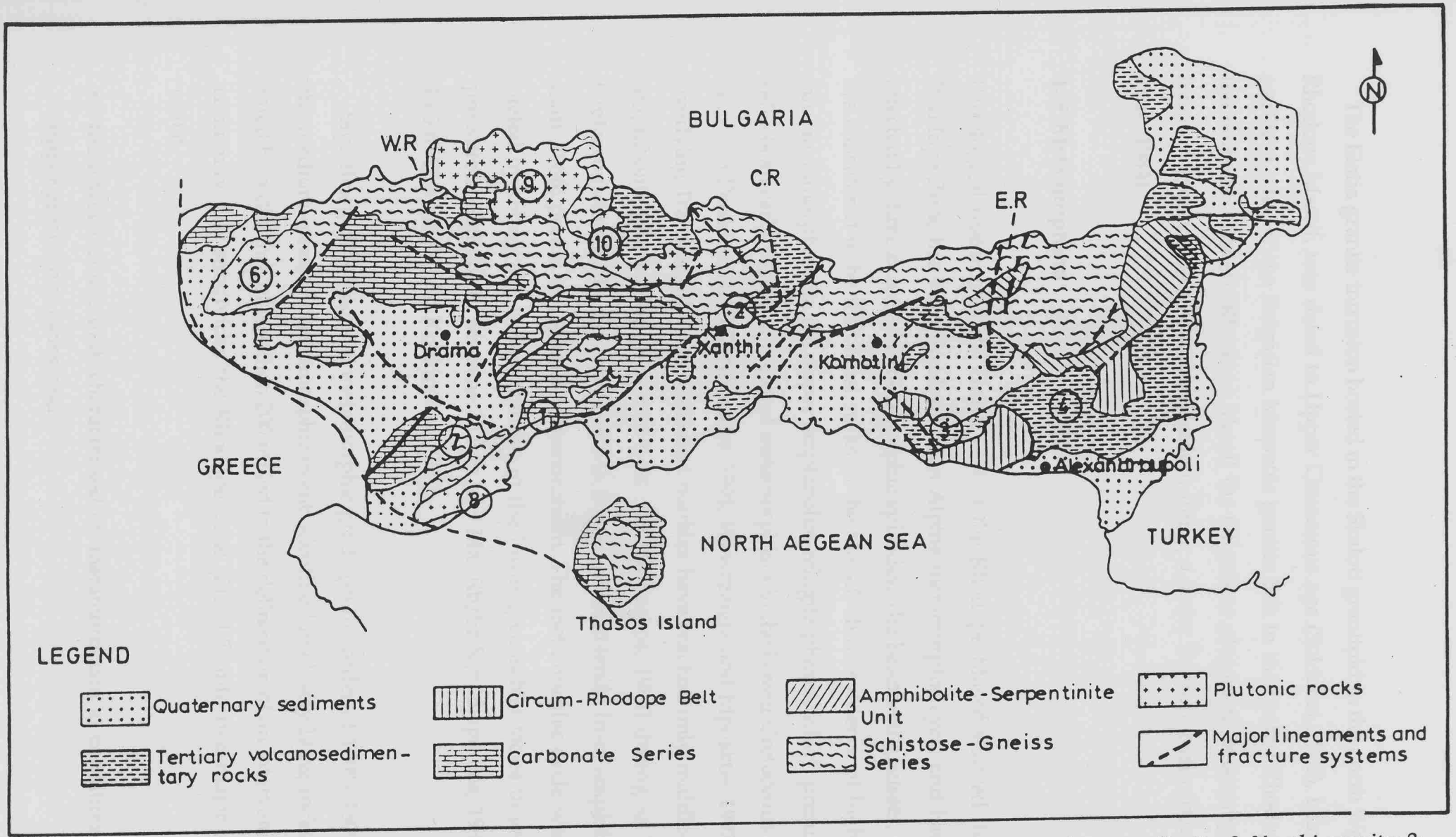

Figure 1.6: Geological map of the Rhodope Massif showing the distribution of the igneous activity (1: Kavala granodiorite; 2: Xanthi granite; 3: Maronia monzodiorite; 4: Kirki-Leptokaria monzodiorite; 6: Vrondou granitoid; 7: Pangeon granodiorite; 8: Symvolon granodiorite; 9: Elatia granodiorite; 10: Skaloti granitoid).

The Elatia granite intrusion hosted in the Skaloti granitoid in the north Western Rhodope Massif, was dated to Upper Cretaceous age (Soldatos, 1985), being the southern edge of the Bulgarian Mesozoic granite belt in the central Rhodope. In the northern Western Rhodope Massif the Oligocene plutonism is accompanied by co-magmatic volcanic rocks (Haidou) filling a major Tertiary basin (Innocenti et al., 1984).

1. 5 Metamorphism

Petrological research in the Greek part of the Rhodope Massif showed that the Rhodope Zone has been involved in an Alpine metamorphic cycle and has been affected by three successive metamorphic episodes. The basement gneisses, which are considered to be the oldest rocks in the Massif, show evidence of high pressure metamorphism in the upper amphibolite-eclogite phases, which presumably reflects an early period of regional metamorphism in the Lower Cretaceous (Mposkos and Perdikatsis, 1987; Mposkos, 1994; Wawrzenitz and Mposkos, 1997). The overlying Transitional Zone rocks and marbles have reached only middle-upper amphibolite phases (Mposkos and Liati, 1993; Mposkos, 1994) during an Upper Cretaceous to Middle Eocene 45-50 Ma (K/Ar in hornblende from amphibolites, Liati, 1986) period of regional metamorphism. The metamorphic cycle was completed by retrograde metamorphism in the lower greenschist facies under low-pressure conditions in Miocene 13.9 to 15.9 Ma (Rb/Sr Kyriakopoulos, 1987) and 15.5 to 17.8 Ma (K/Ar, Kokkinakis, 1980).

Significant differences in metamorphic grade (in the order of 100^0 - 150^0C), for the medium- pressure metamorphic event, identified in closely lying rocks (separated by a distance of less than 200 m) led to the delineation of an intervening discontinuity that subdivides the Rhodope Zone (Fig. 1.7) into two major tectonic units:

- the lower tectonic unit, characterised by metamorphism at conditions of the upper greenschist facies, and

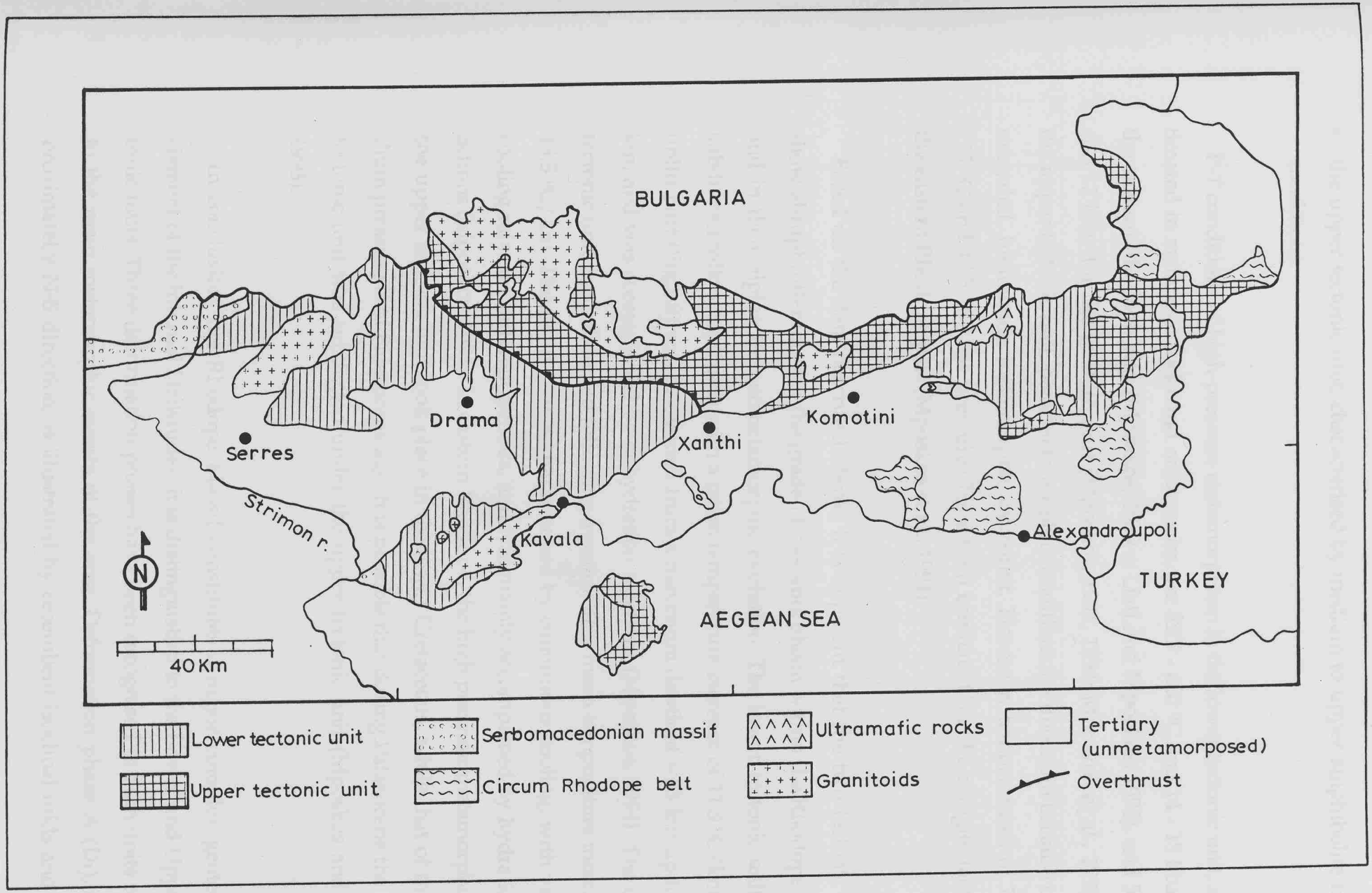

Figure 1.7: Simplified geological map of the Rhodope Massif showing the Lower and Upper tectonic units (in Mposkos, 1994).

- the upper tectonic unit, characterised by medium to upper amphibolite facies conditions.

P-T conditions of high-pressure metamorphism in the lower tectonic unit, as estimated in metabasic rocks and orthogneiss, are 550^0 - 600 ^{0}C and 14 - 15 kbar for the eastern Rhodope part (Mposkos, 1989 c; Liati and Mposkos, 1990), and 520^{0}C and 12 kbar for the western part (Mposkos, 1991, 1994; Mposkos et al., 1998). In the upper tectonic unit, peak metamorphic conditions are uncertain because of the extended, high-grade metamorphic overprint. However, temperatures of 750^0 - 775 ^{0}C and 13.5-16 kbar pressures have been estimated for the eclogite facies in the eastern Rhodope part (Mposkos et al., 1994).

Based on the data described above, it is apparent that the two tectonic units show abrupt differences in the grade of metamorphism within the Rhodope Zone and in their alpine tectonometamorphic evolution. The lower tectonic unit was subducted following a path with a mean temperature increase of 11.5 ^{0}C/km. The uplift part (Fig.1.8) was isothermal from a maximum depth of $\approx$ 53 km up to $\approx$ 14 km, and was accompanied by dehydration reactions (Mposkos, 1994). The upper tectonic unit was subducted following a path with a mean temperature increase of 15.5 ^{0}C/km. The uplift part is characterised by continuous cooling, with various cooling rates for different periods, and was mainly accompanied by hydration reactions (Mposkos, 1994). In eastern Rhodope, the high pressure metamorphism of the upper tectonic unit took place in the lower Cretaceous, while that of the medium pressure is of Palaeocene age. It is possible that during Palaeocene the lower tectonic unit was subducted under the upper tectonic unit (Mposkos and Liati, 1993).

In conclusion, the Rhodope Massif constitutes a major complex geotectonic element of the internal Hellenides. It is distinguished in the Lower and Upper tectonic units. Three deformation phases have been recognised in both units related to the main metamorphic events of the area. Deformation phase A (D_1), of approximatel;y N-S direction, is illustrated by recumbent isoclinal folds and a pri-

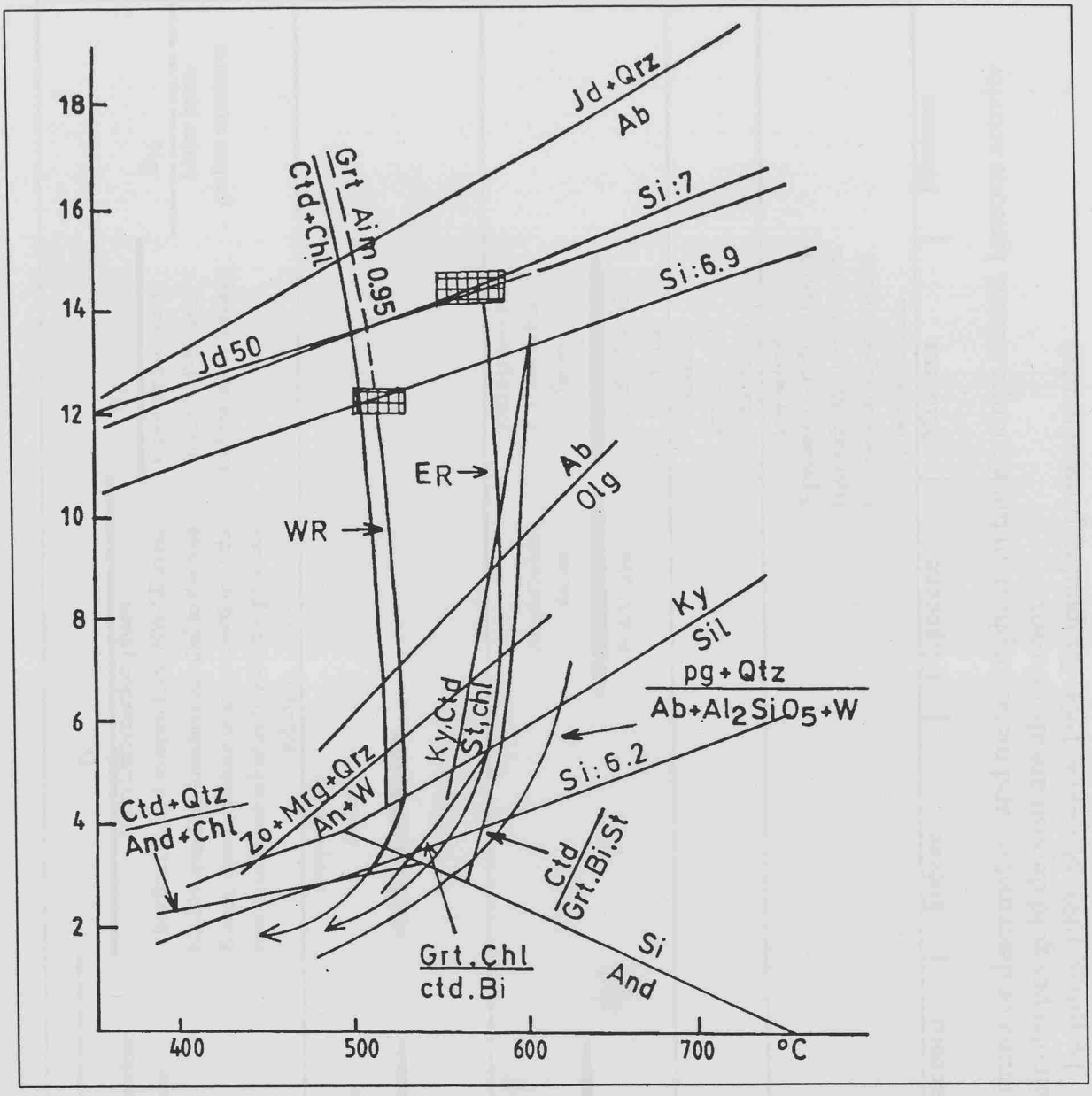

Figure 1.8: P-T conditions of the high-pressure metamorphism and uplift path of the Lower tectonic unit from Rhodope Massif (Mposkos, 1994).
W.R: Uplift path for West Rhodope Zone
E.R: Uplift path of East Rhodope Zone.

mary lineation due to axial plane schistosity. These early structures have been mostly destroyed by those of Deformation phase B (D_2) of NE-SW direction. B phase, which is the main Deformation phase, is characterised by close to isoclinal folds associated to pervasive lineation. Open folds of NW-SE axes mark deformation phase C (D3). The relative time of deformation and metamorphism in the Rhodope Massif is schematically illustrated in Table 1.2. Igneous activity and properties of ore forming fluids of the Asimotrypes mesothermal gold deposit are also shown.

DEFORMATION	D_1 Recumbent isoclinal folds of N-S direction Primary lineation due to axial plane schistosity		D_2 Main Deformation phase Isoclinal, closed to open folds NW-SE axes. NE-SW trending lineation parallel to the fold B-axes, corresponding to intersesection of the new axial plane schistosity with the previous foliation.		D_3 Open ample wavy folds NW-SE axes and fracture cleavage	D_{3b} Major horst-graben structures
METAMORPHISM *Upper Tectonic Unit (E.Rhodope)*	HP-HT Eclogite facies T: 750 - 775 ^{0}C P: 13.5 - 16 kbar		Amphibolite facies P: 4-15 kbar			
Lower Tectonic Unit (W.Rhodope)	HP-HT Eclogite facies T: 550 - 600 ^{0}C P: 14 - 15 kbar			Amphibolite facies P: 4-15 kbar	Retrogression L. Greenschist facies T: 270-340 ^{0}C P: 3.3 kbar	
IGNEOUS ACTIVITY					Nikissiani granodiorite 13 -15 Ma	
ORE FORMING FLUIDS					low salinity 3-phase CO_2-rich inclusions H_2O-rich: XCO_2=c.10 mol% CO_2-rich: XCO_2=c.38 mol% 2-phase inclusions	
	L. Cretaceous	U. Cretaceous	Eocene	Oligocene	Miocene	Pliocene

Table 1.2: Schematic summary of the relative timing of deformation and metamorphism in the Rhodope Massif. Igneous activity and properties of ore forming fluids of the Asimotrypes gold deposit are also shown.
(After Papanikolaou and Panagopoulos, 1981; Tsombos, 1993; Mposkos, 1994; Eliopoulos, present study).

CHAPTER 2

GEOLOGY OF THE PANGEON MOUNTAIN REGION

2.1 General Statement

The Rhodope Massif, on the basis of geological criteria is divided in the Eastern, Central and Western Rhodope Zones. The boundaries between the Western and Central Rhodope Zones are not clearly defined. However, geographically the Western Rhodope Zone includes the following areas: Falakron, Lekani, Pangeon, and Menikion Mountains and the island of Thassos in the Greek territory. The Pirin and the Southern Rila Mountains occur in Bulgaria. (Fig. 1.1 & 2.6).

2.2 Geological Setting of the Pangeon Mountain Region

The Pangeon Mtn. region geologically belongs to the Western Rhodope Zone and forms a highly uplifted, dome like, horst structure composed of metamorphic rocks of Palaeozoic-Mesozoic age, Oligocene magmatic rocks (Meyer, 1968; Kyriakopoulos, 1987), and sedimentary rocks of Upper Miocene age to Recent (Xydas, 1978).

The metamorphic rocks, consisting mainly of marbles, schists, augen gneisses and amphibolites cover the largest part of the area (Fig. 2.1). Granodioritic stocks intrude all the metamorphic formations and occur along a NE-SW trending line. The sedimentary rocks, which are terrestrial, lacustrine to brackish and marine deposits are mainly developed in the western and north-western parts of the area.

LEGEND

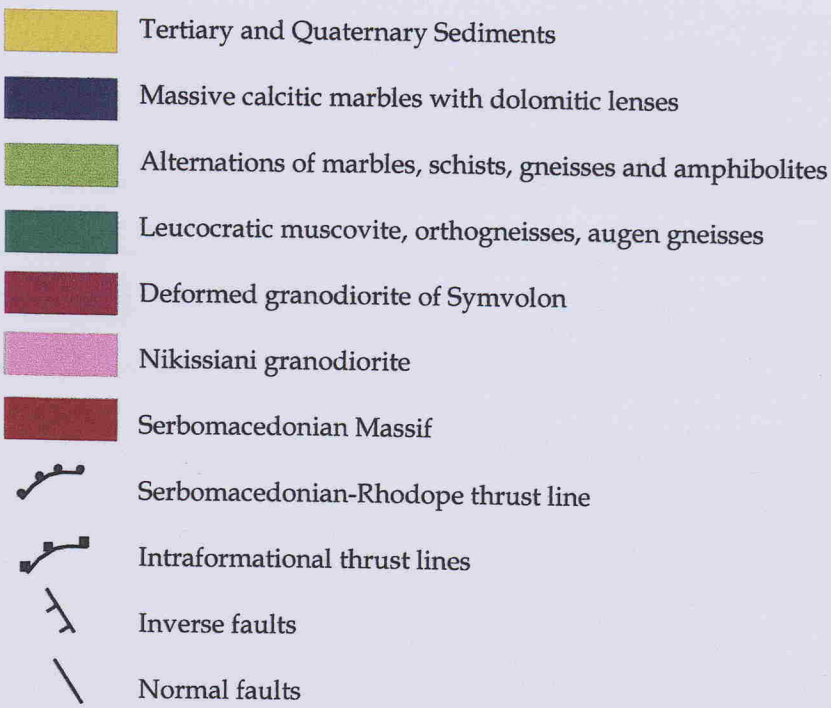
Tertiary and Quaternary Sediments
Massive calcitic marbles with dolomitic lenses
Alternations of marbles, schists, gneisses and amphibolites
Leucocratic muscovite, orthogneisses, augen gneisses
Deformed granodiorite of Symvolon
Nikissiani granodiorite
Serbomacedonian Massif
Serbomacedonian-Rhodope thrust line
Intraformational thrust lines
Inverse faults
Normal faults

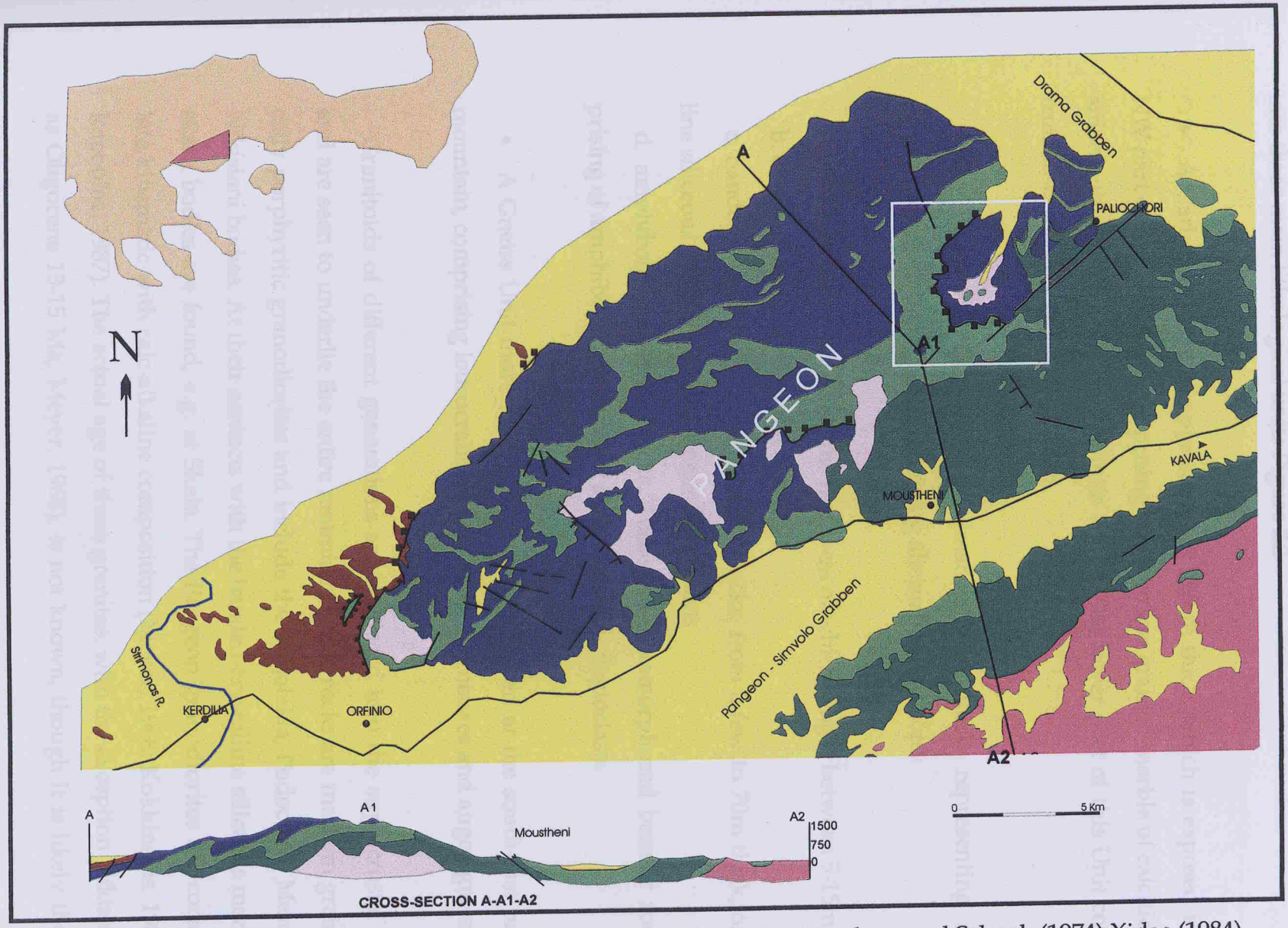

Figure 2.1: Geologic and tectonic map of the Pangeon Mt., after Kronberg and Schenk (1974);Xidas (1984). Modified by Chatzipanagis et al., 1991.

Based on field observations, the metamorphic rocks of the area are sub-divided into three main lithological units Figure 2.2:

- A Carbonate Unit, of approximately 500 m thick, which is exposed in the N-NW part of the mountain, comprising white coarse grained marble of calcitic composition with intercalations of dolomite lenses. The lower part of this Unit consists of banded-crystalline siliceous marbles.

- A Transitional Unit of approximately 600m thick, representing a strong sheared zone consisting of the following alternating horizons:

a. two-mica gneiss horizons, the thickness of which ranges between 5-15m

b. albite-gneisses, 20-25m thick

c. banded crystalline siliceous marble blocks, from a few to 70m thick, or crystalline siliceous marble lenses of longer dimensions

d. amphibolite lenses or blocks. These are metamorphosed basaltic rocks comprising of amphibole (hornblende/actinolite) and plagioclase.

- A Gneiss Unit more than 1000 m thick, exposed at the south-east part of the mountain, comprising leucocratic muscovite, orthogneisses and augen gneisses.

Granitoids of different generations are emplaced into the supracrustal sequence and are seen to underlie the entire mountain. These rocks are medium grained to locally porphyritic granodiorites and include the Mesolakia, Podochori, Mesoropi and Nikisiani bodies. At their contacts with the banded-crystalline siliceous marble, small skarn bodies are found, e.g. at Skala. The Pangeon granodiorites are considered as late kinematic with calc-alkaline composition (Meyer, 1968; Kokkinakis, 1980; Kyriakopoulos, 1987). The actual age of these granites, with the exception Nikisiani (dated as Oligocene 13-15 Ma, Meyer, 1968), is not known, though it is likely they are ge-

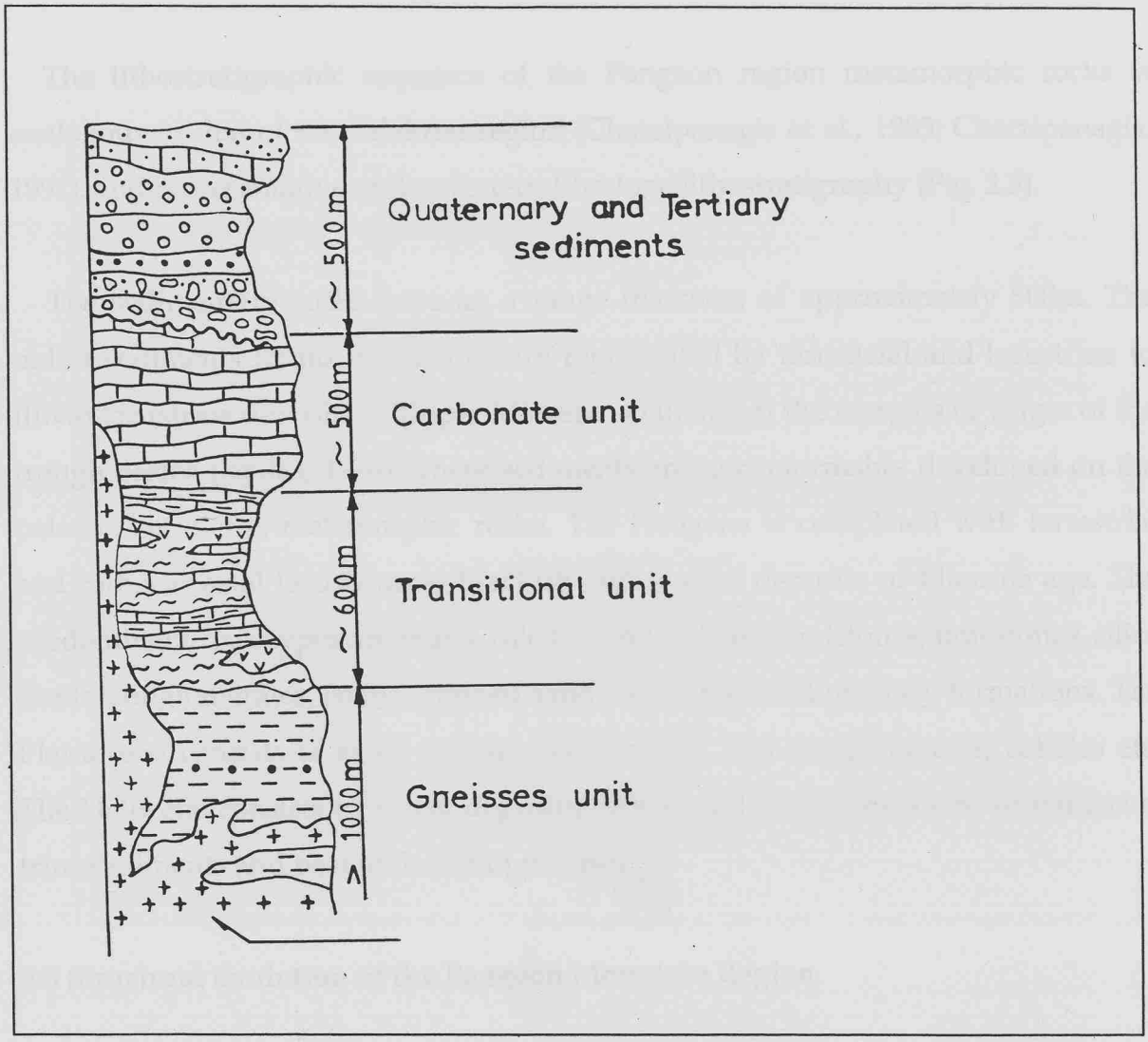

Figure 2.2: Lithostratigraphic unit of the Asimotrypes, Pangeon (Chatzipanagis et al., 1991).

netically related to the Kavala granite with an age of 13.9 to 15.9 ma (Kyriakopoulos, 1987).

The lithostratigraphic sequence of the Pangeon region metamorphic rocks is analogous to that of the Falakron region (Chatzipanagis et al., 1983; Chatzipanagis, 1991), and representative of the western Rhodope lithostratigraphy (Fig. 2.3).

The sedimentary rocks have an average thickness of approximately 500m. The oldest sediments found in the area are represented by terrestrial and lacustrine to fluvio-lacustrine deposits of Upper Miocene occurring at the margins or ridges of the trough basins (Xydas, 1978). These sediments are unconformably developed on the palaeorelief of the metamorphic rocks. The Neogene is completed with terrestrial and rather coastal lacustrine to brackish and marine deposits of Pliocene age. The predominant rock types are marls, calcitic sand, calcitic sandstones, limestones, silica sands, conglomerates, coarse-grained sand and volcanosedimentary formations. The Pleistocene consists of sand, pebbles, sandy clays, and conglomerates, cobbles etc. The Holocene consists of recent deposits, deltaic and coastal deposits, recent lacustrine sediments and peat at the Philippi basin.

2.3 Structural Evolution of the Pangeon Mountain Region

The overall structural evolution of the Western Rhodope Zone rocks shows a complex development of corroborative tectonometamorphic events. Intensive plastic and brittle deformation characterise the Zone. The successive stages of the plastic deformation are overprinted almost in all metamorphic rocks, giving a complete picture of the tectonometamorphic evolution of the Rhodope Massif. Associated brittle deformation, though of great metallogenic significance, is difficult to interpret because only traces of the last tectonic events can be recognised in the field (Chatzipanagis et al., 1992). The major elements of brittle deformation comprise compressional thrust

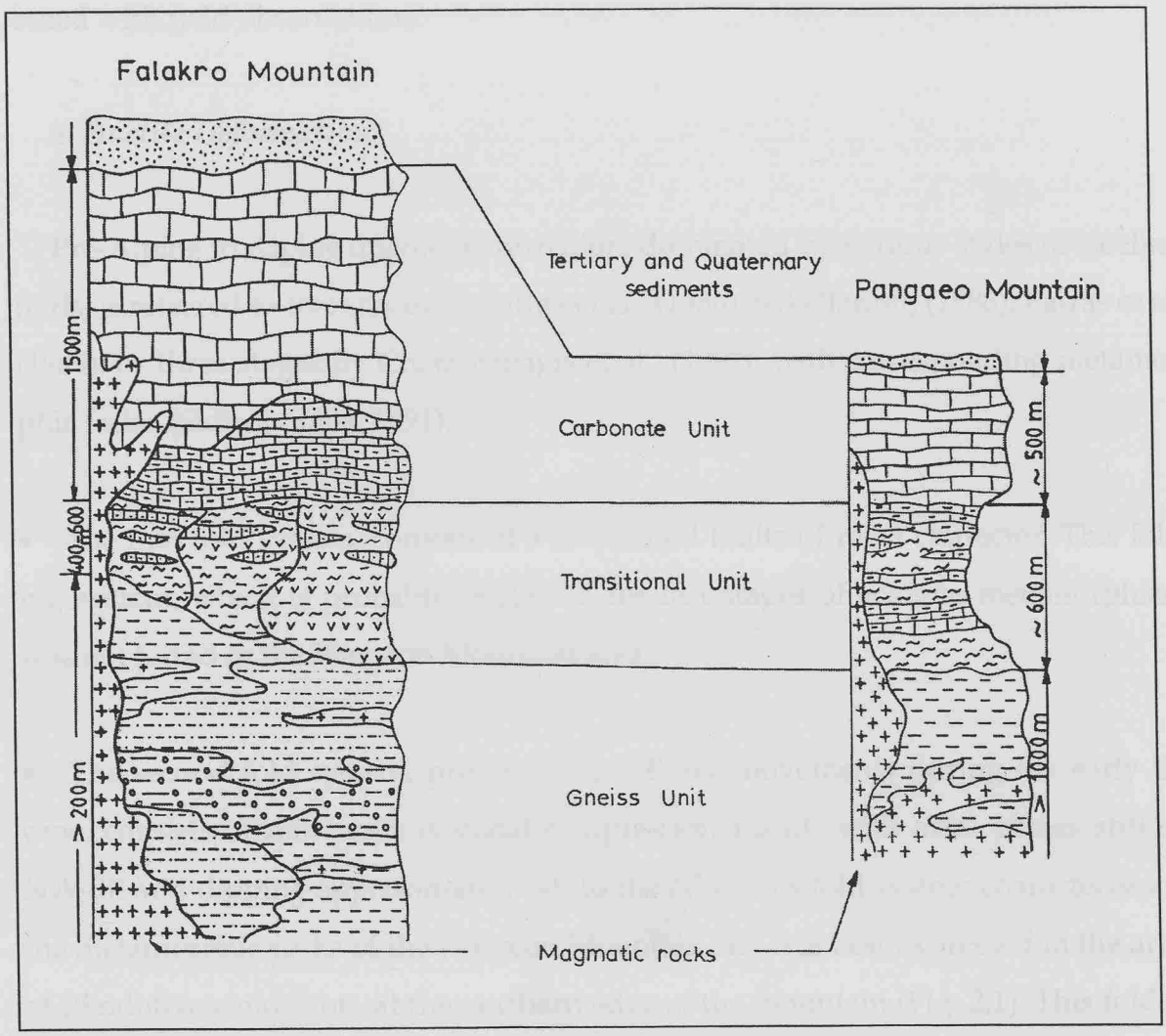

Figure 2.3: Lithostratigraphic correlation of the Falakro and Pangeon Mountains (Chatzipanagis, 1991).

and shear structures, and extensional fault zones. The latter are clearly obtained by integrated interpretation of remote sensing, aeromagnetic, and seismic data combined with field observations.

a. Ductile Deformation

Pre-Alpine to Alpine ductile deformation, dominated by various styles of isoclinal folds, is referred to five stages by Patras et al., (1986); Sakellariou, (1988); Patras et al., (1989), or three stages by Chatzipanagis et al., (1992), with corresponding metamorphic facies (Sidiropoulos, 1991).

- The first fold system, consists of a few closed faults of relict character. This folding system, which is probably related to the last stages of eclogite metamorphism, was not found in the Pangeon Mountain area.

- The second fold system, produced by NE-SW movements during the early Eocene, consists of numerous isoclinal compressional folds with axial planes striking NW-SE and dipping approximately 50° to the NW. This fold system characterises all the metamorphic rocks of the Pangeon Mountain and it is best expressed in the areas of Rhodolivos and Proti, at the northern edge of the mountain (Fig. 2.1). This folding system, related to the medium pressure type metamorphism, has caused reversals of the lithological units locally, and in many cases has increased the initial rock thickness with overthrusts and reversed faults (Fig. 2.4 & 2.5).

- The third fold system is comprised of open drag folds and dissolution cleavages as a result of decompressional forces during the uplift of the (post middle Miocene) Rhodopian orogeny. Major host-graben structures began to develop at this time and movement has continued to the present.

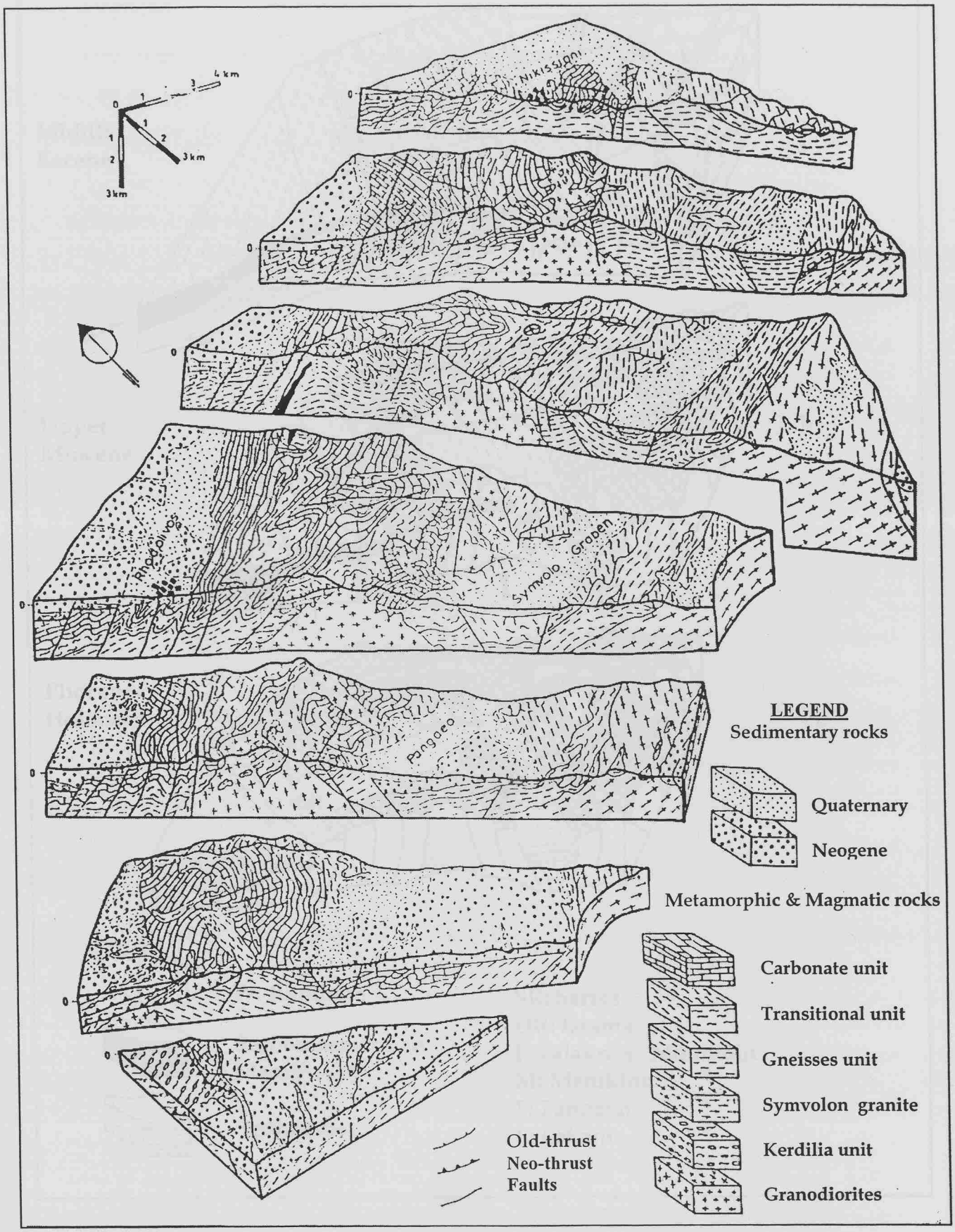

Figure 2.4: Structural sketch map illustrating the evolution of the Pangeon and Symvolon Mountains (Chatzipanagis, 1991).

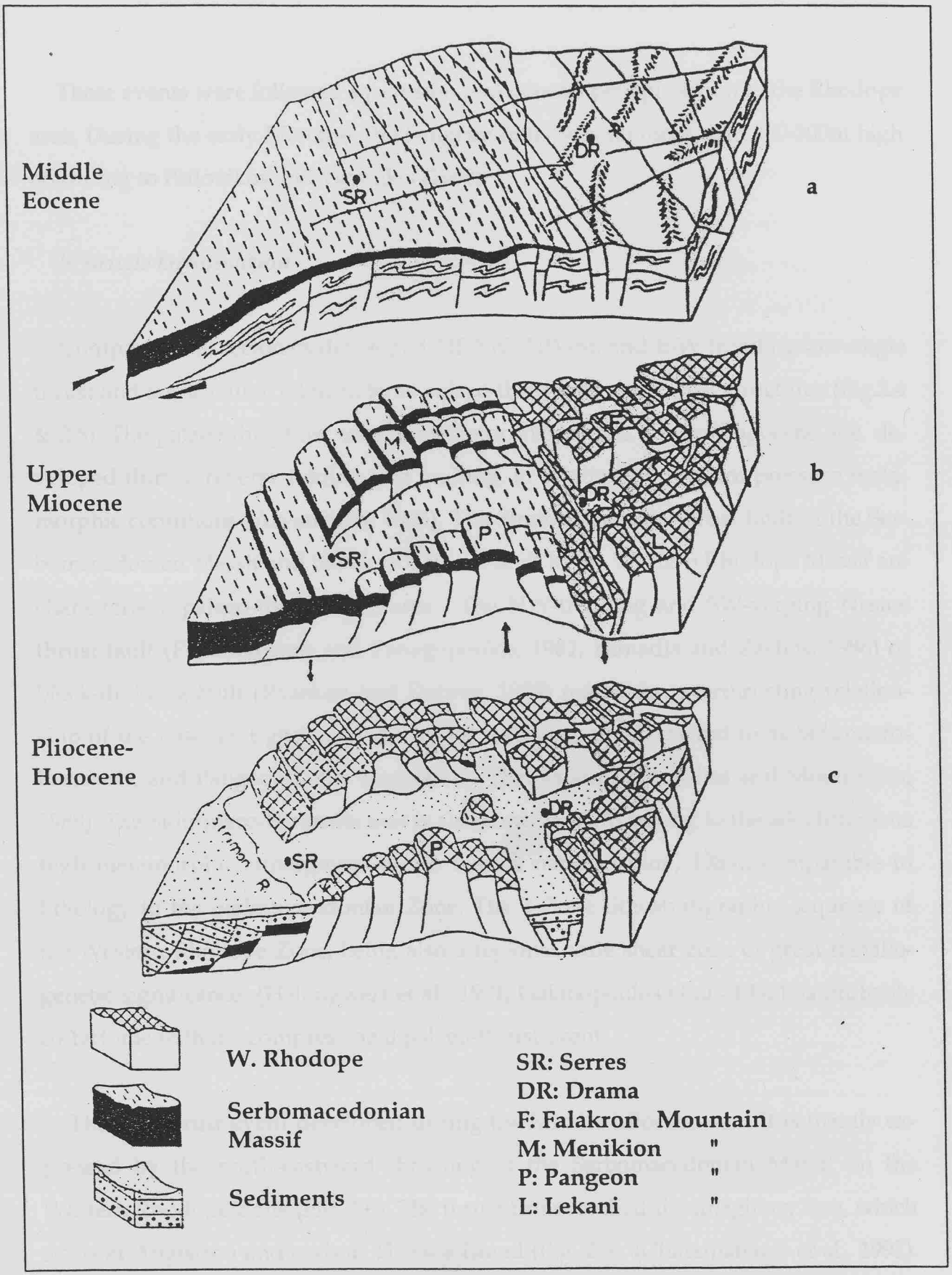

Figure 2.5: Schematic sketches illustrating the evolution of the West Rhodope Zone and the Serbomacedonian Massif, from Middle Miocene up today (Chatzipanagis, 1991).

These events were followed by erosion and general peneplanation in the Rhodope area. During the early Miocene, the Pangeon relief was no more than 200-300m high according to Psilovikos and Vavliakis (1982).

b. Brittle Deformation

Compressional tectonics developed NE-SW, NW-SE and E-W trending low-angle thrust and shear faults, referred to as palaeo-thrust and neo-thrust structures (Fig.2.4 & 2.5). The palaeo-thrust are tectonometamorphic thrusts, of pre-Oligocene age, developed during reverse folding and faulting, in relation to medium pressure metamorphic conditions (Arvanitidis, 1993). The Stratoni-Varvara thrust-fault in the Serbomacedonian Massif and the Nestos thrust-fault in the Western Rhodope Massif are characteristic palaeo-thrust structures. The NW-trending and SW-verging Nestos thrust fault (Papanikolaou and Panagopoulos, 1981; Dimadis and Zachos, 1986) or block-dividing fault (Ryaskov and Dobrev, 1989) marks the overthrusting relationship of the basement gneiss on the upper carbonate unit, referred to as Sidironero-Paranesti, and Pangeon Units respectively (Patras et., 1989; Kilias and Mountrakis, 1989). The Sidironero-Paranesti unit is also considered to belong to the allochthonous high metamorphic supergroup of the Nestos nape (Ivanov, 1989), comparable in lithology to the Serbomacedonian Zone. The T-Zone lithostratigraphic sequence of the Western Rhodope Zone, being also a regional scale shear zone of great metallogenetic significance (Hellingwerf et al., 1991; Galanopoulos et al., 1992), is probably co-tectonic with the compressional palaeo-thrust event.

The neo-thrust event developed during the Middle Miocene, and it is mainly expressed by the north-eastward thrusting of the Serbomacedonian Massif on the Western Rhodope Zone (Fig. 2.6). The thrust front reached the imaginary line, which starts at Angistron and ends at Thassos Island (Fig. 2.6), (Chatzipanagis et al., 1992). Also, during this thrust on the Pangeon Region shear structures and reversed faults

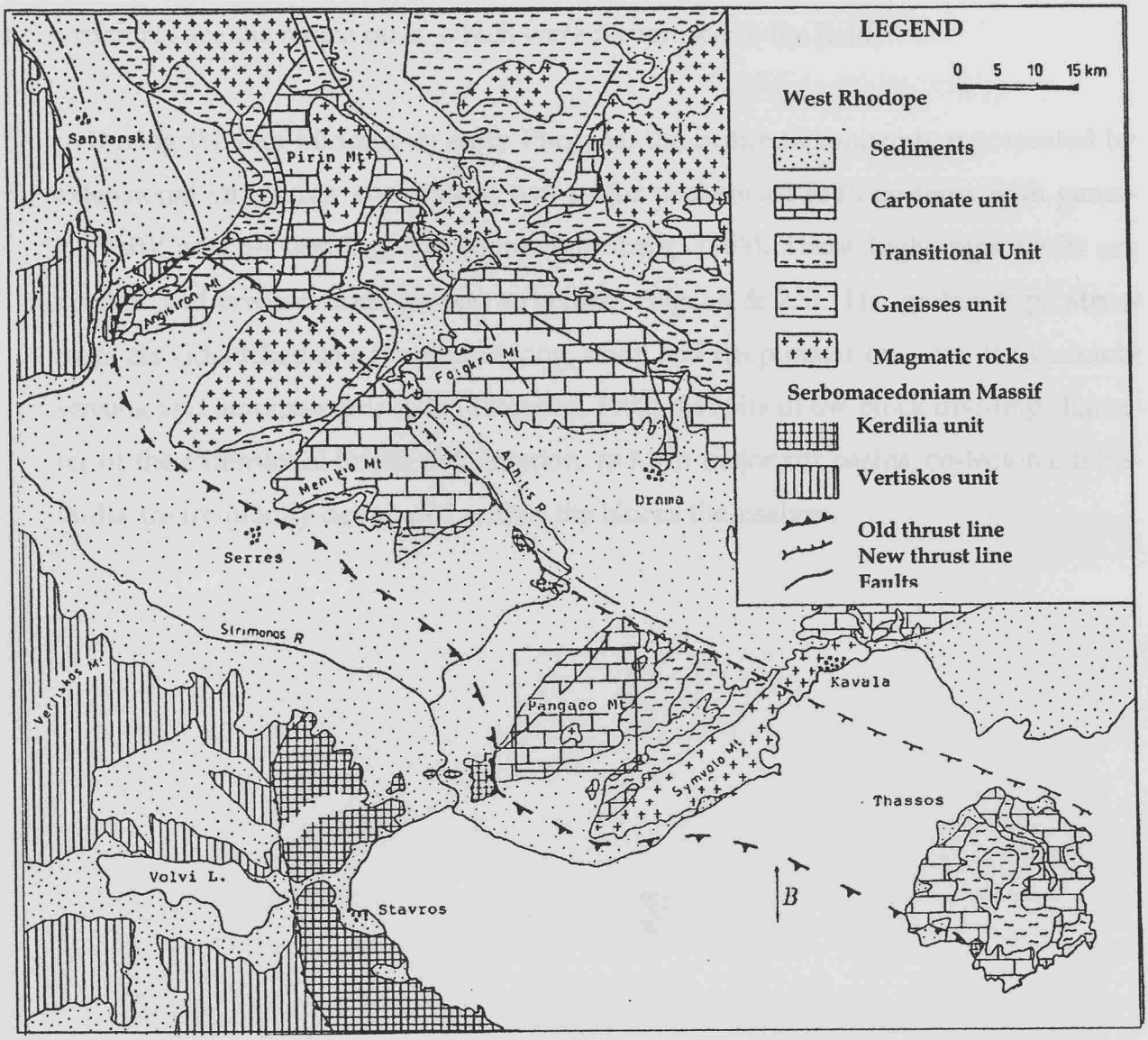

Figure 2.6: The tectonic relationship between the West Rhodope Zone and the Serbomacedonian Massif (Chatzipanagis, 1991).

were created in the rocks underlying the Rhodope Massif. The compressional fault structures are the oldest ones, which were recognised in the field.

During the late Miocene to early Pliocene, the brittle tectonism is represented by extensional structures, comprising two major post-thrust fault systems with generally NW and SE trending directions (Kronberg, 1969). These high-angle faults are vertical and created horst-graben structures (Fig.2.4 & 2.5). The graben type structures also identified as a number of long, steep and deep major lineaments by remote sensing and aeromagnetic data (Tsombos, 1993). In spite of the block dividing character of the extensional brittle deformation, to form major rift basins, co-tectonic intrafaults are frequently developed within the blocks themselves.

CHAPTER 3

ORE GEOLOGY

3.1 General Statement

The Pangeon Mountain Region contains typical examples of vein and shear-hosted precious and base metal deposits. The majority of these deposits were worked in ancient times and especially during the Alexander the Great era, as it is reported by several authors of that time. Kronberg and Schenk (1974), and Xydas (1984) initially mapped the area. During the course of this work only minor modifications were made on the existing geological maps.

The north eastern part of the Pangeon gives a vertical section, greater than 1000 metres, through a vein and replacement style of mineralisation, with a strong structural control on each occurrence. NW-SE sub-vertical fractures can be traced up the mountain with a paragenesis changing from pyrite + quartz to pyrite + quartz + sericite to sericite in the granite underlying the Asimotrypes, and finally pyrite + chalcopyrite + malachite where the veins cross overlying marble and schist units (Fig. 3.1).

The granite is overlain by an alternating sequence of shear banded marbles and sheared supracrustals including amphibolites, gneisses and schists (Fig.3.2). These are in turn overlain by 700 meters of massive marble which is considered as equivalent to the Falakron marble of the Drama region (Chatzipanagis, 1991). The contacts between sheared marbles and sheared supracrustals are low angle shear thrusts, dipping ± 30° to the east. Lenses of arsenopyrite - pyrite quartzite are

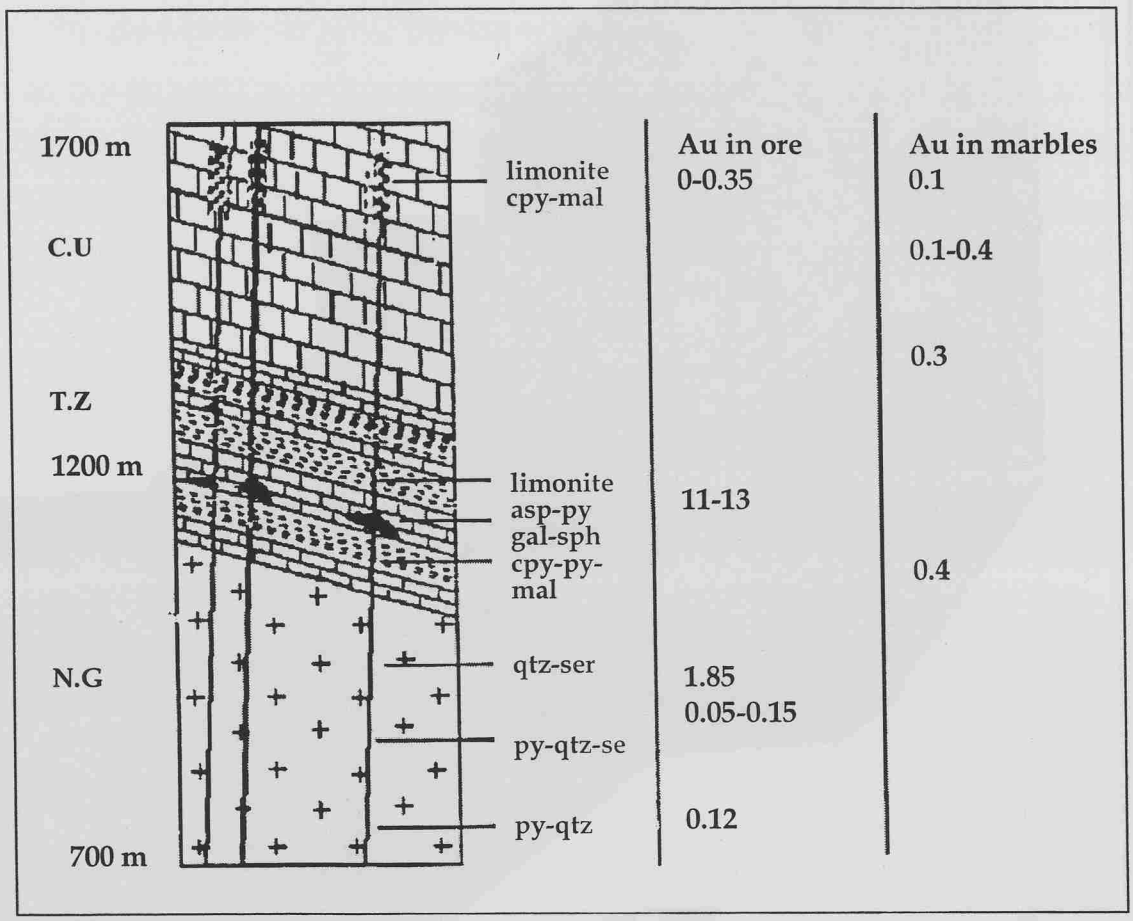

Figure 3.1: Vertical profile through the Asimotrypes mineralising system, showing also Au contents (ppm) in ore and marbles.
N.G: Nikisiani Granodiorite
T.Z: Transitional Zone
C.U: Carbonate Unit

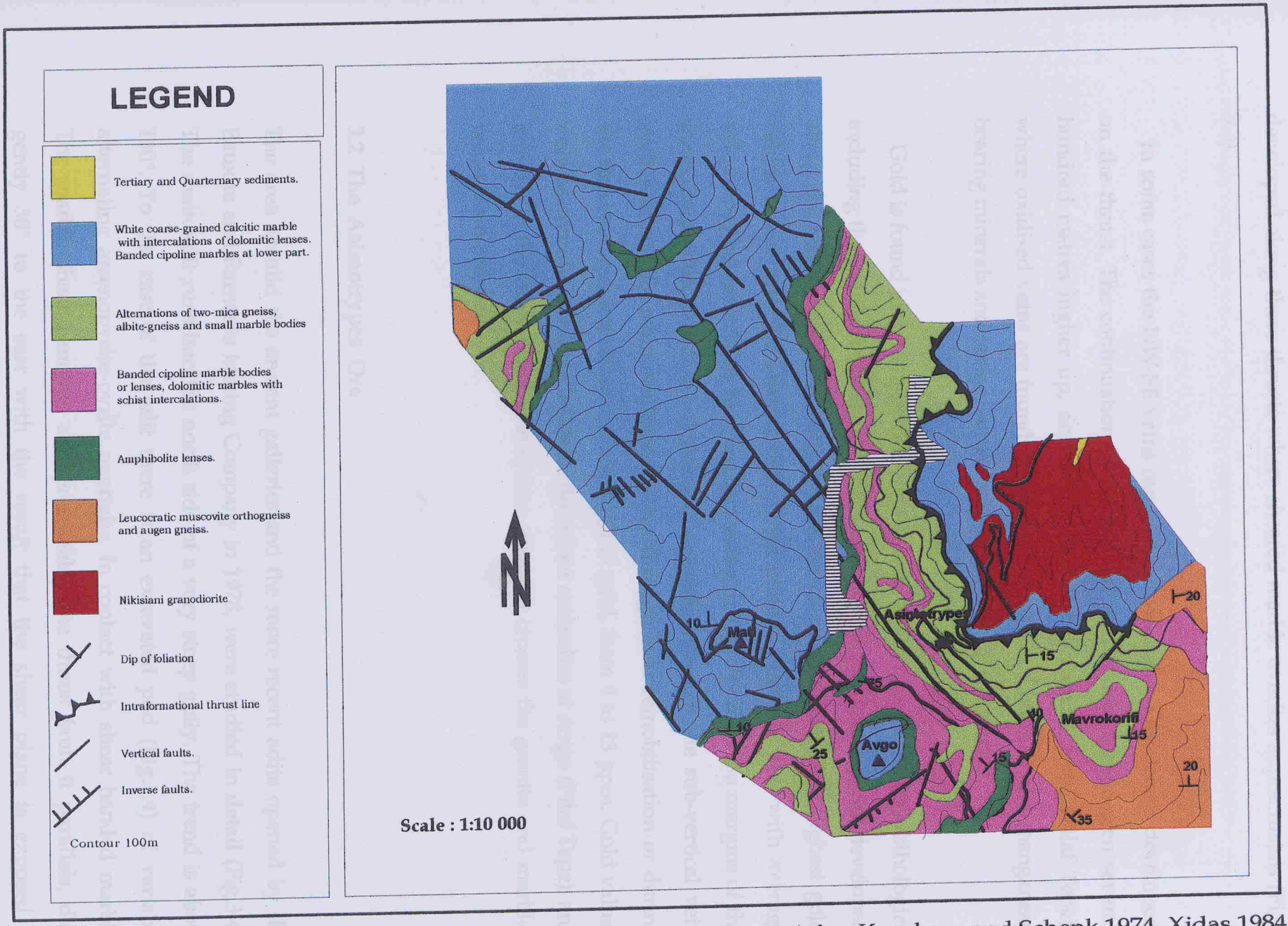

Figure 3.2. Geological map of the N.E. part of the Pangeon Mountain (after Kronberg and Schenk 1974, Xidas 1984. Modified by Eliopoulos.)

developed along these thrusts where sheared marble overlies supracrustals (Fig. 3.3).

In some cases the NW-SE veins can be seen crossing the ore lenses developed on the thrust. The continuation of the NW-SE vein system can be seen several hundred metres higher up, on the top of the mountain at Avgo (Pilaf Tepe), where oxidised veins are found in ankeritised marble. Limonite and manganese bearing minerals and minor malachite traces mostly fill the veins.

Gold is found in the sub-vertical vein system which cuts all the rock lithologies including the granite, as well as in the irregular pods and lenses of ore developed along the thrusted contacts between the marbles and schists. The highest gold values come from the arsenopyrite-pyrite pods at Asimotrypes, with average values ranging from 11 to 16 ppm, decreasing to 1 to 3 ppm at the margins of the pods. Sulphides, which are developed as small lenses in the sub-vertical vein system above the main ore lenses, either through later remobilisation or during the first mineralising phase, are also high in gold, from 4 to 13 ppm. Gold values decrease rapidly at higher levels, in the minor orebodies at Avgo (Pilaf Tepe), and are low in the sub-vertical vein system where it crosses the granite and marbles below Asimotrypes.

3.2 The Asimotrypes Ore

The area around the ancient galleries and the more recent adits opened by the Bauxite and Parnasse Mining Company in 1978, were studied in detail (Fig.3.4). The main adit runs into the north side of a very steep gully. The trend is about 130°. To the east of the adit there is an excavated pod (Fig.3.4) of variably alternating arsenopyrite-pyrite quartzite, in contact with shear banded marble. The marble shear banding, and presumably the thrust fault it parallels, dips gently 30° to the east with the result that the shear plane is exposed at

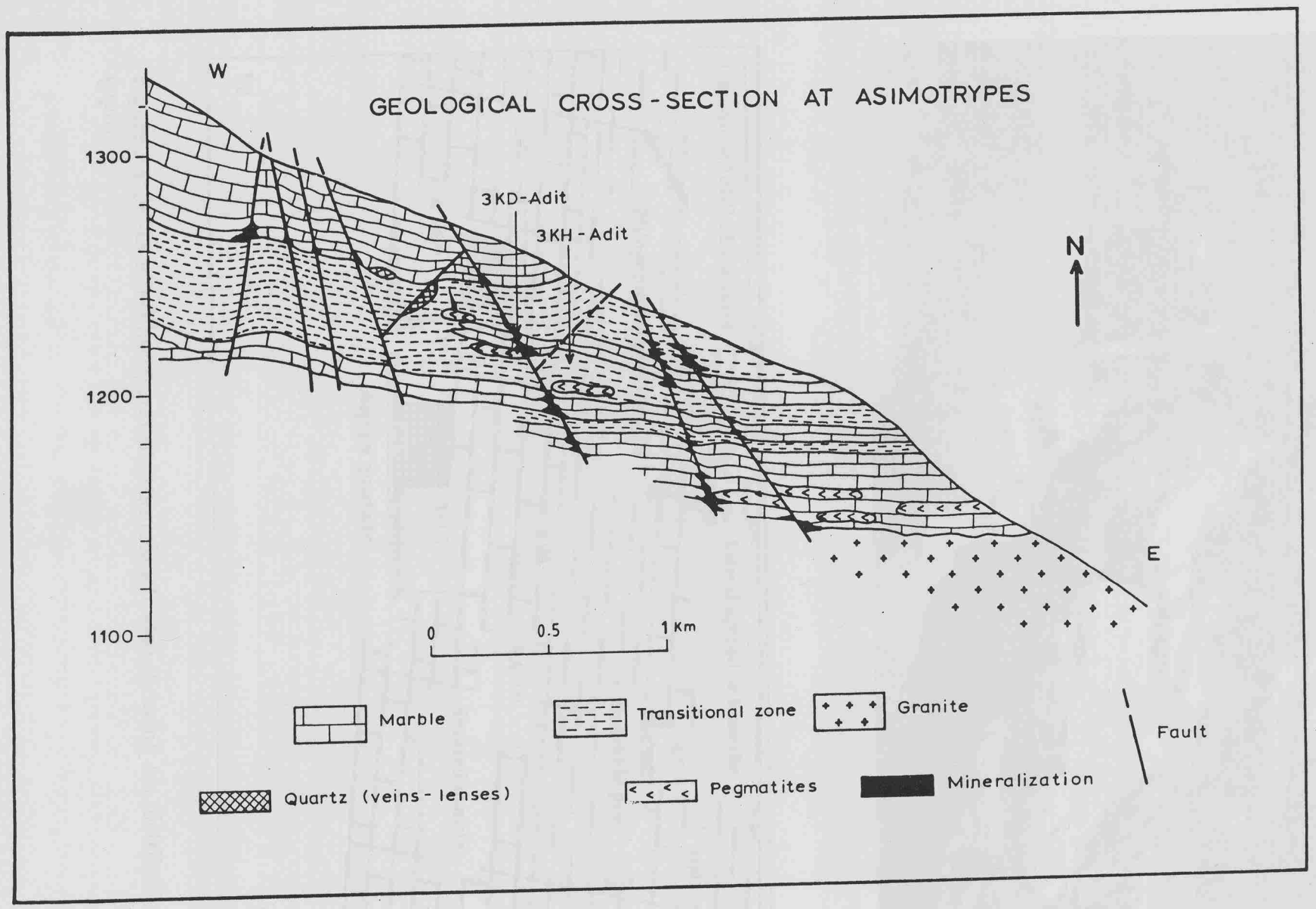

Figure 3.3: Geological cross-section at Asimotrypes, Pangeon.

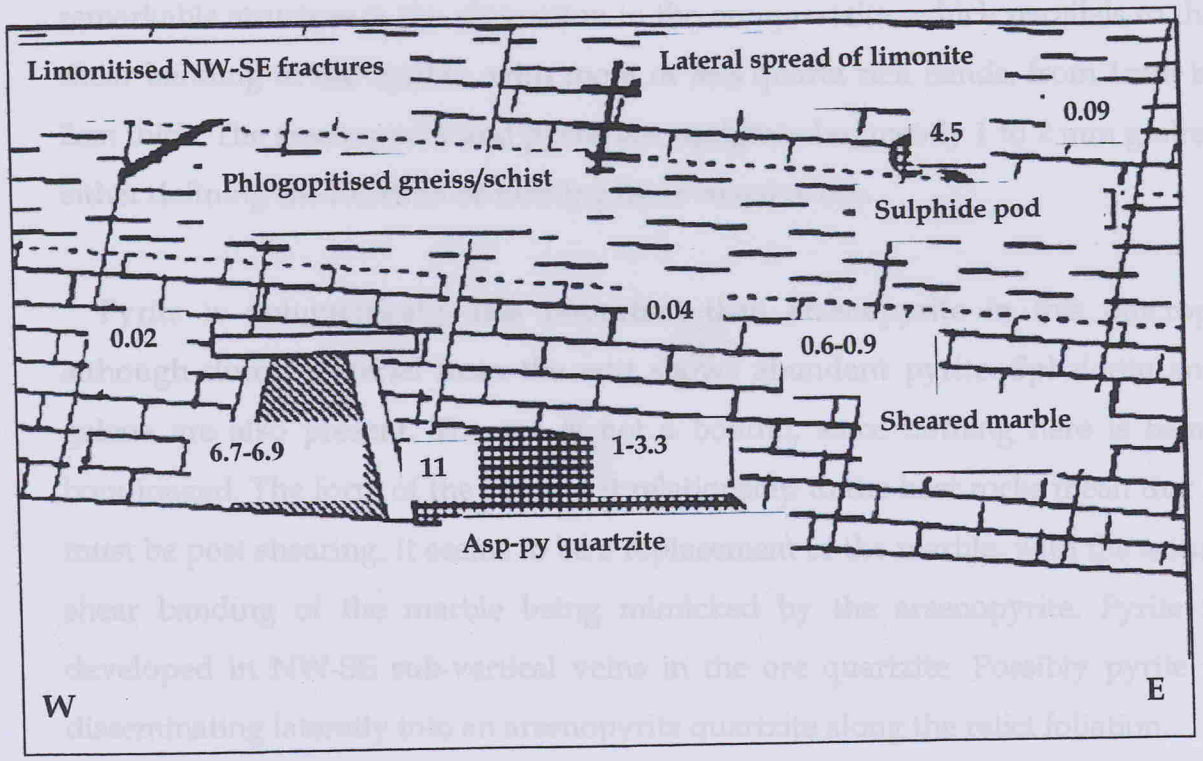

Figure 3.4: 3K-D adit (Photo) and situation sketch, also showing Au distribution in (ppm).

successively higher levels to the west. The Nikisiani granodiorite was found at a depth of 180 meters underneath the Asimotrypes ore, during drilling operations.

The shape of the ore is important in this particular 3K-D adit. It is elongated in the W-E plane of the thrust and constitutes an irregular pod about 1-2 m wide, 1 m thick and 5 m long. A large part of the ore has been removed during mining operations, leaving a skin of sulphides against the marble to the north. The contact between the ore and marble is a 2 cm zone of limonitised material. Importantly there is no skarn development between the sulphides and marble; a calc-silicate assemblage as such is absent. However, the underlying schist seems to have been biotised / phlogopitised, which is the skarn equivalent. Not exposed, but documented, is the orebody that is developed along the contact between the marble and schist, with the marble being replaced. The most remarkable structure is the alternation in the ore quartzite, which parallels to the shear banding in the marble, with more or less quartz rich bands, from 1mm to 2cm thick. The arsenopyrite and pyrite are equigranular, mostly 1 to 2 mm grains, either defining the foliation or forming more massive ore.

Pyrite is volumetrically less important than arsenopyrite in this outcrop, although dump material from the adit shows abundant pyrite. Sphalerite and galena are also present. The ore is not a boudin, since nothing here is being boudinaged. The form of the ore and it relationship to the host rocks mean that it must be post shearing. It seems to be a replacement of the marble, with the actual shear banding of the marble being mimicked by the arsenopyrite. Pyrite is developed in NW-SE sub-vertical veins in the ore quartzite. Possibly pyrite is disseminating laterally into an arsenopyrite quartzite along the relict foliation.

Within the adit entrance there is a major brecciation zone. This NW-SE plane dips 55° N, with abundant limonitisation around the fragments, and truncates the western end of the ore.

The marble above the orebody is crosscut by sub-vertical NW-SE fractures, which are often coated with limonite. In general where the fractures cut schist or gneiss, only limonite is found, whereas where a marble unit is crossed, sulphides may developed. However, this is not uniform since to the east of the adit entrance a NW-SE fracture crossing schists contains malachite, stained quartz as well as thin lenses of arsenopyrite and pyrite.

Quartz boudins are abundant in the sheared marble, and boudinaged and folded quartz layers are seen in the schist sequence. The schist close to the orebody is hydrothermally altered, with what appears to be phlogopitisation. The minor skarn bands with magnetite some 150 m east of the orebody are simply skarn bands in the sheared marble, unrelated to the mineralisation.

Some 200m west up the gully there are several adits dating from the time of Philip of Macedonia - large enough for hopeless slaves to creep into, and often quite extensive. One of these adits was sampled (Fig. 3.5), since it shows the relationship between the thrust related arsenopyrite-pyrite quartzite and the NW-SE fractures. Above the thrust plane ore a NW-SE shear is strongly limonitised, and contains sub-vertical lenses of arsenopyrite-pyrite. These are small compared to the main ore at this point, but indicate an upward movement of hydrothermal fluid along the fracture system, linking the two. The main question here is whether the ore was remobilized from the thrust by later superposition of NW-SE fractures, or whether the fractures acted as channel ways for hydrothermal fluids. These may have resulted in both the sub-vertical mineralised veins and the replacement bodies in marble along the shear contact at the same time. The latter seems more likely at present.

A further point is the potential role of the Nikisiani granidiorite in this and other mineralisations. The presence of the granodiorite intersected by drilling and cropping out in the general region suggests a possible genetic link with the

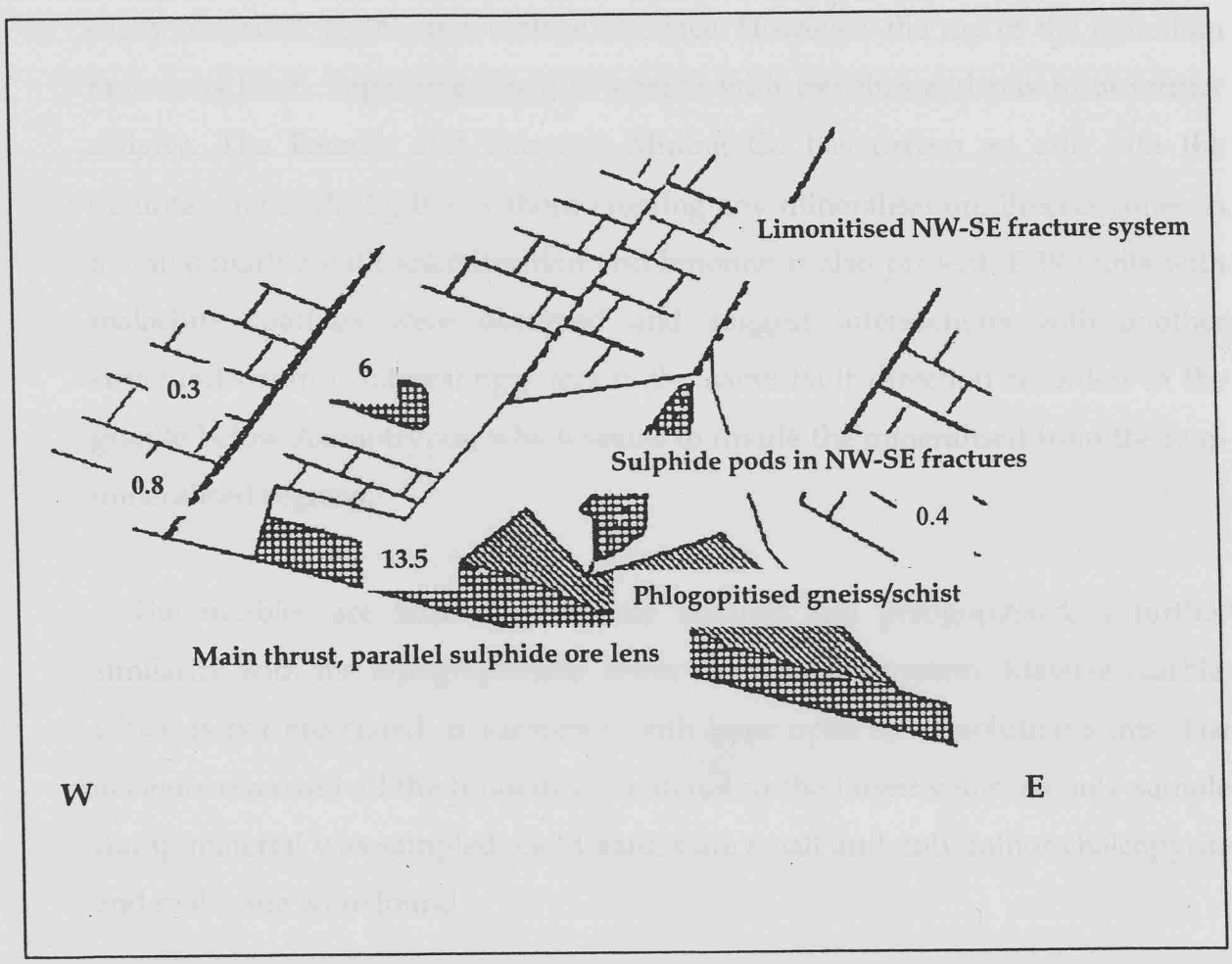

Figure 3.5: Situation sketch of the archaeological adit 3K-H, located above the main adit 3K-D, Asimotrypes. Au contents (ppm) are also illustrated.

mineralisation. This is supported by the presence of weak foliation and NW-SE fracturing together with dispersed pyrite.

3.3 The Avgo (Pilaf Tepe) Mineralisation

The passage of the NW-SE veins through the upper massive marble can not be easily observed, as this is a vertical cliff face. However, the top of the mountain known as Pilaf Tepe (rice bowl) is scarred with trenches and pits from former activity. The Bauxite and Parnasse Mining Co has driven an adit into the mountain (adit 18° S), but without crossing any mineralisation. Breccia zones in massive marble with ankeritisation and limonite is also present. E-W joints with malachite coatings were observed and suggest intersections with another structural control. Interestingly this is the same fault direction recorded in the granite below Asimotrypes, which seems to divide the mineralised from the non-mineralised regions.

The marbles are locally intensively sheared and phlogopitised, a further similarity with the topographically lower Asimotrypes system. Massive marble, which is not brecciated, is karstified, with large open space solution joints. The ancients removed all the limonitised material in the larger veins, so only sample dump material was sampled. Gold values are small and only minor chalcopyrite and malachite were found.

CHAPTER 4

PETROLOGICAL STUDIES OF THE PANGEON LITHOLOGICAL UNITS

4.1 General Statement

Carbonate rocks comprise the main part of the Western Rhodope and the Serbo-macedonian Zones. In the Pangeon Region, marbles form an upper thick unit above a sequence of interlayered gneisses, calcareous schists and banded marbles. The marbles of the upper thick unit of the Pangeon Region have been correlated with the major Falakron Series marbles of the Drama area (Chatzipanagis, 1991). The contact between the Falakron marble and the underlying Pangeon gneiss lies within an early Miocene ductile shear zone (Dinter, 1998). The spatial link of these rocks to the hosted mineralisation is studied in order to define their association and an attempt is made to determine their depositional environment.

The petrological studies in the Pangeon Mountain were carried out in the top section of the central area, namely Avgo and Mati, lithostratigraphically corresponding to the Upper Carbonate Unit, and in the north east area of the mountain along the road from Nikisiani to Asimotrypes, which corresponds to the underlying Transitional Zone, and the basement gneiss unit.

Based on textural and mineralogical criteria and the participating degree of the non-carbonate minerals (insoluble residue), Varti-Matarangas and Eliopoulos (1992); Varti-Matarangas (1993); Varti-Matarangas and Eliopoulos (1999), classified the car-

bonate rocks of the Pangeon Region in six types. Types I to III belong to the Upper Carbonate Unit (Falakron Series), whereas Types IV to VI belong to the Transition Zone.

4.2 Petrography of the Upper Carbonate Unit (Falakron Series)

The complex geological history of the studied area has affected the evolution (genesis, diagenesis and metamorphism) of the crystalline carbonate rocks. All primary features of these rocks have been obliterated. Therefore recognition of the modifications and overprinting of the earlier carbonate rocks is difficult to determine.

Field observations showed that the Carbonate Unit, of 500m thickness, consists of alternations of thick-bedded massive grey marble, with thin banded, dark marbles of smaller thickness. (Plates: 4.1/a-d & 4.2/a-c). The laminated texture in the old surfaces is in the form of relief (Pl. 4.1/a,d). Locally they present a cellular structure.

Type I : Laminated grey to rose-colored marble

The lamination of this marble type is exposed on the weathered surfaces and it is the result of the different degree of dissolution of the dolomitic and calcitic laminae (Pl. 4.1/a,d).

Petrographic studies showed alternations of thin laminae of medium to coarse-grained dolomite with coarsely grained dedolomite (Pl 4.3/a). The coloured laminae consists of coarse non-planar dolomite crystals with very fine opaque minerals, while interstitial dedolomite crystals are developed. Sometimes when the dedolomitisation process is increased the dolomite crystals seem to be residual and float within the dolomite crystals. In other cases, the alternating calcitic laminae do not show dedolomitisation, the size of calcitic crystals has a wide range -fine to coarse- and the

MARBLES FROM THE UPPER CARBONATE UNIT (FALAKRON SERIES)

PLATE 4.1

a: Thick bedded laminated marble, locally with cellular texture in a small quarry.

b & **c**: Alternation of light grey, massive calcitic marble (Petrographic Type III) with thin banded, dark grey to rose marble (Petrographic Type I) in smaller thickness.

d:. White grey, thick bedded dolomitic marble. The laminated texture in the old surfaces is in the form of relief. Cellular texture is locally present.

PLATE 4.2

a & **b**: Alternations of white calcitic marble strongly deformed (Petrographic Type III) with beige dolomitic marble (Petrographic Type II).

c : Alternation of grey laminated marble (Petrographic Type I), with calcitic marble strongly deformed.

PLATE 4.1

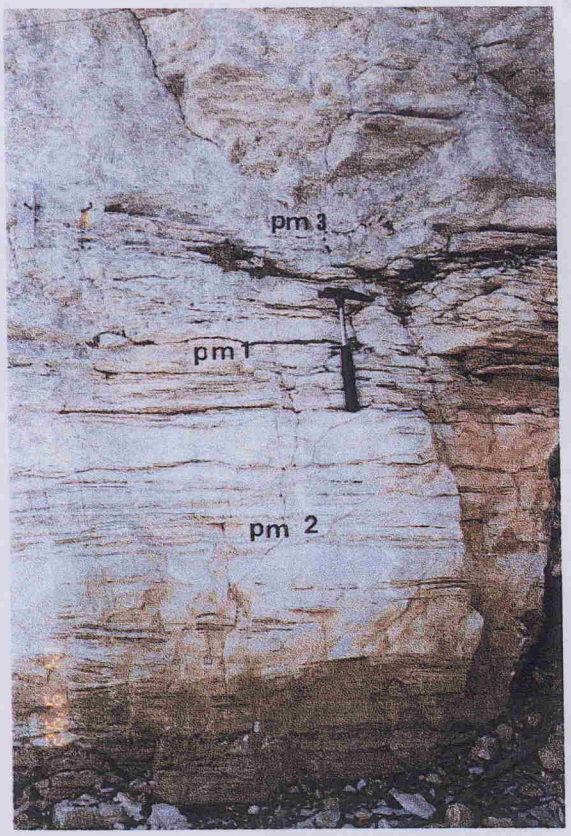

a

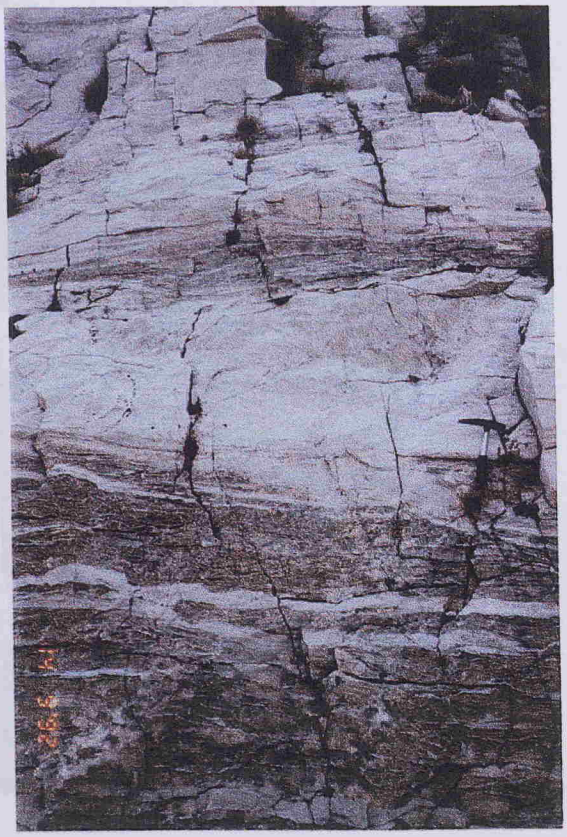

b

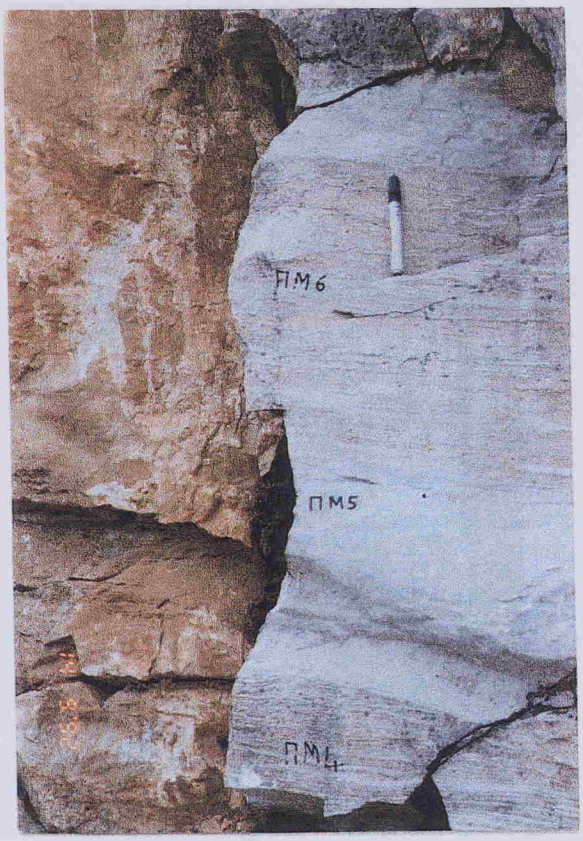

c

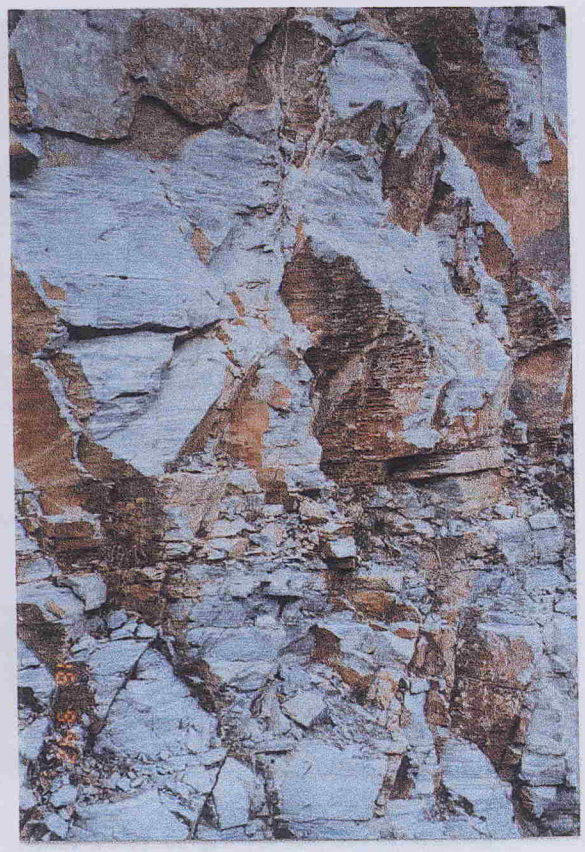

d

PLATE 4.2

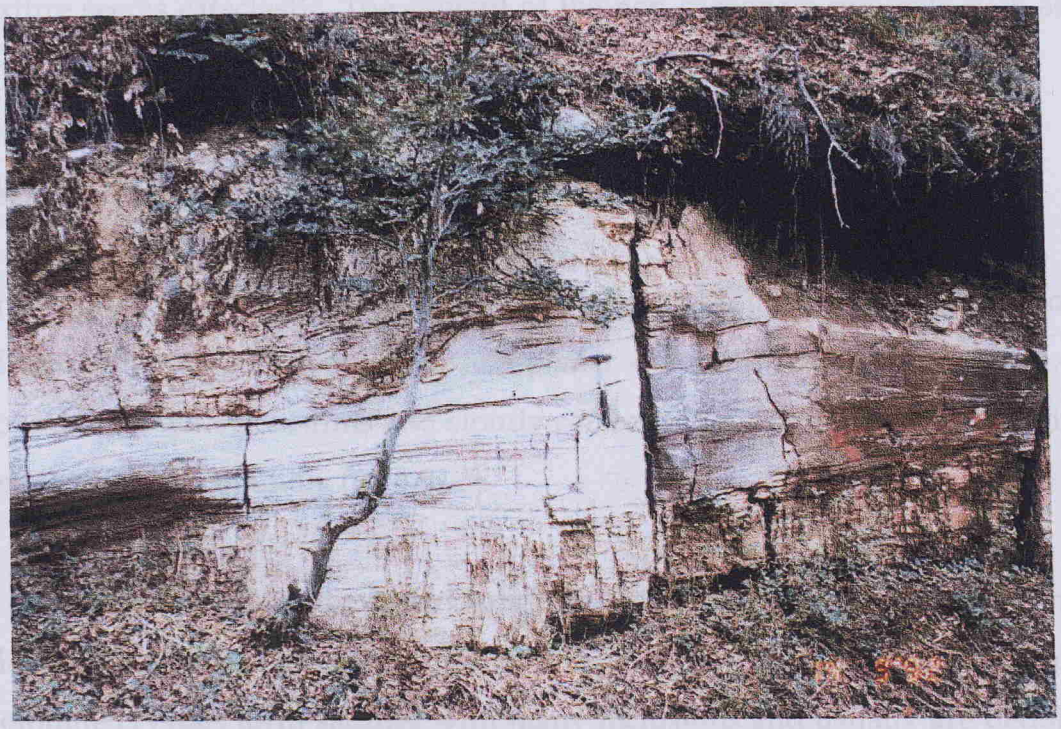

a

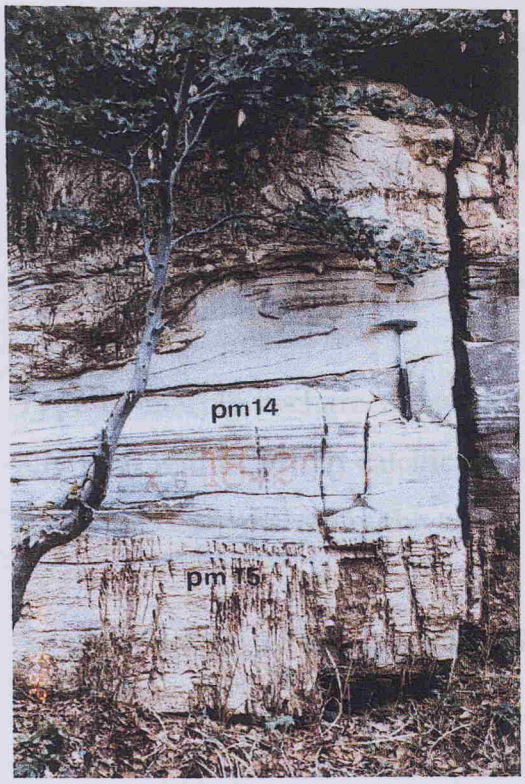

b

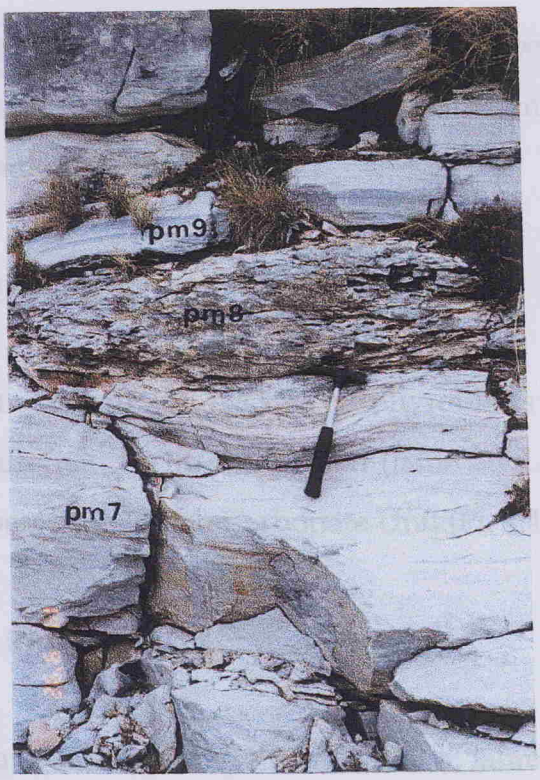

c

texture seems cataclastic. The content of the non-carbonate minerals such as quartz, phyllosilicates and amphiboles is variable and ranges between 15-45%.

Type II : Fine grained non-ferroan dolomitic marble

This type of marble is widespread in the Pangeon Mountain. It is usually comprised of unimodal, slightly elongated, non-planar dolomite crystals (equal size, sutured boundaries) with clear-rims and cloudy centres (Pl. 4.3/b,c). Elongated cavities with dedolomite are common. (Pl. 4.3/d).

In the lower part on the main Carbonate Unit (Falakron series) the dolomitic marble microscopically appears polymodal with non-planar boundaries. The coarser dolomite crystals form saddles with many inclusions and usually are dedolomitised (PL.4.3/d).

This type of marble is strongly tectonised in the upper part of the main Carbonate Unit and less so in the lower parts of the same sequence. Finally, this type often correlates with iron and manganese mineralisation.

Type III : Grey calcitic marble, strongly deformed

Type III marble is characterised by high tectonism and calcitic porphyroblasts usually float within a finer calcitic matrix. It alternates with the Type II (laminated marble) and occurs mainly in the upper members of the main Carbonate Unit (Pl. 4.4).

4.3 Petrography of the Transition Zone Lithologies

The carbonate rocks of the Transitional Zone are medium to thick bedded, laminated to banded, impure calcitic marbles and beige to grey in colour (Pl. 4.5/a,b). They al-

MARBLES FROM THE UPPER CARBONATE UNIT (FALAKRON SERIES)

PLATE 4.3

a: Fine to medium laminated marble (Petrographic Type I). Alternations of thin laminae of medium grained dolomite with coarsely grained calcite, probably dedolomite (After Varti- Matarangas, 1993).

b: Fine to medium grained dolomitic marble (Petrographic Type, II). The dolomite crystals are unimodal and non-planar (After Varti- Matarangas, 1993).

c: Similar to the previous. Elongated cavities fill with dedolomite (After Varti- Matarangas, 1993).

d: Saddle dolomite crystal in the centre of the cavity (After Varti- Matarangas, 1993).

PLATE 4.3

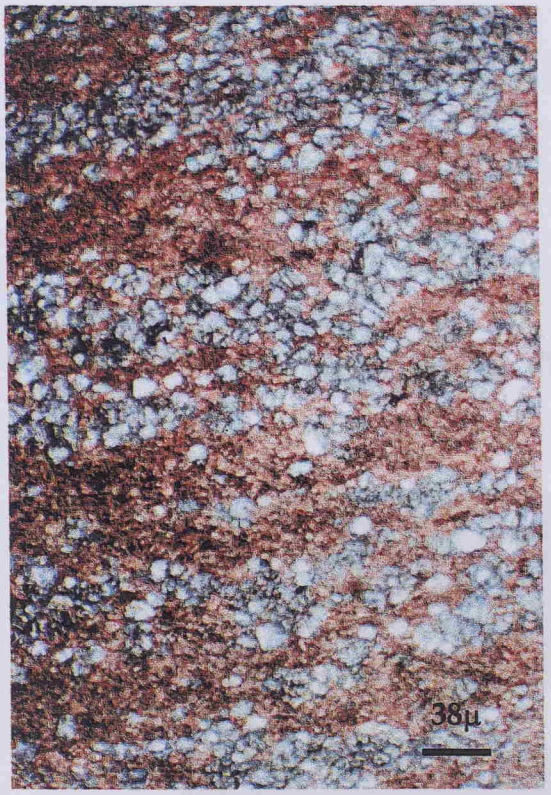

a

b

c

d

PLATE 4.4

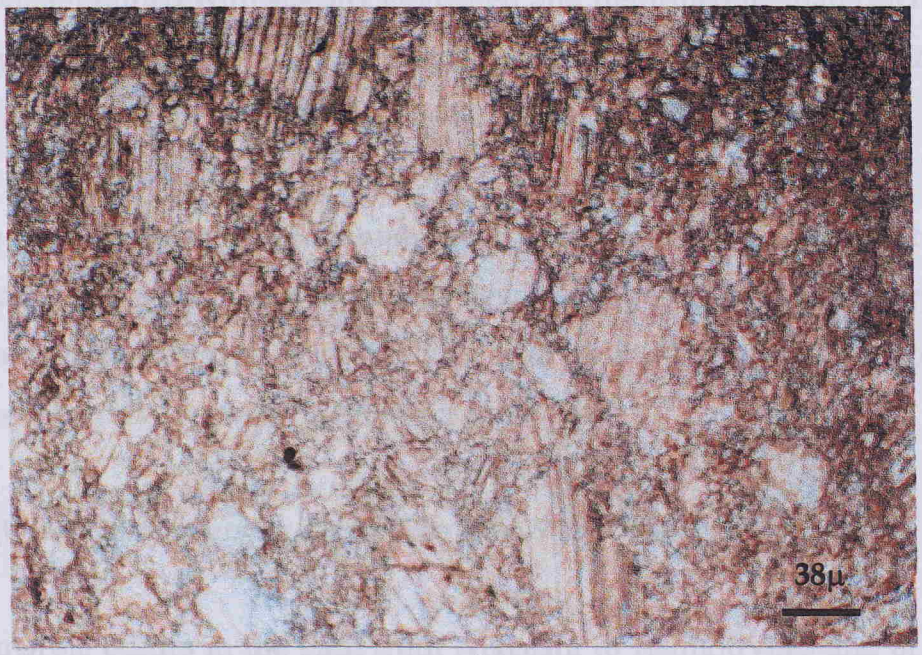

Plate 4.4: Calcitic marble strongly deformed (Petrographic Type V), with calcite pyroclasts and calcite which floats within fine calcitic crystals (After Varti- Matarangas, 1993).

ternate with gneiss and amphibolite beds and are best developed adjacent to the major auriferous mineralisation of Asimotrypes (Plate 4.5/a-c).

Type IV : Impure calcitic marble

The impure calcitic marble (siliceous marble) are medium to thick bedded, laminated to banded, multicoloured and alternate with gneiss and amphibolite beds (Pl.4.5/a-c). It is coarse-grained with slightly elongated and deformed ferroan-calcitic crystals. Boundary shapes are sutured to slightly curved and exhibit deformational twinning and undulate extinction (Pl. 4.6/a & 4.6/b).

The content of the non-carbonate minerals is considerable and ranges between 13-33%. Quartz is the main non-carbonate mineral and usually is finely crystalline or forms elongated aggregates with undulate extinction. Mica and amphiboles, as well as opaque minerals are observed in lesser amounts.

Type V : White, very coarsely crystalline calcitic marble

Type V marble occurs in the path from Nikisiani to Asimotrypes and at the contact with the granite. It is very coarsely crystalline with lobate to sutured boundaries, slight deformational twinning and contains numerous small dolomite exsolutions (Pl. 4.6/c).

Type VI : Dedolomitic marble

Type VI marble is found in the Asimotrypes area and it is associated with the mineralisation hosted within the marbles. It is characterised by mortar texture, deformational twinning and numerous residual dolomite crystals (Pl. 4.6/d).

MARBLES FROM THE TRANSITION ZONE

PLATE 4.5

a: Laminated to banded , medium to thick bedded, beige impure calcitic marble (Petrographic Type IV), alternated with gneiss and amphibolite, in contact with ore at Asimotrypes.

b: Grey laminated, thick bedded calcitic marble (Petrographic Type IV), alternating with amphibolite beds.

c: Alternations of medium bedded calcitic marbles with schist rocks.

PLATE 4.6

a: Impure calcitic marble (Petrographic Type IV) from the lower part of the Transition Zone. Coarse grained with slightly elongated ferroan-calcite crystals, sutured boundaries, deformational twinning and mortar texture (After Varti- Matarangas, 1993).

b: Impure calcitic marble (Petrographic Type IV). Coarse grained with slightly elongated and deformed ferroan calcitic crystals. The boundary shapes are slightly curved to suture (After Varti- Matarangas, 1993).

c: Very coarsely grained calcitic marble (Petrographic Type V) with suture boundaries of the crystals (After Varti- Matarangas, 1993).

d: Dedolomitic marble (Petrographic Type VI). It is characterised by mortar texture, deformational twinning and numerous residual dolomite crystals (After Varti- Matarangas, 1993).

PLATE 4.5

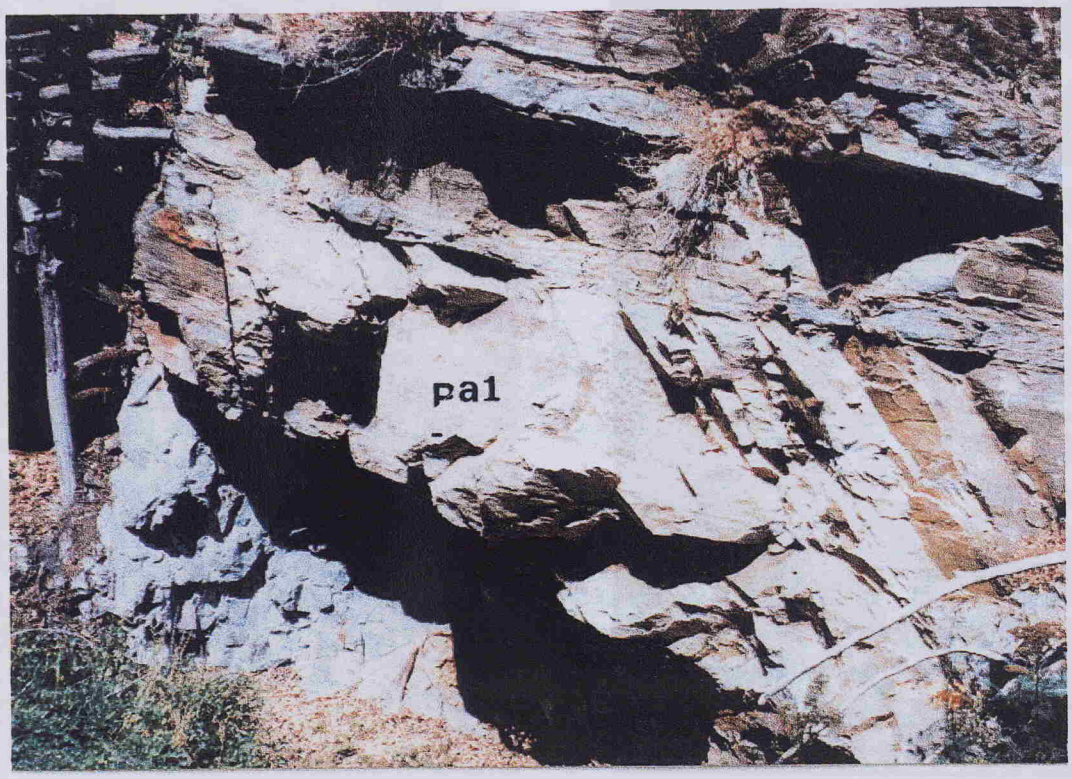

a

b

c

PLATE 4.6

a

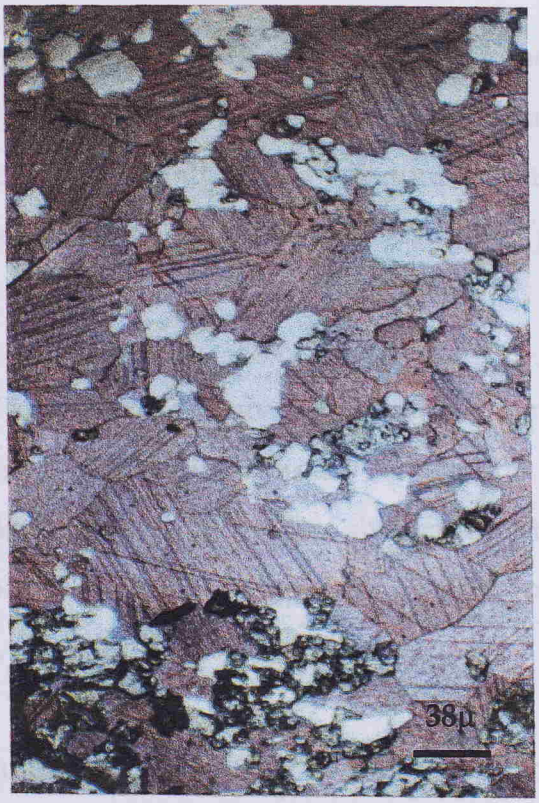

b

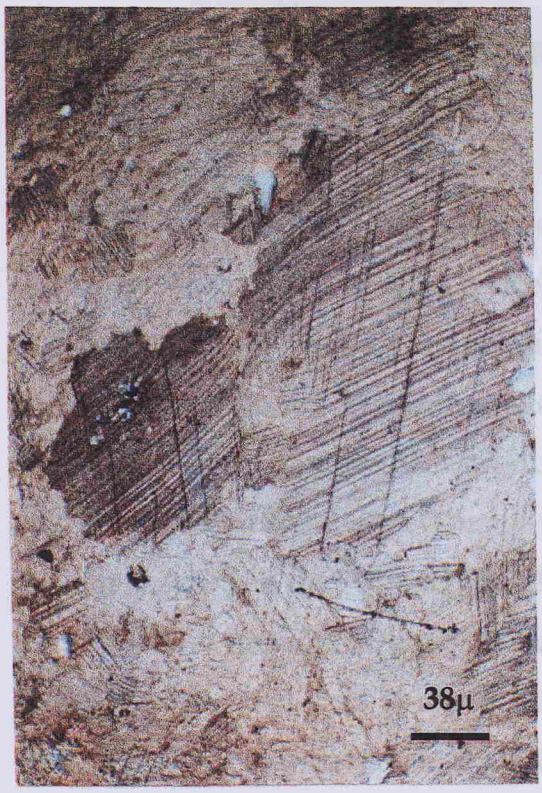

c

d

According to field observations made, more specifically the thickness and banding of marbles of both the Carbonate Unit and the Transition Zone, petrographic studies and the comparison to other carbonate sequences mainly of the Pelagonian tectonic zone, the depositional environment of these rocks seems to be shallow marine (platform or shelf) environment.

The gneiss and mica schist rocks of the Transition zone are mainly pelitic gneisses and two-mica schists alternated with impure calcitic, coarsely crystalline and dedolomitic marbles and amphibolitic rocks. Petrographic studies showed that these pelitic gneisses and two-mica schists consist of albite, oligoclase, quartz, phengite/muscovite, biotite, K-feldspar, garnet, chloritoid, chlorite and clinozoisite.

Quartz veins and small lenses, with minor amounts of sericite, chalcedony and epidote crosscut the two-mica schist rocks of the area. These veins also contain minor amounts of arsenopyrite and pyrite in equal ratio. Some chalcopyrite was found intensively altered to malachite and goethite. Altered chalcopyrite, was also found within the schist rocks.

The amphibolitic rocks of the Pangeon area are made up the following mineral assemblage: hornblende, garnet, albite, pyroxene, clinozoisite, chlorite, quartz, rutile and titanite. Also, minor metallic minerals were found in these amphibolitic rocks, such as pyrrhotite, which is often altered to a mixture of pyrite-marcasite-pyrrhotite characterised as "intermediate product". The pyrrhotite crystals are orientated parallel to the rock schistosity. Usually pyrrhotite is accompanied by chalcopyrite having the same form and orientation. Titanite and leucoxene are the typical accessory minerals. The metallic minerals described above are typical for these amphibolitic rocks and they do not show any genetic link to the main ore in the studied area. Also, the effect of retrograde metamorphism is apparent on these metallic minerals.

The presence of hornblende in the amphibolites and garnet in the amphibolites and metapelites show that the metamorphic conditions in the Pangeon region exceeded those of the middle-greenschist phases. The coexistence of albite and oligoclase in all rock types of the study area suggests that during the metamorphic evolution of the Pangeon region , the degree of metamorphism did not exceed the conditions defining the boundary of the greenschist to amphibolitic phases (albite-oligoclase zone). The P-T conditions for the high pressure metamorphism have been estimated at 520 ^{0}C and 12 kbar by Mposkos (1991, 1994), based on the highest Si (6.9) value in phengite of orthogneisses and the garnet formation in the metapelites.

4.4 Gneiss Basement Unit

The basement gneisses are actually orthogneisses representing magmatic rocks of the pre-Alpine basement which have been folded and metamorphosed at the same time as the overlying sedimentary and igneous rocks (Mposkos et al., 1989). The orthogneisses are distinguished as leucocratic gneisses characterised by the mineral assemblage K-feldspar, albite, oligoclase, quartz, phengite/muscovite and two-mica gneisses with biotite as additional phase. Frequently, in the same rock sample, phengite and phengitic- poor muscovite coexist. The highest Si values are usually found at the centre of phengites exhibiting zonation, whereas the lower Si values are found at the edges of large crystals, which are replaced by secondary biotite and muscovite. This change in the chemical composition of the white K-micas by phengitic to less phengitic, as it is mainly expressed in crystals characterised by zoning, is interpreted by Mposkos (1998) as an evidence of the geological evolution of the Pangeon region from high pressure metamorphic conditions to lower ones.

4.5 Nikisiani Granodiorite

The Nikisiani granodiorite is characterised by the following mineral assemblage: quartz, sericite, plagioclase, microcline, biotite, epidote and opaque minerals. In its peripheral parts the granodiorite shows banded textures with minor re-crystallisation phenomena and retrograde metamorphism. Pyroxene, epidote and titanite form thin bands surrounding the phenocrysts. In places, especially close to the crosscutting quartz veins in contact with the marble, the granodiorite shows intense alteration -sericitisation- transformed to "white granite". The altered granite contains minor pyrite strongly altered to goethite. This "white granite" is intensively tectonised showing cataclastic texture becoming arenaceous.

Numerous quartz veins, with strong marginal development of biotite crosscut the granodiorite. The quartz veins contain abundant iron hydroxides (goethite) and residual pyrite. Four microscopic, 1-5 μm, native gold crystals were located in goethite microfissures.

CHAPTER 5

MINERALOGY

5.1 General Statement

Mineralisation at Asimotrypes is of replacement and shear-zone-controlled style and has the form of irregular quartzite pods or lenses and quartz veins cross-cutting the marbles. The ore occurs in both deformed and undeformed varieties with the former constituting the largest part of the overall sulphide mineralisation. The deformed ore predates the undeformed one and is characterised by intense mylonitisation.

Quartz is a major gangue mineral intimately associated with the sulphide ore and can be distinguished in two types. Type A quartz occurs in well-developed individual euhedral to anhedral crystals. Some triple point junctions occur, interpreted to be the result of hydrothermal recrystallisation. This quartz type shows evidence of deformation, exhibiting wavy extinction and micro-fracturing. Type B quartz is microcrystalline, recrystallised and surrounding Type A quartz crystals. Chalcedony and muscovite-sericite, both in lesser amounts, comprise the gangue material of the mineralisation.

The Asimotrypes ore has a relatively simple sulphide mineral assemblage of arsenopyrite, pyrite, and gold, which forms the bulk of the sulphide material. This ore variety is highly deformed during the brittle/ductile deformation and shear zone precipitation and it is associated to regional uplift. This deformation implies that this

mineralisation variety slightly predates main the deformation. The undeformed ore variety is also comprised of arsenopyrite, pyrite and gold with subordinate sphalerite, galena, chalcopyrite, pyrrhotite, tetrahedrite-tennantite, marcasite, covellite and malachite (Table 5.1).

Ore / Gangue Phase	Deformed	Undeformed	Oxidized
Quartz	———	———	
Chalcedony	———	———	
Muscovite-sericite	———	———	
Arsenopyrite	———	———	
Pyrite	———	———	
Gold	———	———	
Pyrrhotite	———	———	
Chalcopyrite	———	———	
Marcacite	———	———	
Tetrahedrite-tennantite	----	———	
Sphalerite	----	———	
Galena	----	———	
Limonite			———
Malachite			———
Covellite			———
Free gold			———

Table 5.1: Generalised paragenetic sequence for the Asimotrypes ore. Deformed ore is associated with the main deformation stage resulting from regional uplift. Deformation is shown by cataclastic arsenopyrite and pyrite crystals.

Gold mainly occurs as submicroscopic grains in arsenopyrite and less in arsenian pyrite, rarely as free native gold and finally as free gold in the oxidation products. The term submicroscopic gold includes both solid solution and colloidal size (< 1μm in diameter) particulate gold. Both forms are refractory to direct cyanidation , even after pulverising the sulphide minerals.

5.2 Sulphide Mineralisation

The ore mineral association consists of arsenopyrite, pyrite, with subordinate pyrrhotite, sphalerite, chalcopyrite, tetrahedrite-tennantite, and galena, and very rare microscopic native gold.

Arsenopyrite is the dominant ore mineral at Asimotrypes. Arsenopyrite generally occurs as coarse idiomorphic grains; single crystals are found dispersed in the host rock or are concentrated in individual coarse-grained assemblages of large idiomorphic crystals with pyrite. Arsenopyrite is often intensely fractured and displays cataclastic texture where replaced by quartz (Plate 5.1). Frequently arsenopyrite shows intense alteration phenomena at the rim.

Electron microprobe analysis of arsenopyrite crystals showed As-contents range from 41.66 to 43.00 wt% with a mean value of 42.47 (±0.37) and S-contents range from 21.76 to 23.59 wt% with a mean value of 22.72(±0.50). Co, Ni and Sb contents are below the detection limits of the wavelength dispersion analyser. As/S ratios in the arsenopyrite core, outer zones and crystal rims are constant. This internal chemical homogeneity of the arsenopyrite crystals is indicative of chemical equilibrium internally and also with other phases in the Fe-As-S system. In addition, the composition of deformed and undeformed arsenopyrite is the same, indicating similar conditions of formation.

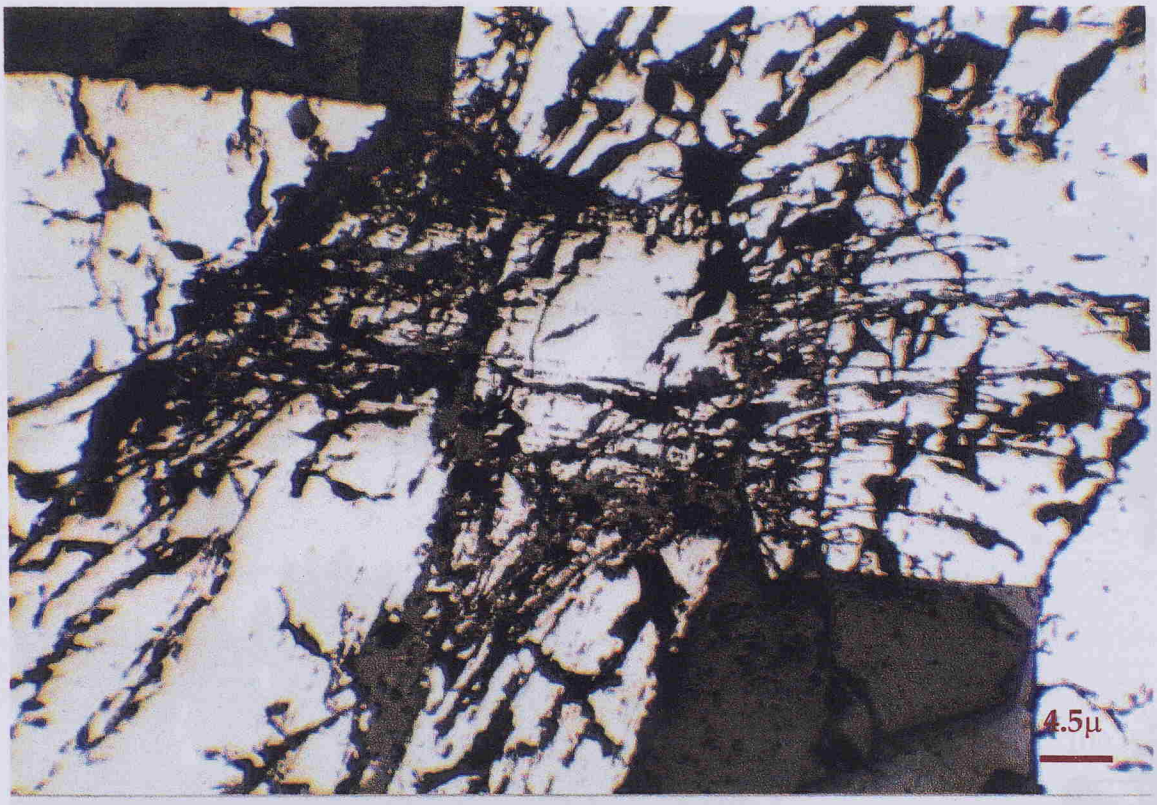

a

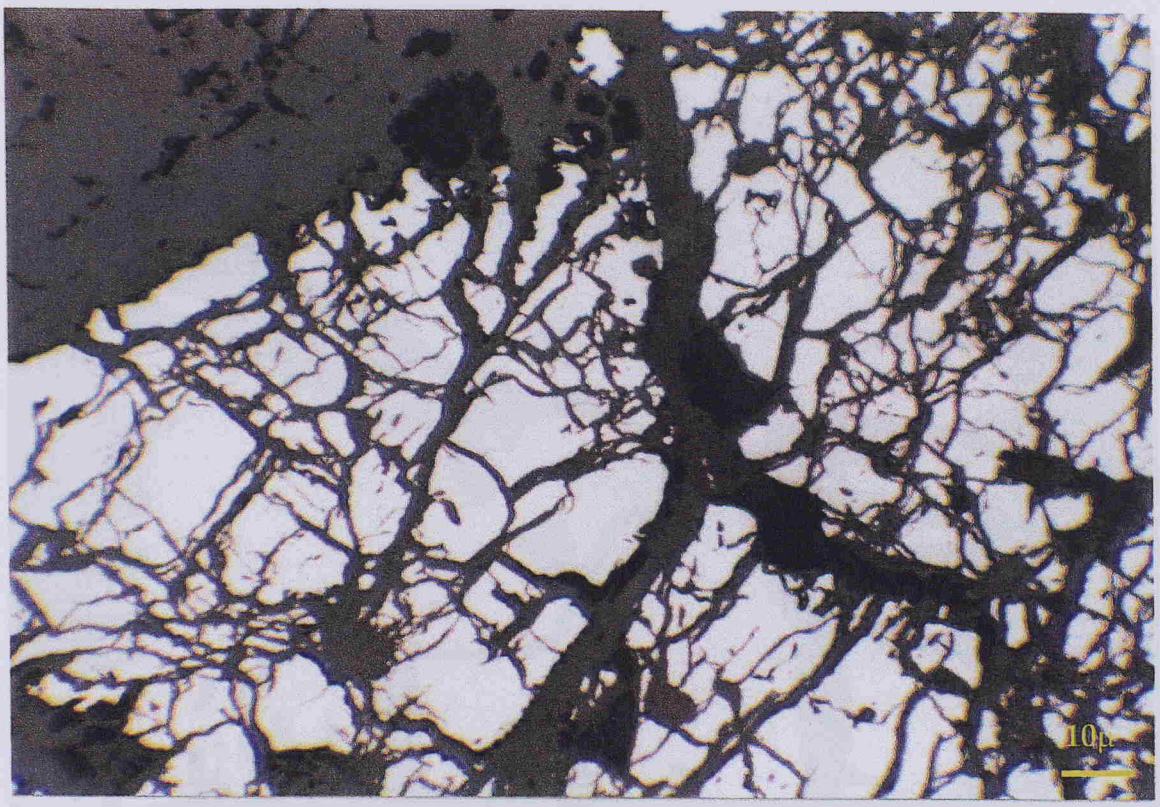

b

Plate 5.1: (a) Replacement of arsenopyrite prismus by quartz. (b) Advanced replacement of arsenopyrite by quartz along cataclastic fractures.

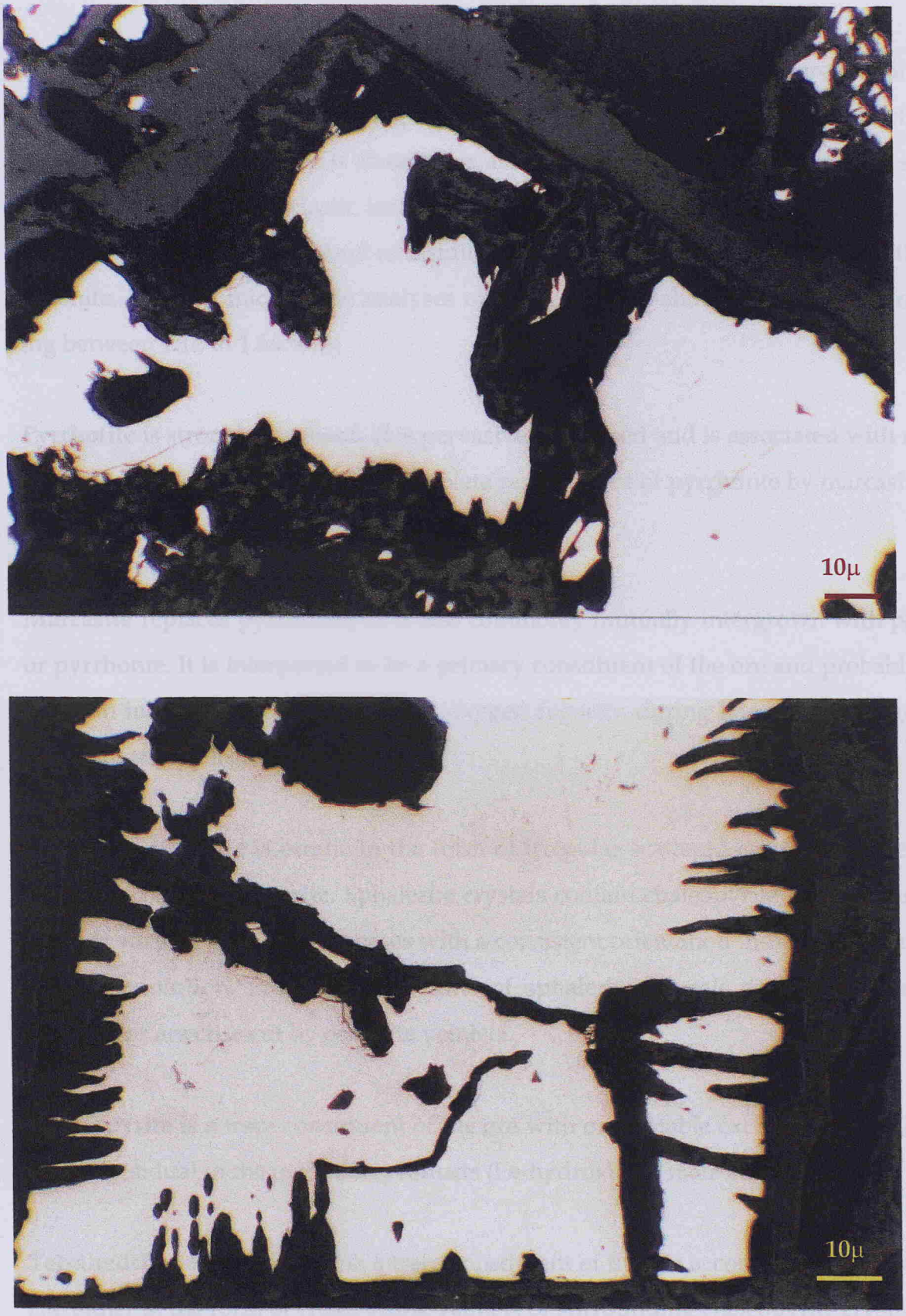

Plate 5.2: Advanced replacement of pyrite prismus by quartz along cataclastic fractures.

Pyrite occurs either as scattered crystals intensely fractured and altered or intergrows with arsenopyrite forming massive agglomerates in varying proportions (Plate 5.2). However, pyrite is always less abundant than arsenopyrite. In some samples pyrite displays cataclastic textures with quartz replacing pyrite (Plate 5.3). Frequently these crystals are found as residuals-inlets within pseudomorphs of goethite-limonite. Electron microprobe analyses of pyrite crystals showed As-contents ranging between 1.12 to 1.66 wt%.

Pyrrhotite is strongly localised. It is pervasively oxidised and is associated with marcasite and chalcopyrite. Partial to complete replacement of pyrrhotite by marcasite or pyrite or both is common.

Marcasite replaces pyrrhotite, or is less commonly mutually intergrown with pyrite or pyrrhotite. It is interpreted to be a primary constituent of the ore and probably reflects an increase in sulphur and /or oxygen fugacity during late waning stages of mineralisation (Oberthur et al. 1997).

Sphalerite presence is erratic in the form of irregular scattered crystals replaced by galena and/or chalcopyrite. Sphalerite crystals contain chalcopyrite drop-like inclusions of varying size, in some cases with a consistent orientation indicative by an origin by exsolution. Frequently the rims of sphalerite crystals are transformed to covellite or are crosscut by covellite veinlets.

Chalcopyrite is a trace constituent of the ore with one notable exception where it occurs as residual in the oxidation products (Fe-hydroxides+malachite) (Plate 5.4).

Tetrahedrite-tennantite is also a trace constituent of the ore accompanying chalcopyrite either in the form of crosscutting veinlets or surrounding chalcopyrite crystals.

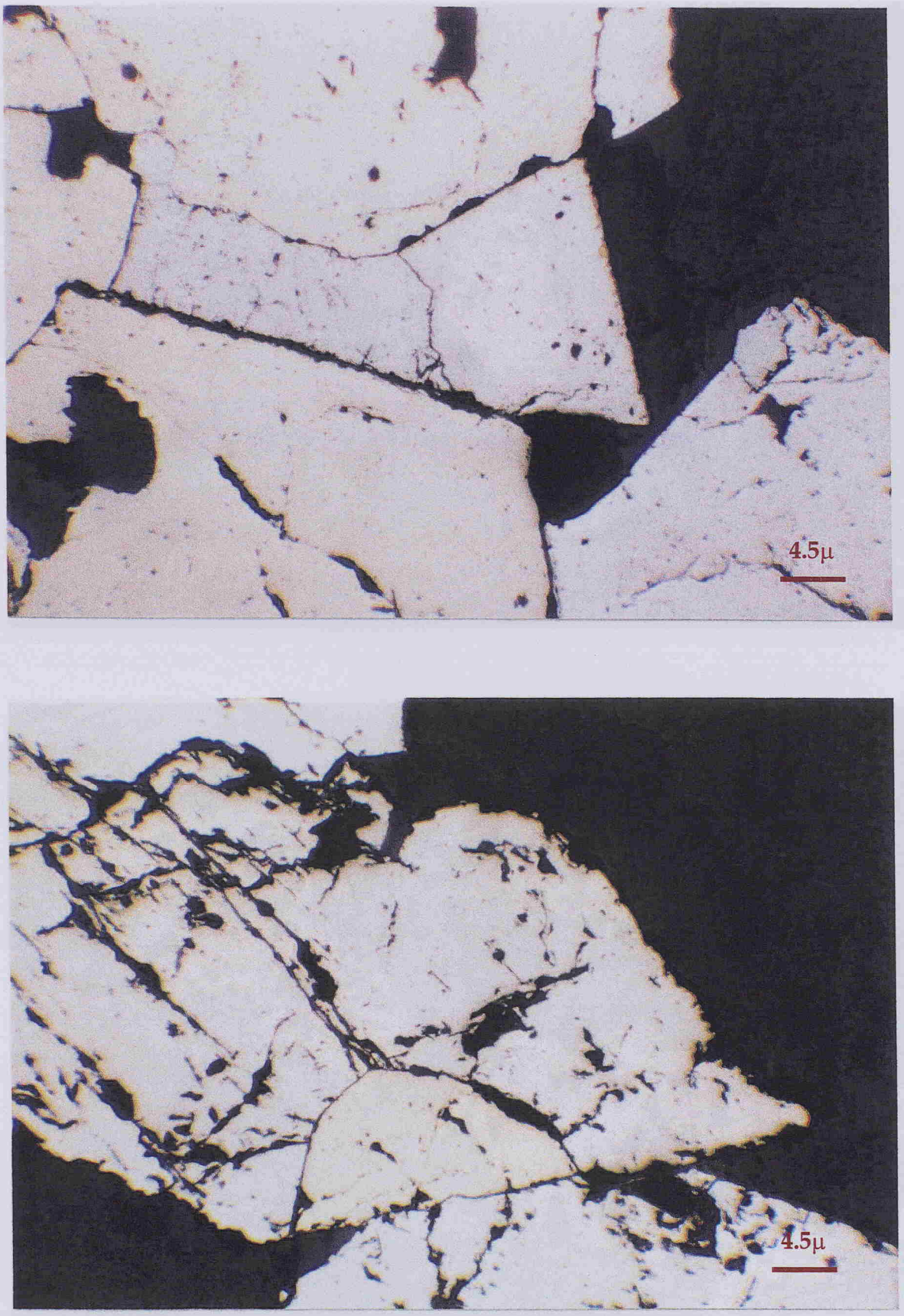

Plate 5.3: (a) Equilibrium deposition of arsenopyrite and pyrite (more yellow).
(b) Intergrowth of arsenopyrite prismus and pyrite (more yellow).

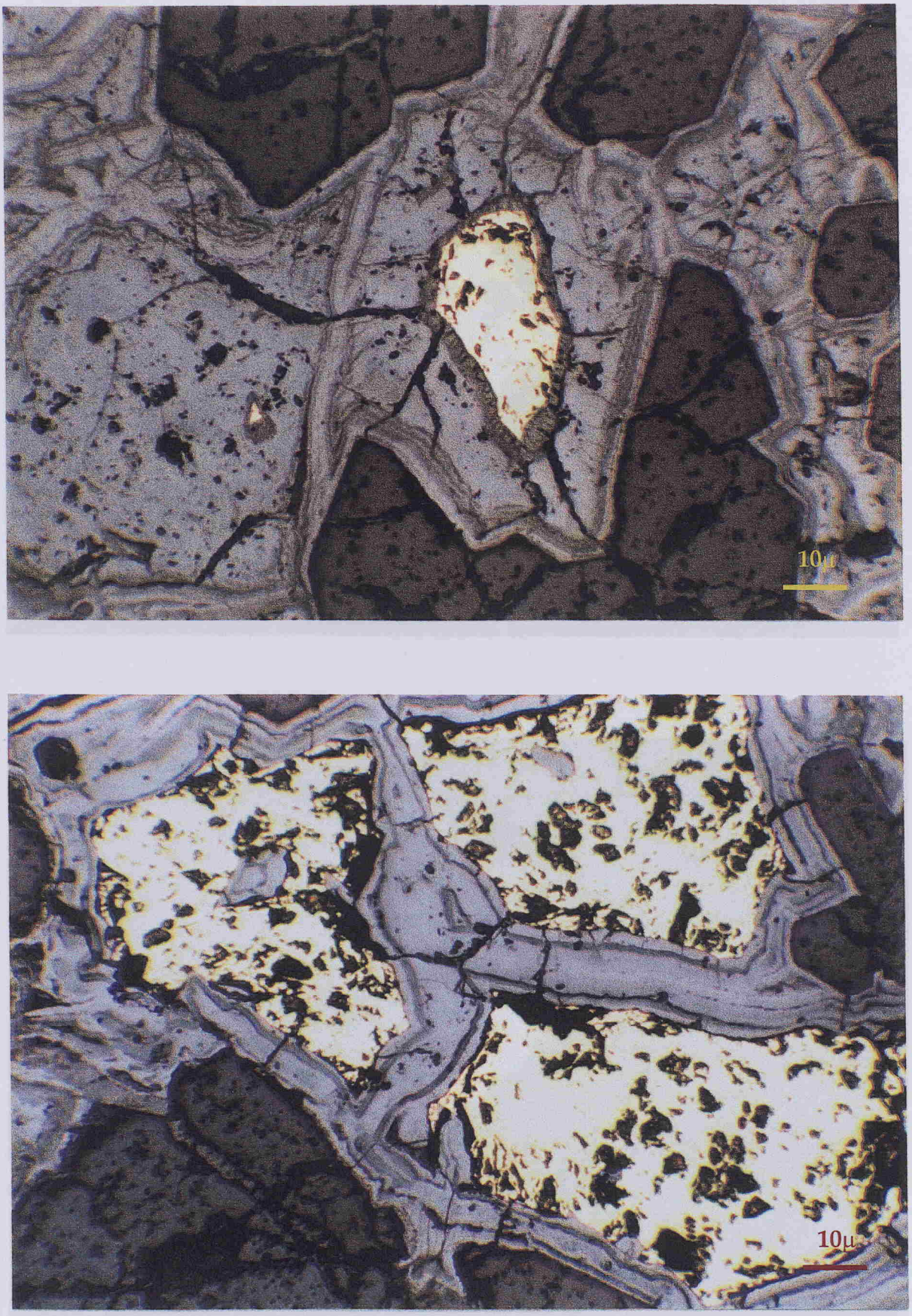

Plate 5.4: Oxidised chalcopyrite in goethite.

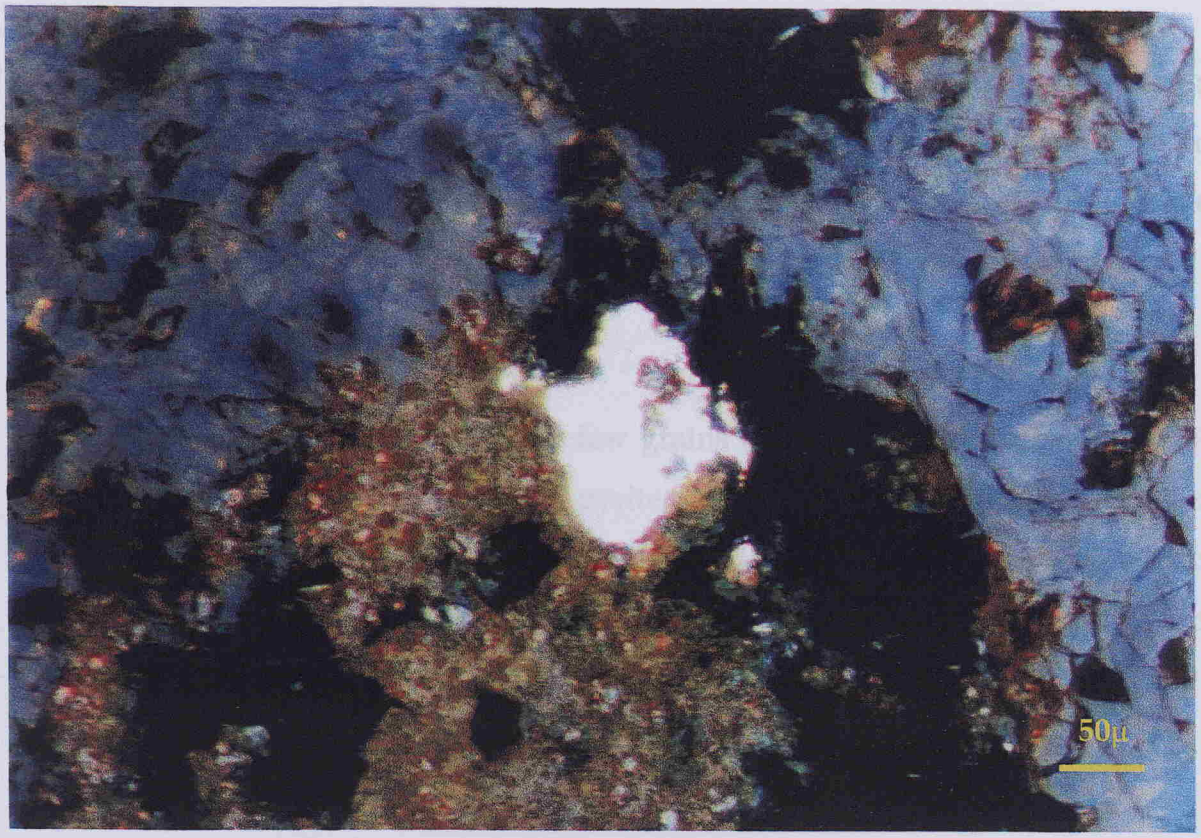

Plate 5.5: Gold in goethite veinlets, as oxidation product.

Likewise the **galena** presence is erratic. In the samples where galena was located although it forms macroscopically visible crystals, it shows intense alteration around its boundaries and appears as residual within cerrussitic mass and hydroxides. Covellite traces within the oxidation products indicates the initial copper presence in the galena.

Free **gold** is rare in the ore and only few grains (< 20 μm) were observed, in Fe-oxide (goethite) veinlets with residual pyrite. Gold grains were generated in goethite fissures, in all likelihood during the oxidation processes (Plate 5.5), exsolved from sulphide minerals. Electron microprobe analysis showed Au-contents range from 90.92 to 91.16 wt%, Ag-contents from 8.54 to 8.87 wt% and Fe-contents from 0.20 to 0.24 wt%.

5.3 Mineralogical Position of Gold in the Sulphide ores

Two representative arsenopyrite-pyrite samples from the Asimotrypes ore were selected for further studies in order to establish the occurrence of gold. Assays of the samples are given in Table 5.2.

Sample No.	Au (gr/t)	As (%)	S (%)
As-14	9.90	32.30	21.90
As-31	16.60	34.70	19.30

Table 5.2: Assays of arsenopyrite-pyrite ore from Asimotrypes.

Gold Minerals

Only a small number (5) of free native gold grains of ≈ 20 μm were identified in the panned concentrates of the studied samples (Plate 5.6). The intensive cyanidation tests on pulverised (-5 μm) samples indicate that only 10% of the gold is soluble in cyanide. Therefore, the remaining 90% must be submicroscopic gold.

SIMS Spot Analysis

Secondary ion mass spectrometry (SIMS) was performed in order to:

- quantify the gold contents in arsenopyrite and pyrite and
- to map the distribution of gold in individual crystals of the same minerals.

Fifty particles of arsenopyrite and pyrite from samples As-14 and As -31 were analysed. The results are shown in Table 5.3

Mineral	n	Au Range (ppm)	Mean (ppm)
Arsenopyrite	34	0.47 - 29.00	11.59
Pyrite	16	0.14 - 11.00	2.31

Table 5.3: Gold contents of the Asimotrypes ore, as determined by SIMS spot analyses on different grains. n= number of grains

Results from the Asimotrypes ore indicate that both arsenopyrite and pyrite are carriers of gold and there is a preferred enrichment of gold in arsenopyrite relative to pyrite. The submicroscopic gold concentration in pyrite ranges from 0.14 to 9.3 ppm with an average of 2.3 ppm gold. The arsenic content of the pyrites ranges from 0.01

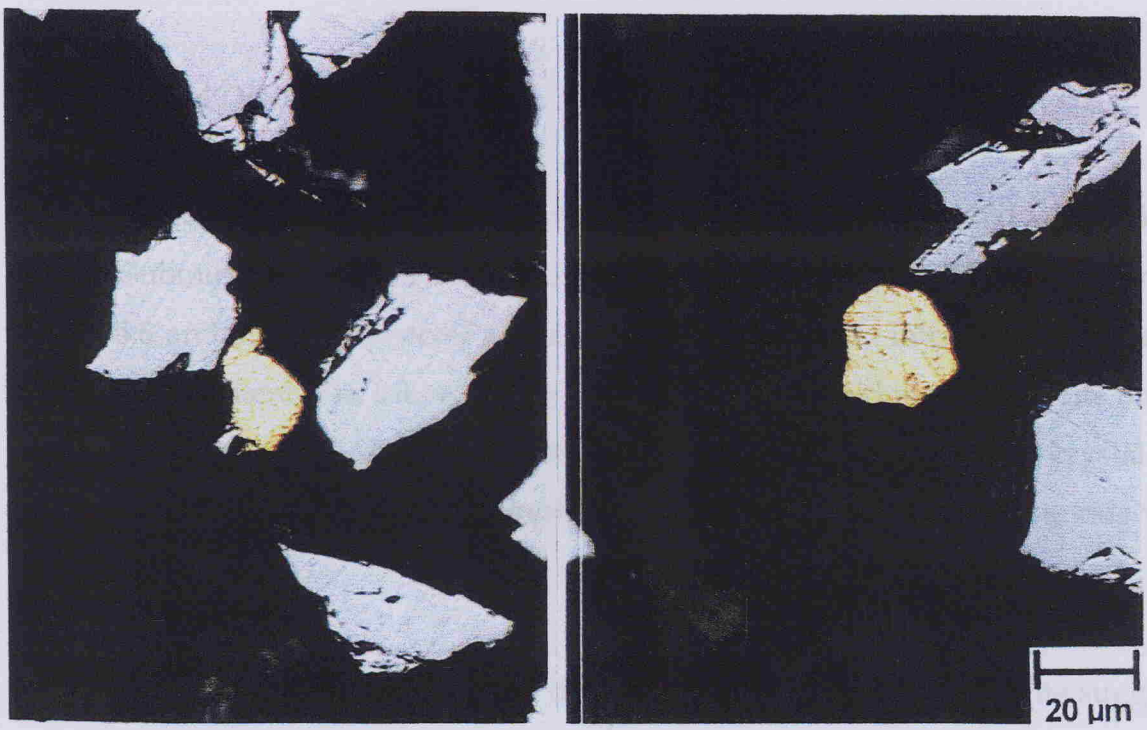

Plate 5.6: Free native gold particles (bright yellow).

to 3.8 wt% averages 1.4 wt%. Submicroscopic gold and arsenic in the pyrite structure are positively correlated (Fig. 5.1). Submicroscopic gold concentrates preferentially in the arsenopyrite (Fig. 5.2). The gold concentration in arsenopyrite ranges from 0.5 up to 29 ppm with an average of 12±5.3 ppm. The partition coefficient of gold between arsenopyrite and pyrite is 12/2.3=5. The large range of gold concentrations of the spot analyses point to the inhomogeneous distribution of gold in the arsenopyrite crystals. The gold deportment is depicted graphically in Figure 5.3.

SIMS Gold Distribution Mapping

SIMS gold distribution mapping revealed the actual location of gold in sulphide crystals. Submicroscopic gold in arsenopyrite shows a zoned distribution pattern (Plates 5.7, 5.8 and 5.9) with several zones of high concentration interspaced with zones of low gold content. The inhomogeneous distribution of gold in arsenopyrite implies an intermittent supply of gold, and less likely periods of arsenopyrite crystal growth with gold being allowed to incorporate in the lattice followed by periods where it was not.

The excellently preserved gold distribution patterns in arsenopyrite suggests that remobilisation of gold played a minor role in the post-depositional history of the gold mineralisation investigated in this study and that most of the sulphide-bound gold is still in place where it was crystallised first.

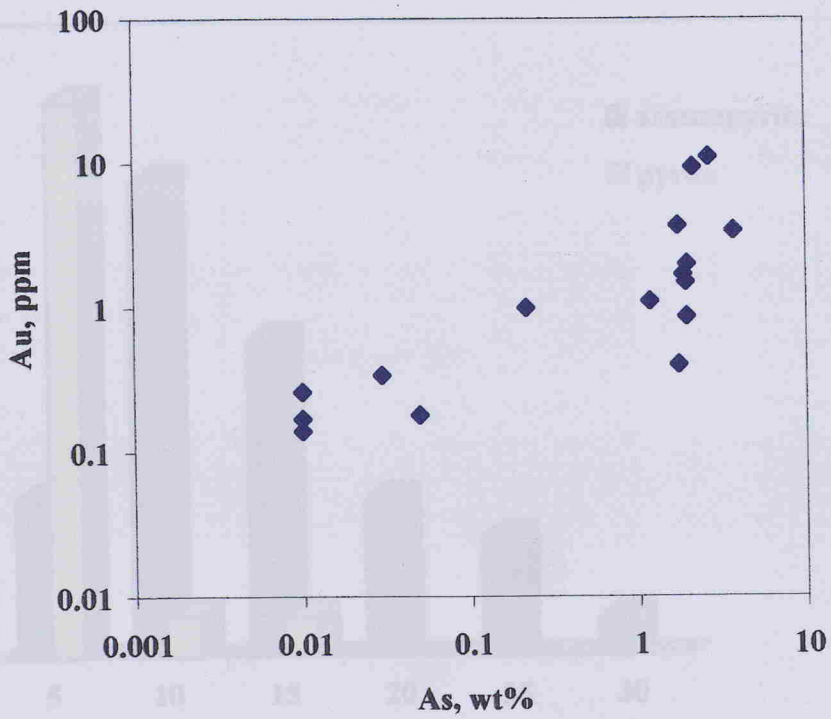

Figure 5.1: Correlation of gold with arsenic in the Asimotrypes pyrites.

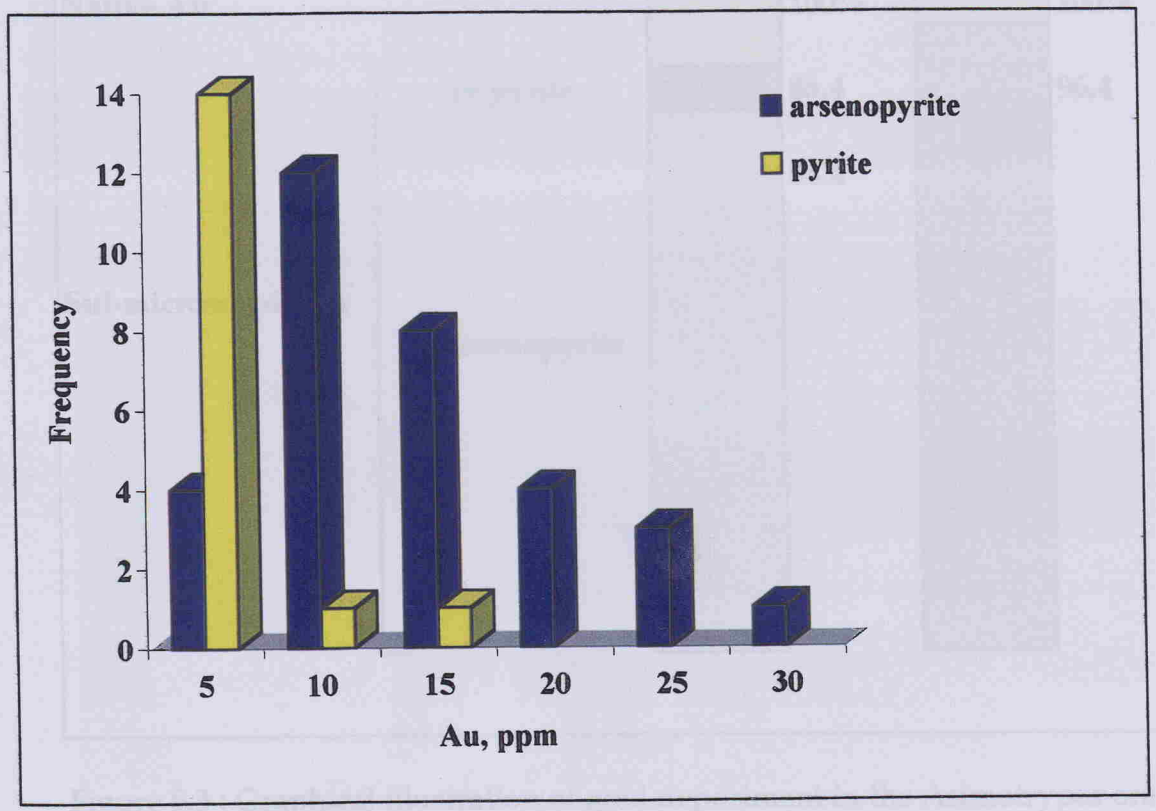

Figure 5.2: Histogram of submicroscopic gold concentration in arsenopyrite and pyrite in the Asimotrypes ore.

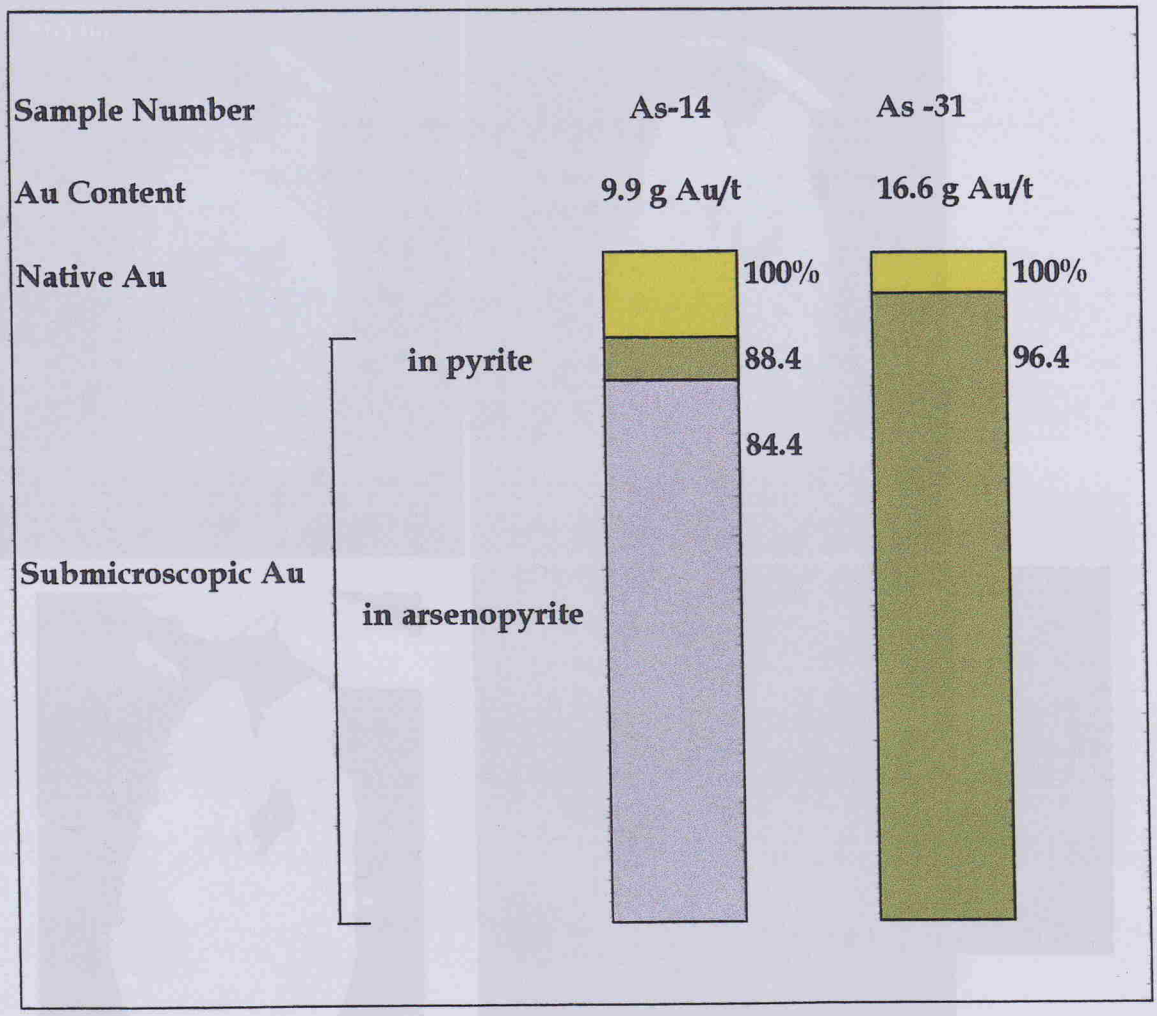

Figure 5.3 : Graphical illustration of gold deportment in the Asimotrypes ore.

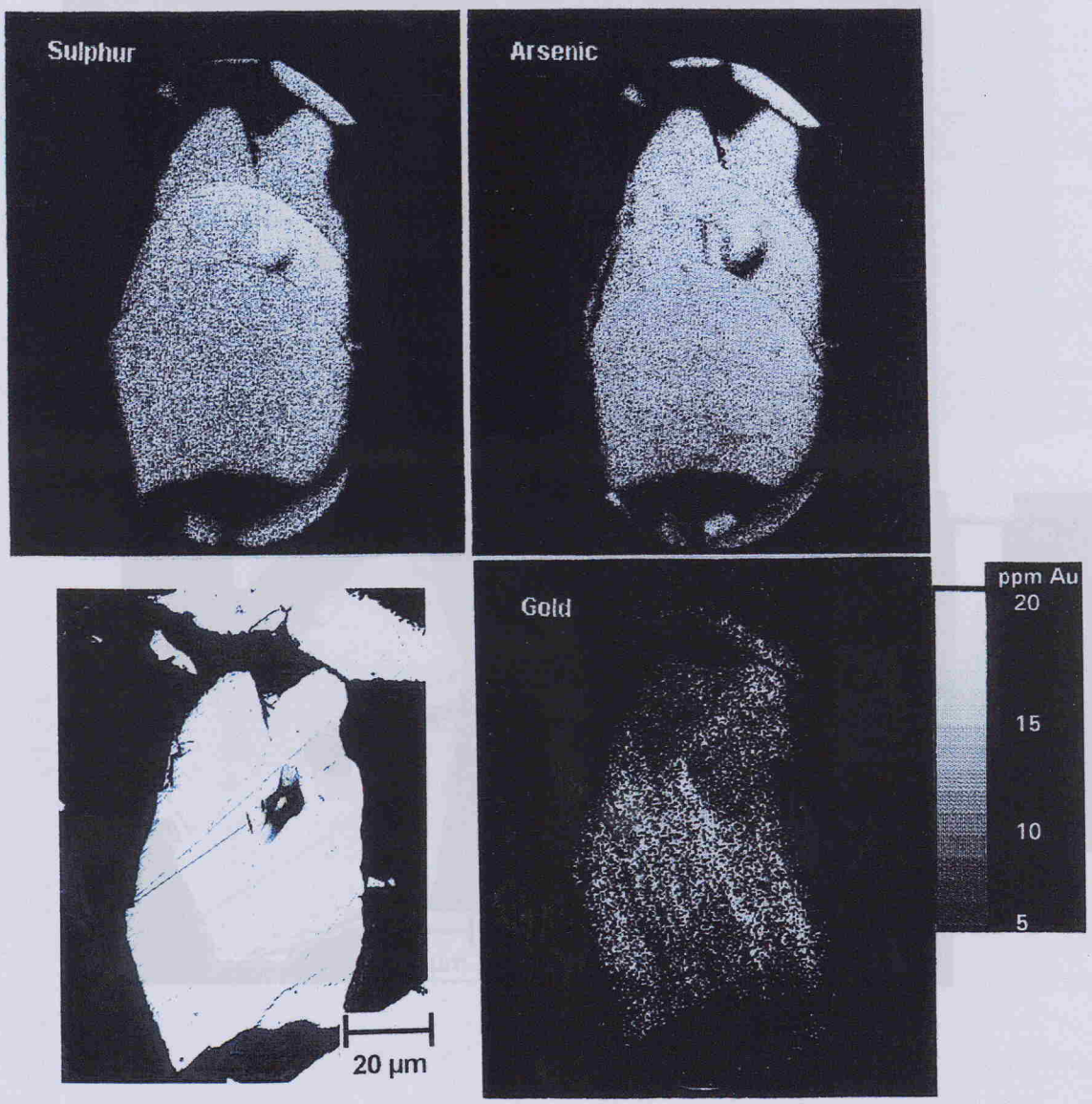

Plate 5.7: Zoned distribution of gold in arsenopyrite. The dark spot is the area analyzed. The gray scale gives the range of gold content noted in the particle.

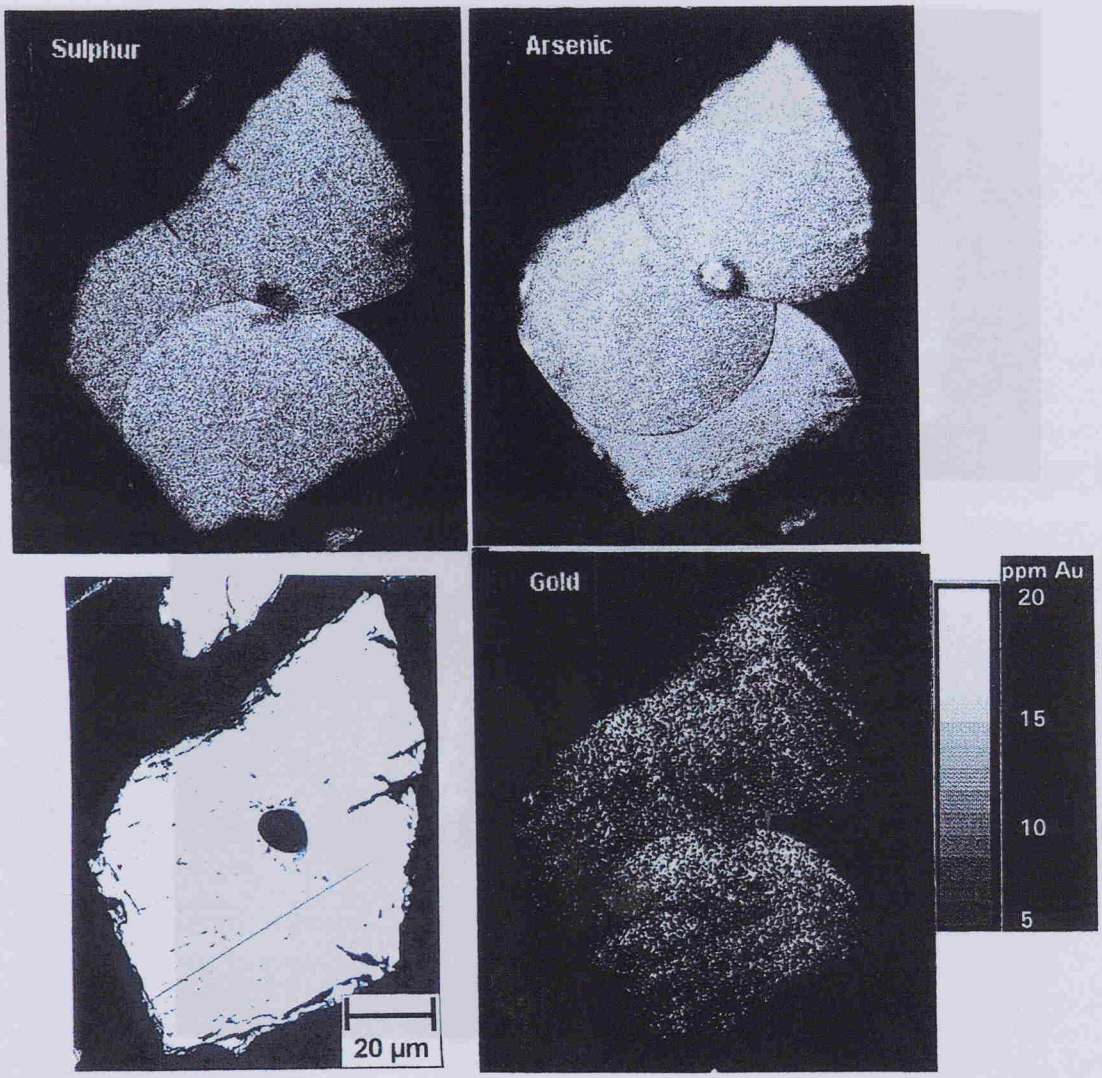

Plate 5.8: Zoned distribution of gold in arsenopyrite. The dark spot is the area analysed. The gray scale gives the range of gold content noted in the particle.

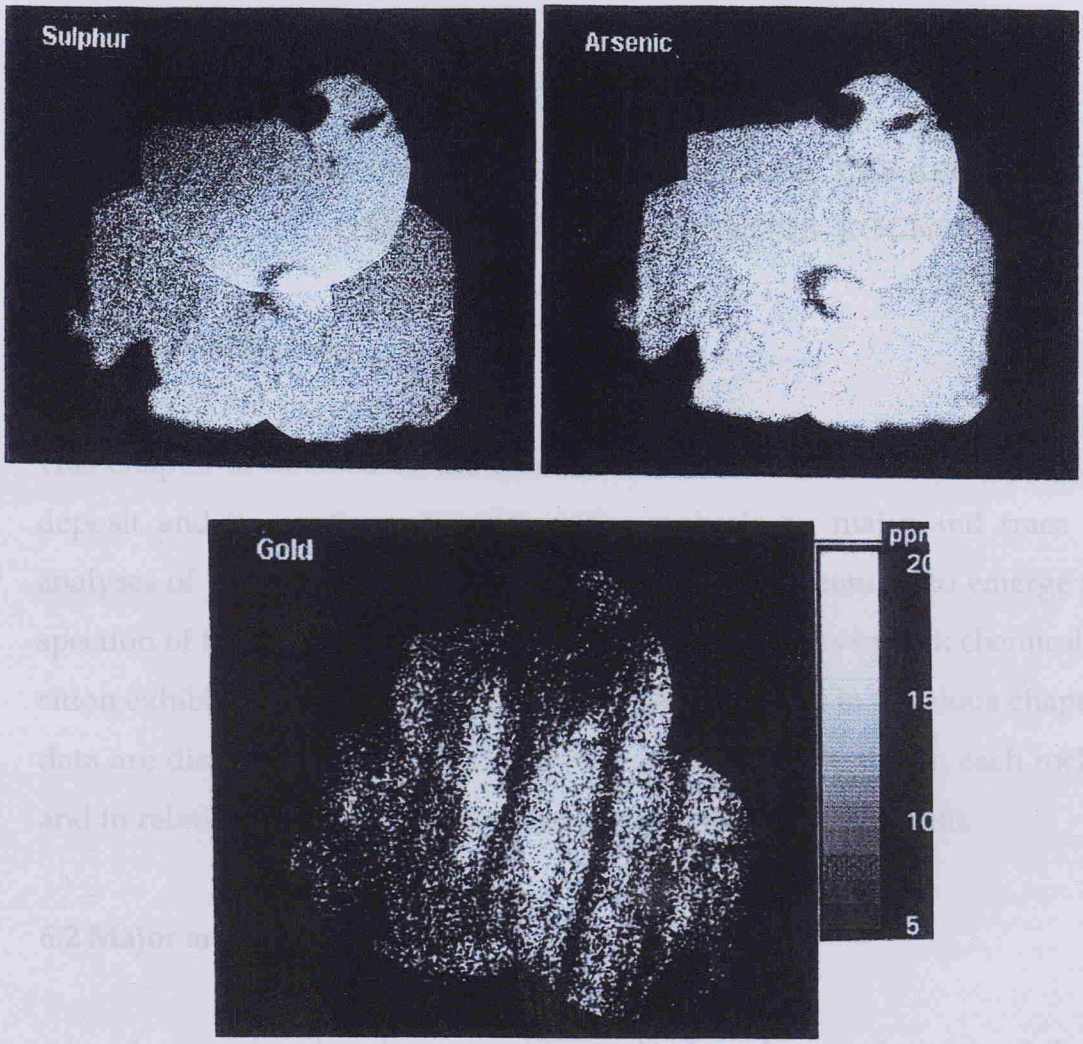

Plate 5.9: Zoned distribution of gold in arsenopyrite. The gray scale gives the range of gold content noted in the particle.

CHAPTER 6

GEOCHEMICAL CHARACTERISTICS OF THE ASIMOTRYPES ORE AND ITS CONTIGUOUS ROCKS

6.1 General Statement

This chapter is devoted to the chemical characteristics of the Asimotrypes gold deposit and its contiguous rocks, with emphasis on major and trace element analyses of whole rocks and ore samples. The salient features to emerge from inspection of the chemical data is the substantial variations in bulk chemical composition exhibited by the different rock groups as defined in previous chapters. The data are discussed below with respect to its significance within each rock group, and in relation to the overall chemical environment of the deposit.

6.2 Major and Trace Element Geochemistry

Abundances of major element oxides and selected trace elements of the Asimotrypes gold deposit are reported in Tables 1-10, Appendix III.

Marbles

SiO_2 contents in the analysed marbles range between 0.30-6.30 wt% except for the ones adjacent or close to the ore which are highly silicified and where the SiO_2 content ranges up to 35 wt% (Table 1, Appendix III).

The spatial distribution of Fe_2O_3 parallels that of SiO_2. The average concentration of total iron in the carbonate rocks of Pangeon is 482 ppm (Table 2, Appendix

III). However, the average concentration of iron in the calcitic marbles is 200 ppm, in the dolomite 508 ppm, and in the impure calcitic marbles of the Transitional Zone is 743 ppm. Finally in the dolomitic marbles near to the Fe, Mn, mineralisation the iron concentration ranges from 5692 to 7216 ppm.

The correlation of iron with the percentage of insoluble residue is relatively strong (Fig. 6.1) and the iron enrichment is developed in the non-carbonate minerals. The average values of dolomites (508 ppm) fall within the range of those at other deep burial and/or late diagenetic dolomites (Mattes and Moyntjoy, 1980; Budaj et al., 1984; Zenger and Dunham, 1988). The relatively high concentration of iron could be attributed to burial diagenetic modification because of its large distribution coefficient D Fe_{dol} >1. The iron concentration of the impure calcitic marbles in the Asimotrypes area is likely due to the hydrothermal activity and the high percentage of the non-carbonate minerals.

The average manganese concentration in the carbonates of Pangeon is 91 ppm. (Table 2, Appendix III). More specifically, the average manganese concentration in the dolomitic marbles is 120ppm and that in the calcitic ones is 23 ppm. In the impure calcitic marbles of the Transitional Zone the average concentration is 123ppm, and in the dolomitic samples near to the Fe, Mn mineralisation ranges from 2964 to 3294 ppm.

The correlation of manganese with the percentage of insoluble residue is relatively strong (Fig. 6.1), and the manganese enrichment is also developed -like iron- in the non-carbonate minerals. The correlation of manganese with iron is also similar. The relatively low manganese content, as well as the low Fe and Sr contents may be attributed to the high degree, of major element stoichiometry of these dolomites. However, the manganese concentration in dolomites is relatively enriched compared to the calcitic marbles.

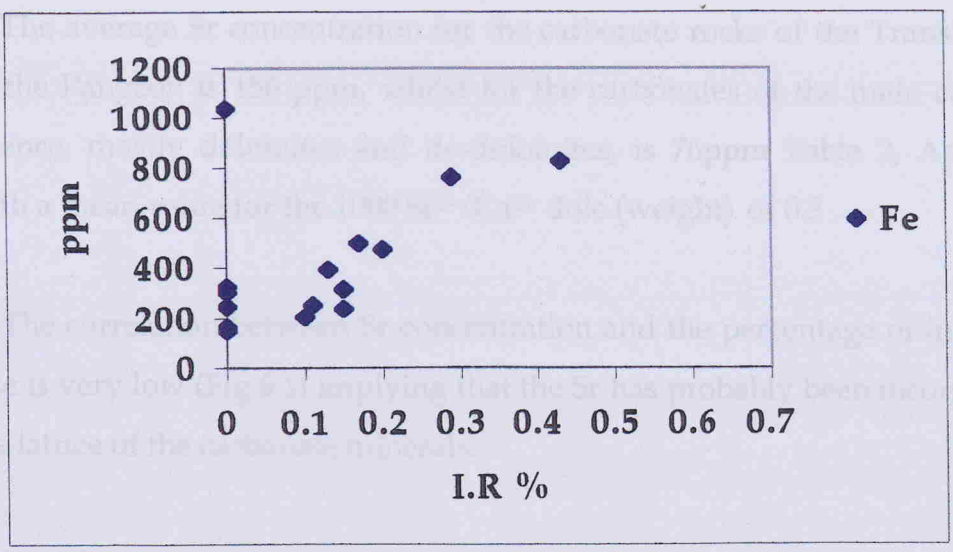

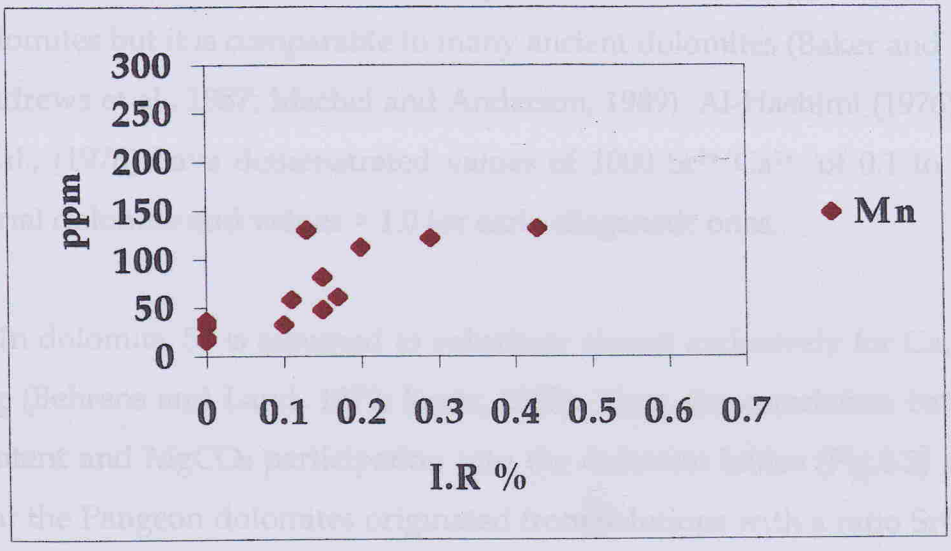

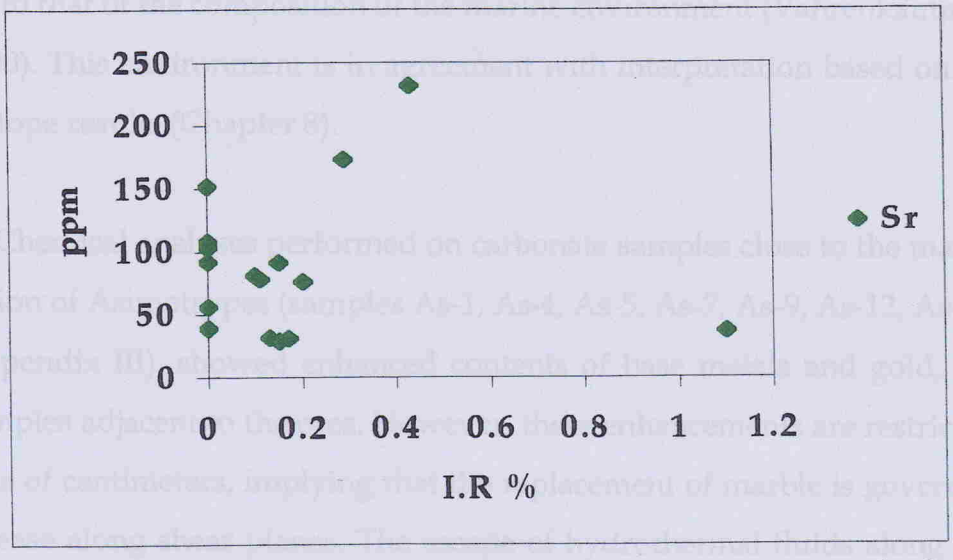

Figure 6.1: Correlation of Fe, Mn and Sr concentration and the insoluble residue. Correlation of Sr is low, implying incorporation into the lattice of carbonate minerals.

The average Sr concentration for the carbonate rocks of the Transitional Zone of the Pangeon is 156 ppm, whilst for the carbonates of the main carbonate sequence, mostly dolomites and de-dolomites, is 76ppm Table 2, Appendix III), with a mean value for the 1000 Sr^{2+}/Ca^{2+} dolo (weight) of 0.3 .

The correlation between Sr concentration and the percentage of insoluble residue is very low (Fig.6.1) implying that the Sr has probably been incorporated into the lattice of the carbonate minerals.

The Sr concentration of the Pangeon dolomites is lower than all Holocene dolomites but it is comparable to many ancient dolomites (Baker and Burns, 1985; Andrews et al., 1987; Machel and Anderson, 1989). Al-Hashimi (1976) and Veizer et al., (1978) have demonstrated values of 1000 Sr^{2+}/Ca^{2+} of 0.1 to 0.3 for post burial dolomite and values > 1.0 for early diagenetic ones.

In dolomite, Sr is assumed to substitute almost exclusively for Ca, and not for Mg (Behrens and Land, 1972; Kretz, 1982). Thus, the correlation between the Sr content and $MgCO_3$ participation into the dolomite lattice (Fig.6.2) may suggest that the Pangeon dolomites originated from solutions with a ratio Sr^{2+}/Ca^{2+} similar to that of the composition of the marine environment (Vahrenkamp and Swart, 1990). This environment is in agreement with interpretation based on C, O stable isotope results (Chapter 8).

Chemical analyses performed on carbonate samples close to the main mineralisation of Asimotrypes (samples As-1, As-4, As-5, As-7, As-9, As-12, As-32, Table 1, Appendix III), showed enhanced contents of base metals and gold, but only in samples adjacent to the ores. However, these enhancements are restricted to a few tens of centimeters, implying that the replacement of marble is governed by fluid release along shear planes. The escape of hydrothermal fluids along these structural pathways meant that was no reason for any diffusion into the surrounding marbles.

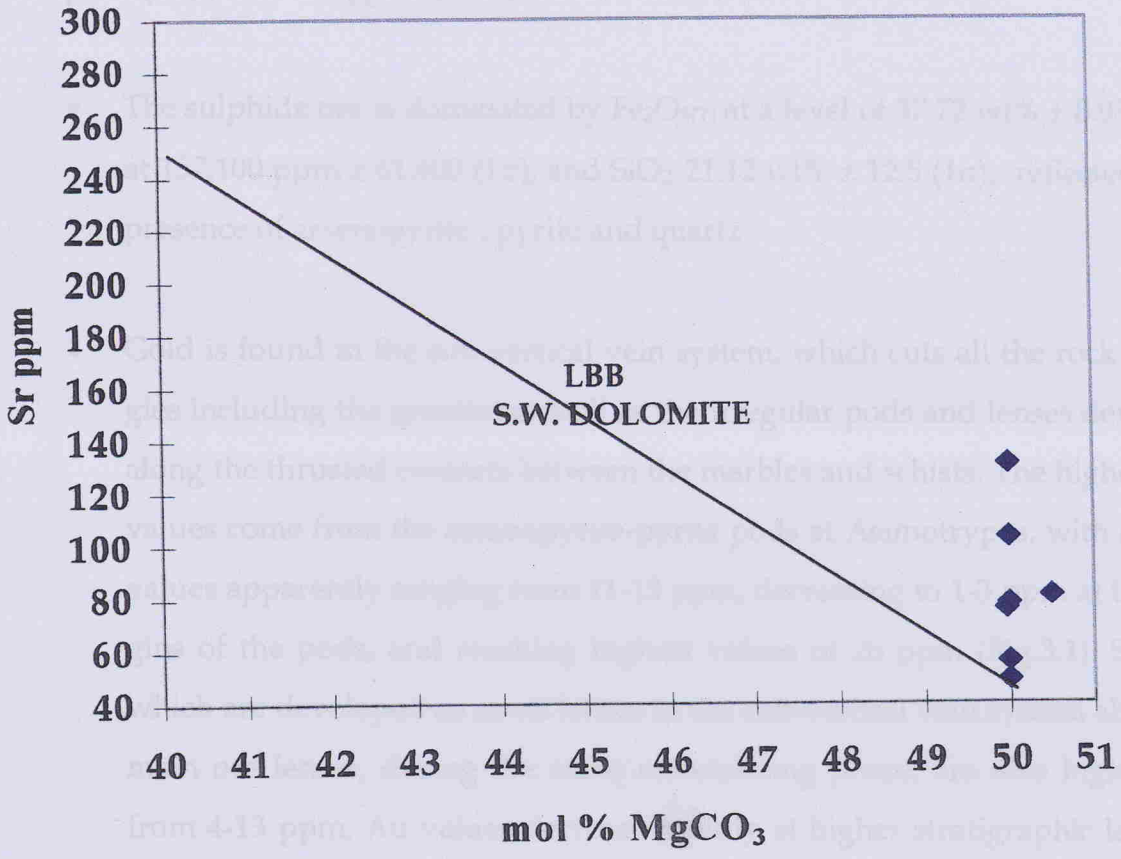

Figure 6.2: $MgCO_3$ wt%, versus Sr ppm, diagram suggesting that the Pangeon carbonates originate from solutions with compositions similar to that of marine environment (Vahrenkamp and Swart, 1990).
LBB: Little Bahama Bank
SW: Seawater

Orebodies

The salient geochemical features of the Asimotrypes carbonate-hosted gold deposit (Tables 3-10 Appendix III) are as follows:

- The sulphide ore is dominated by $Fe_2O_{3(T)}$ at a level of 37.72 wt% ± 8.93 (1σ), S at 157,100 ppm ± 61,400 (1σ), and SiO_2 21.12 wt% ± 12.5 (1σ), reflected in the presence of arsenopyrite , pyrite and quartz.

- Gold is found in the sub-vertical vein system, which cuts all the rock lithologies including the granite, as well as the irregular pods and lenses developed along the thrusted contacts between the marbles and schists. The highest gold values come from the arsenopyrite-pyrite pods at Asimotrypes, with average values apparently ranging from 11-13 ppm, decreasing to 1-3 ppm at the margins of the pods, and reaching highest values of 26 ppm (Fig.3.1). Sulfides, which are developed as small lenses in the sub-vertical vein system above the main ore lenses, during the same mineralizing phase, are also high in Au, from 4-13 ppm. Au values decrease rapidly at higher stratigraphic levels, in the minor mineralisation at Avgo (Pilaf Tepe), and are low in the sub-vertical vein system where it crosses the granite and marbles below Asimotrypes.

- Silver distribution is variable and is concentrated at a level of 31.71 ppm ± 49.6 (1σ). Silver exhibits a distinct correlation with gold, indicating a close association between Ag and Au deposition. Ratios of Au/Ag are scattered, but the median ratio for the ore samples is ≈ 0.9, whilst the Ag/Pb ratio is 0.03 ± 0.02 (1σ).

- The arsenic content of auriferous rocks is high at 188,637 ppm ± 166,473 (1σ) compared to most mesothermal gold deposits (Boyle, 1979), endorsing the so-called Au-As association. The correlation between Au and As is high, and

taking into account that Au is located within the arsenopyrite crystals, suggests that the deposition of these two elements was contemporaneous.

- Antimony shows the same overall distribution as arsenic through the sulphide ore, but at lower absolute levels 58.5 ppm ± 25 (1σ).

- Bismuth is a characteristic element in association with many types of hydrothermal gold deposits, but analytical data are notably scarce. According to the present study and data from literature, Bi is commonly enriched in mesothermal gold deposits, although concentration varies markedly between individual deposits. At Asimotrypes Bi contents are at the level of 53.4 ppm ± 20 (1σ). Bismuth shows a fairly good correlation with Au implying coeval deposition of the elements.

- Cr, Ni and Co are mostly somewhat depleted in carbonate-hosted mesothermal gold deposits (Boyle, 1979). However, concentration of Cr is at the level of 159.6 ppm ± 60 (1σ), of Ni at 66.15 ppm ± 20.8 (1σ), and of Co at 69 ppm ± 17 (1σ). These enrichments may be attributed to the host-rock lithology explained by the presence of metabasite and ortho-rocks in the Transitional Zone.

- In general, the base metal content is uniformly low with Cu content at a level of 550 ppm ± 956 (1σ), Pb at 1660 ppm ± 1987 (1σ), and Zn at 1391 ppm ± 1864 (1σ). Base metals do not show any affinity for gold, nor does Mn or Fe. This agrees with the observations that malachite bearing vein samples are low in Au.

Statistical analysis has been used to define geochemical associations i.e., elements that are geochemically linked or follow each other using the Microstat Software Package (1987). Critical values for (1-Tail, 0.05) and (2-Tail, 0.05) are +/- 0.42706 and 0.49580 respectively. The correlation coefficiant for the ore grade

samples with >0.5 ppm Au shows that As, S, Bi and Ag are well correlated with gold (Table 6.1). These correlations are relatively high given the complex nature of hydrothermal systems. Although the magnitude of correlation varies, these elements also correlate well with each other.

However, it is apparent that there is a single auriferous mineralising system, which at this structural level is low in base metals. In this respect the Asimotrypes gold deposit conforms to the general pattern of highly enriched rare elements coupled with low degrees of enrichment of base metals, characteristic of many mesothermal lode gold deposits of both vein and chemical sedimentary types.

Table 6.1: Correlation coefficients for ore grade samples with >0.5 ppm Au in the Asimotrypes geochemical data set. Correlations above 0.42 are statistically significant at the 90% confidence level.

	Au	Ag	S	As	Sb	Bi	Pb	Zn	Cu	Cr	Ni	Co
Au	1.000											
Ag	0.510	1.000										
S	0.595	0.090	1.000									
As	0.750	0.469	0.694	1.000								
Sb	0.182	0.282	0.498	0.284	1.000							
Bi	0.583	0.447	0.349	0.531	0.144	1.000						
Pb	0.272	0.448	0.022	0.208	0.019	0.105	1.000					
Zn	0.038	0.079	0.064	0.183	0.018	0.007	0.112	1.000				
Cu	0.398	0.849	0.179	0.378	0.421	0.544	0.014	0.122	1.000			
Cr	0.382	0.717	0.178	0.451	0.072	0.471	0.001	0.344	0.784	1.000		
Ni	0.105	0.125	0.067	0.055	0.505	0.173	0.008	0.164	0.092	0.138	1.000	
Co	0.144	0.114	0.489	0.273	0.104	0.066	0.228	0.179	0.093	0.439	0.049	1.000

Number of observations: 16

CHAPTER 7

FLUID INCLUSION STUDIES

7.1 General Statement

The main mineralisation of the Pangeon Mnt is located at Asimotrypes and it is of shear-zone controlled and replacement style. All fluid inclusions studied are hosted in gangue quartz. On the basis of microscopic examination this quartz can be distinguished in two types:

Type A quartz occurs in well-developed individual euhedral to anhedral crystals. Some triple point junctions occur which are interpreted to be the result of hydrothermal recrystallization. Type A quartz crystals show evidence of deformation, exhibiting wavy extinction and micro-fracturing. Type B is microcrystalline, recrystallised quartz, surrounding Type A quartz crystals.

All fluid inclusions studied are concentrated towards the sulphide-rich areas in quartz which is always in intimate association with the ore sulphides and appears to be in textural and physicochemical equilibrium with them (Plate7.1).

7.2 Background Information

The application of fluid inclusion investigations to geological problems has been the subject of numerous studies since the middle of nineteenth century (Sorby, 1858; Smith, 1953). Fluid inclusion examination began with the search for the composition of the ore-forming fluids and the conditions of genesis of mineral deposits. Today fluid inclusion work, excellent reviews of which are given by

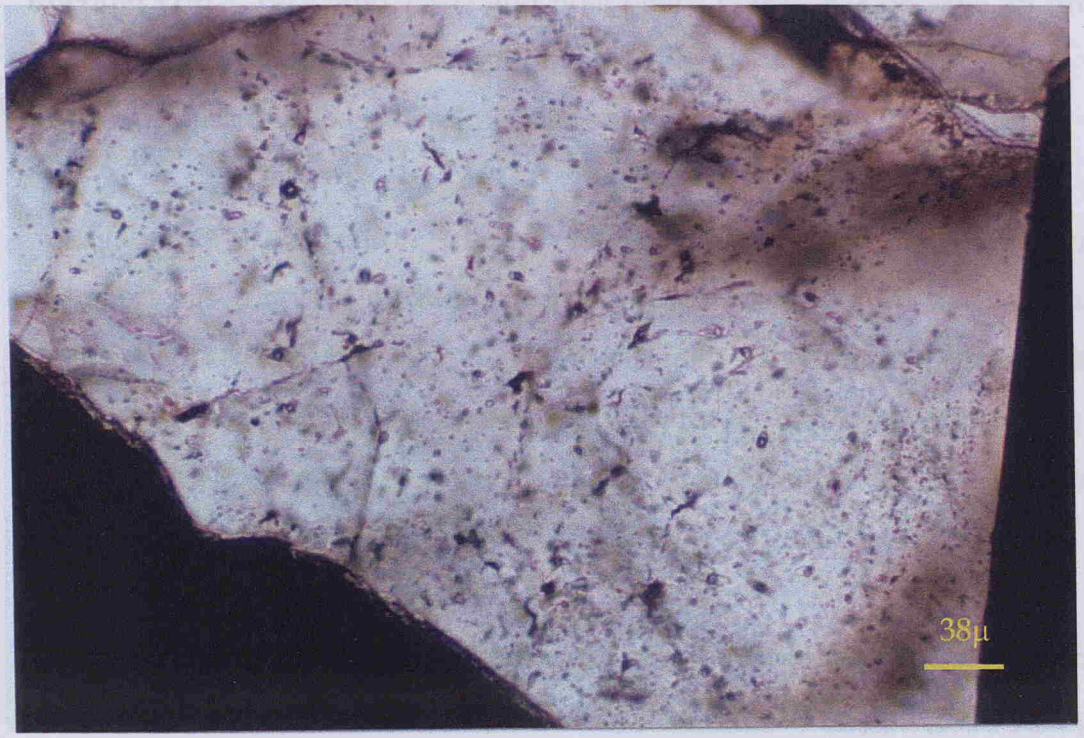

a

b

Plate 7.1 : Quartz in textural equilibrium with (a) undeformed (euhedral) and (b) cataclastic arsenopyrite replaced by quartz precipitated in active tectonic environment (shear zone). Random distribution of primary Type I inclusions.

Roedder (1972, 1979, and 1981) and Sheppherd (1985), has become an important tool in understanding ore formation processes. Unless otherwise noted the following discussion is based on Roedder's summaries.

Elaborate classification schemes have been proposed by a number of researchers based on the differing proportions of solids, liquids and vapour in the inclusions. Such schemes are certainly easier to use than paragenetic classifications because subjectivity is kept to a minimum. A simple but convenient classification scheme based on the major phases present at room temperature is discribed by Shepherd et al., (1985) and it is illustrated in Table 7.1.

When a mineral grows or recrystallises in a fluid medium, any process that hinders the growth of prefect crystals may result in the trapping of small portions of the fluid within the crystal. If this fluid is trapped during the formation of the enclosing crystal, the result is a primary fluid inclusion (Plates 7.2, 7.3, 7.4 a). Secondary inclusions form when later and entirely different fluids become trapped in cracks during fracturing or recrystallisation (Plate 7.6b). A fluid inclusion that becomes sealed off in a healing fracture before complete formation of the hosting crystal is called pseudosecondary.

Thus, fluid inclusions represent microscopic samples of fluids associated with the geological history of the hosting crystal.

Distinction of types of fluid inclusions is of fundamental importance. This is because the time elapsed between the trapping of primary and secondary inclusions, sometimes millions of years, may result in inclusions of extremely different compositions and P-T histories. Unfortunately, the inclusion's origin cannot always be inferred with certainty because of lack of genetic information. The most important suggestive criteria for assigning a primary origin is the absence of any planar arrangement. Primary inclusions can be reliably identified if they can be related to growth phenomena. Secondary inclusions usually mark healed frac-

INCLUSION TYPE	ESSENTIAL PHASES	TYPICAL EXAMPLES	ABBREVIATION
Monophase liquid	L=100%		L
Liquid-rich, two-phase	L > 50%		L + V
Vapour-rich two-phase	V = 50 to 80%		V + L
Monophase vapour	V ≈ 100%		V
Multiphase solid	L = variable S < 50%		S + L ± V
Multisolid	S > 50% L,V variable	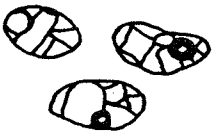	S + L ± V
Immiscible liquid	L_1 , L_2		$L_1 + L_2 \pm V$
Glass	GL > 50%	not shown	GL ± V ± S

Table 7.1: Classification scheme for liquid and melt inclusions in minerals based upon phases observed at room temperature. L = liquid, V = vapour, S = solid, GL = glass. (After Shepherd et al., 1985).

tures, are small in size, on the order of a few microns (μ), and exhibit divergent behaviour during heating or freezing runs, in relation to nearby primary inclusions. Pseudosecondary inclusions are in many cases associated with fractures or dislocation surfaces that can be traced to an abrupt ending within the crystal.

Of importance in the application of fluid inclusion research, is whether necking down or leakage has occurred. Necking down is the process during which large inclusions split into a series of smaller ones.

If several liquid and/or gas phases have been equilibrated in the original inclusion, the resulting inclusions will exhibit varying phase ratios and a spread of microthermometric data. Choosing isolated inclusions to work on would eliminate inclusions that might have necked down. Leakage is the non-isochemical addition or removal of inclusion material between trapping and experiment. Some inclusions have been shown to leak under conditions that do not represent those in nature. The systematic variation of results from fluid inclusion studies of zoned single crystals (Roedder, 1963) and the demonstrated endurance of CO_2-rich inclusions to severe internal pressure at high temperatures (Roedder, 1965), constitute the greatest evidence against significance leakage.

The trapped fluid may be homogeneous, carry solid particles in suspension, or be composed of two or more immiscible components or have a gas phase (i.e. boiling fluid). Water, with rare exceptions, is the dominant constituent. The total dissolved salt content is usually expressed in terms of equivalent weight percent NaCl and is referred to as salinity.

After trapping, the inclusion follows a cooling and presumably isochoric and isodensity path and it may evolve into a multiphase inclusion. The phase transition or unmixing occurs on the solvus of the corresponding chemical system. A trapped aqueous brine may evolve a vapour bubble because of differential ther -

mal contraction of the host crystal and the fluid. These bubbles should be distinguished from the primary gas trapped from a boiling fluid.

If an H_2O-CO_2 fluid was trapped at elevated temperature, it may unmix below 300 ^{0} C, due to H_2O, CO_2 immiscibility, and separate CO_2 into a second fluid phase. If the CO_2 concentration is high enough, or if the CO_2 partial pressure exceeds 75 bars, gaseous CO_2 will separate usually below the critical point for pure CO_2, 31^0 C.

Regularity both of phase volume ratios and microthermometric data provides the best evidence available that the original fluid was homogeneous.

Decreasing solubility during cooling may result in saturation with respect to the solutes and precipitation of daughter minerals.

The composition, density and P-T conditions of the inclusions can be deduced from univariant phase transitions observed during cooling and heating experiments assuming that the inclusions retain constant volumes. The temperature of homogenisation of the inclusion (T_H) on heating can be used to estimate the trapping temperature. T_H represents a minimum trapping temperature and a pressure correction must be applied to compensate for the pressure differences between the experiment and the trapping, and for the salinity of the fluid. An independent estimate of pressure or temperature can be used for pressure correction. Pressure can be evaluated from fluid inclusion studies in a limited number of cases (Roedder and Bodnar, 1980). Salinity can be estimated by freezing the inclusion and recording the temperature at which melting of the frozen inclusion occurs. The melting point is related to the composition of the dissolved salts. In CO_2-bearing inclusions, the clathrate compound, carbon dioxide hydrate ($CO_2$5.75 H_2O) forms upon freezing. When pure this compound melts at about +10^0 C (Collins, 1979). Solutes present depress the clathrate melting point, providing an estimate for the salinity, for the case of CO_2-inclusions.

However, methane and solutes exert opposed effects on the clathrate melting behaviour: thus melting point data from CO_2-bearing liquid inclusions are not easy to interpret without knowledge of the gas species present.

Cooling CO_2-rich inclusions to temperatures as low as -80^0 C causes freezing of the CO_2 phase. Melting of solid CO_2, upon heating, in equilibrium with liquid and vapour CO_2, at a temperature of T=-56.6 ^{0}C, is the best indication yet available in fluid inclusion research, of the purity of the CO_2-phase. The temperature (T -56.6 ^{0} C) where three CO_2 phases (solid, liquid, vapour) coexist is known as the CO_2 triple point (Weast, 1974).

The values obtained for homogenisation temperatures and salinity can then be compared to experimental results on fluid phase equilibrium systems: H_2O + NaCl (Sourirajan and Kennedy, 1962); H_2O + CO_2 (Takenouchi and Kennedy, 1964); H_2O + CO_2 + NaCl (Takenouchi and Kennedy, 1965; Gehring te al., 1979; Hendel and Hollister, 1981) in order to infer trapping conditions (i.e. boiling or immiscibility) or interpret homogenisation behaviour.

7.3 Compositional Types of Fluid Inclusions

A total of 19 samples were collected from this locality for fluid inclusion microthermometry and gas analysis. These wafers were prepared from quartz associated with massive, arsenopyrite-pyrite quartzite lenses in contact with the shear banded marble from the main adit at Asimotrypes, and sub-vertical sulphide-bearing quartz veins, cutting gneiss-schist, which has been biotized/ phlogopitized, 10m north-west of the main adit.

The shape of the inclusions is irregular to euhedral with smooth boundaries and their size varies from <4 to 20 μm. Three types of inclusions are recognised in the studied samples on the basis of the phases present at room temperature:

- *Type I: 3-phase CO_2 - rich inclusions: $L_1 + L_2 + V$*

Type I aqueous-carbonic fluid inclusions are restricted in Type A quartz and are characterised at room temperature by visible amounts of both undersaturated aqueous liquid plus carbon dioxide and consist of three phases: liquid H_2O-rich (L_1) + liquid CO_2 (L_2) + vapour CO_2 (V). Type I inclusions are characterised by highly variable CO_2 to H_2O ratios. (Plates 7.2 & 7.3). Type I inclusions are further subdivided to Type Ia and Type Ib which are H_2O- and CO_2-rich respectively. The vol. % of the CO_2 phase, as estimated visually at 25 °C, range from 10 to 50 in Type Ia, although most inclusions contain between 20 and 30 vol. % CO_2, and 70 to 90 in Type Ib (Fig. 7.1).

- *Type II: 2-phase inclusions: L + V aqueous*

Type II aqueous fluid inclusions occur in Type A quartz and at room temperature they contain both H_2O liquid + vapour phases with L>V (Plate 7.4). The vapour bubble typically occupies 10-20 vol. % of the inclusion volume. Clathrate hydrate melting characteristics observed at temperatures above 0 ^{0}C, indicate that Type II inclusions actually contain traces of CO_2, possible maximum 2.2 molal (Hendequist and Henley, 1985).

- *Type III: Decripitated and/or leaked inclusions: V + L*

Type III inclusions are small in size -up to 15 μm- and range from irregular, through elongate to ovoid in shape. They occur at the interfaces of dynamically recrystallised Type B quartz and between grains of strained and unstrained Type A quartz (Plate 7.5). They characterise the migration fronts of grain boundaries and are interpreted as leaked and decripitated inclusions swept up by the boundary as it migrates through the strained material (Giles and Marshall, 1994). The inclusions-free cores of recovered grains support this. Indeed, in highly recovered

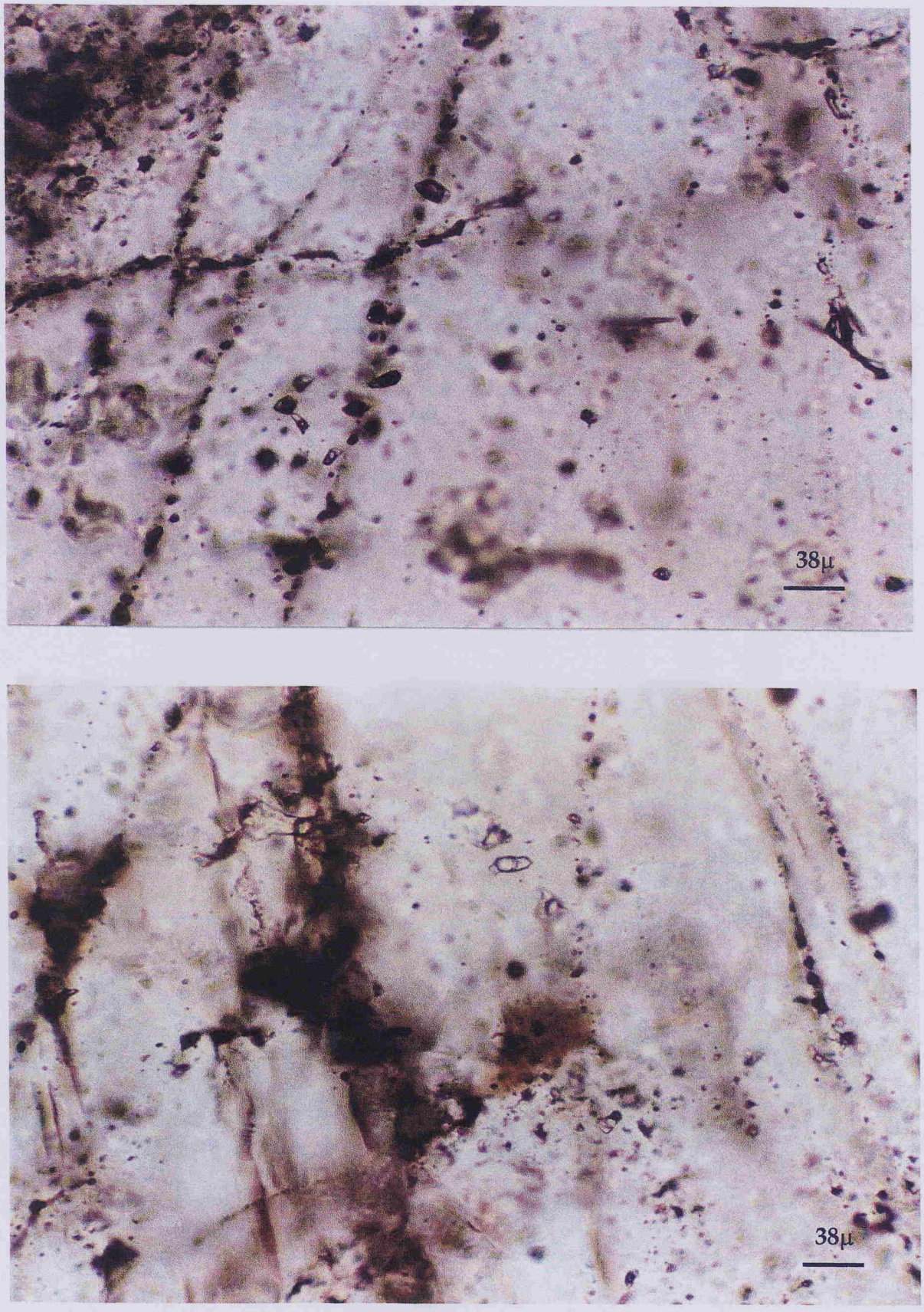

Plate 7.2: 3phase CO_2-H_2O Type I inclusions along intragranular fractures in quartz Type A. Note the variable CO_2/H_2O ratios, implying immiscibility phenomena.

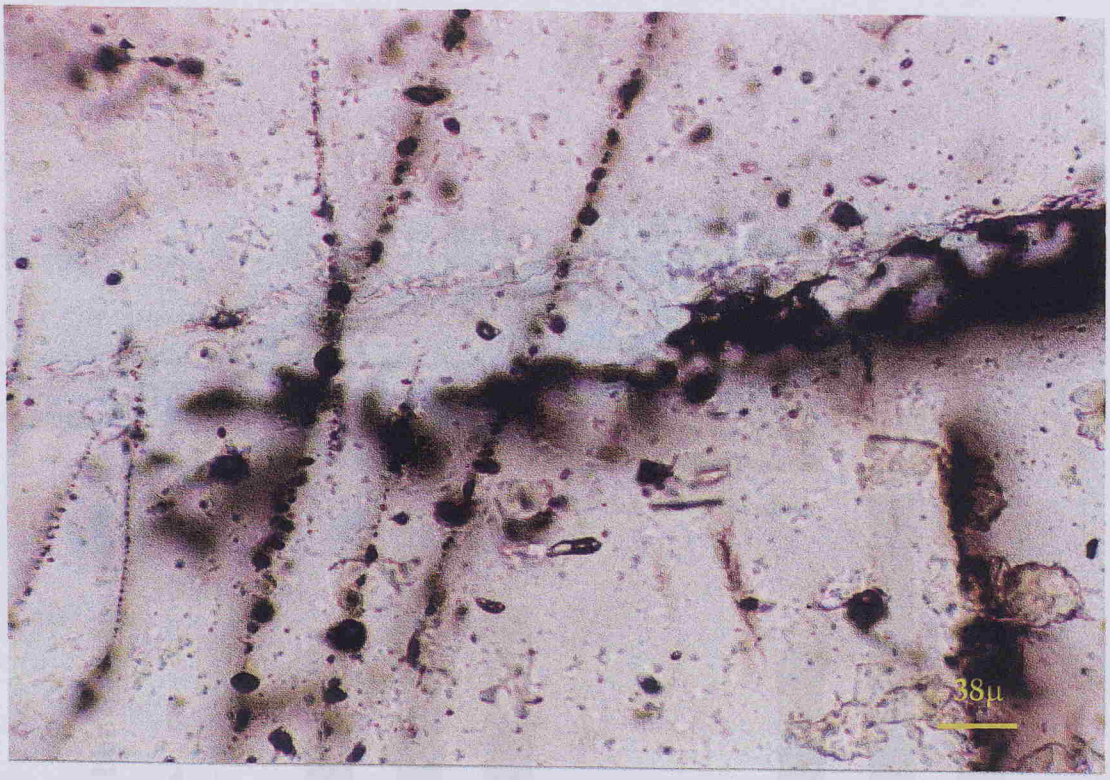

a

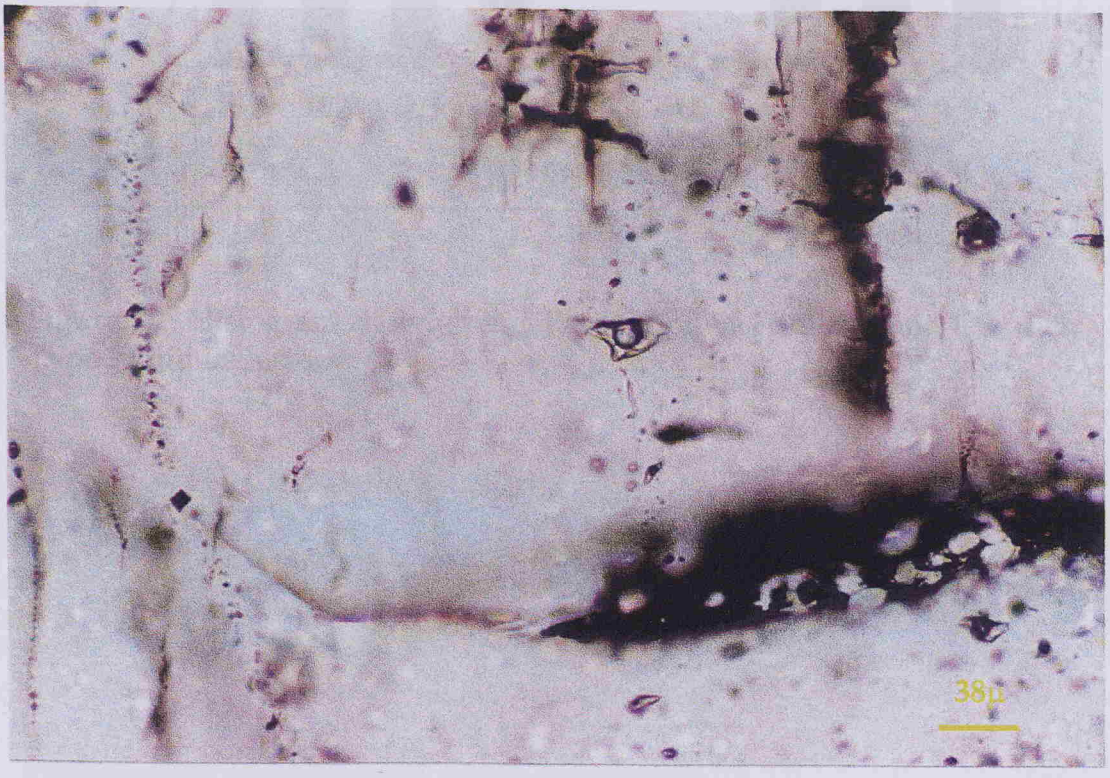

b

Plate 7.3: Variable CO_2/H_2O ratio in Type I inclusions indicating immiscibility. Note that some inclusions in (a) have been decripitated to vapour phase before homogenisation.

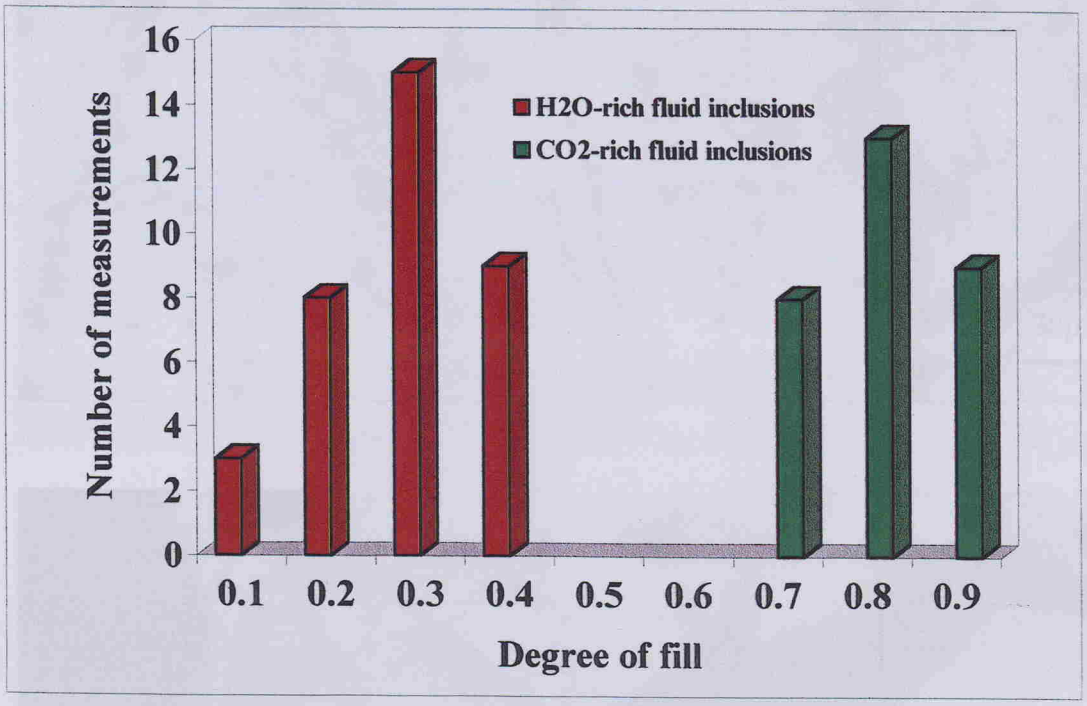

Figure 7.1: Histogram showing the distribution of H_2O-rich and CO_2-rich Type I fluid inclusions.

a

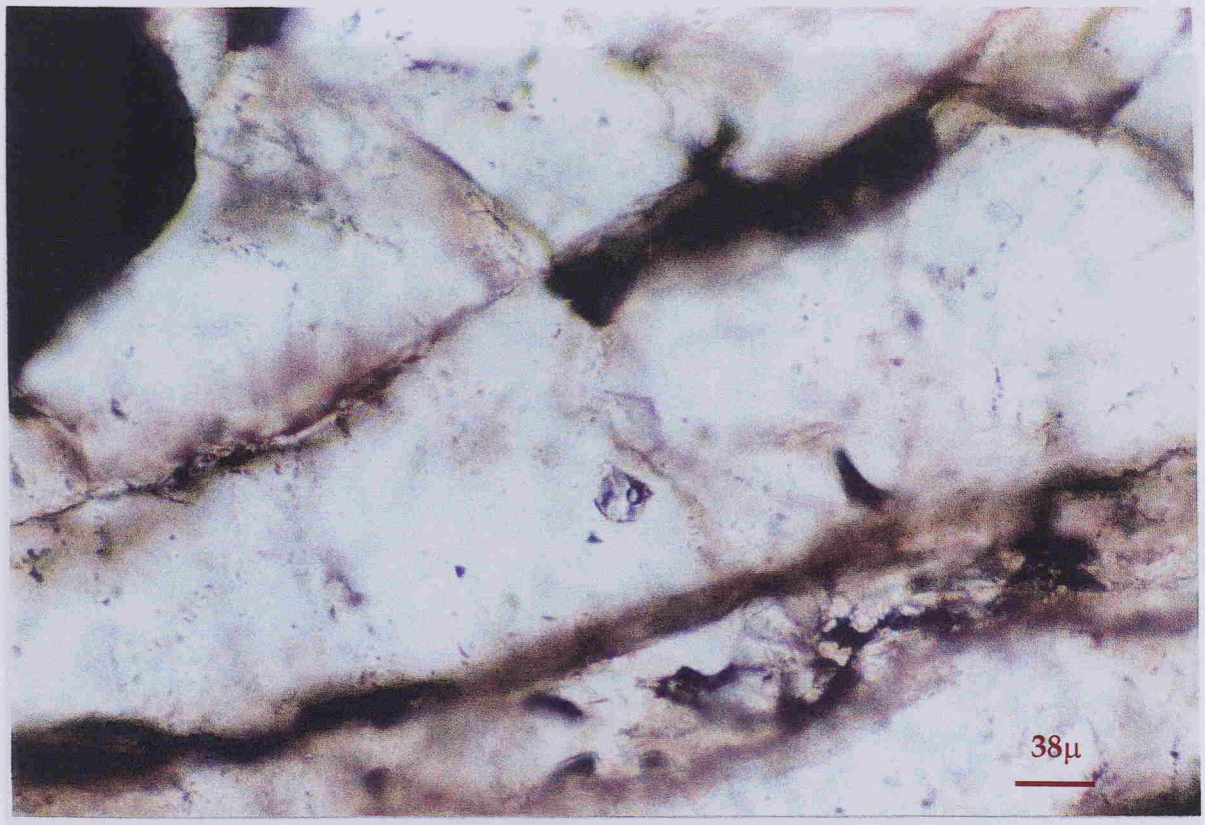

b

Plate 7.4: (a) Type I fluid inclusions aligned along intragranular fractures, suggesting quartz precipitation in a tectonic active environment (shear zone). (b) Primary, low temperature, Type II, 2 phase liquid vapour, H_2O inclusions. Negative crystal shape.

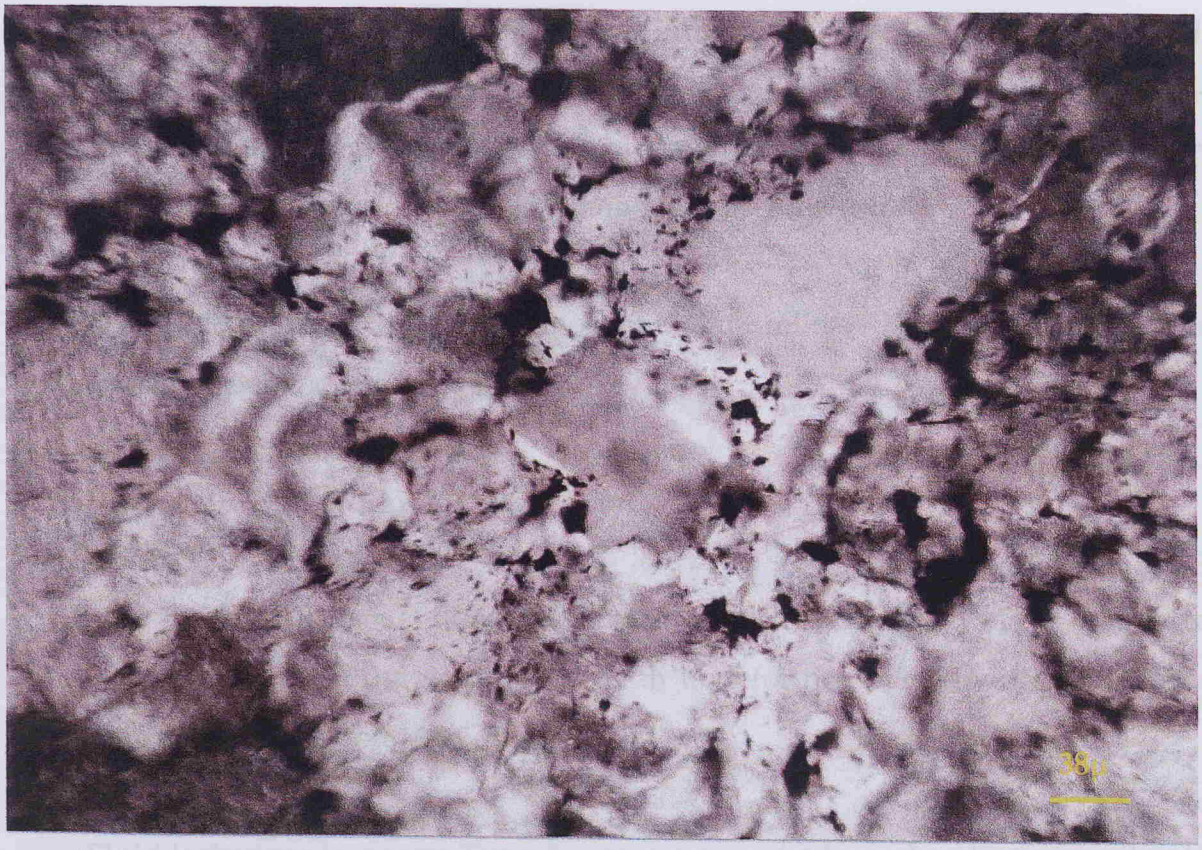

a

b

Plate 7.5: Type III fluid inclusions, (a) decripitated at grain boundaries of hydrothermally recrystallised quartz B, (b) leaked.

(recrystallised) quartz, the frequency and size of inclusions diminishes until all inclusions are eliminated. Kerrich (1976) and Wilkins and Barkas (1978) have suggested that the process of recovery and re-crystallisation progressively eliminate both pre-existing inclusions and the grain boundary inclusions.

Type I inclusions are by far the most abundant followed by Types II and III in decreasing frequency of occurrence.

7.4 Occurrence of Fluid Inclusions

All the fluid inclusions studied are hosted by clear domains of Type A quartz crystals being in textural equilibrium with undeformed arsenopyrite. No workable inclusions were found in Type B.

Fluid inclusions in quartz Type A may occur as: (a) irregular clusters randomly distributed of Types I and II inclusions (Plate 7.2), (b) single isolated Type I inclusions, (c) irregular groups of Type I inclusions with variable CO_2 / H_2O ratio (Plates 7.2 & 7.3), and (d) trails along narrow well healed intragranular microfractures of Type I inclusions (Plate 7.6). Occurrence types a, b, and c conform to those suggested for primary fluid inclusions, whereas type d conform with pseudosecondary origin (Roedder 1984). Most Type II inclusions occur along narrow well healed transgranular microfractures (Plate 7.6) and are of secondary origin.

No systematic differences were observed in fluid inclusion characteristics in the various samples studied.

7.5 Microthermometry Results

Types Ia and Ib inclusions described are considered to belong to the same ore-forming event related to the sulphide mineralisation, whilst Type II inclusions report later introduction of meteoric water into the mineralising system.

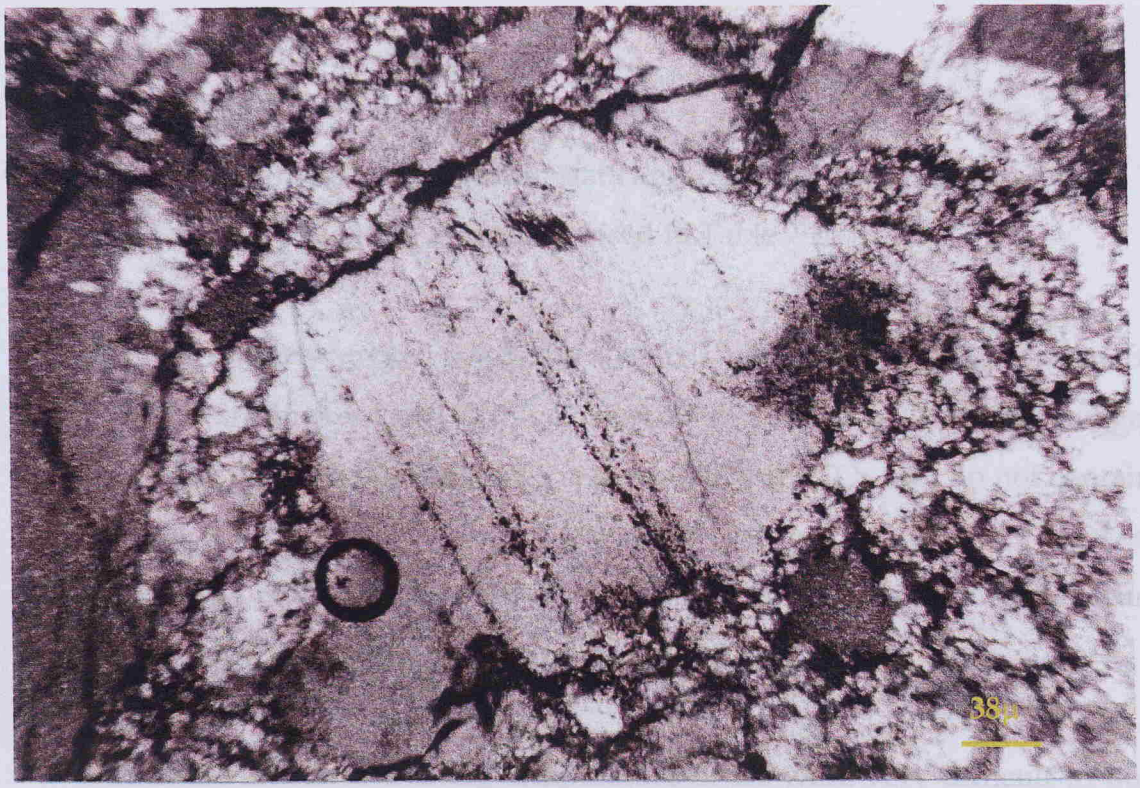

a

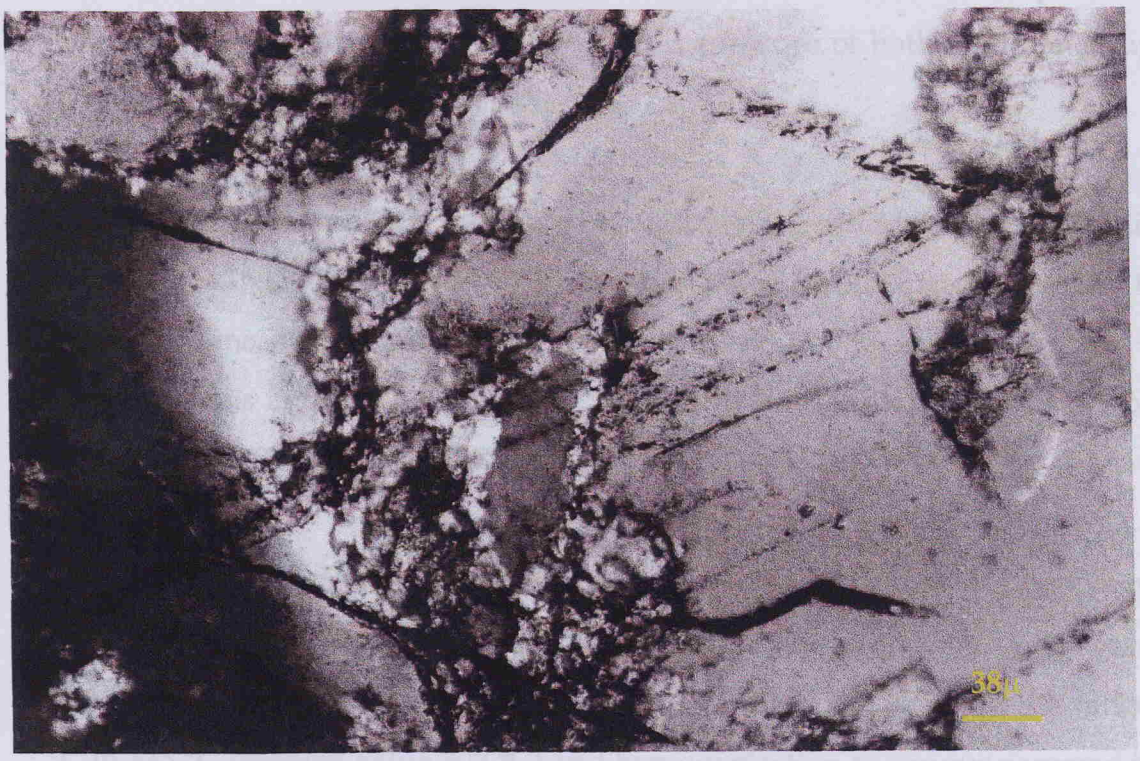

b

Plate 7.6: (a) Type I inclusions along intragranular fractures in quartz Type A surrounded by microcrystalline recrystallised quartz Type B. (b) Type II, secondary inclusions in transgranular well healed fractures, cross-cutting quartz Types A and B.

Type I : 3 phase CO_2 - rich inclusions

Fluid inclusion microthermometric data and ore-fluid properties of Type I, H_2O-rich (Ia) and CO_2 -rich (Ib) are summarised in Table 7.2.

Melting temperatures of solid CO_2 (Tm_{CO2}) in Type I inclusions range from -56.9 to -56.2, which is close to the triple point of pure CO_2 (- 56.6 °C), suggesting that the gas phase in the inclusions is predominantly CO_2 and do not contain significant amounts of other dissolved volatiles such as CH_4, N_2 etc. This was also confirmed by bulk volatile analyses (see later). Homogenisation temperatures of the CO_2 phase (Th_{CO2}) range from +25.5 to +29.4 °C (Fig.7.2).

An initial and final melting temperature of ice were very difficult to observe due to the small size of the inclusions and has not been recorded. Temperatures of melting of clathrate hydrate (Tm_{Clath}) in the presence of both liquid and vapour CO_2 range from + 7.7 to +8.8 °C (Fig. 7.3).

Microthermometric data were used to calculate the salinity and bulk density of the fluid (FLINCOR, Brown, 1989). Salinities range from 2.61 to 7.31 wt% NaCl equiv. (Collins, 1979) and bulk densities from 0.88 to 0.99 $gr.cm^{-3}$ for the H_2O - rich inclusions and 0.61 to 2.22 wt% NaCl equiv. and bulk densities 0.37 to 0.52 $gr.cm^{-3}$ for the CO_2 - rich inclusions.

Total homogenisation temperatures (Th) for Type I inclusions range between 275 °C and 340 °C and homogenisation to both liquid and vapour was observed. Homogenisation to liquid occurred in the H_2O - rich inclusions in the range 275 °C to 335 °C (median value 302 °C) and homogenisation to vapour occurred in the CO_2 - rich inclusions in the range 308 °C to 340 °C (median value 322 °C). Homogenisation temperatures in either phase cluster between 300 °C and 330 °C (Fig. 7.3).

Table 7.2 : Microthermometric data and ore-fluid properties of Type Ia and Type Ib fluid inclusions from the Asimotrypes area.

Incl. type		Tm_{CO2} ^0C	Tm_{Clath} ^0C	Th_{CO2} ^0C	Th ^0C	Degree fill. %	Salinity * wt% NaCl equiv.	D Bulk* gr.cm^{-3}	XNaCl mol %	XCO_2 mol %	XH_2O mol %
Ia	Min.	-56.9	6.1	25.5 (V)	275 (L)	0.10	2.61	0.88	0.80	3.05	81.85
H_2O-rich	Max.	-56.2	8.7	27.5 (V)	335 (L)	0.40	7.31	0.99	1.99	16.16	96.15
	n	35	35	35	35	35	35	35	35	35	35
	Mean	-56.6	7.9	26.5 (V)	302 (L)	0.25	4.41	0.94	1.39	9.65	88.50
Ib	Min.	-56.9	8.9	26.5 (V)	308 (V)	0.70	0.61	0.37	0.09	22.38	45.35
CO_2-rich	Max.	-56.2	9.7	29.4 (V)	340 (V)	0.90	2.22	0.52	0.50	54.57	77.08
	n	30	30	30	30	30	30	30	30	30	30
	Mean	-56.6	9.3	27.9 (V)	322 (V)	0.80	1.63	0.47	0.32	38.47	61.21

Tm_{CO2} : CO_2 melting temperature

$Tm_{Clathrate}$: Clathrate melting temperature

Th_{CO2} : Partial CO_2 homogenization

Th : Total homogenization temperature

X: Bulk inclusion composition

* Calculated using FLINCOR (Brown, 1989) and Brown and Lamb (1989) Equations of State.

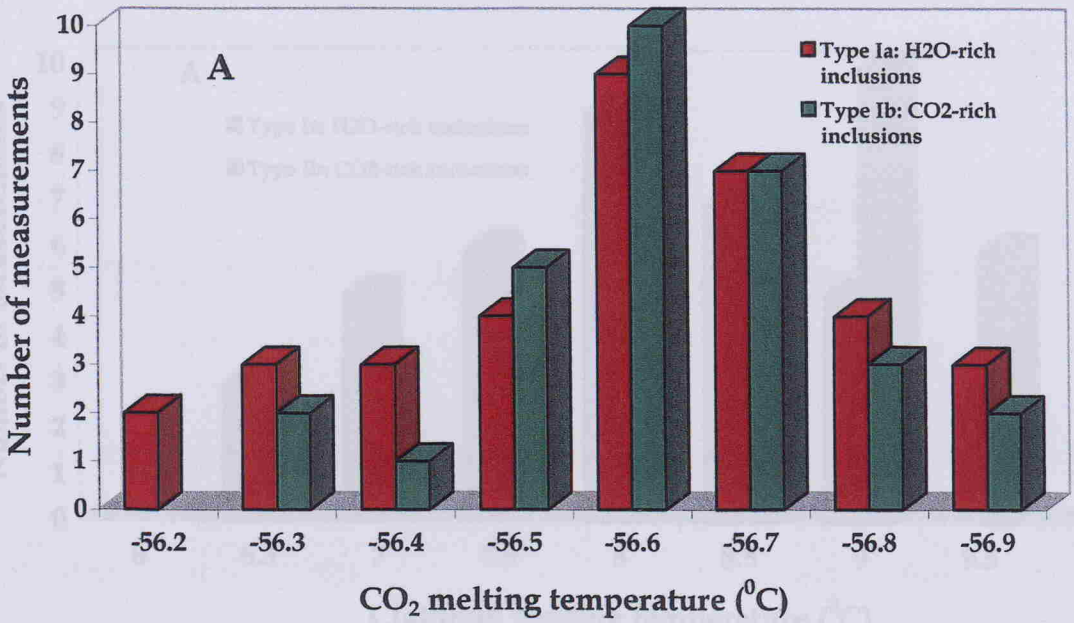

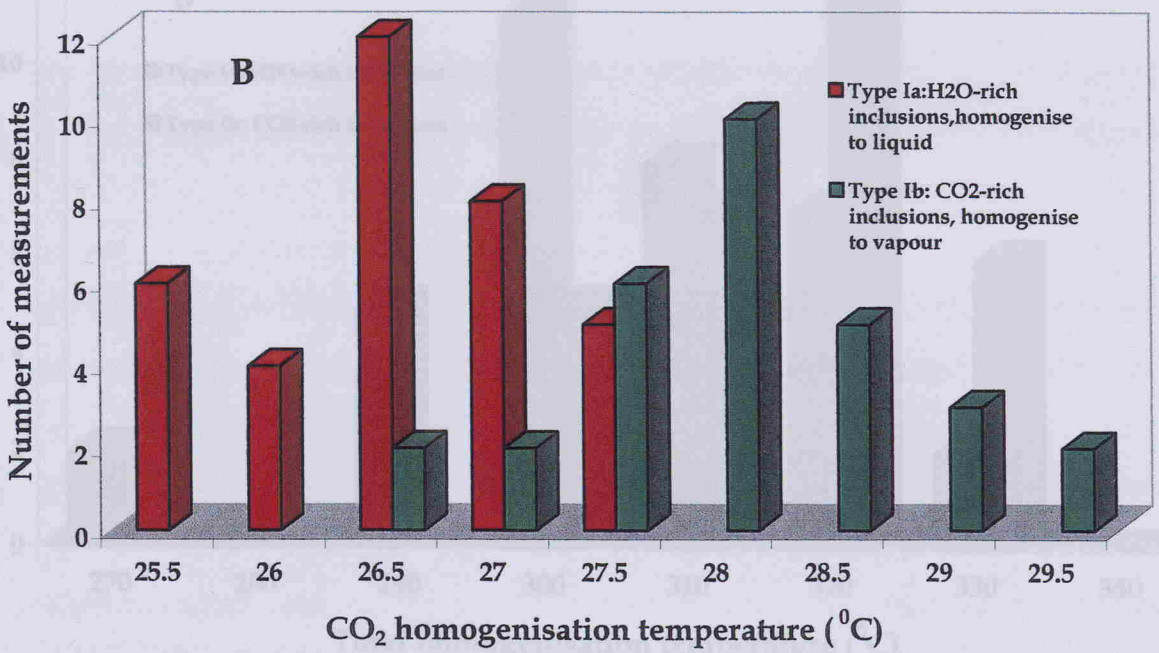

Figure 7.2 : Microthermometry data on Type I inclusions in quartz.
A. Temperatures of final melting of CO_2
B. Temperatures of homogenisation of CO_2 liquid and vapour.

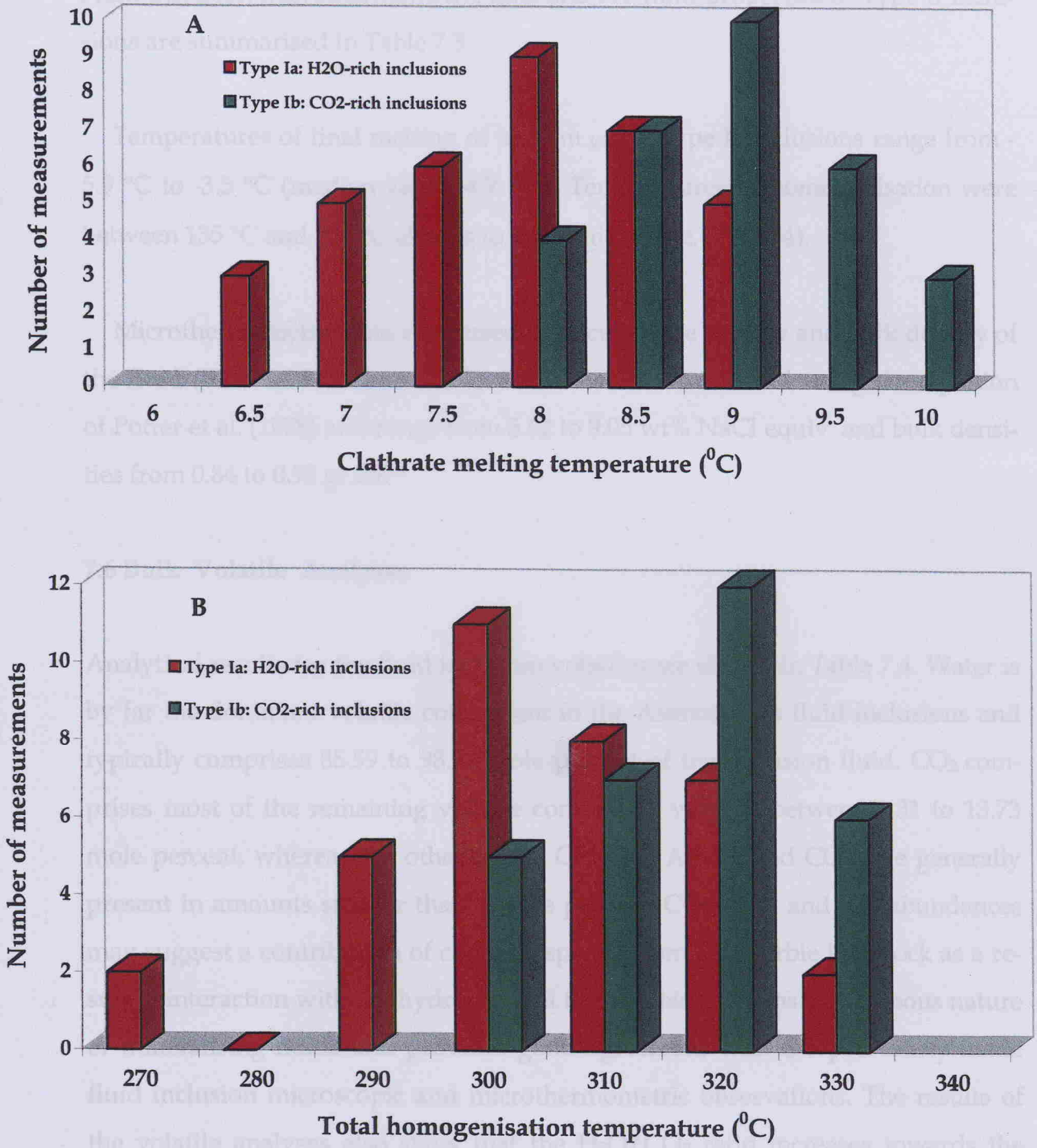

Figure 7.3: Microthermometry data on Type I inclusions in quartz.
A. Temperatures of final melting of clathrate in Type I inclusions
B. Temperatures of homogenisation to liquid (L) or vapour (V) of Type I inclusions

Type II: 2- phase inclusions

Fluid inclusion microthermometric data and ore-fluid properties of Type II inclusions are summarised in Table 7.3.

Temperatures of final melting of ice (Tm_{ice}) in type II inclusions range from -5.9 °C to -3.5 °C (median value -4.7 °C). Temperatures of homogenisation were between 135 °C and 256 °C always to the liquid phase. (Fig. 7.4).

Microthermometric data were used to calculate the salinity and bulk density of the fluid (FLINCOR, Brown, 1989). Salinities were calculated using the equation of Potter et al. (1978) and range from 5.62 to 9.05 wt% NaCl equiv. and bulk densities from 0.84 to 0.98 $gr.cm^{-3}$.

7.6 Bulk Volatile Analyses

Analytical results for the fluid inclusion volatiles are shown in Table 7.4. Water is by far the dominant volatile component in the Asimotrypes fluid inclusions and typically comprises 85.59 to 98.18 mole percent of the inclusion fluid. CO_2 comprises most of the remaining volatile component varying between 1.31 to 13.73 mole percent, whereas the other gases- CH_4, N_2, Ar, H_2 and CO - are generally present in amounts smaller than 1 mole percent. CO_2, CH_4, and CO abundances may suggest a contribution of carbonic species from the marble host rock as a result of interaction with the hydrothermal fluids. This confirms the aqueous nature of mineralising fluids and provides good agreement with the previously made fluid inclusion microscopic and microthermometric observations. The results of the volatile analyses also show that the H_2O/CO_2 ratio increases towards the mineralisation. In samples which contain predominantly CO_2-bearing inclusions, the composition estimated from microthermometry agrees closely with that obtained by bulk volatile analyses. Finally, data for the principal volatiles H_2O, CO_2, combined with geological data shows that structures hosting gold mineralisation

Table 7.3 :Microthermometric data and ore-fluid properties of Type II inclusions from the Asimotrypes area

	Tm_{ice} ^0C	Th ^0C	Degree fill. %	Salinity* t% NaCl equiv	Bulk dens. $gr.cm^{-3}$
Min.	-5.9	135 (L)	10	5.62	0.84
Max.	-3.5	256 (L)	20	9.05	0.98
n	19	25	25	25	25
Mean	-4.7	190 (L)	15	7.33	0.91

m_{ice}: Melting temperature

Th : Total homogenization temperature

* Calculated using FLINCOR (Brown, 1989)

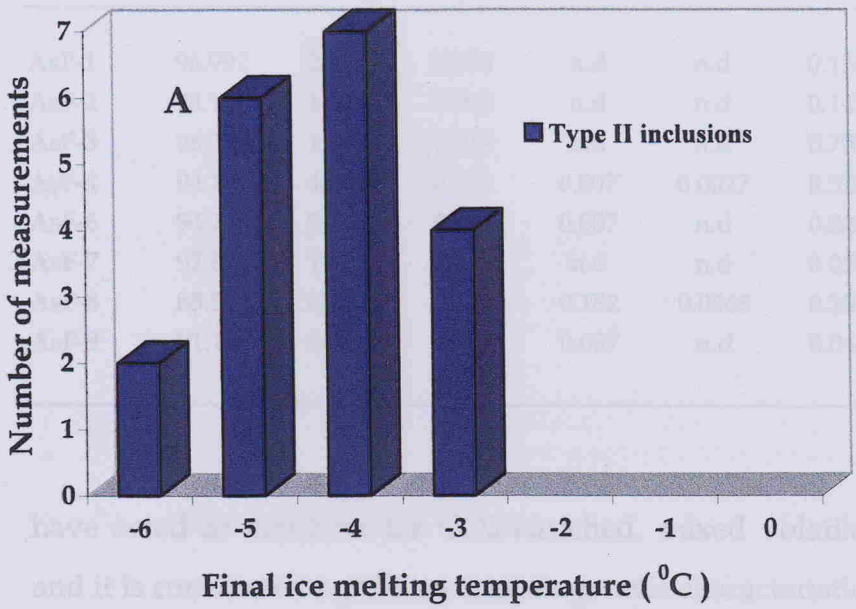

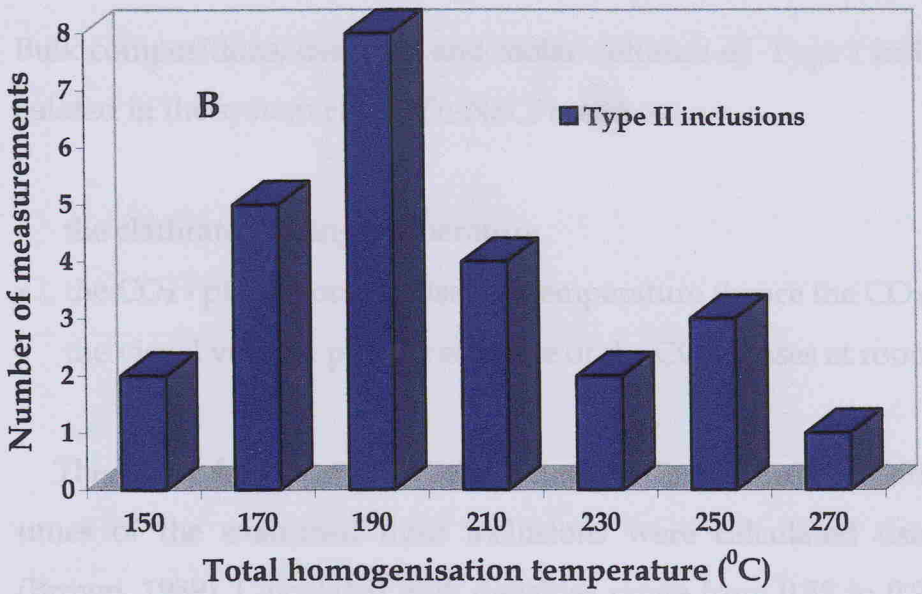

Figure 7.4 Microthermometry data on Type II inclusions in quartz.
A. Temperatures of final ice melting in Type II inclusions.
B. Temperatures of homogenisation (to liquid) of Type II inclusions

Table 7.4 : Volatile data table (mole %) for samples from the Asimotrypes ore

Sample	H2O	CO2	CH4	N2	Ar	H2	CO
AsF-1	96.992	2.366	0.075	n.d	n.d	0.134	0.433
AsF-2	98.184	1.315	0.093	n.d	n.d	0.145	0.264
AsF-3	96.716	1.666	0.519	n.d	n.d	0.705	0.405
AsF-4	94.770	4.995	0.016	0.007	0.0027	0.320	0.289
AsF-6	94.245	5.160	0.008	0.057	n.d	0.325	0.205
AsF-7	97.845	1.620	0.202	n.d	n.d	0.050	0.283
AsF-8	85.592	13.739	0.014	0.182	0.0043	0.281	0.188
AsF-9	91.130	8.750	0.006	0.007	n.d	0.047	0.060

have acted as conduits for CO2-enriched, mixed volatile H_2O-CO_2-NaCl fluids and it is considered a primary metallogenetic characteristic.

7.7 Compositions, Bulk Densities and Molar Volumes of Type I and II Inclusions

Bulk compositions, densities and molar volumes of Type I inclusions can be calculated in the system H_2O-CO_2-NaCl based on:

- the clathrate melting temperature
- the CO_2 - phase homogenisation temperature (hence the CO_2 - phase densities)
- the visual volume percent estimate of the CO_2 phases at room temperature.

The molar fractions of H_2O, CO_2 and NaCl, and bulk densities and molar volumes of the examined fluid inclusions were calculated using the FLINCOR (Brown, 1989). Calculated bulk densities range from 0.88 to 0.98 gr.cm^{-3} (median value 0.92) and 0.39 to 0.52 gr.cm^{-3} (median value 0.42) for Types Ia and Ib inclusions respectively (Table 7.2).

Calculated bulk densities range from 0.84 to 0.98 gr.cm^{-3} with median value at 0.91 (Table, 7.3). The presence of a possible maximum of 2.2 molal CO_2 in these H_2O - rich inclusions would decrease the density by 0.03 to 0.05 gr.cm^{-3} (Hendequist and Henley, 1985).

7.8 Fluid Immiscibility and P-T Conditions of Entrapment

Three types of fluid inclusions have been observed in quartz from the Asimotrypes mineralisation:

- Type I, containing liquid H_2O + liquid CO_2 + vapour CO_2 phase, with varying CO_2 to H_2O ratios
- Type II, containing H_2O-rich liquid + vapour phase with liquid > vapour, and
- Type III, decripitated and/or leaked inclusions.

Textural observations suggest that Type A quartz and arsenopyrite, which is the main gold host mineral, have co-precipitated and that the fluids represented by Type I and Type II inclusions are related to the ore-forming event, whereas fluids represented by Type III inclusions are related to the uplift.

The FLINCOR program (Brown, 1989) was used to calculate the pressure at homogenisation for Type I inclusions. Using the Brown and Lamp (1989) equation of state, calculated pressures range from 2.7 to 4.3 kbar and cluster around a median value of 3.3 kbar.

Coexisting Type Ia and Ib inclusions with highly variable CO_2/H_2O-phase ratios which homogenise into the H_2O or CO_2 phase over the same temperature range (Fig. 7.3) strongly suggests the existence of a fluid which has undergone CO_2-H_2O separation prior to or during entrapment as fluid inclusions (Ramboz et al., 1982). The variable phase ratios of Type I inclusions may due to mixed entrapment of variable physical proportions of immiscible H_2O-rich and CO_2-rich

components. In this context the CO_2-rich Type Ib inclusions may represent an end product of complete CO_2-H_2O phase unmixing; Type II inclusions corresponding to the "tail" of the histogram of Figure 7.4 represent continuing effervescence with decreasing temperature depleting the fluid in CO2.

Additional evidence that Type I inclusions represent the products of immiscibility is that the estimated salt contents increase in more H_2O-rich inclusions (Fig.7.6). The higher salinity of H_2O-rich Type Ia inclusions is produced by unmixing of a relatively low salinity, CO_2-H_2O fluid, because salt will preferentially partition into the H_2O-rich liquid rather than into the CO_2-rich vapour (Bowers and Helgeson, 1983b).

Fluid inclusions representing entrapment of immiscible fluids in the H_2O-CO_2-NaCl system should homogenise on the solvus curve corresponding to the specific immiscible fluid compositions at the pressure of entrapment. In the CO_2-H_2O system, the solvus top at 2 kbar is at a temperature of 269 ^{0}C and for a mole fraction of CO_2 of 0.37 (Stemer and Bodnar, 1991). Addition of NaCl to the system raises the crest of the solvus to higher temperatures and broadens its limbs, as illustrated in Figure 7.5 for a content of 6 wt% NaCl relative to the aqueous phase at 2 kbar pressure (Hendel and Hollister, 1981; Bowers and Helgeson, 1983; Gehring, 1986). Included in Figure 7.5 are total homogenisation temperatures obtained on Type I inclusions as a function of their mole % CO_2 content. The overall distribution of data in Figure 7.5 strongly suggest entrapment on a solvus curve. Most data lie between 2 kbar CO_2-H_2O solvus and the CO_2-H_2O 6 wt% NaCl solvus. This is in agreement with the salinities estimated from clathrate melting data of 2.61 to 7.31 equivalent wt% NaCl.

As shown in Tables 7.2 and 7.3 and Figure 7.6, Type Ia inclusions show a trend of increasing salinity with decreasing temperature, whilst Types Ib and II inclusions define the opposite. Such salinity patterns indicate fluid unmixing (Types Ia and Ib) and cooling and dilution (Type II).

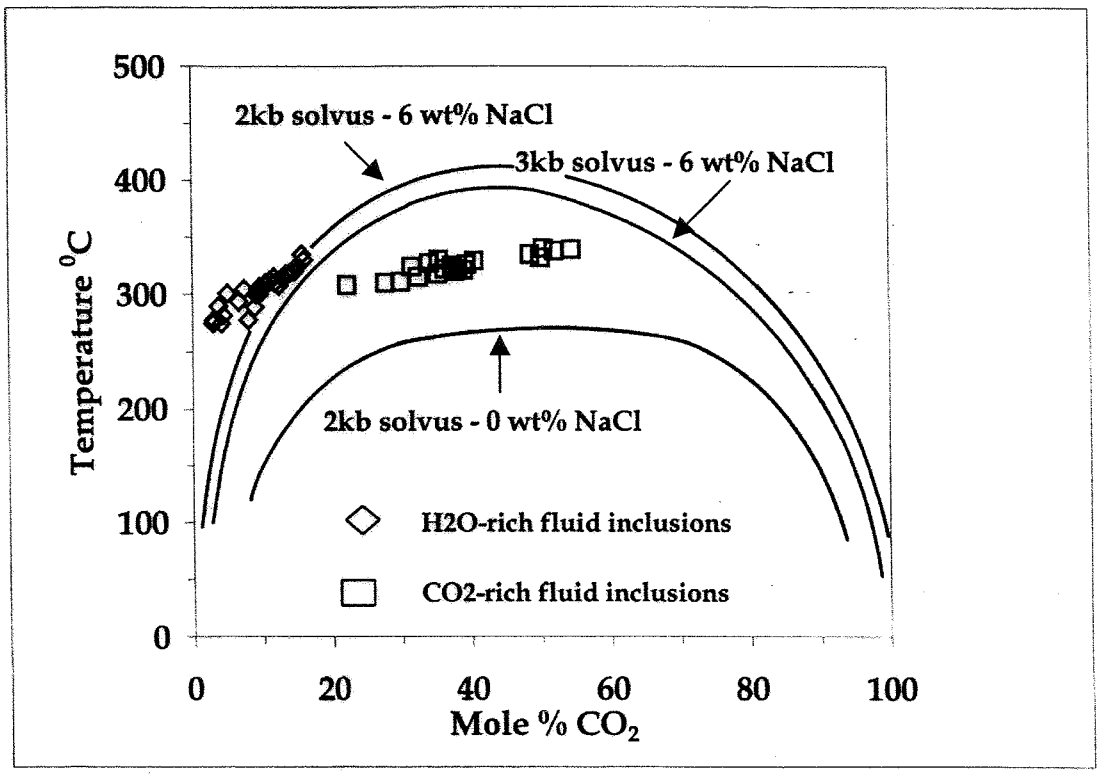

Figure 7.5: Total Homogenisation Temperature versus calculated mole % CO_2 content of Type I inclusions. Also shown are solvi for the H_2O-CO_2 system at 2 kb (Sterner and Bodnar, 1991) and the H_2O-CO_2-NaCl system at 2kb (Bowers and Helgeson, 1983) and 3 kb and 6 wt% NaCl relative to the aqueous phase (Naden and Shepherd, 1989) in Antona et al. (1994).

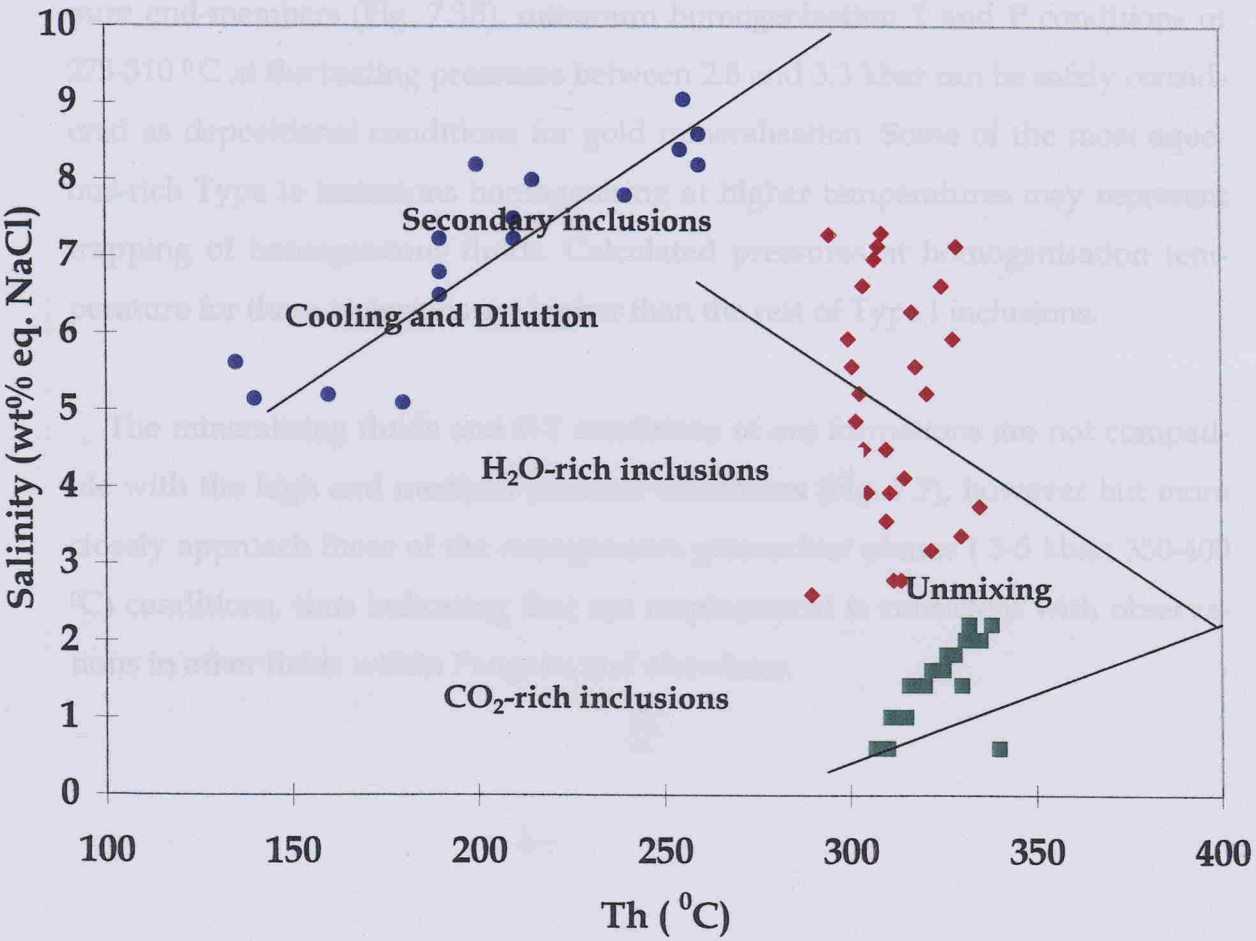

Figure 7.6: Total homogenisation temperatures versus salinity diagram for fluid inclusions from the Asimotrypes ore. CO_2-rich and H_2O-rich inclusions represent unmixing of a low salinity H_2O-CO_2 fluid, whilst secondary fluids record later incursion of more dilute waters.

Since immiscibility has been strongly indicated, fluid inclusion homogenisation conditions represent trapping conditions and thus depositional conditions of Type A quartz and sulphide + gold mineralisation. Considering that for coeval inclusions, the minimum homogenisation temperatures for inclusion homogenisation into the H_2O, and into the CO_2, phases, are provided by inclusions trapping pure end-members (Fig. 7.3B), minimum homogenisation T and P conditions of 275-310 ^{0}C at fluctuating pressures between 2.8 and 3.3 kbar can be safely considered as depositional conditions for gold mineralisation. Some of the most aqueous-rich Type Ia inclusions homogenising at higher temperatures may represent trapping of homogeneous fluids. Calculated pressures at homogenisation temperature for these inclusions are higher than the rest of Type I inclusions.

The mineralising fluids and P-T conditions of ore formations are not compatible with the high and medium pressure conditions (Fig. 7.7), however but more closely approach those of the retrogressive greenschist phases (3-5 kbar; 350-400 ^{0}C) conditions, thus indicating that ore emplacement is consistent with observations in other fields within Pangeon and elsewhere.

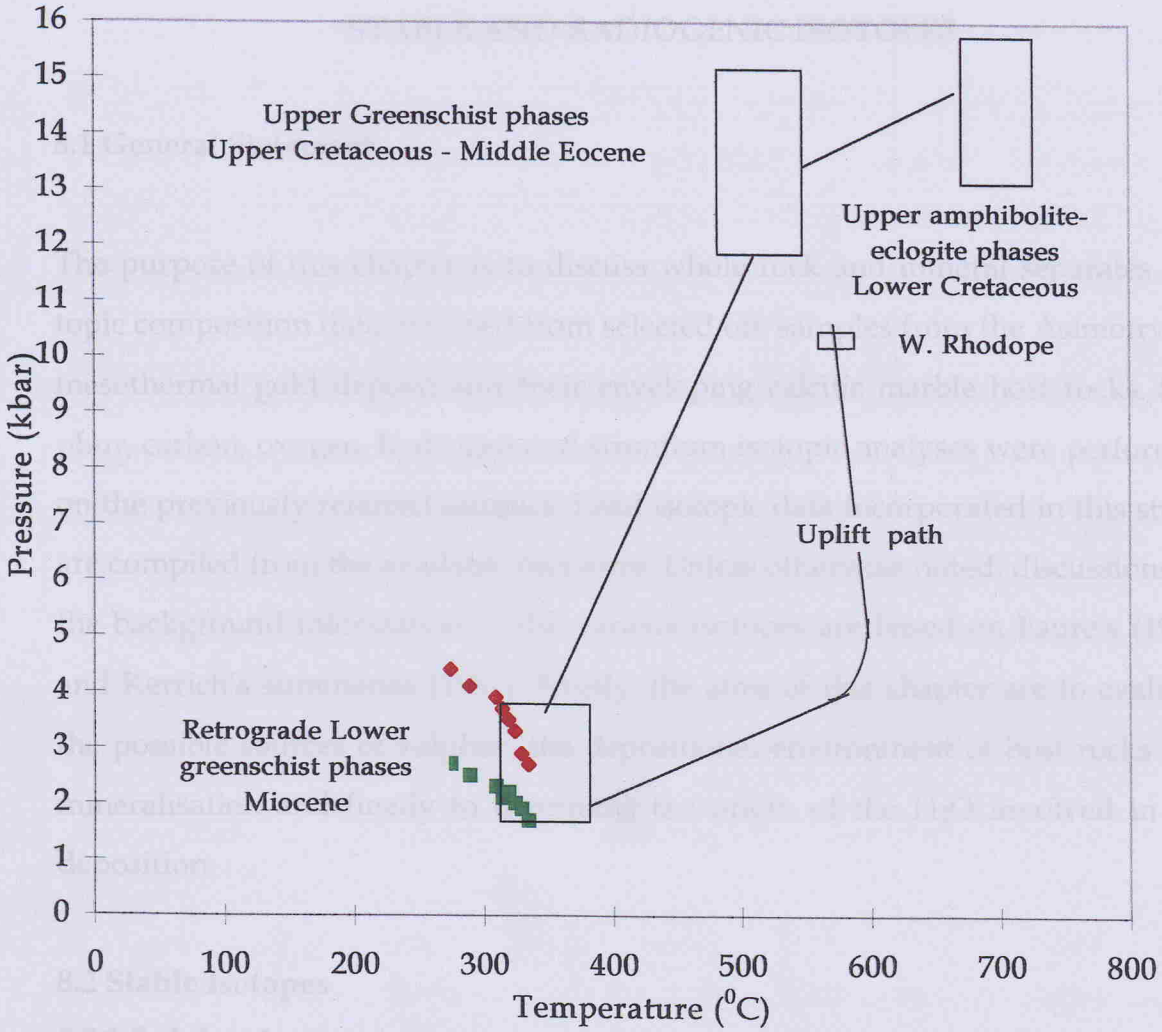

Figure 7.7: Pressure-temperature diagram showing calculated homogenisation conditions for Types Ia and Ib inclusions in relation to inferred regional metamorphic conditions in the Rhodope Massif (Mposkos, 1994).

CHAPTER 8

STABLE AND RADIOGENIC ISOTOPES

8.1 General Statement

The purpose of this chapter is to discuss whole rock and mineral separates isotopic composition data obtained from selected ore samples from the Asimotrypes mesothermal gold deposit and their enveloping calcitic marble host rocks. Sulphur, carbon, oxygen, hydrogen and strontium isotopic analyses were performed on the previously referred samples. Lead isotopic data incorporated in this study are compiled from the available literature. Unless otherwise noted, discussions on the background information of the various isotopes are based on Faure's (1986) and Kerrich's summaries (1987). Finally, the aims of this chapter are to evaluate the possible sources of sulphur, the depositional environment of host rocks and mineralisation and finally to determine the origin of the H_2O involved in ore deposition.

8.2 Stable Isotopes

8.2.1 Sulphur Isotopes

8.2.1.1 Background Information

Sulphur has four stable isotopes with the approximate natural abundance of ^{32}S = 95.02 %, ^{33}S = 0.75 %, ^{34}S = 4.2 % and ^{36}S = 0.017 %. Although some studies have been made on the variation of $^{36}S/\ ^{32}S$ ratios in natural samples, the majority of sulphur isotopic studies deal with the variation of $^{34}S/^{32}S$ ratios. The sulphur isotopic composition of a compound is usually expressed as $\delta\ ^{34}S$ value, which is defined as a per mil deviation of the $^{34}S/^{32}S$ ratio of the compound relative to that of

the troilite phase of the Canyon Diablo meteorite:

$$\delta\ ^{34}S = [\ (^{34}S/^{32}S)_{spl} - (^{34}S/^{32}S)_{std} / (^{34}S/^{32}S)_{std}\ ] \times 10^3$$

Variations in the isotopic composition of sulphur are caused by two kinds of processes: (i) reduction of sulphate ions to hydrogen sulphide by certain anaerobic bacteria which results in the enrichment of hydrogen sulphide in ^{32}S; (ii) various isotopic exchange reactions between sulphur-bearing ions, molecules, and solids by which ^{34}S is generally concentrated in compounds having the highest oxidation state of S, or greatest bond strength (Bachinski, 1969).

Granitic rocks contain S with variable isotopic compositions because the magma from which they crystallised either formed by melting of sedimentary rocks or because the magma was contaminated with S of biogenic origin in the crust. Some plutonic and volcanic igneous rocks of basaltic composition also contain fractionated S. It is unlikely that such variations are attributable to differences in the isotopic composition of S in the mantle. Instead, they can be caused by (i) contamination of magma with crustal S in a process called sulphurisation; (ii) alteration by seawater; and (iii) outgassing of SO_2 from the magma at different oxygen fugacities.

One of the principal objectives of the study of S isotopes in geology is to contribute toward a better understanding of the origin and conditions of formation of sulphide ore deposits. The origin of sulphur in ore deposits is defined by the calculated isotopic composition of the total sulphur in solution ($\delta\ ^{34}S_{\Sigma S}$). Based on the summaries of $\delta\ ^{34}S_{\Sigma S}$ data for 15 representative hydrothermal ore deposits made by Rye and Ohmoto (1974), the $\delta\ ^{34}S_{\Sigma S}$ values fall into three groups. One group has slightly positive $\delta\ ^{34}S_{\Sigma S}$ values, the second has values between 5 and 15 per mil, and the third has average values near 20 per mil. These groups reflect the three major sources of sulphur in hydrothermal ore deposits.

Deposits such as Providencia and Casapalca that have $\delta\ ^{34}S_{\Sigma S}$ values near 0 per mil are associated with felsic igneous rocks. Their sulphur was probably derived from igneous sources, which include sulphur released from silicate melts and sulphur leached from sulphides in igneous rocks. Igneous sulphur must be derived either from the upper mantle or from the homogenisation of large volumes of deeply buried or subducted crustal material.

Deposits such as Kuroko, Echo Bay, and Pine Point have $\delta\ ^{34}S_{\Sigma S}$ values close to that of sea-water sulphates. The sulphur in these deposits was most likely derived either from ocean water, as at the Kuroko and Echo Bay deposits, or from marine evaporites, as at Pine Point.

Deposits such as Cortez and the Black Hills Tertiary deposits whose fluids have intermediate $\delta\ ^{34}S_{\Sigma S}$ values probably collected their sulphur from local country rocks -from either disseminated sulphides or older ore deposits. The sulphur in the Bluebell deposit was probably a mixture of sulphur from evaporites and sedimentary sulphides. Rye and Ohmoto (1974) determined the proposed source of sulphur in each of these deposits by the relationship of the time and space distribution of their $\delta\ ^{34}S_{\Sigma S}$ values to geologic details. The range of $\delta\ ^{34}S_{\Sigma S}$ values in deposits where sulphur is derived from sedimentary or mixed sources can be large or small depending on the extent to which the sulphur was homogenised by the ore-generating event. The reasonably narrow range of $\delta\ ^{34}S_{\Sigma S}$ values for the Bluebell fluids indicates that the different sulphur components were fairly well mixed in the hydrothermal solutions.

The previous discussion is related to the principles of application of sulphur isotope data to undisturbed ore deposits. The question is what happens to sulphur isotope distributions in sulphide minerals during metamorphism. Several detailed studies on metamorphosed stratiform deposits have been published and two principles of sulphur isotope distribution during metamorphism of these deposits are summarised by Rye and Ohmoto (1974). These principles are:

(i) Large - scale premetamorphic $\delta\ ^{34}S$ variations are generally preserved. The average $\delta\ ^{34}S$ for sulphides in major units such as formations are generally not changed.

(ii) Small scale sulphur isotope changes are in many cases superimposed upon the original sulphur isotope distribution during metamorphism. These include: (a) redistribution of sulphur isotopes among coexisting minerals that define the temperature of metamorphism, and (b) local $\delta\ ^{34}S$ variations which reflect the structural or chemical metamorphic history.

These principles can be illustrated from the data for the Homestake, South Dakota, gold deposit (Rye and Rye, 1974). The ore occurs mainly in the Homestake formation and sulphides also occur in the overlying Ellison and underlying Poorman formations. Each formation has a distinct lithology and the $\delta\ ^{34}S$ distribution is 6-10 ‰ , 4 -30 ‰ and 3-5 ‰ respectively. Stratigraphic dependence of $\delta\ ^{34}S$ values in metamorphosed sulphide deposits has also been observed in the massive sulphide deposits at Bathust, New Brunswick (Lusk, 1972), and Ducktown, Tennessee (Mauger, 1972). The fact that original large-scale $\delta\ ^{34}S$ were retained in these deposits indicates that large amounts of sulphur were added to and not subtracted from the system during metamorphism and that remobilization of sulphur was restricted to a small scale during metamorphism.

8.2.1.2 Analytical Results

Ten representative sulphide samples from the 3K-D and 3K-H adits at Asimotrypes were collected for sulphur isotope analysis.

The sulphur isotope results are presented in Table 8.1. The $\delta\ ^{34}S$ values for arsenopyrite, pyrite and chalcopyrite from the Asimotrypes deposit are 2.19 to 2.89, 2.28 to 3.13 and 2.17 to 2.24 per mil respectively. No significant variations are observed within the Asimotrypes gold deposit, and the mean $\delta\ ^{34}S$ for the sulphides is 2.54 per mil $\pm$ 0.29 (1σ). Microscopic textural evidence from this study indicates

Table 8.1:Sulfur Isotope Ratios of Sulfide Minerals from the Asimotrypes area, Pangeon

		Sulfide Sulfur isotope compositions (CDT in per mil)		
Sample No	Remarks	δ^{34} S asp	δ^{34} S py	δ^{34} S cpy
As-11		2.82		
As-14	Coexisting sulfides	2.72	2.47	
As-16		2.19		
As-19		2.58		
As-21	Coexisting sulfides	2.82	2.28	
As-37			3.13	
As-44			2.38	2.17
As-46			2.31	2.24
As-71	Coexisting sulfides	2.89	2.35	
As-72	Coexisting sulfides	2.77	2.42	

Abbreviations: asp=arsenopyrite, py=pyrite, cpy=chalcopyrite

that arsenopyrite and pyrite were deposited contemporaneously and, hence sulphur isotopic equilibrium might have existed between them. Also, the Δ Asp-Py fractionation values, for all arsenopyrite and pyrite separates that have been analysed, are similar with a range from 0.25 to 0.54 and mean value of 0.39 per mil, and these small differences indicate that isotopic equilibrium did exist between arsenopyrite and pyrite. Theoretical (Sakai, 1968) and experimental studies (Kajiwara and Krouse, 1971), indicate that under isotopic equilibrium conditions $\delta\ ^{34}S$ py > $\delta\ ^{34}S$ cpy. The samples analysed in this study (Table 8.1) follow this trend suggesting that isotopic equilibrium was attained. The extent to which isotopic equilibrium has been attained cannot be evaluated by utilising the various plotting techniques of Smith et al. (1977, 1978) and Shelton and Rye (1982) because of the limitations of the available data.

$\delta\ ^{34}S$ values of primary sulphide minerals from the Asimotrypes ore have a mean value of 2.54 which is generally considered characteristic for a felsic igneous rock source for the sulphur (Ohmoto, 1972; Rye and Ohmoto, 1974).

Fluid temperatures were calculated from the pyrite-chalcopyrite pair in equilibrium using the Ohmoto and Rye (1979) equations. Calculated temperature is in the range of 274 ^{0}C. The validity of the estimates of depositional temperatures on the basis of minimum fluid inclusion (Th) between 270 ^{0}C and 280 ^{0}C, is supported by independent estimates of 274 ^{0}C of the pyrite-chalcopyrite equilibrium sulphur isotope pairs. The excellent fit of the minimum fluid inclusion homogenisation temperatures (270 ^{0}C to 280 ^{0}C) with the deposition temperatures determined from sulphur isotopes, indicate that a formation pressure of 3.3 kbar is acceptable for the Asimotrypes gold ore.

The absence of sulphate minerals at Asimotrypes is characteristic of Mesozoic mesothermal gold deposits (Taylor, 1987) and suggests that H_2S was the dominant sulphur species in the ore fluid (Ohmoto and Rye, 1979). From diagrams showing the relationship between oxygen fugacities and pH, and between log S^{34}

H_2S and pH, for specific sulphide $\delta\ ^{34}S$ values (Ohmoto, 1972; 1985), upper limits for fo_2 at 10^{-31} and for pH at 6.5 are obtained for $\delta\ ^{34}S_{\Sigma S} = 0$ per mil and $\Sigma S \leq 0.01$ moles/ kg H_2O (Ohmoto, 1985).

8.2.2 Carbon Isotopes

8.2.2.1 Background Information

Carbon has two stable isotopes: $^{12}C = 98.89$ % and $^{13}C = 1.11$ %. In addition radioactive ^{14}C occurs in nature due to its formation in the upper atmosphere.

The carbon isotopes are fractionated by a variety of natural processes, including photosynthesis and isotope exchange reactions among carbon compounds. Photosynthesis leads to enrichment of ^{12}C in biologically synthesised organic compounds. On the other hand, isotope exchange reaction between CO_2 gas and aqueous carbonate species tend to enrich carbonates in ^{13}C. As a result, the isotopic abundance of ^{13}C in terrestrial carbon varies by about 10 %.

The isotopic composition of carbon is expressed in terms of the delta notation used also for oxygen and hydrogen and it is defined by the parameter:

$$\delta\ ^{13}C = [\ (^{13}C/^{12}C)_{spl} - (^{13}C/^{12}C)_{std} / (^{13}C/^{12}C)_{std}\ ] \times 10^3$$

The reference standard is CO_2 gas obtained by reacting belemnites of the Peedee Formation with 100 percent phosphoric acid, that is, the PDB standard of the University of Chigago.

The principles of the application of carbon isotope data to hydrothermal ore deposits are similar to those of sulphur. The carbon content of hydrothermal ore deposit is represented primarily by carbonates of calcium, magnesium, iron and manganese and by CO_2 and CH_4 gas in fluid and gaseous inclusions in ore and gangue minerals.

The isotopic composition of carbon in hydrothermal carbonates depends not only on the $\delta^{13}C$ of the total carbon in the ore-bearing fluid but also on the fugacity of oxygen, the pH, the temperature, the ionic strength of the fluid, and on the total concentration of carbon. These relationships have been investigated by (Ohmoto, 1972) and were reviewed by Rye and Ohmoto (1974). The dependence arises from the fact that various physical and chemical parameters control the concentrations of different carbon-bearing ions and molecules, which fractionate carbon isotopes depending on the temperature. A change in any one of the above physical or chemical parameters affects the chemical equilibrium by which the ions and molecules are related and thereby also changes their isotopic composition.

In order to determine the carbon isotope composition of the fluids from which ores actually precipitated, we need to have $\delta^{13}C$ analyses of total carbon, usually CO_2 , in fluid inclusions. Available analyses for $\delta^{13}C$ in CO_2 in fluid inclusions for a number of hydrothermal ore deposits range from about -4 to -12 per mil (Rye and Ohmoto, 1974). In these analysed samples $\delta^{13}C_{CO2} \cong \delta^{13}C_{\Sigma C}$, so the data reflect the carbon isotopic composition of the hydrothermal fluids. The ranges of $\delta^{13}C$ values for the major reservoirs of carbon in hydrothermal systems are:

(i) marine limestones, which have average $\delta^{13}C$ values near 0 per mil

(ii) deep-seated carbon, which has an average $\delta^{13}C$ value of about -7 per mil as indicated by analyses of carbonatites, and

(iii) reduced or organic carbon in sediments which normally has $\delta^{13}C$ values of less than -15 per mil.

In low-temperature environments where bacteriogenic sulphides are produced, anaerobic bacteria also produce CO_2 and CH_4 from the associated organic matter, which they consume as an energy source (Cheney and Jensen, 1965). Depending upon the depositional environment and the proportion of carbonate derived from CO_2 and CH_4, precipitated carbonates may show a wide and random spread of variations in $\delta^{13}C$ values, including some large negative values. Very

large negative $\delta^{13}C$ values, however, can also be produced in syngenetic carbonates in volcanic environments by the refluxing of organic carbon from restricted ocean basins, and a wide range of $\delta^{13}C$ values can be produced in the carbonates by changes in the fo_2 of the depositional environment or by mixing of refluxed organic carbon with marine or deep-seated carbon (Rye and Rye, 1974).

Preliminary carbon isotope data from Precambrian iron carbonates in the Homestake gold deposit indicate that no significant change in average $\delta^{13}C$ values of major units occurred during metamorphism (Rye and Rye, 1974). Detailed studies of marbles representative of a wide range of metamorphic grades, including marbles in anatectic granites, indicate that $\delta^{13}C$ values of carbonates are, in general, little changed during regional metamorphism events, when the metamorphic fluid/rock ratios are high and the fluids are CO_2-rich. Exceptions may occur, where the marbles have been decarbonated (Rye and Ohmoto, 1974).

The possible sources for CO_2 in ore-forming fluids with respect to $\delta\ ^{13}C$, suggested by various authors, are as follows:

- Metamorphic decarbonation or dissolution reactions of carbonate (Ohmoto and Rye, 1979). The $\delta\ ^{13}C$ value of such a metamorphic fluid will depend on: (1) the degree of decarbonation or dissolution, (2) the $\delta\ ^{13}C$ value of the carbonate minerals, and (3) the isotopic fractionation factor between CO_2 and the carbonate mineral which is temperature dependent (Ohmoto, 1986). According to Bottinga (1968) and Kerrich (1990) CO_2 liberated by such reactions at 400^0 and 500 ^0C would be enriched by about 3 per mil relative to the source. Carbon isotopic ratios of Greek marbles range from -2 to +6 per mil, with most values clustering between 0 and +4 per mil (German et al., 1980). Consequently, liberated CO_2 can be expected to have $\delta\ ^{13}C$ values ≥ 0 per mil. In addition carbon isotope data for calcites in synvolcanic sea-floor alteration of basaltic origin, metamorphosed to low amphibolite or low- to mid-greenschist facies indicate $\delta\ ^{13}C$ values ranging from -2.1 to +1.4 per mil (Groves et al., 1988). Considering that high-temperature disso-

lution in such low-carbonate rocks produces CO_2 that is isotopically similar to or slightly heavier than the original carbonate (Ohmoto and Rye, 1979) sea floor carbonate may produce $\delta\ ^{13}CO_2$ close to 0 per mil. Ohmoto (1986) has calculated that under most geologic conditions the $\delta\ ^{13}C$ of CO_2 derived from carbonate rocks may fall between -8 and +4 per mil.

- Oxidation of organic carbon in the rocks during metamorphism. According to Schidlowski (1988) the bulk of $\delta\ ^{13}C$ values for organic carbon are -26 ± 7 per mil throughout the geologic record. Also $\delta\ ^{13}C$ from -1 to -5 per mil might be expected if CO_2 from a decarbonation source exchanged with graphite or mixed with CO_2 resulting from oxidation of graphite. However, mass balance calculations indicate that rather large amounts of graphite are needed to bring the $\delta\ ^{13}C$ of decarbonation down to values between -1 and -5 per mil (Kreulen, 1980).

- CO_2 may be of deep seated origin and represent either juvenile CO_2 , possibly derived from degassing of the upper mantle (Touret, 1981), or magmatic CO_2 (Ohmoto and Rye, 1979; Taylor, 1986). Juvenile CO_2 is generally accepted to have $\delta\ ^{13}C$ values between -3 and -8 per mil based on isotopic analyses of carbonatites (Deines and Gold, 1973), and diamonds (Deines, 1980; Milledge et al., 1983). The characteristic $\delta\ ^{13}C$ of most magmatic-melt carbon is generally considered as being between -8 and -5 per mil (Taylor, 1986). CO_2 - melt fractionations are approximately 3 per mil such that magmatic CO_2 is -5 to -2 per mil (Taylor, 1986). Kreulen (1980), in a study of the Naxos metamorphic terrain in Greece, identified a population of CO_2 - rich fluids occurring in low-grade to high-grade schists, and pegmatites, with $\delta\ ^{13}C$ values of -5 to -1 per mil, as probably deep seated origin.

8.2.2.2 Analytical Results.

Fifteen representative calcite samples from the Asimotrypes area were collected along a profile away from the arsenopyrite-pyrite ore on the main thrust zone between gneisses and sheared marbles, at a distance from a few cm up to 50 m

from the ore and subsequently were analysed for their ^{13}C isotopic composition.

The results of the carbon isotope analyses are given in Table 8.2. Carbon isotope values are remarkably constant over a narrow range between 1.89 to 2.94 per mil and median value 2.54 ± 0.34 (1σ). The constancy of the $\delta\ ^{13}C$ values shows that fugacities were well above the H_2CO_3 / CH_4 equal concentration boundary. This implies that log oxygen fugacities were most probably within the range -30 to -32 at 312 ^0C (Ohmoto, 1972; Steed and Morris, 1997). Fluid inclusion studies showed that CO_2 was a major constituent in the ore fluids. In these circumstances $\delta\ ^{13}C$ for CO_2 (or H_2CO_3 apparent) will be essentially the same as for total carbon in the ore fluid. The fractionation equation for calcite-CO_2 presented by Friedman and O' Neil (1977) at 275 ^0C and 340 ^0C , suggests that the $\delta\ ^{13}C$ in the ore fluid was 4.12 ± 0.35 (±) and 4.68 ± 0.35 (1σ) respectively during the ore deposition stage.

$\delta\ ^{13}C$ isotope data of 2.54 ± 0.34 (1σ) per mil is consistent with a marine environment of deposition for the Asimotrypes marbles that is commonly associated with $\delta\ ^{13}C$ of 0 ± 4 per mil (Veizer and Hoefs, 1976; Ohmoto and Rye, 1979). A plot of the $\delta\ ^{13}C$ versus $\delta^{18}O$ values of calcite is illustrated in Figure 8.1, and it is also suggesting a marine environment of deposition (Ohmoto and Rye, 1979; Faure, 1986; Kerrich, 1987). In addition, field data (thickness and banding of marbles), Sr geochemistry (Chapter 6) and isotopic composition (later in this Chapter) also indicate a marine environment of deposition for the Asimotrypes marbles.

The rather high $\delta\ ^{13}C$, above +2 per mil suggests a shallow sea and warm climate conditions (Woo et al. 1992). Evaporation of seawater increases the $\delta\ ^{18}O$ values, but on the other hand , higher temperatures lowers the fractionation between the water and carbonates. Increased temperatures, however, explain the carbonate $\delta\ ^{13}C$ values, which are increased by +1 to +2 per mil.

Table 8.2 : Carbon Isotope Composition of Calcite and Corresponding Equilibrium in Fluids at 275 ^{0}C and 340 ^{0}C from Ore-host Marbles, Asimotrypes area, Pangeon

Sample	Rock Type	$\delta^{13}C_{PDB}$ per mil	$\delta^{13}C_{PDB}$ FLUID[1] per mil	
			275 ^{0}C[2]	340 ^{0}C[2]
As-1	Impure calcitic marble, Type I, 20cm from ore	2.67	4.44	4.77
As-4	Impure calcitic marble, Type I, hanging wall	2.57	4.14	4.67
As-5	Impure calcitic marble, Type I, 5m above ore	2.88	4.45	4.98
As-7	Fresh, impure calcitic marble,Type I, 10m above ore	2.59	4.16	4.69
As-9	Impure calcitic marble, Type I, 5m east of ore	2.49	4.06	4.59
As-12	Impure calcitic marble, Type I, 8m from ore, inside adit	2.61	4.18	4.71
As-18	Dedolomitic marble, Type VI,15 m west of adit 3K-D	2.94	4.51	5.04
As-22	Dedolomitic marble, Type VI, 15 m west of adit AS-4	2.92	4.49	5.02
As-23	Fine-medium grain. marble, Type II, 6m west AS-4	2.94	4.51	5.04
As-32	Impure calcitic marble, Type I, in contact with granite	2.11	3.68	4.21
As-50	Coarse calcitic marble,Type IV, 735m elevation	1.90	3.47	4.00
As-52	Recrystallized dedolomitic marble, Type VI	1.89	3.46	4.19
As-53	Fine grained impure calcitic marble, Type I	2.60	4.17	4.90
As-54	Impure calcitic marble, Type I	2.61	4.18	4.91
As-56	Dedolomitic marble, Type VI	2.47	4.04	4.77

[1] Fractionation equation of Friedman and O' Neil (1977)

[2] T (^{0}C), based on fluid inclusion microthermometry (Table 7.2)

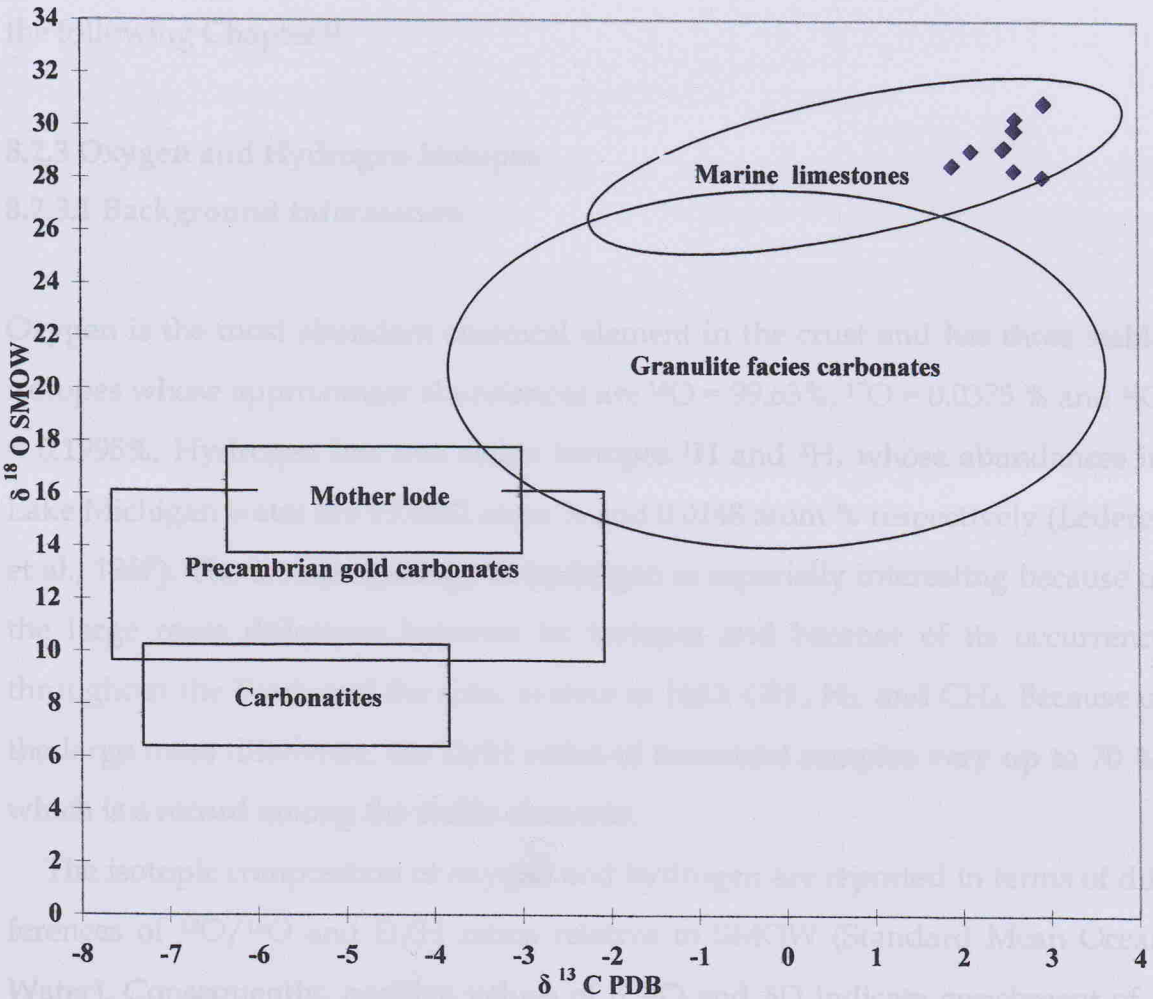

Figure. 8.1: Variation diagram for $\delta^{18}O$ versus $\delta^{13}C$. Precambrian gold carbonates from Kerrich (1989), Mother Lode carbonates from Weir and Kerrick (1987), Taylor (1986) and Rosenbaum and Taylor (1984); fields for granulite-facies carbonates, Phanerozoic marine limestones and carbonatites from Valley (1986).

Finally, $\delta\ ^{13}C$ values in the fluid of 4.68 ± 0.35 (1σ) (Table 8.2) are consistent with CO_2 of metamorphic origin produced during metamorphic decarbonation reactions of carbonate rocks (Ohmoto and Rye, 1979). This interpretation is in agreement with de-dolomitisation processes in marbles as these are discussed in the following Chapter 9.

8.2.3 Oxygen and Hydrogen Isotopes

8.2.3.1 Background Information

Oxygen is the most abundant chemical element in the crust and has three stable isotopes whose approximate abundances are ^{16}O = 99.63%, ^{17}O = 0.0375 % and ^{18}O = 0.1995%. Hydrogen has two stable isotopes ^{1}H and ^{2}H, whose abundances in Lake Michigan water are 99.9852 atom % and 0.0148 atom % respectively (Lederer et al., 1967). The isotope geology of hydrogen is especially interesting because of the large mass difference between its isotopes and because of its occurrence throughout the Earth and the solar system in H_2O, OH^-, H_2, and CH_4. Because of the large mass difference, the D/H ratios of terrestrial samples vary up to 70 %, which is a record among the stable elements.

The isotopic composition of oxygen and hydrogen are reported in terms of differences of $^{18}O/^{16}O$ and D/H ratios relative to SMOW (Standard Mean Ocean Water). Consequently, positive values of $\delta\ ^{18}O$ and δD indicate enrichment of a sample in ^{18}O and D compared to SMOW, whereas negative values imply depletion of those isotopes in the sample relative to the standard.

The isotopic compositions of oxygen and hydrogen of a sample are expressed as per mil differences relative to SMOW:

$$\delta\ ^{18}O = [\ (\ ^{18}O/^{16}O\ )_{sp1} - (\ ^{18}O/^{16}O\ )_{smow} / (\ ^{18}O/^{16}O\ )_{smow}\ ]\ X\ 10^3$$

$$\delta\ D = [\ (\ D/H\ )_{sp1} - (\ D/H\ )_{SMOW} / (\ D/H\ )_{SMOW}\ ]\ X\ 10^3$$

Two methods are utilized to determine $^{18}O/^{16}O$ and D/H ratios of natural hydrothermal fluids: (i) direct measurement of the fluid itself in a geothermal area or fluid inclusions in the minerals of an ore deposit, and (ii) isotopic analyses of minerals, calculation of temperatures of formation utilizing various geothermometers, and finally, calculation of D/H and $^{18}O/^{16}O$ ratios of waters in equilibrium with the assemblages at their temperatures of formation.

Water is the dominant constituent of ore-forming fluids and the knowledge of its origin is fundamental to any theory of ore formation. The ultimate source of the H_2O can be best deciphered by studying some geochemical parameter based on the water molecules themselves. Stable isotope analyses provide just such a parameter, because natural waters of various origins exhibit systematic differences in their deuterium and ^{18} O contents. At present the most useful application lies in using D/H and $^{18}O/^{16}O$ analyses as indicators of the origin and history of the H_2O in hydrothermal fluids. Hydrothermal fluids may have originated as meteoric water, sea water, geothermal waters variously enriched in ^{18}O, connate or formation waters with variable δ D and $\delta^{18}O$ values, metamorphic and magmatic waters as well as mixtures of several of the above. Mixing of waters of different sources in fact seems to be one of the most characteristic features of ore deposition and hydrothermal alteration in a number of localities world-wide.

The $\delta^{18}O$ and δ D of average modern meteoric waters are related by the meteoric line equation:

$$\delta D = 8\,\delta^{18}O + 10 \quad (1)$$

Local extremes in temperature, relative humidity and evaporation rate will change the slope of the above equation (1). Any change in the $\delta^{18}O$ of seawater (relative to SMOW) however, would have been accompanied by corresponding shift in the intercept of equation (1).

Seawater refers to water from open oceans unchanged by local evaporation (which enriches the water in D and ^{18}O) or admixture of fresh waters (which decreases the δ D and $\delta^{18}O$ seawater). Sheppard (1986) summarised the modern range in δ-values as δ D from -7 to +5 per mil, and $\delta^{18}O$ from -1.0 to +0.5.

Formation waters include the common oil-field brines, as well as waters of variable salinity often referred to as connate waters. Formation waters from various basins trend away from the meteoric water line towards higher oxygen and hydrogen isotope values. Samples at the highest temperatures and with the highest salinities are normally more enriched in ^{18}O and D. The coolest, least saline waters within a given basin generally have the lowest $\delta^{18}O$ and δ D values. Formation waters from sedimentary basins at high latitudes tend to plot along trends that intersect the meteoric water line at lower $\delta^{18}O$ and δ D values than formation waters from basins located at lower latitudes. This systematic behaviour strongly suggests that meteoric water comprise an important fraction of the formation waters in such basins.

Metamorphic water is defined as water associated with, or in equilibrium, with metamorphic rocks during metamorphism. It has long been recognised that during contact metamorphism, waters of dehydration, pre-intrusion pore fluids, meteoric water and magmatic water may all be involved to various degrees (Valley, 1986). A wide range of $\delta^{18}O$ values (+5 to +25 per mil) is often attributed to metamorphic water (Taylor, 1979), reflecting a wide range in both metamorphic temperatures and isotopic compositions of metamorphic rocks. The δ D values for metamorphic fluids in general may range from ≈ 0 to -70 per mil. Devolatilisation can be modelled as either continuous (closed system) or fractional (Rayleigh; open-system) devolatilisation, but with a changing bulk fluid-rock fractionation factor (Valley, 1986).

Magmatic fluids are those volatile compounds of H, C, and S which exsolve from magmas, usually as H_2O, CO_2, SO_2, and H_2S. The isotopic composition of

these volatiles varies as a function of both source material and isotopic fractionation during degassing (Taylor, 1986). The term juvenile water refers to water, which has never passed through the hydrologic cycle. The solubility of water in mafic and ultramafic magmas is small and its contribution to the crustal reservoir is probably insignificant.

The $\delta^{18}O$ values of magmatic water is typically assumed to be in the range of +5.5 to +10 per mil (Taylor, 1979). The δ D of magmatic water varies during degassing , resulting in a positive correlation between δ D and the residual water content of igneous rocks (Taylor ,1986). The initial δ D of magma is defined as the δ D value of the magma prior to any degassing. The subsequent variation in δ D value of the magma and the exsolved H_2O depends on whether the degassing is dominantly an open- or closed-system process (Taylor, 1986). The δ D value of the first exsolved water will be approximately 20 to 25 per mil enriched relative to the bulk magma. The δ D of most of the water exsolved from many felsic melts is in the range of -30 to -60 per mil, but the associated magmatic rocks may be significantly depleted.

The δ D value of a magma is generally determined by its source material plus any crustal material assimilated during emplacement of the magma; direct contamination by non-magmatic waters appears to be rare. For most felsic magmas, magmatic water represents recycled water derived primarily from the melting of hydrous crust (largerly fractionated seawater, Magaritz and Taylor, 1976). Water associated with mafic magmas appears to have somewhat lower δ D values -50 to -70 per mil than that associated with felsic magmas. The δ D value of apparently unaltered MORB is approximately -80 ± 10 per mil (Kyser and O'Neil, 1984).

Much progress has been made in measuring oxygen and hydrogen fractionation factors between minerals and water at varying temperatures. Equations expressing isotope fractionation of oxygen and hydrogen between minerals and water over a range of temperature can be combined to give mineral isotope-thermometry equations. In general, the minerals of volcanic rocks indicate rea-

sonable temperatures of crystallisation while those of plutonic rocks yield lower temperatures due to re-equilibration of oxygen isotopes during slow cooling.

The differences in $\delta\ ^{18}O$ of minerals in metamorphic rocks generally decrease with increasing grade of metamorphism. Temperatures calculated from mineral pairs are concordant and also increase with metamorphic grade. However, they do not necessarily reflect the maximum temperatures because of reequilibration during cooling. This effect is particularly noticeable in high-grade metamorphic rocks and minerals, such as calcite and feldspar, which equilibrate oxygen isotopes rapidly.

The volume of rock within which oxygen isotopes are re-equilibrated by exchange with an aqueous fluid or with CO_2 during metamorphism depends on the permeability of the rocks. The development of fractures enhances the opportunity for isotope exchange in large volumes of rocks. In the absence of adequate permeability, large isotopic differences may persist over short distances.

8.2.3.2 Analytical Results

Oxygen Isotopes

δ^{18} O values for marble calcites are closely grouped, with a range of 28.11 to 30.93 per mil SMOW, with a median value of 29.31 ± 0.94 (1σ) per mil and are presented in Table 8.3. Oxygen isotopic values of around 30 per mil are considered as metamorphic oxygen values (Taylor, 1979). The range of marble δ^{18} O values could be either a primary oxygen isotopic range caused by increased temperature conditions during carbonate deposition or caused by weathering at an ancient sub-surface. Equilibrium isotopic fractionation in the system calcite -water implies that the δ^{18} O in the fluid was 22.94 ± 0.93 (1σ) per mil and 24.77 ± 0.93 (1σ) per mil for 275 ^{0}C and 340^{0}C respectively. These values clearly imply a metamorphic origin of the ore fluids (Sheppard, 1986).

Table 8.3 : Oxygen Isotope Data of Calcite and Corresponding Equilibrium in Fluids at 275 ^{0}C and 340 ^{0}C from Ore-host Marbles, Asimotrypes area, Pangeon

Sample	Rock Type	δ^{18}O SMOW per mil	δ^{18}O SMOW FLUID [1] per mil	
			275 ^{0}C[2]	340 ^{0}C[2]
As-1	Impure calcitic marble, Type I, 20cm from ore	29.93	23.56	25.43
As-4	Impure calcitic marble, Type I, hanging wall	28.41	22.05	23.91
As-5	Impure calcitic marble, Type I, 5m above ore	28.44	22.08	23.94
As-7	Fresh, impure calcitic marble,Type I, 10m above ore	29.92	23.55	25.42
As-9	Impure calcitic marble, Type I, 5m east of ore	29.23	22.86	24.73
As-12	Impure calcitic marble, Type I, 8m from ore, inside adit	30.32	23.95	25.82
As-18	Dedolomitic marble, Type VI,15 m west of adit 3K-D	30.93	24.56	26.43
As-22	Dedolomitic marble, Type VI, 15 m west of adit AS-4	28.11	21.75	23.61
As-23	Fine-medium grain. marble, Type II, 6m west AS-4	30.88	24.51	26.26
As-32	Impure calcitic marble, Type I, in contact with granite	29.09	22.72	24.59
As-50	Coarse calcitic marble,Type IV, 735m elevation	28.54	22.17	23.92
As-52	Recrystallized dedolomitic marble, Type VI	28.51	22.14	23.89
As-53	Fine grained impure calcitic marble, Type I	28.35	21.99	23.85
As-54	Impure calcitic marble, Type I	29.86	23.49	25.24
As-56	Dedolomitic marble, Type VI	29.18	22.81	24.56

[1] Fractionation equation of Friedman and O' Neil (1977)

[2] T (^{0}C), based on fluid inclusion microthermometry (Table 7.2)

Taking into account the remarkably constant carbon isotope values for the same samples it is suggested that replacement of the marbles by the sulphides obviously took place along sharply restricted zones, e.g. fault planes channelling the metal bearing fluids. Directly outside the channel zones only weak, if any, oxygen isotopic exchange between the marble and the fluids occurred, with the carbon isotopic signature remaining undisturbed.

Quartz δ^{18} O values consistently lie between 20.82 and 22.58 per mil with a mean value of 21.87 ± 0.52 (1σ) and are presented in Table 8.4. The quartz-water fractionation of Matsuhisa et al., (1979) was used to derive the oxygen isotopic composition of the hydrothermal fluid which equilibrated with quartz at 275^0 and 340 ^{0}C from the trapping and hence deposition temperatures derived from fluid inclusion studies (Table 7.2).The calculated fluid values range between 13.01 and 14.77 per mil with a mean value of 14.06 ± 0.52 (1σ) at 275^0 and 15.25 and 17.01 per mil with a mean value of 16.31± 0.52 (1σ) at 340 ^{0}C. These compositions are consistent with values of metamorphic fluids (3 to 20 per mil, Sheppard, 1986). The δ^{18} O of the hydrothermal fluids reflects the original isotopic composition of the source fluid modified by mixing of fluids, unmixing (immiscibility), fluid rock reactions, or by any other chemical change of the fluid. Immiscible separation of CO_2 is a consistent feature of most mesothermal lode gold deposits (Robert and Kelly, 1987). Separation of gaseous CO_2 from an H-C-O fluid may act to perturb isotopic relationships in hydrothermal systems. Higgins and Kerrich (1982) have calculated that separation of 20 mole % CO_2 at 300 ^{0} C would induce a 3 per mil depletion in the residual fluid, given a $CO_{2\,(gas)}$ - $H_2O_{(liquid)}$ fractionation of 14 per mil at this temperature (Bottinga, 1968). Differences between single-stage quantitative separation and Rayleigh fractionation are only apparent for fluids where the molar proportion of CO_2 is in excess of 35 percent. Smith and Kesler (1985) estimate that the molar proportions of CO_2 are in the range of 1 to 12 per cent, such that the magnitude of the effect is restricted to <-2 per mil. This in turn, is consistent with the previously discussed uniformity of the quartz δ^{18} O values.

Table 8.4 : Quartz and Silicate Oxygen Isotope Data and Corresponding Equilibrium in Fluids at 275 ^{0}C and 340 ^{0}C, Asimotrypes area, Pangeon

Sample	Mineral	δ^{18} O SMOW per mil	δ^{18} O SMOW FLUID [1] per mil	
			275 ^{0}C[2]	340 ^{0} C[2]
AsO-1	Quartz	20.82	12.93	15.29
AsO-2	Quartz	22.15	14.26	16.62
AsO-3	Quartz	21.44	13.55	15.91
AsO-4	Quartz	22.58	14.69	17.05
AsO-5	Quartz	21.87	13.98	16.34
AsO-6	Quartz	21.63	13.74	16.10
AsO-7	Quartz	22.25	14.36	16.72
AsO-8	Quartz	22.48	14.59	16.95
AsO-9	Quartz	21.70	13.81	16.17
AsO-10	Quartz	21.84	13.95	16.31
AsO-11	Muscovite	13.62	9.59	11.18
AsO-12	Muscovite	12.93	8.91	10.50
AsO-13	Muscovite	14.10	10.07	11.66
AsO-14	Muscovite	13.15	9.12	10.71
AsO-15	Muscovite	13.88	9.85	11.44

[1] Fractionation equation for qtz-H_2O of Matsuhisa et al. 1979

[1] Fractionation equation for musc-H_2O of Friedman and O' Neil (1977)

[2] T (^{0}C), based on fluid inclusion microthermometry (Table 7.2)

The values for δ^{18} O for sericites range between 12.28 to 14.33 per mil with a mean value of 13.38 ± 0.86 (1σ) and are presented in Table 8.4. The fractionation equation for water-muscovite of Friedman and O' Neil (1977) was utilised to derive the oxygen isotopic composition of the hydrothermal fluids. The calculated δ^{18} O values at 275 ^{0}C and 340 ^{0}C range between 8.25 to 10.30 per mil with a mean value of 9.41 ± 0.81 (1σ) per mil and 9.76 to 11.76 per mil with a mean value of 10.88± 0.84 (1σ) per mil respectively. These values are consistent with metamorphic fluids, although the lower $\delta^{18} O_{fluid}$ values (less than 10 per mil) overlap with the uppermost values of magmatic water (5.5 to 10 per mil, Taylor, 1979a).

Fluid temperatures were calculated from two quartz-muscovite pairs in equilibrium from the Asimotrypes ore. The δ^{18} O analyses of quartz and muscovite separates yield $\Delta_{quartz\text{-}muscovite}$ ($\delta^{18} O_{quartz}$ - $\delta^{18} O_{muscovite}$) values of 9.87 and 9.17 for sample pairs AsO-2 and AsO-5 respectively. Calculated temperatures for the pairs using the equations of Matsuhisa et al., (1979), and Friedman and O' Neil (1977) yielded temperatures of 327 ± 10 ^{0}C. The average observed homogenisation temperature for inclusions for the area is 312 ^{0}C. This difference of the quartz-muscovite temperature relative to the fluid inclusion temperature may reflect a certain amount of retrograde re-equilibration of the quartz-muscovite oxygen isotope fractionation or the difference is small and overlaps with analytical error.

Whole rock oxygen isotope data are presented in Table 8.5. Whole rock δ^{18} O values for the Asimotrypes ore lie within a narrow range from 15.79 to 16.48 per mil and with a mean value of 16.15 ± 0.26 (1σ). δ^{18} O whole rock values for the Nikisiani granite-granodiorite consistently lie between 10.59 to 12.24 per mil with a median value of 11.58 ± 0.65 (1σ) per mil. It is apparent that whole rock δ^{18} O values for the Asimotrypes ore and the Nikisiani granite-granodiorite show a narrow spread and are consistent with values of metamorphic fluids.

Summarising, oxygen isotope results obtained for samples from the Asimotrypes mesothermal gold deposit are as follows:

Table 8.5: Whole Rock Oxygen Isotope Data, Asimotrypes area, Pangeon.

Sample	Rock Type	δ^{18} O SMOW per mil
As-11	As-py quartzite	16.16
As-14	massive arsenopyrite ore	15.83
As-16	massive arsenopyrite ore	16.24
As-19	As-py quartzite	16.32
As-21	As-py quartzite	15.79
As-31	massive pyrite ore	16.42
As-15	amphibolite	15.87
As-17	amphibolite	16.48
As-62	amphibolite	16.26
As-33	foliated granite	11.65
As-34	granite	11.02
As-35	white, altered granite	10.59
As-38	granodiorite	12.11
As-39	granodiorite	12.24
As-40	granodiorite	11.90

Median $\delta^{18}O$ values for marble calcites, quartz, sericite and whole rock are 29.31 ± 0.94 (1σ) ‰, 21.87 ± 0.52 (1σ) ‰, 13.38 ± 0.86 (1σ) ‰, and 16.15 ± 0.26 (1σ) ‰ respectively, and are considered as metamorphic oxygen values. Calculated median ore fluid composition at 275^0 C and 340^0 C in the system calcite-water is 22.94 ± 0.93 (1σ) ‰ and 24.77±0.93 (1σ) ‰, in the quartz-water system is 14.06 ± 0.52 (1σ) ‰ and 16.31± 0.52 (1σ) ‰ and in the water-muscovite is 9.41± 0.52 (1σ) ‰ and 10.88 ± 0.52 (1σ) ‰ respectively. These values are consistent with values of metamorphic fluids.

Hydrogen Isotopes

Hydrogen whole rock isotopic analysis was performed on eight representative samples from the main ore, the Transition zone and the granite. The aim of these analyses is to use the D/H values combined with $^{18}O/^{16}O$ as indicators of the origin and history of the H_2O in the ore forming fluids.

Whole rock hydrogen isotopic data are presented in Table 8.6. These are the first δ D values reported for ore in the Rhodope massif and there is no other comparative database. δ D values for the ore are in the range of -105 to -125 per mil, with a median of -117 ± 7.5 (1σ) per mil and for the granite are in the range of -79 to -89 per mil with a median value of -82 ± 6.21 (1σ) per mil. The δ D values reported above imply that all fluids contained in the Asimotrypes ore and granite fluid inclusions represent evolved meteoric waters (Shelton et al., 1988; Nesbitt et al., 1989). The isotopically light δ D values cannot be the result of incorporation of modern surface waters or metamorphic waters -20 to -65 per mil (Taylor, 1979), since those reservoirs are significantly heavier isotopically.

Table 8.6 : Whole Rock Hydrogen Isotope Data, Asimotrypes area, Pangeon

Sample	Rock Type	δ D SMOW per mil
As-11	As-py quartzite	-115
As-14	massive arsenopyrite ore	-105
As-16	massive arsenopyrite ore	-120
As-19	As-py quartzite	-125
As-21	As-py quartzite	-110
As-31	massive pyrite ore	-125
As-15	amphibolite	-120
As-17	amphibolite	-110
As-62	amphibolite	-125
As-33	foliated granite	-79
As-34	granite	-75
As-38	granodiorite	-89
As-39	granodiorite	-85

8.3 Radiogenic Isotopes

8.3.1 Strontium Isotopes

8.3.1.1 Background Information

Strontium has four naturally occurring isotopes ^{88}Sr, ^{87}Sr, ^{86}Sr and ^{84}Sr all of which are stable. Their isotopic abundances are approximately 82.53 %, 7.04%, 9.87 % and 0.56 % respectively. The isotopic abundances of strontium isotopes are variable because of the formation of radiogenic ^{87}Sr by the decay of naturally occurring ^{87}Rb. For this reason, the precise isotopic composition of strontium in a rock or mineral that contains rubidium depends on the age and Rb/Sr ratio of that rock or mineral.

The isotopic composition of Sr in circulation in the hydrosphere depends on the $^{87}Sr/^{86}Sr$ ratios of the rocks that interact with water at or near the surface of the earth. The Sr released into solution is homogenised isotopically by mixing during transport until it arrives in the oceans or in a closed basin on the continents. From there the Sr re-enters the rock cycle primarily by co-precipitation with calcium carbonate. The sedimentary carbonate and evaporite rocks of the world have therefore preserved a record of the changing isotope composition of Sr in the oceans throughout Proterozoic and Phanerozoic time.

Analysis of marine carbonates indicates that the $^{87}Sr/^{86}Sr$ ratio of the oceans has varied systematically throughout Phanerozoic time (Figure 8.2), and has apparently been constant in modern oceans at 0.70906±0.00033 (Faure, 1986). The reasons for the isotopic homogeneity of Sr in the oceans are: (i) the long residence time of about 5×10^6 years compared to the mixing time of the oceans of about 10^3 years, and (ii) the concentration of Sr in the oceans is high (7.7 μg/g) compared to average river water (0.068 μg/ml). The time-dependent variation of this ratio in the oceans can be explained in terms of changing proportions of strontium contributed to the oceans from different sources, which are hydrothermal circulation and continental input.

The $^{87}Sr/^{86}Sr$ ratio of seawater is controlled by mixing of three isotopic varieties of strontium derived from the following sources: (i) young ocean-floor volcanic rocks, (ii) old sialic rocks of the continental crust and (iii) marine carbonate rocks of Phanerozoic age. Therefore, the $^{87}Sr/^{86}Sr$ ratio of seawater is an indirect indicator of the kinds of rocks that are exposed to chemical weathering on the surface of continents and in the ocean basins. It also is an indicator of overall climate (arid-wet), of geomorphology-peneplanation or recent collision tectonics. These considerations lead to the observation that the $^{87}Sr/^{86}Sr$ ratio has varied during the course of geologic time in response to changes in the kinds of rocks exposed to chemical weathering; essentially an interplay between riverine input of Sr exchange at the ocean ridges.

The isotopic homogeneity of Sr in the oceans may allow us to use the observed time-dependent variation of the $^{87}Sr/^{86}Sr$ ratio to date marine carbonate rocks. The systematic variation in the $^{87}Sr/^{86}Sr$ ratio of the oceans since Cambrian time indicates that the three principal sources of Sr identified above have contributed varying proportions of Sr entering the oceans at different times. During the Palaeozoic era the $^{87}Sr/^{86}Sr$ ratio of the oceans fluctuated repeatedly from a high value of about 0.70910 in Late Cambrian time to about 0.70680 during the Late Permian period. After an initial increase to about 0.70770 in Middle Triassic time the ratio declined again to 0.70680 in Middle to Late Jurassic time and then increased during the Cretaceous and Tertiary periods with only a few minor fluctuations in Mid-Cretaceous and Early Tertiary time.

8.3.1.2 Analytical Results

^{87}Sr / ^{86}Sr isotope ratios are presented in Table 8.7 and vary from a maximum of 0.708040 to a minimum of 0.707850 with an average of 0.707920 ± 0.00010 (1σ) (Fig.8.2). These values are consistent in all three samples analysed close and away from the ore. The ^{87}Sr / ^{86}Sr ratio range is consistent with a Lower Carboniferous

Table 8.7 : Sr Isotope Data for Calcites from Impure Calcitic Marbles, Asimotrypes area, Pangeon.

Sample	Rock Type	Mineral	$(^{87}Sr / ^{86}Sr)_{measured}$
As-4	Calcitic marble	Calcite	0.707850
As-5	Calcitic marble	Calcite	0.708040
As-53	Calcitic Marble	Calcite	0.707870

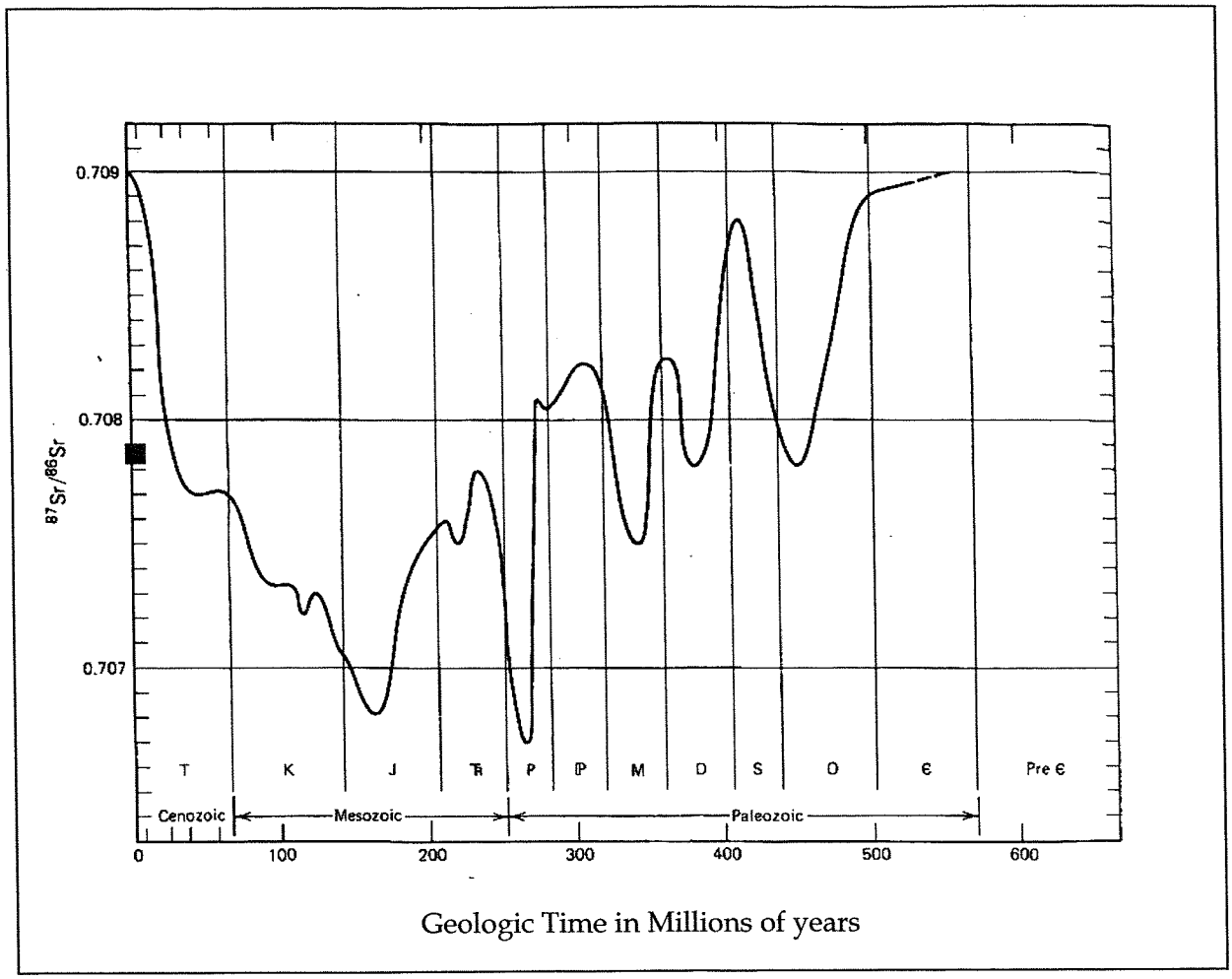

Figure 8.2: Variation of the $^{87}Sr/^{86}Sr$ ratio of marine carbonates in Phanerozoic time. (in Faure, 1986).
Square dark spot, is the average $^{87}Sr/^{86}Sr$ ratio for the Asimotrypes calcitic marbles.

sea water age (Peterman et al., 1970; Dasch and Biscaye, 1971). This age determination is in agreement with field and geologic interpretation. The seawater Sr derivation is consistent with interpretation made based on bulk rock geochemistry results (Chapter 6) and conclusions drawn from C and O isotope results from ore-host calcitic marbles (this Chapter).

8.3.2 Lead Isotopes

8.3.2.1 Background Information

Ordinary lead has four naturally occurring isotopes: ^{208}Pb, ^{207}Pb, ^{206}Pb, and ^{204}Pb. The first three are products of decay of uranium and thorium and only ^{204}Pb is not radiogenic, although it is very weakly radioactive and decays to stable ^{200}Hg by alpha emissions with a half-life of $1.4X10^{17}$ years (Faure, 1986). Because of its long half-life, ^{204}Pb is treated as a stable reference isotope.

Lead is widely distributed throughout the earth and occurs not only as the radiogenic daughter of U and Th but also forms its own minerals from which U and Th are excluded. Therefore the isotopic composition of Pb varies between wide limits from the highly radiogenic Pb in very old U, Th-bearing minerals to the common Pb in galena and other minerals that have low U/Pb and Th/Pb ratios. Galena is frequently associated with other sulphide minerals, which enables us to study the origin of metallic ore deposits by the isotope composition of Pb in galena and other common Pb minerals.

Lead is also a trace element in all kinds of rocks. Its isotopic composition in different kinds of rocks contains a record of the chemical environments in which Pb resided. These may include the mantle, crustal rocks, or Pb ores. Each of these environments has different U/Pb and Th/Pb ratios that affect the isotopic evolution of Pb. The Pb/Pb and Th/Pb ratios are changed by magma generation and fractionation, by hydrothermal and metamorphic processes and by weathering and other low temperature processes at the earth's surface. The isotopic composition

of a particular sample of Pb may be modified both by decay of U and Th and by mixing with Pb having different isotope compositions.

As a result, the isotopic compositions of Pb in rocks and ore deposits display complex patterns of variation that reflect their particular geological histories.

In the simplest case, represented by the single-stage Holmes-Houtermans model, Pb evolved in a homogeneous reservoir having characteristic U/Pb and Th/Pb ratios until it was withdrawn from that reservoir and was sequestered in a Pb mineral such as galena. The equations describing Pb evolution in this model require knowledge of the isotope ratios of primordial Pb and the age of the earth. These were determined from analyses of Pb in stony and iron meteorites.

The single stage model was found to apply only to a small number of conformable ore deposits associated with sequences of volcanic and sedimentary rocks deposited near island arcs and subduction zones. However, even for conformable ore deposits the dates calculated from the single-stage model do not agree well with the geologic ages of the associated rocks. Moreover, most other metallic ore deposits yield single-stage model dates that are highly discrepant and, in some cases, even negative, i.e., associated with the future rather than with the past.

The isotope ratios of so-called «anomalous» leads that do not fit the single-stage model form linear arrays in the Pb evolution diagram. Such anomalous-Pb lines may be caused by the addition of varying amounts of radiogenic Pb to ordinary single-stage Pb. If that is true, the slope of the anomalous Pb line can be used to derive information about the age and the Th/Pb ratio of source rocks that provide the radiogenic lead. In addition, estimates can be made of the time of withdrawal of the single-stage Pb from its reservoir and the age of ore deposit in which the Pb now resides. In this case the linear data array defines a mixing line whose slope does not convey information about the age of such leads.

The two-stage model of Stacey and Kramers (1975) is based on a selected data set and proposes that ore leads evolved in two reservoirs having different U/Pb and Th/Pb ratios. The change in these ratios took place at about 3.7 Ga and was caused by the geochemical differentiation of the earth. The mantle of the earth may have been the first reservoir but after 3.7 Ga, Pb evolution probably occurred in frequently- mixed continental sediments from which Pb was extracted during subduction into the mantle. The two-stage model yields dates for Pb in galena and K-feldspar that agree much better with their geologic ages than dates derived from single-stage models.

The isotope ratios in volcanic rocks from mid-ocean ridges, oceanic islands, island arcs, and continental regions tend to form linear arrays on the Pb-evolution diagrams. The co-linearity of Pb-isotope ratios may be caused by the heterogeneity of the magma sources with respect to the U/Pb and Th/Pb ratios. In this case the lines are secondary or higher order isochrons whose slopes depend on the time elapsed since the last homogenisation of Pb in the magma sources. Dates calculated on the basis of this assumption from Pb-Pb isochrons of MORBs and OIBs range from 1.0 to 2.0 Ga and suggest the occurrence of large- scale geochemical differentiation in the mantle under the oceans.

However, the linear data arrays of Pb in young volcanic and plutonic rocks in subduction zones and in continental regions are probably caused by mixing of mantle-derived Pb associated with crustal rocks. This interpretation is consistent with the evidence provided by other radiogenic isotopes (Sr, Nd, Hf) that intrusive and extrusive rocks in these geologic settings are extremely contaminated by interactions between magma and the country rock. Such contamination of magma is less likely in the oceans but cannot be ruled out entirely.

8.3.2.2 Analytical Results

Lead isotopic analyses from the main polymetallic sulphide deposits, and repre-

sentative mineralised occurrences from the Rhodope and Serbomacedonian Massifs, have been carried out in the past by various researchers and data with corresponding reference are shown in Table 8.8.

^{207}Pb / ^{204}Pb versus ^{206}Pb/ ^{204}Pb ratios of Uranogenic lead in galenas from ores hosted in the Rhodope and Serbomacedonian Massifs are plotted in Figure 8.3, according to the data of Table 8.8. Growth curves and isochrons of the diagram are according to the models: plumbotectonics (upper crust, orogene, mantle), Cumming and Richards (C-R), Stacey and Kramers (S-K), Amov (A). It is clear that the ^{207}Pb / ^{204}Pb ratios vary within a small range between the growth curves of orogene and upper crust. This indicates a uniform, crustal type, source for the rocks and ores in which crustal material predominates.

The overall isotopic pattern of the studied ores are very similar and their data fields overlap significantly. This can be taken as an indication for a similar crustal evolution and a more or less contemporaneous ore deposition period in both the massifs. On the basis of lead isotopic data it is not possible to distinguish between different ore types. Pb-Zn ± Au replacements, vein and stratiform type ores and porphyry copper style ores show all very similar lead isotope signatures. Variations in the isotopic compositions of ore minerals in the studied ores however exist and they are suggested to reflect local structural inhomogeneities (Frei, 1992).

Lead isotope patterns with spreads in the ^{207}Pb / ^{204}Pb and ^{208}Pb / ^{204}Pb ratios similar to those defined by the ore leads from the Rhodope and Serbomacedonian Massifs are typically observed in cases where older crustal components are involved in young orogenies. Using the average crustal lead evolution model proposed by Stacey and Kramers (1975), it is possible to obtain an approximate minimum age for the crustal material in the Rhodope and Serbomacedonian Massifs from the ore lead isotopic data points. The slopes of the tangents through the data points to the growth curve represent the momentary production rates of ^{207}Pb / ^{204}Pb at the time these leads started to evolve independently in distinct res

Table 8.8: Lead Isotopic Ratios for Polymetallic Sulphide Deposits for the Greek Serbomacedonian and Rhodope Massifs. ( )* Number of analyses.

LOCALITY	TYPE	$^{206}Pb / ^{204}Pb$	$^{207}Pb / ^{204}Pb$	$^{208}Pb / ^{204}Pb$	REFERENCES
Serbomacedonian Massif					
(1) Myriophyto	Vein	18.335	15.663	38.480	Amov et al., 1991
(2) Madem Lakkos (14)*	Replacement	18.744 (± 0.011)	15.656 (± 0.006)	38.853 (± 0.033)	Chalkias and Vavelidis, 1988; Kalogeropoulos et al., 1989; Kilias, 1990; Nabel et al., 1991.
(3) Olympias (13)	Replacement/vein	18.773 (± 0.011)	15.671 (± 0.008)	38.869 (± 0.028)	Chalkias and Vavelidis, 1988; Kalogeropoulos et al., 1989; Kilias, 1990; Frei, 1992.
West Rhodope Massif					
(4) Dafnoudi	Stratabound	18.820	15.740	39.030	Gale,1978.
(5) Kato Nevrokopi (4)	Karst/Stratabound	18.726 (± 0.020)	15.665 (± 0.013)	38.855 (± 0.049)	Frei, 1992.
(6) Pangeon (4)	Replacement/vein	18.715 (± 0.008)	15.640 (±0.002)	38.755 (±0.020)	Gale, 1978.
(7) Thassos (6)	Karst	18.788 (± 0.020)	15.683 (± 0.021)	38.905 (± 0.052)	Gale, 1978; Vavelidis et al., 1985.
(8) Thassos (4)	Calamine	18.760	15.650	38.810	Vavelidis et al., 1985.
(8) Thassos (5)	B.I.F.	18.560	15.640	38.590	Vavelidis et al., 1985.
(9) Farasino	Vein	18.714	15.670	38.922	Vavelidis et al., 1985.
Central Rhodope Massif					
(10) Thermes (29)	Replacement/vein	18.694 (± 0.006)	15.663 (± 0.003)	38.919 (± 0.018)	IGME, Xanthi ,Changkakoti et al., 1990.
(11) Kaloticho (4)	Vein/Stockwork	18.655 (± 0.016)	15.655 (± 0.027)	38.850 (± 0.045)	Gale, 1978; Frei,1992.
(12) Xylagani (3)	Stratiform	18.375 (± 0.003)	15.560 (± 0.001)	38.855 (± 0.030)	Frei, 1992.
(13) Palea Kavala	Gossan	18.739	15.678	38.856	Amov et al., 1991.
(13) Palea Kavala	Limonite	18.732	15.685	38.851	Amov et al., 1991.
East Rhodope Massif					
(14) Kirki (18)	Vein	18.704 (± 0.014)	15.654 (± 0.006)	38.787 (±0.021)	IGME, Xanthi ;Frei, 1992
(15) Essimi (33)	Stratiform	18.740 (± 0.006)	15.667 (± 0.015)	38.826 (± 0.031)	IGME, Xanthi ;Frei, 1992, Changkakoti et al., 1990.

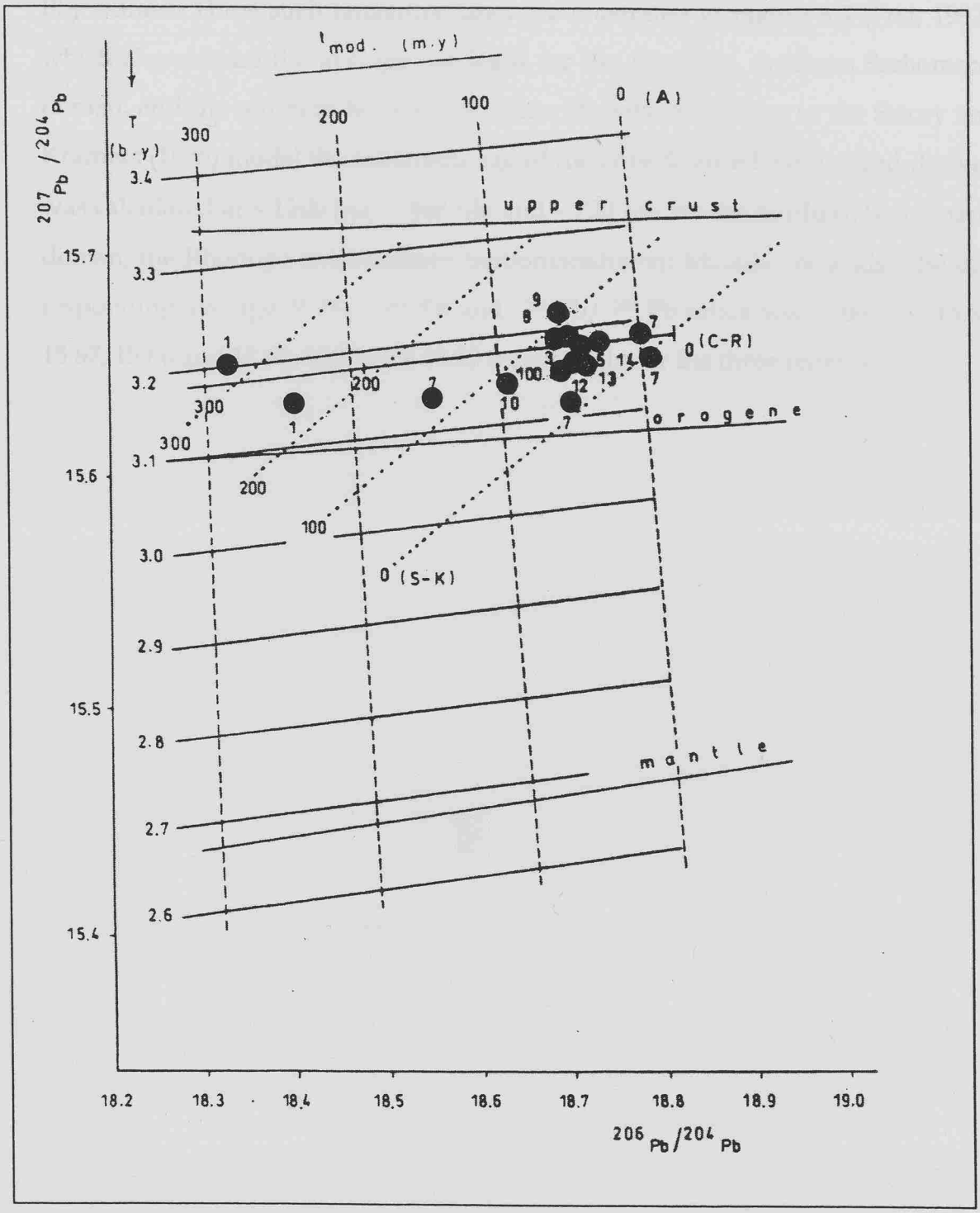

Figure 8.3: $^{207}Pb/^{204}Pb$ versus $^{206}Pb/^{204}Pb$ composite diagram for Uranogenic lead in galenas from ores in the Serbomacedonian and Rhodope Massifs, with growth curves and isochronons according to the models: Plumbotectonics (upper crust, orogene, mantle), Cumming and Richards (C-R), Stacey and Kramers (S-K) and Amov (A). Data from Table 8.8; numbers of dark circles correspond to numbers in brackets in Table 8.8.

ervoirs which were characterised by different μ_2 ($^{238}U/^{204}Pb$) and W_2 ($^{232}Th/^{204}Pb$) values. Three such tangential lines are illustrated in Figure 8.4 (Frei, 1992), which characterise the average ore leads for the Rhodope, northern Serbomacedonian, and the southern Serbomacedonian Massifs. According to the Stacey and Kramers (1975) model the minimum age of the crust from which the lead derived was calculated at ~ 1100 Ma, ~ 800 Ma and ~ 720 Ma for the northern Serbomacedonian, the Rhodope and southern Serbomacedonian Massifs ore leads. The corresponding average $^{207}Pb/^{204}Pb$ and $^{206}Pb/^{204}Pb$ ratios were taken as 15.68, 15.67, 15.66 and 18.68, 18.73 and 18.80 respectively for the three regions.

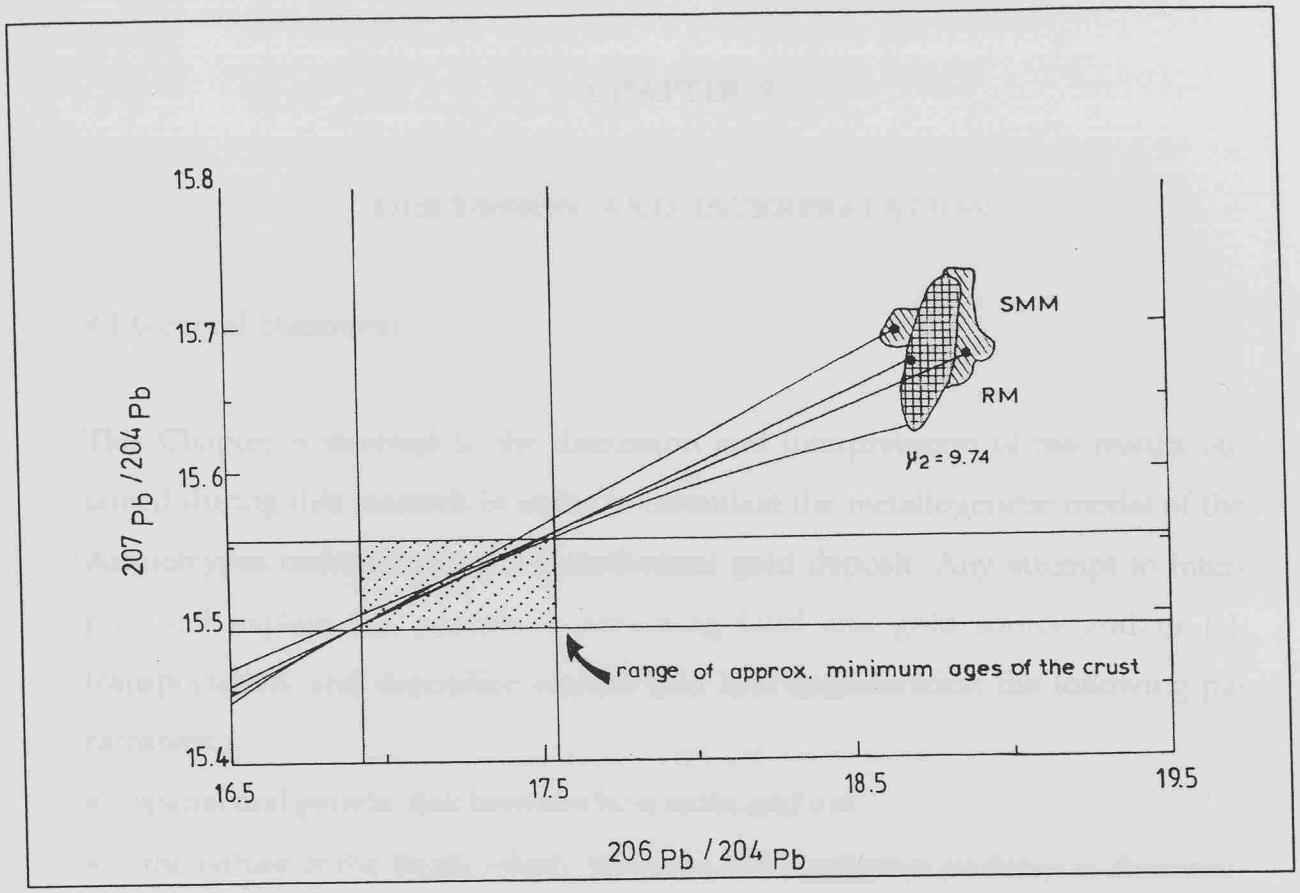

Figure 8.4: ^{207}Pb / ^{204}Pb versus ^{206}Pb /^{204}Pb diagram showing the fields defined by ore leads from the Serbomacedonian Massif (diagonally hatched) and the Rhodope Massif (cross-hatched). The three data points correspond to the average lead isotope values of ores from the northern Serbomacedonian Massif (^{207}Pb / ^{204}Pb =15.68, ^{206}Pb /^{204}Pb =18.70), from the southern Greek Serbomacedonian Massif (^{207}Pb / ^{204}Pb =15.66, ^{206}Pb /^{204}Pb =18.80) and from the Rhodope Massif (^{207}Pb / ^{204}Pb =15.665, ^{206}Pb /^{204}Pb =18.74). The three tangents to the Stacey and Kramers average crustal lead evolution curve (μ_2=9.74) define a range between ~ 720 to 1100 Ma for the minimum age of the crust, from which the leads were derived (in Frei, 1992).

CHAPTER 9

DISCUSSION AND INTERPRETATION

9.1 General Statement

This Chapter is devoted to the discussion and interpretation of the results obtained during this research in order to formulate the metallogenetic model of the Asimotrypes carbonate-hosted mesothermal gold deposit. Any attempt to interpret and explain the possible mineralising fluid and gold source and/or (s), transportation, and deposition should take into consideration the following parameters:

- spatial and genetic link between host rocks and ore;
- the nature of the fluids which, based on fluid inclusion evidence is characterised by high but variable contents of CO_2 and traces of CH_4 , H_2O - CO_2 phase separation during mineralization at P - T conditions of 3.3 kbars and 312 ^{0} C respectively, and relatively low aqueous phase salinity at $\approx$ 4 wt% NaCl equivalent;
- the relationship of the ore to the retrograded amphibolite to lower greenschist facies metamorphic terranes coupled with the presence of the spatially related syn-kinematic granite-granodiorite of Nikisiani;
- the oxygen and carbon isotopic composition of the fluids in addition to the hydrogen and sulphur isotopic signatures;
- devolatilisation/decarbonation reactions during regional metamorphism;
- uplift acting as the heat source for deep circulating meteoric waters mixing with metamorphic waters;
- hydrothermal fluids generated by any combination of the above.

9. 2 Comparison of the Asimotrypes Gold Deposit with Archean Mesothermal Gold Deposits of the N. American Cordillera and Mesozoic Korean Gold Deposits.

Geological and geochemical characteristics of Phanerozoic mesothermal gold deposits (Table 9.1) , show that many characteristics, especially in timing of ore formation, structure, metamorphism, ore morphology, textures, associated elements, mineralogy, paragenesis, fluid inclusions, and stable and radiogenic isotopes, exhibit a considerable degree of similarity among the major districts, world-wide. The existence of this degree of similarity suggests that in many respects the genetic processes are similar as well. The principal differences between districts , largerly in host-rock type, hydrothermal alteration, and relation to plutons, most likely reflect local geological heterogeneities. The most important conclusion arising from Table 9.1 is the close similarity between Archean and Phanerozoic mesothermal gold deposits, also reported by Hutchinson (1987) and Kerrich (1987)..

Fluid inclusion data from the present study indicate that sulphides and associated gold were deposited between 340^0 and 275^0 C from relatively dilute fluids ($\approx$4 wt% equiv. NaCl) and mean calculated pressure 3.3 kbars (Table 9.2). Gold deposition was likely a result of decrease sulphur activity caused by sulphide deposition and/or H_2S loss accompanying fluid unmixing combined with cooling and dilution of the ore-forming fluids.

Measured and calculated compositions of ore fluids in the Asimotrypes area showed $\delta\ ^{18}O$ between 14 to 16 per mill and δD between -75 to -125 per mil (Table 9.2), indicating that gold was deposited from a highly evolved meteoric water that underwent extreme ^{18}O enrichment and moderate D enrichment. Mineralogy and ore fluid chemistry of the Tertiary Asimotrypes deposit are similar to those of mesothermal lode gold deposits of the Canadian Cordillera occurring in Canadian Archean greenstone belts, the Mother Lode district of California and the Mesozoic

Table 9.1: General geological and geochemical characteristics of Phanerozoic mesothermal gold deposits (Nesbitt, 1993).

Tectonics	Typically in accreted, deformed and metamorphosed continental margin or island arc terranes.
Host lithology	Widely variable; greywackies-pelites, chemical sedimentary units, volcanics, plutons, ultramafics.
Metamorphism	Typically sub-to upper greenschist; occasionally host terranes are metamorphosed to higher grade prior to mineralisation.
Relations to plutons	Variable; some areas close spatial and probable genetic link; other districts no evidence of plutonic activity.
Structure	Varies from fold to fault control; where fault controlled, mineralisation is generally confined to second-order faults related to major structures.
Timing	Late in orogenic sequence; subsequent to principal deformation and metamorphism.
Ore morphology and textures	Thick quartz veins, typically banded, occasionally vuggy with high-grade ore shoots; vertically continuous, mineralised zones; occasional stockwork and disseminated mineralisation.
Mineralogy and paragenesis	Early phases: quartz, Ca-Mg-Fe carbonates, arsenopyrite, pyrite, albite, sericite, chlorite, scheelit, stibnite, pyrrhotite, tetrahedrite, chalcopyrite, and tourmaline. Late phases: gold, galena, sphalerite, tellurides.
Hydrothermal alteration	Carbonitisation, albitisation, sericitisation, silicification, sulphidation, chloritisation; listwanite development.
Zoning and elemental geochemistry	Au:Ag typically >1; associated elements: Ag, Sb, As, W, Hg, Bi, Mo, Pb, Zn, Cu, Ba. Zoned from high temperature Au ± Ag, As, Mo, W to Sb ± Au, Hg, W to Hg ± Sb.
Fluid inclusions	H_2O-CO_2 inclusions, typical X CO_2 0.05 to 0.2; < 5 equiv. wt% NaCl; T homogenisation 250-350 ^{0}C, P > 1000 bars.
Stable isotopes	Typical values: $\delta\ ^{18}O$ (Qzt) = +11 to 18 ‰; $\delta\ ^{13}C$ (Cb) = -25 to -3 ‰; δ D (fluid inclusions) = -160 to -30 ‰, $\delta\ ^{34}S$ = -10 to + 10 ‰ .
Radiogenic isotopes	Indicate heterogeneous crustal sources for Sr, Pb, and Nd.

Table 9.2: Fluid inclusion and Stable isotope data (in per mil) from Phanerozoic mesothermal gold deposits (Nesbitt, 1993).

Area	Homogenisation Temperature ^0C	Estimated mole% CO_2	Salinity Wt% NaCl equiv.	$\delta\ ^{18}O$	$\delta\ ^{13}C$	δ D	$\delta\ ^{34}S$
Victoria	160-330	~ 5	1-9	+14 to +21 (Qtz) +11 to +18 (Cb)	-20 to -3 (Cb)		-10 to +10 (Py,Po,Asp)
Nova Scotia	200-400	13-14	< 4-6	+12 to +18 (Cb)	-25 to -14 (Cb)		
California	150-280	< 11	< 2	+14 to +23 (Qtz) +13 to +19 (Cb)	-6 to +7 (Cb) -5 to -2 (CO_2) -25 to -23 (CM)	-100 to -30 (FI) -60 to -40 (Sil)	-4 to +6 (Py,Po,Gl,Spl)
Canadian Cordillera	200-350	5-20 (up to 100)	2-8	+13 to +18 (Qtz) +13 to +17 (Cb)	-10 to -2 (Cb) -17 to -8 (CO_2) -26 to -25 (CM)	-160 to -100 (FI)	+8 to +13 (Py, Asp)
Alaska	150-310	5-20 (up to 50)	< 5	+14 to +18 (Qtz)		-100 to -120 (FI) ~ -60 (Sil)	
Korea	290-375	15-25	~ 4	+11 to +15 (Qtz) +6 to +9 (Cb)	-6 to -5 (Cb)	-110 to -80	+4 to +12 (Py, Po, Gl, Spl)
China	100-350	< 5	~ 4	+6 to +13 (Qtz) +6 to +9 (Cb)	-8 to -3 (Cb)	-140 to -60 (FI)	-8 to +16 (Py)
Asimotrypes, Greece*	275-340	3-38	< 5	+28 to +30 (Ca) +20 to +23 (Qtz) +12 to +14 (Sil) +15 to +17 (WR)	+2 to +3 (Ca)	-100 to -120 (WR)	+2 to +3 (Py,Asp,Cpy)

Abbreviations: Qtz, quartz; Cb, carbonate; Ca, calcite; FI, fluid inclusions; CM, carbonaceous material; Sil, silicate; WR, whole rock; Py, pyrite; Asp, arsenopyrite, Cpy, chalcopyrite, Po, pyrrhotite; Gl, galena, Spl, sphalerite.
* Data from present study.

gold-rich mesothermal vein deposits of the Republic of Korea (Table 9.2).

The geochemical similarity and more specifically the fluid inclusion and isotopic data of the Asimotrypes mesothermal gold deposit to those of the Canadian Cordillera and the Republic of Korea, of different age and occurrence may suggest a more general application of the meteoric model for the origin of mesothermal lode gold deposits. As emphasised by Nesbitt et al., (1986), the diversity of host rocks of Canadian and other mesothermal deposits (mafic to felsic volcanic rocks and intrusions, serpentinites, and clastic and chemical sedimentary rocks) indicates that the host rock petrology is not a controlling factor in the formation of such deposits. The occurrence of the Tertiary Asimotrypes mesothermal gold deposit at the contact of marbles and gneisses and the geochemical data derived from this study corroborate this point and validate a more general application of meteoric models to the formation of mesothermal gold deposits.

9.3 Dolomitisation

Field observations and detailed petrographic studies in the main carbonate sequence of the Pangeon indicate that the dolomite rocks are widespread. The complex diagenetic-metamorphic history of the carbonates is one of the main difficulties in interpreting the origin of the dolomites and the process of dolomitisation. Generally the various processes that would lead to the dolomitisation of limestones or calcareous sediments (Morrow, 1982) can be divided in two groups:

- early diagenetic processes involving modified or unmodified seawater (Adams and Rhodes, 1960; Badiozamani, 1973; Folk and Land, 1975; and

- late diagenetic or epigenetic processes, commonly involving magnesium-rich, basin derived fluid (Zenger, 1983; Gregg, 1985; Machel and Moyntjoy, 1986; Hardie, 1987).

On the basis of field observations, petrographic characteristics and geochemical data it can be concluded that the last dolomitisation process in Pangeon results from processes in the second group. In the Pangeon area, dolomites do not form large units, and are not present as fronts. On the contrary, the alternations of dolomitic and calcitic marbles are clear. The dominant dolomite type, the unimodal, nonplanar, medium to coarse crystalline dolomites as well as the minor saddle dolomite types show the petrographic criteria that support a burial environment of dolomitisation.

In the studied areas, the crystal size of dolomites ranges from medium to coarse. Zenger (1983) and Gregg (1985) used coarse crystallinity as one of the criteria for a deep burial origin and it is suggestive of higher temperature. The presence of even minor saddle dolomite indicates that these rocks have undergone some burial, probably to epigenetic conditions. The near stoichiometry ($Ca_{49.5}$ $Mg_{50.5}$ to $Ca_{50.03}$ $Mg_{49.97}$) of the dolomites reflects burial conditions (Zenger and Danham, 1988) and either neomorphism and stabilisation of early diagenetic dolomites or replacing crystalline dolomite formed initially in the mesogenetic zone (Lumsden and Chimahuski, 1980).

It is difficult to interpret the trace element content of ancient dolomite quantitatively (Hardie, 1987) because of a number of factors including uncertainty about appropriate distribution coefficients, although general statements can be made. The trace element (Sr, Fe, Mn, and Pb, Zn) content indicates, as in most ancient carbonates, the effects of late diagenesis and some signatures from seawater origin of the initial dolomitised fluids. Most of the previous evidence could be accounted for either by neomorphism of an earlier dolomite or replacement of limestone under burial conditions. The fact that the dolomitisation is widespread and therefore vast amounts of Mg are needed, as well as that it is lithostratigraphically controlled, leads to the hypothesis that neomorphic process of an earlier dolomite took place.

9.4 De-dolomitisation

The de-dolomitization process (calcitisation of dolomite), including the selective dissolution of dolomite as well as the replacement of dolomite by calcite, is widespread in Pangeon. The de-dolomitisation is often interpreted as a near surface diagenetic product either reflecting near surface alteration associated with subaerial exposures, unconformity, fault and fractures related surfaces or late alteration during burial (Goldberg, 1967; Scholle, 1971; Chafetz, 1972; Budaj, 1984). As with dolomite formation, relations between depth, temperature and calcitisation of dolomite are very poorly constrained (Enamy, 1963; Katz, 1971; Frank, 1981).

All possible transitions from partial to almost complete de-dolomitisation of the whole rock are developed in the studied area. De-dolomite ranges from a minor to a major component of the investigated carbonate rocks and it is associated with the Petrographic types I and VI. Corrosion boundaries between calcite and dolomite constitute the main textures mainly in the Petrographic type I. In the initial stages of de-dolomitisation, the dolomite may be attacked at its edges producing centripetal corrosion. The corrosion continues and the de-dolomitisation moves towards the centre of the crystal either along particular fractures or cleavage planes in the crystal or as embayments.

Additional alteration of the dolomite produces a mosaic of calcite enclosing small relics of euhedral dolomite. This texture is mainly present in the de-dolomitic marble type VI. Usually, the de-dolomitisation process starts from the larger (saddle) dolomite crystals. Small grains of iron oxides and hydroxides may occur with these crystals which are thought to be by-products of the de-dolomitisation process of ferroan dolomite (Enamy, 1963; Katz, 1971; Frank, 1981). The two classic de-dolomite fabrics, rhombohedral calcite after dolomite and granular calcite after dolomite (Enamy, 1967) are present, but are not common in the carbonates. Based only on petrography it is difficult to distinguish the possible

existence of more than one de-dolomitisation phase.

The calcite related to the de-dolomitisation process, in the samples examined is Mg and Fe enriched. The enrichment of de-dolomite in Mg is most probably due to the high Mg quantities freed during de-dolomitisation (Richter, 1974). These geochemical data confirm the petrographical evidences, as described above. According to the existing field data, petrographic and geochemical studies, we can assume that the de-dolomitisation took place under near surface, oxidised conditions and close to tectonic discontinuities, such as faults, fractures and other disconformities. These surfaces also are favourable for ore deposition. Fracture related de-dolomite has also been reported in connection to tectonic vein type mineralisation (Budaj, 1984). Moreover, the ore oxidation is favourable for de-dolomitisation mechanisms, without precluding the elevated temperature of hydrothermal solutions, which may also cause the de-dolomitisation. In experimental work by Kastner (1982), calcitisation of dolomite took place at temperatures up to 200 ^{0}C. Based on the above, we can explain the positive relationship between the de-dolomitisation and mineralisation.

9.5 Dolomitisation and Mineralisation Processes

The fourth petrographic type (impure calcitic marble) belonging to the alternation zone is correlated to the arsenopyrite + pyrite ore. The Petrographic types I and VI are correlated to the oxidised sulphide ore within the marbles and the Petrographic type II with the manganese oxide mineralisation. The relationship between the dolomitisation and the mineralisation bearing carbonate rocks is debatable. Significant differentiations of the petrographic and geochemical characteristics were not observed either close or away from the ore body. The ore hosted in carbonate rocks of the Transitional Zone (impure calcitic marble) do not show any relation with the dolomitisation. The inverse process of dolomitisation, the de-dolomitisation has a positive relationship with the ore hosted within the marbles. It is probably due to the similar favourable conditions for de-dolomitisation and ore deposition processes, which are related to the tectonic discontinuities and/or

the elevated temperature of hydrothermal solutions.

9.6 Origin of the Asimotrypes Fluids

The fluid composition range ($\delta^{18}O_{fluid}$ 14.38 - 16.14 per mil, δD_{fluid} - 117 ± 7.5 per mil) is shown on a δD versus $\delta^{18}O$ plot (Fig. 9.1). Also shown for reference are the regions occupied by metamorphic and magmatic waters (Sheppard, 1986). The cluster of $\delta^{18}O_{quartz}$ values between 20.82 to 22.58 per mil (Table 8.4) and the calculated average $\delta^{18}O_{fluid}$ value of 15.43 ± 0.52 per mil (Table 8.4) are somewhat enriched in $\delta^{18}O$ relative to the most mesothermal lode gold deposits, which generally display regional homogeneity in $\delta^{18}O_{fluid}$ values (Kerrich, 1989; Nesbitt and Muehlenbachs, 1989a). However, for the Asimotrypes fluids shown in Figure 9.1, the δD_{fluid} values clearly lie outside of the magmatic and metamorphic water field.

Any interpretation of the stable isotope results must address the question of the origin of the seeming incongruity of ^{18}O - enriched and D - depleted ore fluids. As shown in Figure 9.2, the $\delta^{18}O$ values for the ore fluids of the Asimotrypes mesothermal gold deposit are in good agreement with results from other mesothermal gold deposits. However, the δD values from the Asimotrypes gold deposit are slightly heavier than observed values in other mesothermal deposits (Fig. 9.2). As pointed out in Nesbitt et al. (1986), these δD results unequivocally indicate the involvement of meteoric water in the formation of mesothermal deposits.

Mechanisms, which have been invoked to account for generation of the mineralising fluids involved in mesothermal gold deposits genesis, include:

- lateral secretion (Boyle, 1979)
- mantle degassing - granulitisation (Colvine et al., 1984; Cameron, 1988)
- meteoric water circulation (Nesbitt et al., 1986; Shelton et al., 1988)
- metamorphic devolatilisation (Kerrich and Fyfe, 1981; Goldfarb et al., 1989),

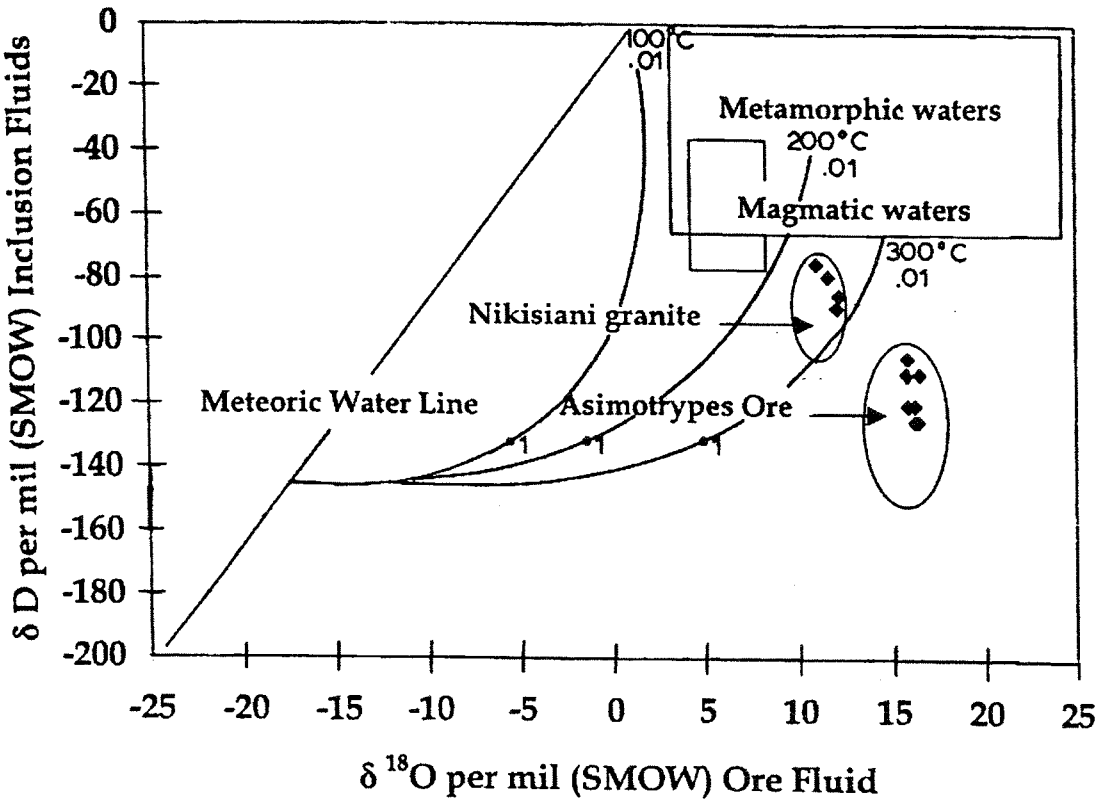

Figure 9.1: Plot of δ D inclusion fluids versus δ ^{18}O fluids of the Asimotrypes mesothermal gold deposit and the Nikisiani granite. The isotopic composition of the Asimotrypes fluids clearly lie outside of the metamorphic and magmatic water fields. Metamorphic and magmatic water fields from Sheppard (1986). Curvilinear trajectories represent the evolution in isotopic composition of meteoric water undergoing exchange at conditions low water/rock ratios for specified temperatures (in Kerrich, 1987).

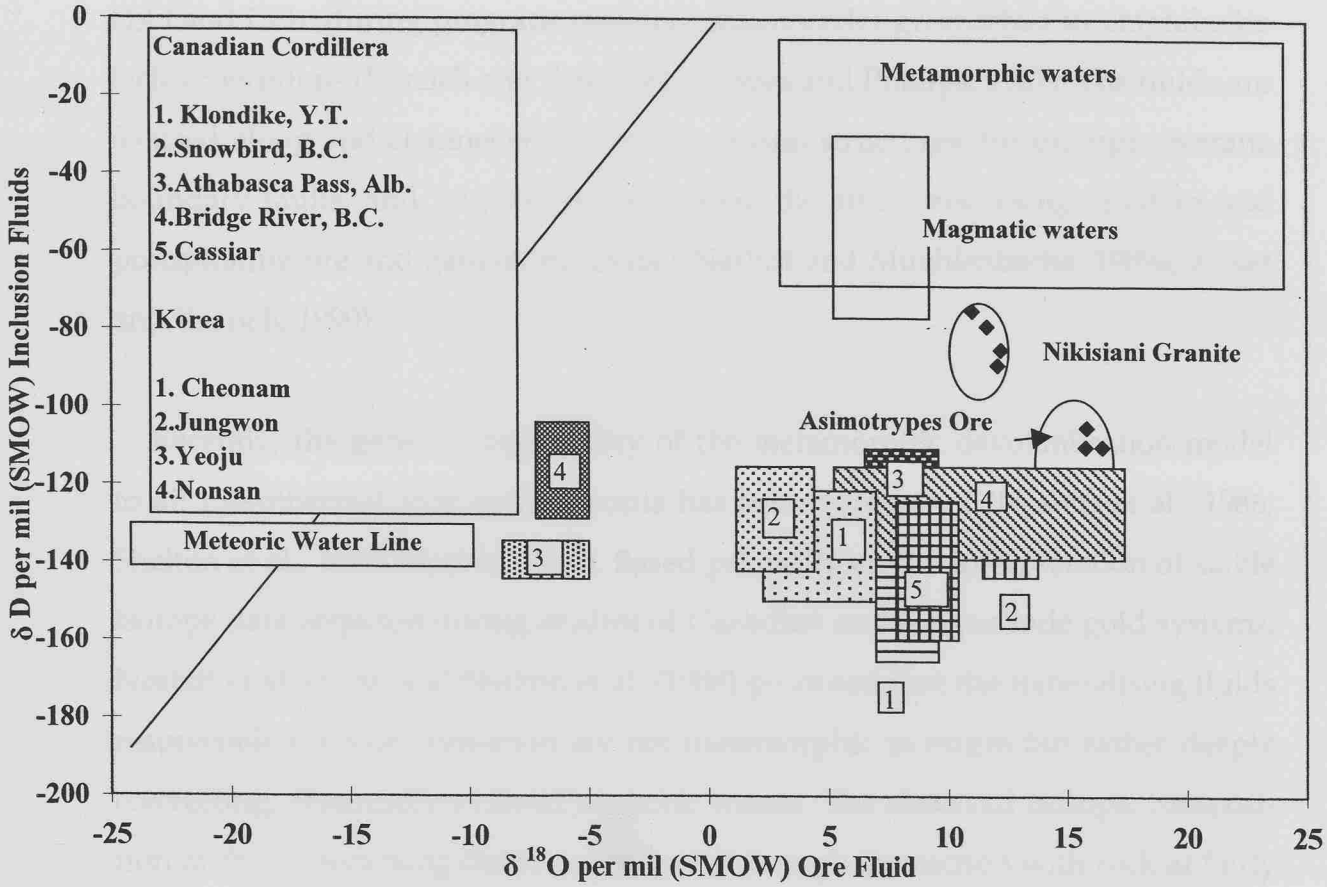

Figure 9.2: Plot of $\delta D_{\text{inclusion fluids}}$ versus $\delta {}^{18}O_{\text{fluids}}$ of the Asimotrypes mesothermal gold deposit. The isotopic composition of the Asimotrypes fluids clearly lies outside of the metamorphic and magmatic water fields (Sheppard, 1986). Data for Klondike from Rushton et al., (1993): Snowbird from Madu et al., (1990); Athabasca Pass, from Shaw et al., (1991); Bridge River, From Maheux, (1989); Cassiar, from Nesbitt et al., (1989a). Korean deposits data from Shelton et al., (1988).

and

- orthomagmatic origin (Colvine et al., 1984; Hattori, 1987)

The genetic model which is presently more widely accepted is the generation of H_2O and CO_2 during prograde metamorphism under greenschist to amphibolite facies conditions (Kerrich and Fyfe,1981; Groves and Phillips, 1987). The fluids are focused along and channelled into major crustal structures, for example, terrane boundary faults, and migrate upward along the structures losing volatiles and precipitating ore and gangue minerals (Nesbitt and Muehlenbachs, 1989a; Kyser and Kerrich, 1990).

Recently, the general applicability of the metamorphic devolatilisation model to all mesothermal lode gold deposits has been questioned (Nesbitt et al., 1986; Shelton et al., 1988; Nesbitt, 1990). Based primarily on the interpretation of stable isotope data acquired during studies of Canadian and Korean lode gold systems, Nesbitt et al. (1986) and Shelton et al. (1988) proposed that the mineralising fluids responsible for lode formation are not metamorphic in origin but rather deeply convecting, chemically evolved meteoric waters. The observed isotopic composition of the mineralising fluids is generated through interaction with rock at fairly high temperatures (275^0 - $340\ ^0$C) and low water / rock (w/r) ratios (Nesbitt and Muehlenbachs, 1989a).

In epithermal Au ± Ag deposits, where the involvement of meteoric water is widely recognised, δD values are generally low, latitudinally dependent, and are accompanied by correspondingly low $\delta^{18}O$ values. In mesothermal gold deposits, on the other hand, low δD values are latitudinally dependent but accompanied by high and latitudinally independent $\delta^{18}O$ values. The origin of this pattern of isotope enrichment and depletion is a direct result of relatively low water / rock ratios in the mesothermal systems. Shown in Figure 9.1 are a set of varying water / rock ratio at varying temperatures (Kerrich, 1987). The initial large shift in $\delta^{18}O$ with little change in δD at relatively high water / rock values is a result of the

high O / H ratio typical of most rocks. Due to the high O / H ratio of rocks, the $\delta^{18}O$ values of fluids will be influenced even at relatively high water / rock values with little effect on δD values. Only with a very low water / rock ratios the δD of the fluids will be affected significantly (Fig. 9.1). As shown in Figure 9.1, the fluid evolution curves readily indicate the water / rock and thermal conditions necessary to generate the isotopic chemistry of fluids in mesothermal gold deposits. Also demonstrated in Figure 9.1 is the fact that in order to obtain typical $\delta^{18}O$ values of the ore fluids, the fluids must have interacted with sedimentary rocks (Nesbitt and Muehlenbachs, 1989a). The $\delta^{18}O$ values of pristine igneous rocks are too low to generate the observed $\delta^{18}O$ values.

The model predicts that the δD_{fluid} values should retain much of their original meteoric signature, whereas the $\delta^{18}O_{fluid}$ values should reflect equilibration with the oxygen composition of the host-rock mass, a process which is reflected in the Canadian Cordillera mesothermal gold deposits and the Asimotrypes results as well. The meteoric water model was proposed by Nesbitt and Muehlenbachs (1989a) to account for the common observation in Cordilleran lode deposits that δD values of inclusion fluids in quartz are extremely depleted in deuterium relative to the magmatic and metamorphic water fields. Also, the δD_{fluid} values demonstrate a systematic latitudinal dependence, in that they become progressively more depleted in deuterium at higher latitudes. A metamorphic dehydration model can not explain this observation.

From Figures 9.1 and 9.2, the area occupied by the Asimotrypes fluids lies outside of the metamorphic and magmatic water fields and could only be derived from these fluids through a significant negative shift in the δD_{fluid} values. It is suggested therefore, that the Asimotrypes mineralising fluids are of meteoric origin, perhaps incorporating a metamorphic fluid component, and that the observed fluid composition was derived by substantial interaction of this fluid with the rock mass. However, it is difficult to estimate the degree of this interaction, since the isotopic composition of the Palaeozoic to Upper Miocene meteoric water

in the study area is unknown, and hence the absence of a fluid evolution curve in Figure 9.1. The incorporation of the metamorphic fluid component in the Asimotrypes mineralised fluids is further evidenced from fluid inclusion microthermometric studies, where estimated P - T trapping conditions coincide with those of the retrograde metamorphism (Chapter 7, Fig. 7.6).

The apparent time lag between peak metamorphism and the onset of mineralisation is a common feature in many mesothermal gold deposits and it is a recurring problem for those in favour to the metamorphic dehydration model (Kyser and Kerrich, 1990; Nesbitt, 1991). To account for the discrepancy, Kyser and Kerrich (1990) suggest that in collisional belts which have experienced significant crustal thickening, peak metamorphism at depth may post-date peak metamorphism at shallower levels by up to tens of millions of years, thus accounting for the apparent discrepancy in age between mineralisation and metamorphism.

However, theoretical modelling by Connolly and Thompson (1989) suggest that much of the fluid generated by prograde reactions at depth is probably consumed by retrograde hydration reactions in the overlying dehydrated rocks. They also suggest that the amount of silica transported by metamorphic fluids is insufficient to explain the volume of quartz veining seen in metamorphic terranes, unless significant convective re-circulation of fluids occurs.

9.7 Transport of Gold

Most experimental studies pertaining to the transport of gold in hydrothermal ore solutions have focused on the role of chloride and reduced sulphur - containing ligands, although other complexes such as thio-arsenites and tellurium species may play some role (Seward, 1984). Gold solubility studies in chloride (Ogryzlo, 1935; Henley, 1973; Vilor, 1973; Wood et al., 1987; Zotov and Baranova, 1989; Seward, 1991; Gammons and Williams-Jones, 1995) and reduced sulphur - containing solutions (Ogryzlo, 1935; Zviaginicev and Paulsen, 1940; Weissberg, 1970; Se-

ward, 1973; Shenberger and Barnes, 1989; Renders and Seward, 1989; Hayahi and Ohmoto, 1991; Pan and Wood, 1994; Gibert et al., 1993; Zotov and Baranova, 1995; Benning and Seward, 1996) have demonstrated that under typical hydrothermal conditions (low oxidation potential, neutral to slightly acid pH), the dominant gold complexing ligands are reduced sulphur species. The stability constants for Au (I) chloride complexes at 25 ^{0}C, are up to twenty orders of magnitude smaller than those of Au (I) hydrosulphide complexes are (Seward, 1991) and, therefore the latter predominate. Despite this observation, the stability constants for Au (I) hydrosulphide complexes in high temperature and high-pressure environments are not yet well defined. This is particular true for low pH regions where no satisfactory data are available.

It is generally accepted that in near neutral pH, reduced sulphur bearing solutions, the dominant Au (I) hydrosulphide complex is $Au(HS)^-_2$ (Seward, 1973; Shenberger and Barnes, 1989; Renders and Seward, 1989; Zotov and Baranova, 1995). The stoichiometry of this complex has been firmly established over a wide range of temperatures (from 25 ^{0}C to 350 ^{0}C) and pressures up to 1000 bar. However, the high temperature equilibrium formation constants for this species from the different studies, vary up to 1.5 log units. The maximum solubility of gold as $Au(HS)^-_2$ is found where pH = pK_1 of H_2S. With increasing temperature, in accordance with the shift of pK_1 of H_2S towards more alkaline pH (Ellis and Giggenbach, 1971; Suleimenov and Seward, 1995), the maximum gold solubility also shifts to higher pH. Consequently, above 300 ^{0}C the species stable at lower pH will become increasingly important for gold transport (Benning and Seward, 1996).

For the acid pH region, two complexes have been proposed: $AuHS^0$ and $HAu(HS)^0_2$. For the neutral species, $AuHS^0$, proposed as the stable species at high temperatures by Seward (1973), the stoichiometry and stability constant were clearly determined at 25 ^{0}C by Renders and Seward (1989). Zotov and Baronova (1995) have conducted experiments at 350 ^{0} C in acid H_2S bearing solutions and

also suggested $AuHS^0$ as the stable species. The protonated complex, $HAu(HS)^0_2$, was suggested by Hayashi and Ohmoto (1991) on the basis of experiments in NaCl- and H_2S-bearing aqueous solutions at 250-350 ^{0}C. Gibert et al., (1993) have determined the solubility of gold in KCl solutions at temperatures up to 450 ^{0}C. From their data, $AuHS^0$ is likely to be the dominant species.

Recent studies by Benning and Seward (1996) in sulphide solutions at near neutral pH showed that the complex $Au(HS)_2^-$ is the dominant gold species. However, with increasing temperature, in accordance with the shift of pK_1 of H_2S towards more alkaline pH, the maximum solubility also shifts to higher pH values and consequently, at high temperatures the species stable at lower pH will dominate. It has been proven that over a wide range of temperatures and pressures in reduced sulphur-containing hydrothermal solutions of low pH, the stoichiometry of the dominant Au(I)-hydrosulphide complex, is $AuHS^0$. High temperature and high pressure equilibrium constants for the formation of the Au(I)-hydrosulphide complexes, $AuHS^0$, and $Au(HS)_2^-$, pertaining to the equilibrium

$$\mathbf{Au_{(S)} + H_2S = AuHS^0 + 1/2\ H_{2\,(g)}} \qquad (1)$$

and

$$\mathbf{Au_{(S)} + H_2S + HS^- = Au(HS)_2^- + 1/2\ H_{2\,(g)}}, \qquad (2)$$

have been calculated by Benning and Seward (1996). The equilibrium constant for reaction (1) varies from $\log K_1$ =-6.81 at 150 ^{0}C / 500 bar to a maximum of -5.90 at 200 ^{0}C / 1500 bar and decreases again at higher temperatures. For reaction (2) , a similar variation occurs: $\log K_2$ = -1.45 at 150 ^{0}C / 500 bar to a maximum of -1.03 at 200 ^{0}C / 1500 bar and decreases again at higher temperatures. The equilibrium constants for the uncharged complex $AuHS^0$, show that this species plays an important role in the transport and deposition of gold in ore depositing environments which are characterised by low pH fluids.

Data obtained through this study allow the following summation to be made

regarding the mineralising fluid, which formed the Asimotrypes carbonate-hosted mesothermal gold deposit. Mineralisation was formed at a mean temperature of 312 ^{0}C and a mean pressure of 3.3 kbars; the average mole fraction carbonic species in the fluids was about 0.06 as determined by the mass spectrometer gas analyses, and fluid salinities range from 0.61 to 7.31 wt% NaCl equivalent with an average of 4.41 wt% NaCl equivalent, as indicated by microthermometric calculations. Furthermore, δ^{34} S and δ^{13} C analyses and interpretation suggest that the log oxygen fugacities were most probably within the range -30 to -32 and pH near neutral at 6.5 (Chapter 8). At Asimotrypes there is no indication that sulphates were ever deposited and thus it is likely that $f\,O_2$ levels were below those at the SO_4 / H_2 S equal concentration boundary during all phases of mineralisation (Ohmoto, 1972; Ohmoto and Rye, 1979). Further evidence for this is the relative constancy of δ^{34} S values for all the main sulphides. The presence of pyrrhotite in association with pyrite (Chapter 5) is an indicator for strongly reducing conditions (Ohmoto, 1972). Although in the Asimotrypes ore, pyrrhotite is strongly localised, it is fairly common in otherwise similar arsenopyrite-pyrite mineralisations (Steed and Morris, 1997). It is not certain that the two minerals were simultaneously deposited and thus this can only be taken as an indication of a generally reduced environment. However, additional evidence for a reducing environment is the presence of CH_4 in the mineralising fluids.

Based on the above, it is suggested that sulphide species, such as $Au(HS)_2^-$, were probably the most effective complexing agents for gold in the Asimotrypes hydrothermal fluids which were typically low in salinity. A relative paucity of base metals in the ore may also indicate that chloride complexing of gold was not important.

9.8 Mechanisms of Gold Deposition.

Gold is precipitated from hydrothermal ore fluids in response to changes in the physicochemical conditions of the fluid at the site of ore deposition. These specific

changes in ore-fluid chemistry can result from a number of processes, including:

- pH changes toward more acidic or alkaline conditions from near neutral solutions
- fO_2 shifts via redox reactions and / or CO_2 immiscibility
- a decrease of the reduced sulphur species activity due to sulphide precipitation
- wall-rock alteration and / or H_2S loss accompanying fluid unmixing
- cooling and dilution of ore fluids

It is never only one factor which causes gold to precipitate from the transporting solution but a mixture of interdependent factors which are different from deposit to deposit. The main reasons for decreasing the solubility of gold in high temperature sulphide solutions are because of changes in pH and/or total reduced sulphur concentrations. In ore depositing systems, this is achieved by wall-rock interaction, oxidation of the fluids (e.g. mixing with meteoric or seawater), boiling with loss of the volatile components (H_2S, H_2, CO_2) or precipitation of sulphide minerals. A temperature and pressure decrease is often assumed to cause precipitation. The effect of temperature on the solubility of gold in sulphide solutions is very strongly related to the total sulphur concentration and the oxygen fugacity. In systems where high sulphur and low oxygen fugacities occur, decreasing temperature may play an important role in the precipitation. It has been shown experimentally by Benning and Seward (1996), that in acid pH solutions, a decrease in pressure will favour the precipitation of gold from solution, whereas in near neutral solutions, a drop in pressure will increase the solubility of gold, and, therefore, precipitation will be impeded. However, this effect is probably only important in the near neutral region.

The pH change was not an effective cause for gold precipitation at Asimotrypes, because wall-rock alteration, if any, was too weak. This is suggested by $\delta^{18}O$ and $\delta^{13}C$ isotopic analyses (Chapter 8). Finally, the gold ore at Asimotrypes is restricted to thrust and shear planes.

The oxygen fugacity of the earliest Asimotrypes fluids decreased through interaction with wall-rock carbon, with a likely reduction in solubility of the gold bisulphide complex. However, this mechanism was also not a major control on gold deposition because there is no spatial relationship between gold concentration and amount and distribution of carbon in ore hosting marbles.

A decrease of sulphur species activity and cooling are suggested to be the favoured depositional mechanisms for Asimotrypes. Figure 9.3 shows a probable mechanism for gold precipitation based on mineralogical and fluid inclusion constraints. The close association of gold and sulphides indicates that sulphide precipitation caused a decrease of sulphur activity, and thus decreased the solubility of gold thio-complexes (Groves et al., 1987; Neall and Phillips, 1987). Fluid immiscibility and accompanying H_2S loss to the vapour during entrapment of early, CO_2 -rich fluids could also enhance the decrease of sulphur activity (Walsh et al., 1988; Lu and Seccombe, 1993). Total sulphur concentrations in ore fluids are assumed to have decreased from approximately 0.01 to 0.001 moles. Evidences of cooling and dilution include the presence of aqueous fluid inclusions as samples of late stage, cooler and more dilute fluids, and interpretation of available mineral assemblages.

Role of CO_2

Although detailed textural evidence for CO_2 effervescence is generally equivocal or circumstantial, the areal fluid composition trends documented in this research are compelling evidence in favour of effervescence of CO_2 from the mineralising fluids. Effervescence of CO_2 may have occurred either in response to a switch from lithostatic to hydrostatic fluid conditions as the fluid was forced through the solvus in the H_2O-CO_2-NaCl system, or during regional uplift.

If loss of CO_2 from an effervescing system accounts for the areal trends seen at

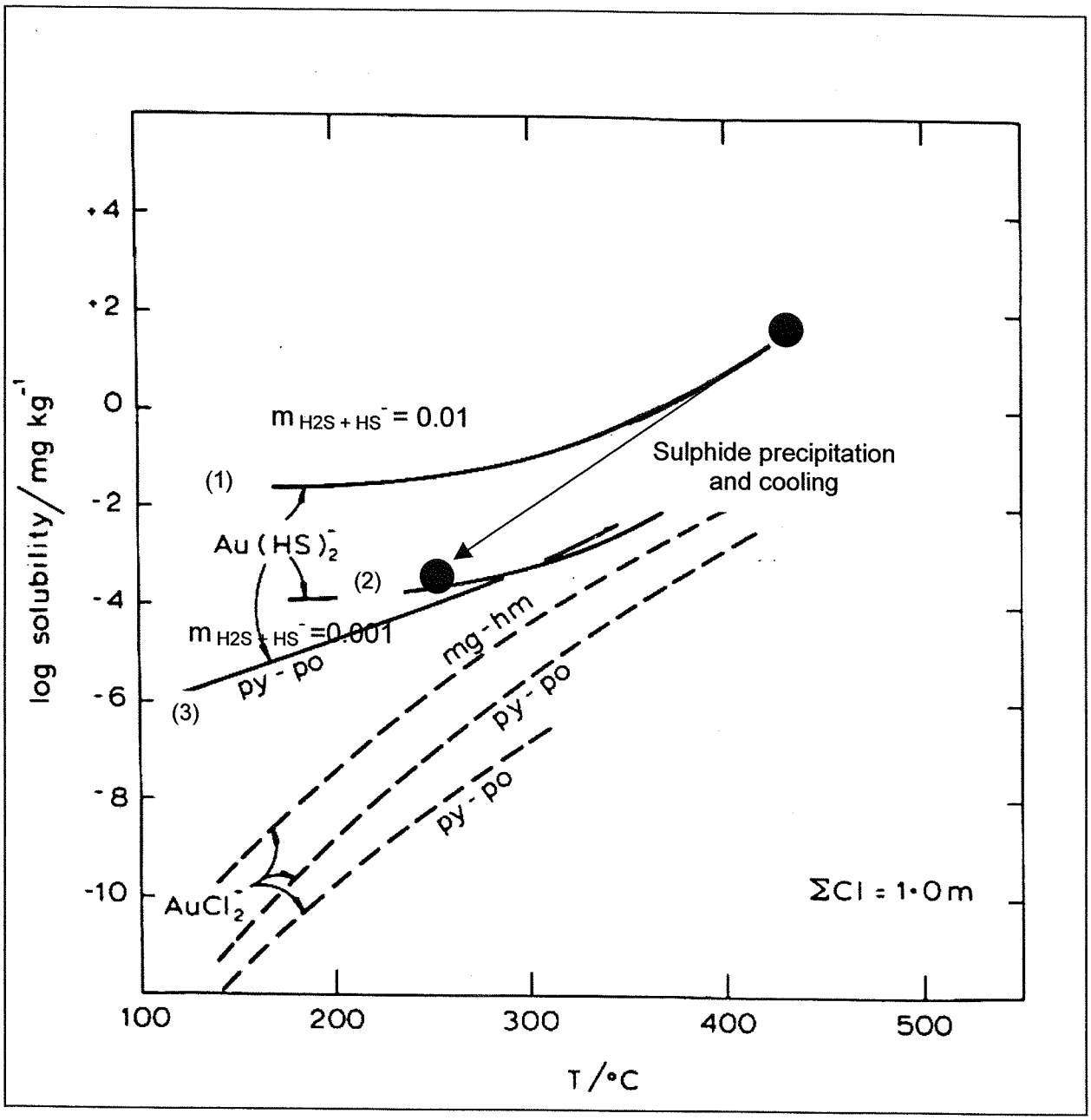

Figure 9.3: Logarithm of the solubility of Au versus temperature for solutions containing 1.0 m chloride; curves (1) and (2) are the solubility of Au as $Au(HS)^-_2$ in equilibrium with pyrite + pyrrhotite at pH=5 and total reduced sulphur ($H_2S + HS^-$) = 0.01 and 0.001 m respectively and are from Seward, 1982; curve (3) is the same as (1) and (2), but with no excess sulphur and is from Belevantsev et al., 1982.

Asimotrypes, the peak in homogenisation temperatures observed in the studied area becomes readily explainable. When the P-T path of an H_2O-CO_2-NaCl fluid intersects the solvus, a CO_2-rich phase is exsolved. As the fluid is trapped on the solvus, the fluid inclusion homogenisation temperatures will be approximately equal to the trapping temperature but will be higher than homogenisation temperatures recorded for higher density fluids trapped at greater depths and higher pressures within the hydrothermal system. Thus, as fluid decreases, homogenisation temperatures would be expected to increase to a maximum at the point of CO_2 loss. The system then becomes H_2O-NaCl ($\pm$ CO_2), and as the fluid density increases with decreasing temperature, progressively lower homogenisation temperatures will be recorded by primary inclusions. Thus homogenisation temperatures would be expected to peak at the point of CO_2 effervescence.

The general trends observed in the Asimotrypes P-T-X data correspond well with this model, implying that the loss of CO_2 from the system occurred in response to a gradual pressure drop as the fluid moved up through a large scale hydrothermal system or more likely as regional uplift forced the hydrothermal system through the solvus in the H_2O-CO_2-NaCl system, rather than in response to rapid pressure loss due to the fault-valve action or seismic pumping (Sibson, 1990). This argument is supported in part by the general lack of brecciation of the mineralisation.

Finally, Shelton et al., (1988), Nesbitt and Muehlenbachs (1989), Rushton et al., (1993), and So and Yun (1997) have shown that decrease of sulphur activity via sulphide precipitation and/or H_2S loss accompanying boiling and CO_2 effervescence was the most important and critical mechanism for gold deposition in the Korean and Canadian Cordillera mesothermal gold deposits.

9.9 Heat Source

Uplift rates in some metamorphic belts have been shown to be very high. Craw

(1988) reported that uplift rates in the Alpine schists in New Zealand were as high as 10 km per million years, approximately equal to removal of the entire greenschist facies. In such areas, crustal geotherms tend to curve upward toward the surface. Theoretical modelling of the thermal state of high uplift regions by Craw and Coons (1988) indicates those uplift rates of greater than 2mm per year (2km/m.y.) result in temperatures of greater than 300 °C at depths of less than 5 km. In this type of system, fluid flow is initiated by buoyancy effects because of the high heat flow as a result of topographic effects due to uplift. Also, hydrothermal fluid systems in these areas are likely to be longer lasting than, say, pluton related systems, because the heat source is a regional feature (Norris and Heley, 1976; Nesbitt, 1990).

In the Western Rhodope the regional uplift started in the Eocene and it was completed in the Miocene. During this time the Lower Tectonic Unit was isothermally uplifted from an approximate depth of 53 km to 14 km (Mposkos, 1994). This implies that for the time given, the rate of uplift was 1mm per year (1 km/m.y.) for temperatures over 300 °C, estimated from fluid inclusions microthermometry (Table 7.2). Thus it is conceivable that the Asimotrypes system was of sufficient duration to allow mineralisation to occur during significant vertical uplift; perhaps as much as approximately 30 Km during the life of the hydrothermal system , if uplift rates were high enough. Perturbation of the normal geothermal gradient caused by uplift would probably be sufficient to drive convection of meteoric fluids in the rock mass.

9.10 Genetic Model for the Asimotrypes Carbonate-hosted Mesothermal Gold Deposit

The results of this research on the genesis of the Asimotrypes carbonate-hosted mesothermal gold deposit suggest deep convection and chemical evolution of meteoric water. In this model, meteoric water penetrates rock units of the brittle regime of the continental crust to a depth limited by the brittle-ductile transition,

which occurs at depths of approximately 14 Km and temperatures of 350^0 to 450 ^{0}C in terranes undergoing strike-slip faulting (Sibson, 1986). Beneath this boundary, the permeability of the rock units most likely undergoes a major reduction, which serves as a hydrologic barrier for the lower extension of the convection cell.

During fluid influx in this system, the downward migrating water will be exposed to a large rock surface area producing low water/rock ratios. This is reflected in the light $\delta\ ^{18}O$ values for the ore-forming fluids, which have been strongly enriched in ^{18}O and are relatively uniform throughout the system. As these fluids move through the brittle regime at temperatures up to 400 ^{0}C, they will approach equilibrium with the rock units, which are undergoing active, low-grade metamorphism. This interaction with the rock units at a low water/rock ratio will tend to produce values for variables, such as X_{CO2} , $f\,O_2$, $f\,S_2$, pH etc., which are buffered by the rock units. In addition, the fluid acquires the Si, W, As, Sb, and Au, which are later precipitated.

As the fluids begin to rise, they cool and depressurise. At approximately 2.7 kbar pressure, immiscible separation of the CO_2-rich phase occurs, decreasing the density of the residual H_2O-rich phase. At approximately neutral pH of 6.5 with Au in $Au(HS)_2^-$ complexes, and at 300 ^{0}C sulphides will be precipitated due to decrease of sulphur activity resulting in decreased solubility of gold thiocomplexes (Groves et al., 1987; Neall and Phillips, 1987; Benning and Seward, 1996). This process will cause Au superaturation and precipitation.

The genetic model proposed requires convection of meteoric water down through the brittle regime to the brittle-ductile transition. This can be tested using the Rayleigh-Darcy equation:

$$\mathbf{Ra = (ga\rho(\rho Cp)\Delta THK/\upsilon\lambda)}$$

whereas: Ra = Rayleigh number, g = gravity, a = thermal expansity, ρ = density, Cp = heat capacity, ΔT = temperature difference, H = thickness of permeable

unit, K = intrinsic permeability, υ = viscosity, λ = thermal conductivity. In convective regimes, values for Ra are greater than 40 (Straus and Schubert, 1977).

Russel (1983), Criss and Taylor (1986) and Nesbitt (1988) have considered applications of the Rayleigh-Darcy equation to the evaluation of convection in the brittle crustal regime among others. In each of these studies the limiting factor in the determination whether fluids will convect or not is invariably the permeability. There is general agreement between the various authors that a permeability of approximately 10^{-17} m^2 or greater is necessary for convection. Due to the highly fractured nature of the rock units in active continental margins, permeabilities in excess of 10^{-17} m^2 are typical and may be as high as 10^{-14} m^2 (Brace, 1980). The presence of strike-slip fault zones is particularly important, because the zones provide highly permeable, vertically continuous pathways for fluid movements. Consequently, convection of meteoric water can and must occur within the brittle regime of active continental margins with a probable lower limit provided by the brittle-ductile transition (Nesbitt and Muehlenbachs, 1989).

As described above, the convecting meteoric water passes through rock units undergoing active, low-grade metamorphism. Consequently, the fluid phase will be a mixture of the convecting meteoric water and the fluids produced by metamorphic devolatilisation. Some first approximation calculations can serve to determine how significant the contribution of each fluid source is to the ore fluid (Nesbitt and Muehlenbachs, 1989). A typical estimate for the velocity of the convecting meteoric water in these systems is 1 m/year (Chris and Taylor, 1986), combining this figure with a density for H_2O at 300 ^0C and 1 kbar of 0.83 g/ cm^3 (Burnham et al., 1969) and porosity estimates varying from a maximum of 1 percent to a minimum of 0.1 percent (Chris and Taylor, 1986) infers a maximum flux rate of meteoric water of 8.3 kg/m^2/year and a minimum rate of 0.83 kg/m^2/year (Nesbitt and Muehlenbachs, 1989). Estimates by Walter and Orville (1982) of the total fluid flux of devolatilisation fluids during metamorphism range from a maximum of 0.3 kg/m^2/year to a minimum of 0.03 kg/m^2/year, passing verti-

cally through a column of rock. The results of this calculation indicate that the component of convecting meteoric water constitutes about 95 percent of the fluid in the brittle regime.

In the previous Chapters and sections an attempt has been made to describe the regional structural setting of the Asimotrypes ore, its mineralogy and geochemistry, P-T conditions, fluid chemistry and source in order to define the genetic model. A final attempt will be made to link the origin of the mineralisation and ore formation with a coherent geologic model in which ore formation occurred during, and in response to, an extended regional tectonic event.

- Deposition of carbonates in a shallow marine environment during Paleozoic-Mesozoic, followed by diagenesis, lithification and metamorphism.

- Thrusting of marine carbonates over a quartzo-feldspathic basement sequence; shear zones are concentrated in the Transitional Zone along schist-gneiss-marble contacts. Subduction of the whole unit to a maximum depth of ≈53 Km in the ductile deformation zone, following a path with a mean temperature increase of 11.5 ^{0}C/Km, during Palaeocene to Eocene. Ductile deformation is dominated by compressional tectonics in depth resulted in the formation of isoclinal folds corresponding to high-pressure eclogite metamorphic phases.

- Uplift, following an isothermal path reached the brittle deformation zone ≈ 14 Km, accompanied by dehydration reactions. Brittle tectonism characterised by compressional tectonics developed NE-SW, NW-SE and E-W trending low-angle thrust and shear faults referred to as palaeo-thrusts of pre-Oligocene age and neo-thrusts of Middle Eocene. These thrusts are tectonometamorphic events associated with medium pressure metamorphic phases. During late Eocene to early Miocene the brittle tectonism is due to extensional deformation. This event, accompanied by the intrusion of the Nikisiani granodiorite in Oligocene, formed subsequently the horst-graben structures. Descending meteoric water mixed with

ascending metamorphic fluids generated by dehydration reactions, initiate a metallogenic hydrothermal convective system driven by uplift rates in the transition of the ductile-brittle zone.

- Post magmatic development of sub-vertical faults and veins along the margins and the interior of the horst, related to retrograde metamorphism in Miocene, acted as channels driving the metalliferrous fluids into the tectonically prepared sites and replacement type mineralisation was formed. Mineralisation cross-cuts the granodiorite and follows earlier shears.

- Uplift continues with cooling and basins are developed in the intervening areas; oxidation of sulphide ores.

CHAPTER 10

CONCLUSIONS

As outlined in Chapter 1, the purpose of this study was to investigate the Asimotrypes carbonate-hosted mesothermal gold deposit from a geochemical standpoint in order to define its nature and origin. The conclusions arrived at, on the basis of the interpretations placed on the data acquired in this study include the following:

- The Asimotrypes carbonated-hosted mesothermal gold deposit is of replacement and shear-style mineralisation. Precious and base metal mineralisation is emplaced as irregular pods along thrusts between marble units and schists within the Transitional Zone, or as small quartz veins within the marbles. Mineralisation has also been located in vertical fault zones which extend upwards through the underlying schists and appear to be feeders for the main mineralisation.

- According to field observations and petrographic studies, the carbonate rocks of Pangeon can be grouped in six types. Dolomites rocks, partially or completely de-dolomitised, are abundant and they are lithostrigraphically controlled. Field observations combined with petrographical textures and geochemical data could be accounted for by either neomorphism of an earlier dolomite or by replacement of a limestone under burial conditions.

- The impure calcitic marble (Type I) is correlated with mineralisation and Types II and VI are correlated with the oxidised sulphide mineralisation. The relationship of dolomitisation and the mineralisation bearing carbonate rocks is debatable. The inverse process of dolomitisation, de-dolomitisation has a positive relationship with

the mineralisation within the marbles, which is probably due to similar favourable conditions for the de-dolomitisation mechanism and ore deposition.

- The mineral paragenesis through a NW-SE sub-vertical fracture up the mountain changes from pyrite + quartz, to pyrite + quartz + sericite, to sericite in the granite overlying the Asimotrypes, to pyrite + sulphides where the veins cross overlying marble and schist units. The Asimotrypes ore consists mainly of arsenopyrite, pyrite and gold, with subordinate sphalerite, galena, chalcopyrite, pyrrhotite, tetrahydrite-tennantite, marcasite, covellite and malachite. Gangue minerals include dominantly quartz and lesser muscovite-sericite.

- Gold appears relatively early in the sulphide paragenetic sequence. Gold mineralisation is often typified by refractory ore as solid solution in arsenopyrite and less frequently in arsenian-pyrite, or can be found free in Fe-oxide (goethite) veinlets with residual pyrite.

- Gold is found in the sub-vertical vein system, which cuts all the rock lithologies including the granite, as well as in irregular pods and lenses developed along the thrust contacts between the marbles and schists. The highest gold values come from the arsenopyrite-pyrite pods at Asimotrypes, with average values ranging from 11-13 ppm. Sulphides developed as small lenses in the sub-vertical vein system are also rich in gold.

- The base metal content is uniformly low. In this respect the Asimotrypes gold deposit conforms to the general pattern of highly enriched rare elements coupled with low degrees of enrichment of base metals, characteristic of many mesothermal lode gold deposits of both vein and chemical sedimentary types.

- Three types of fluid inclusions (with subtypes) were recognised based on con-

stituent phases at room temperature and microthermometric behaviour:

(i) H_2O-CO_2 3-phase inclusions: L_1 (H_2O) + L_2 (CO_2) + V (CO_2), characterised by highly variable CO_2/H_2O volumetric ratios. These inclusions are further subdivided into H_2O-rich inclusions (10-40 volume CO_2) which homogenise to the liquid (aqueous) phase and CO_2-inclusions (70-90 volume % CO_2) which homogenise to the vapour (carbonic) phase.

(ii) Aqueous 2-phase inclusions: L+V. These contain an aqueous liquid and an aqueous vapour phase occupying 10-20 % of the inclusion volume. They always homogenise to the liquid phase.

(iii) Naturally decripitated and/or leaked inclusions: V or L+V. Decripitated inclusions are either empty or contain a vapour phase, whereas leaked varieties exhibit inconsistent vapour/liquid ratios.

- Mineralising fluid pressures and temperatures indicate early ore deposition during phase separation at temperatures between 275^0 C and 310^0 C at calculated pressures between 2.7 and 3.1 kb followed by late deposition at temperatures down to 130^0 C and very low near-surface pressures.

- Mineralising fluid temperatures and pressures approach closely those of regional retrogressive greenschist facies metamorphism (T=350^0 - 400^0 C, P=3-5 kb), and attest to the conditions of syn-to post-metamorphic cooling.

- The $\delta\ ^{34}S$ values for arsenopyrite, pyrite and chalcopyrite from the Asimotrypes ore are 2.19 to 2.89, 2.28 to 3.13 and 2.17 to 2.24 per mil respectively. Petrographic textural evidence and Δ Asp-Py fractionation values indicate that isotopic equilibrium did exist between arsenopyrite and pyrite. $\delta\ ^{34}S$ values have a mean value,

which is generally considered characteristic for a magmatic source for the sulphur and it is recorded for magmatic intrusions in the surroundings of the mineralised sites.

- From diagrams showing the relationship between oxygen fugacities and pH for specific sulphide $\delta\,^{34}S$ values, upper limits for fo_2 at 10^{-31} and for pH 6.5 are obtained.

- Carbon isotope values from calcite marbles are remarkably constant over a narrow range between 1.89 to 2.94 per mil, and the $\delta^{13}C$ in the fluid was 4.12 ± 0.35 (1σ) and 4.68± 0.35 (1σ) at 275^0 C and 340^0 C respectively, during ore deposition stage. $\delta^{13}C$ values around 0 ± 4 per mil are indicative of a marine environment for ore deposition. A plot of $\delta^{13}C$ versus $\delta\,^{18}O$ values of calcite show also a marine environment of deposition. The rather high $\delta^{13}C$, above +2 ‰ suggest a shallow sea and warm climate conditions. $\delta^{13}C$ values of 4.68 ± 0.35 are consistent with CO_2 of metamorphic origin produced during decarbanation reactions of carbonate rocks, interpretation in agreement with the de-dolomitisation processes in marbles.

- Median $\delta^{18}O$ values for marble calcites, quartz, sericite and whole rock are 29.31 ± 0.94 (1σ) ‰, 21.87 ± 0.52 (1σ) ‰, 13.38 ± 0.86 (1σ) ‰, and 16.15 ± 0.26 (1σ) ‰ respectively, and are considered as metamorphic oxygen values. Calculated median ore fluid composition at 275^0 C and 340^0 C in the system calcite-water is 22.94 ± 0.93 (1σ) ‰ and 24.77±0.93 (1σ) ‰, in the quartz-water system is 14.06 ± 0.52 (1σ) ‰ and 16.31± 0.52 (1σ) ‰ and in the water-muscovite is 9.41± 0.52 (1σ) ‰ and 10.88 ± 0.52 (1σ) ‰ respectively. These values are consistent with values of metamorphic fluids.

- The remarkably constant carbon and oxygen isotope values for marble samples, close and away from the ore, suggest that replacement of the marbles by the sulphides obviously took place along sharply restricted zones, i.e. fault planes channelling the metal bearing fluid. Directly outside the channel zones only weak, if any,

oxygen isotopic exchange between the marble and the fluids occurred, with the carbon isotopic signature undisturbed.

- Whole rock hydrogen isotopic data for the Asimotrypes ore and the Nikisiani granite have a median value of -117 ± 7.5 (1σ) ‰ and -82 ± 6.21 (1σ) ‰ respectively. These values imply that ore fluids represent meteoric waters.

- The Asimotrypes mineralising fluids are of meteoric origin, perhaps incorporating a metamorphic fluid component.

- ^{87}Sr / ^{86}Sr isotope ratios have an average of 0.707920 ± 0.00010 (1σ) implying a seawater derivation of Sr that is consistent with interpretation made based on bulk rock geochemistry results and conclusions drawn from C and O isotope values from ore-host marble samples.

- Lead isotope data in ores from the Rhodope and Serbomacedonian Massifs are largely uniform and show a crustal affinity with high ^{208}Pb / ^{204}Pb ratios.

- Sulphide species, such as $Au(HS)_2^-$, were probably the most effective complexing agents for gold in the Asimotrypes hydrothermal fluids which were typically low in salinity. A relative paucity of base metals in the ore may also indicate that chloride complexing of gold was not important.

- A decrease of sulphur species activity and cooling are suggested to be the favoured depositional mechanisms for Asimotrypes. The close association of gold and sulphides indicates that sulphide precipitation caused a decrease of sulphur activity, and thus decreased the solubility of gold thiocomplexes. Fluid immiscibility and accompanying H_2S loss to the vapour during entrapment of early, CO_2 -rich fluids could also enhance the decrease of sulphur activity. Evidences of cooling and dilu-

tion include the presence of aqueous fluid inclusions as samples of late stage, cooler and more dilute fluids, and interpretation of available mineral assemblages.

- Regional uplift started at Eocene in Western Rhodope Massif and it was completed in Miocene. During this time the Lower Tectonic Unit was isothermally uplifted from an approximate depth of 53 km to 14 km, in the transition of the ductile-brittle zone. Perturbation of the normal geothermal gradient caused by the regional uplift was probably sufficient to drive convection of meteoric fluids in the rock mass.

- Combined with geological evidence, the fluid inclusion and stable isotope data of the Asomotrypes gold mineralisation, are consistent with genesis from deeply convecting meteoric water driven by regional uplift through rocks undergoing retrogressive greenschist facies metamorphism.

- Finally, the present study and the comparison of the Asimotrypes Tertiary mesothermal gold deposit with other similar Archean and Phanerozoic mesothermal deposits, revealed an apparent and close similarity among them. Some differences between the compared districts, largely in rock-host type, hydrothermal alteration, and relation to plutons, most likely reflect local geological heterogeneities. Recognition and documentation of the similarities between Archean and Phanerozoic mesothermal deposits stated above reported also by Hutchinson (1987) and Kerrich (1987), support a classification scheme of a single general category of mesothermal lode gold deposits encompassing mesothermal ores ranging from Archean to Tertiary in age.

APPENDIX I

SAMPLE DESCRIPTIONS

Sample Descriptions

Samples As-1 to As-18, As-31 and As-65, As-66, As-67, As-71, As-72 and As-75 are from the main 3K-D adit, altitude 1200 m above sea level (Fig.1). It is a wide construction made by Bauxite Parnassus Company, who opened three adits into the Asimotrypes mineralisation in order to investigate the continuation and quality of the ore exploited by the ancients. On the East Side of the adit entrance an arsenopyrite-pyrite sub-horizontal lens is exposed against shear banded marble. The lack of skarn between the ore lens and the marble is noticeable. Only a 2cm thick skin of limonite.

In addition to the sub-horizontal lenses, sub-vertical ± 130 ^{0} trending faults are present crossing in some cases the ore lenses and are variably mineralised with pyrite, limonite and sometimes malachite. At a higher level above the adit entrance thin sub-vertical limonite filled structures are present, with limonite disseminating laterally out along sub-horizontal planes in the marble. It is apparent that the 130 ^{0} fracture system is post shearing.

As-1: Shear banded, impure calcitic Type IV marble, with thin fractured zones.
As-2: Limonitic banded rock, forming skin to sulphide ore.
As-3: Limonite with pyrite, skin to arsenopyrite-pyrite lens.
As-4: Shear banded, impure calcitic Type IV marble, hanging wall.
As-5: Shear banded, impure calcitic Type IV marble, 5 m above As-4.
As-6: Phlogopitised gneiss with pyrite, above the As-5.
As-7: Fresh, shear banded, impure calcitic Type IV marble, 10 m above the 3K-D adit entrance.
As-8: Phlogopitised gneiss schist, intercalated in impure calcitic Type IV marble.
As-9: Shear banded, impure calcitic Type IV marble to the east of As-8.
As-10: Phlogopitised gneiss schist, highest point above the 3K-D adit entrance.

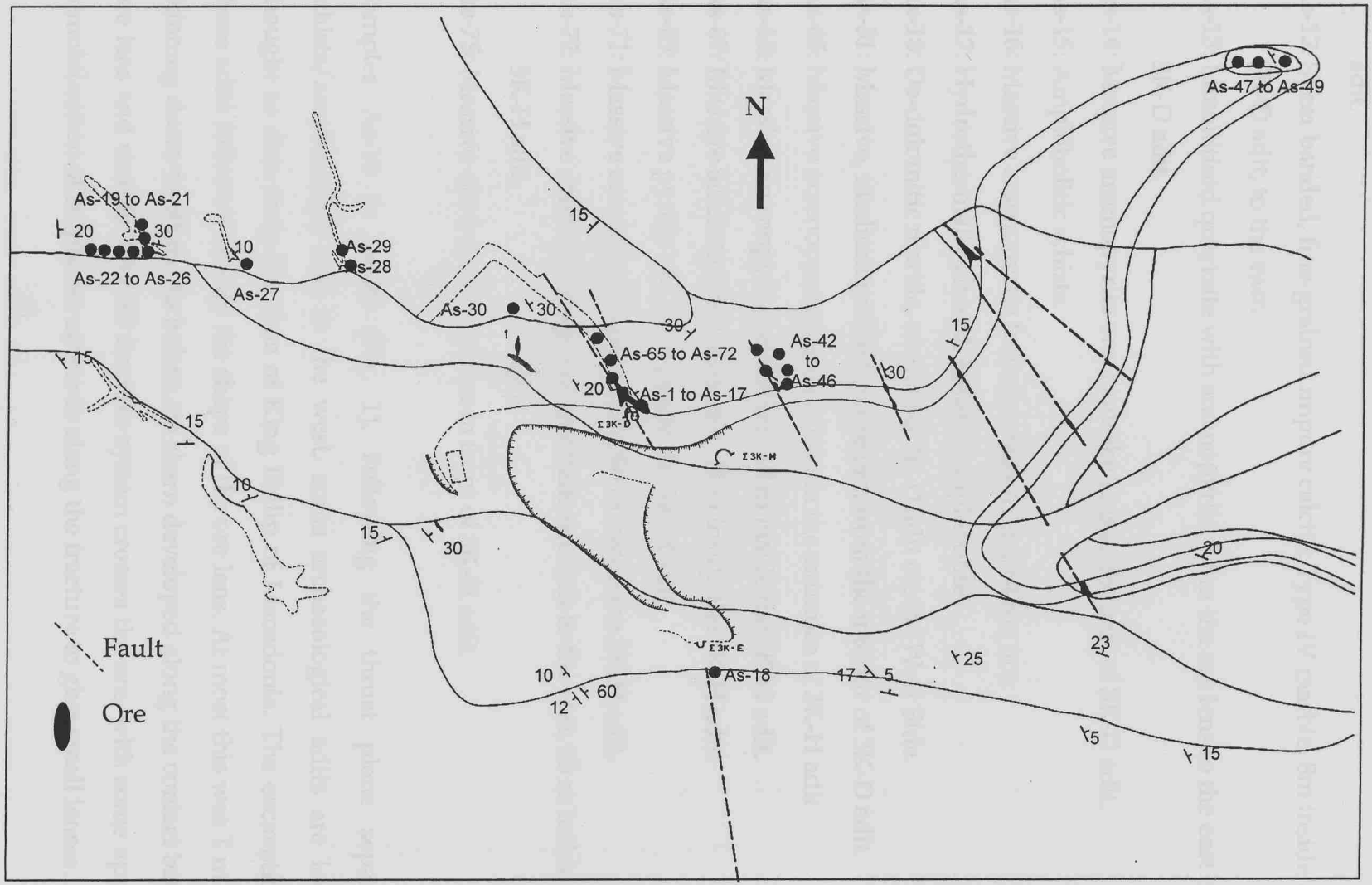

Figure 1: Sample location map in 1:500 scale, Asimotrypes mine area.

As-11: Massive arsenopyrite-pyrite quartzite, from the ore lens to the east of 3K-D adit.

As-12: Shear banded, fine-grained impure calcitic Type IV marble, 8m inside the 3K-D adit, to the east.

As-13: Limonitised quartzite with arsenopyrite, from the ore lens to the east of 3K-D adit.

As-14: Massive arsenopyrite ore, from the lens to the east of 3K-D adit.

As-15: Amphibolitic schists.

As-16: Massive arsenopyrite from the eastern end of the ore.

As-17: Hydrothermally altered, foliated amphibolite.

As-18: De-dolomitic marble, overlying 3K-D adit on the West Side.

As-31: Massive, medium grained pyrite ore, from the interior of 3K-D adit.

As-65: Massive arsenopyrite-pyrite ore from the entrance of 3K-H adit

As-66: Massive arsenopyrite-pyrite ore, 10 m inside the 3K-H adit.

As-67: Massive arsenopyrite-pyrite ore, 20 m inside the 3K-H adit.

As-69: Massive pyritic ore, 40 m inside the 3K-H adit.

As-71: Massive arsenopyrite-pyrite ore, 60 m inside the 3K-H adit.

As-72: Massive arsenopyrite-pyrite quartzite ore lens to the east, 65 m inside the 3K-H adit.

As-75: Massive ore from the dumps in front of 3K-H adit.

Samples As-19 to As-30 (Fig. 1). Following the thrust plane separating schists/amphibolites and to the west, some archaeological adits are located, thought to date from the time of King Philip of Macedonia. The excavations at these adits followed exactly the shape of the ore lens. At most this was 1 m thick, thinning down to 60cm. As before, no skarn developed along the contact between ore lens and marble. NW-SE fracture system crosses the ore, with some apparent remobilisation of sulphides upwards along the fracture to give small lenses.

As-19: Massive arsenopyrite-pyrite pods from sub-vertical fault zone.

As-20: Limonitic coating on NW-SE sub-vertical faults.

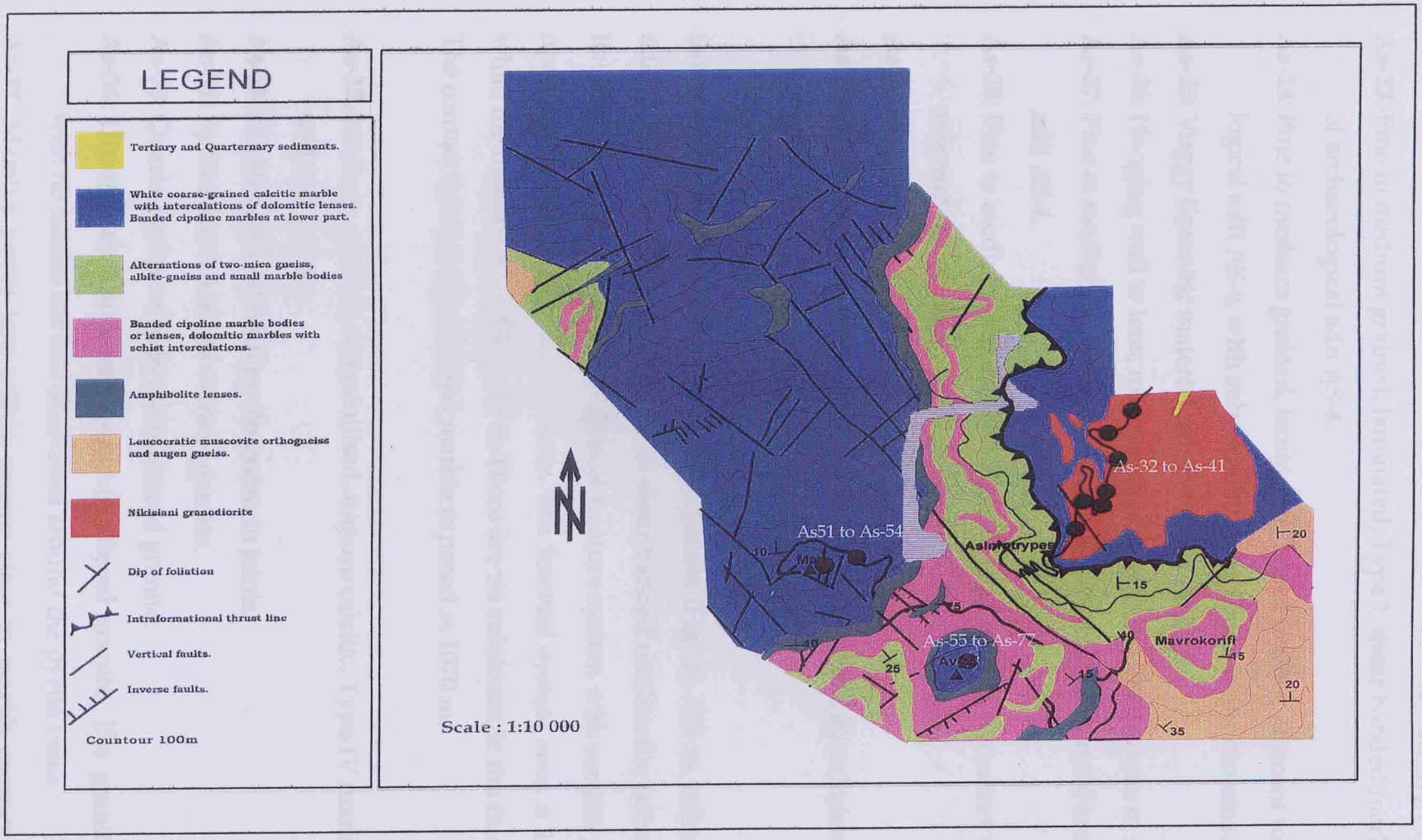

Figure 2: Sample location map in 1:10000 scale, Asimotrypes regional area.

As-21: Coarse arsenopyrite-pyrite ore from sub-horizontal thrust plane.

As-22: De-dolomitic shear banded marble, 15 m west of archaeological adit AS-4.

As-23: Fine to medium grained, laminated, Type I, shear banded marble, 6 m west of archaeological adit AS-4.

As-24: Fine to medium grained, laminated, Type I marble, adjacent to archaeological adit AS-4, with sub-parallel crosscutting limonite veins.

As-25: Vuggy limonitic material parallel to the foliation.

As-26: Hanging wall to lens; manganese and limonite filled cracks in marble.

As-27: Fine to medium grained, laminated, Type I marble, west of archaeological adit AS-4.

As-28: Fine to medium grained, laminated, Type I marble, in contact with limonite and manganese.

As-29: As in As-28.

As-30: Fine to medium grained, laminated, Type I marble, 80 m before 3K-D main adit.

Samples As-32 to As-41 in and around granite (Fig. 2), 120 m below 3K-D main adit. A 3m wide aplitic vein crosscuts shear banded marble; the vein is weakly foliated, and cut by an open sub-vertical fracture system with sericite growing into open spaces and across the fractures. The fracture system runs ± 150 / 70^0 W, while the foliation runs 120 / 40^0 S. There are no sulphides in the fracture system. The contact between granite and marble exposed at 1070 m.

As-32: Medium grained, recrystallised, impure calcitic, Type IV marble, in contact with the granite.

As-33: Foliated granite with pyrite grains in joints.

As-34: Pyrite-quartz-sericite veins in granite.

As-35: Quartz-pyrite veins in white altered granite.

As-36: Disseminated and vein pyrite in altered granite. The granite is leached, with no mafics left in a 20cm zone around the pyrite veins.

As-37: Massive pyrite lens within granite close to marble contact. There is no

skarn developed along the contact, and the pyrite is developed in the granite and not in the marble.

As-38: Thin, 2cm breccia zone in granite.

As-39: Weakly foliated, fresh granodiorite; minor amounts of mafic inclusions, no alteration, no mineralisation.

As-40: Blocks of limonitised, pyritised granite.

As-41: Quartz veins with pyrite in granite.

Samples As-42 to As-50 (Fig. 1), starting 20 m west of the main 3K-D adit to 200 m west.

As-42: Sub-vertical, barren quartz vein.

As-43: Sub-horizontal, barren quartz lenses in gneiss-schist.

As-44: Massive arsenopyrite-pyrite lenses in sub-vertical limonite zones.

As-45: Quartz veins with malachite and chalcopyrite.

As-46: Malachite disseminations in gneiss-schists hosting samples As-45 and As-46.

As-47: Single outcrop and series of blocks of shear banded marble in which magnetite-epidote-hornblende-chlorite ± garnet skarn is developed. The skarn bands are mostly thin , 10 cm seems to be the maximum. There is no relation of the skarn to the mineralisation, since this kind of skarn banding is common in marbles throughout the region.

As-48: Thin, folded skarn - magnetite bands in marble.

As-49: Intensely folded magnetite and marble bands; minor garnet.

As-50: White, very coarsely crystalline calcitic marble, Type V, 735 m elevation. Locally sheared and banded. A thin aplite vein runs parallel to the banding.

Samples As-51 to As-54 are from the highest point of the Pangeon, at 1956 m elevation, vertically above Asimotrypes, west side (Fig. 2).

As-51: Sheared, fine to medium grained dolomitic marble, Type II, with fine manganese network veining.

As-52: White, recrystallised de-dolomitic marble, Type VI. Part of a 700 m thick unit above the thrust.

As-53: Sheared, fine grained, impure calcitic marble, Type IV.

As-54: Phlogopitised, mm-cm banded, impure calcitic marble, Type IV.

Samples As-55 to As-77 are from the ancient adits at Avgo (Pilaf Tepe), vertically above Asimotrypes to the east (Fig. 2). Mineralisation has been totally exhausted by the ancients.

As-55: Massive, fine to medium grained non-ferroan dolomitic marble, Type II, with manganese veinlets and disseminations.

As-56: White, fine grained dedolomitic marble, Type VI.

As-57: Limonitic ore material as crust on the marble.

As-58: Mn veinlets and disseminations in marble.

As-77: Massive, fine to medium grained non-ferroan dolomitic marble, Type II.

As-78: White, fine grained de-dolomitic marble, Type VI.

Samples As-60 to As-64 are from the valley at the lowest part of Pangeon (Fig. 2).

As-60: Barren quartz vein with sericite.

As-61: Limonitised, pyrite-quartz-sericite vein, hosted in granite.

As-62: Altered amphibolite.

As-63: Quartz vein with disseminated pyrite crystals.

As-64: Limonitised, disseminated pyrite-chalcopyrite in quartzite.

APPENDIX II

SAMPLE PREPARATION
AND
ANALYTICAL METHODS

1. MICROPROBE ANALYSES

The chemical composition of arsenopyrite, pyrite and gold were determined at I.G.M.E utilising a JEOL Superprobe 733. Operating conditions included an operating voltage of 20 kV, a beam current of 5nA and 20-second count times. Mineral standards were used, and an on line ZAF corrections were carried out using a PDP-11/04 computer. The error in the iron content is less than 0.2 mol%.

2. SECONDARY ION MASS SPECTROMETRY (SIMS)

The selected samples were crushed and the wet screened at 38 and 5 μm. Each size fraction was gravity separated by superpanning to concentrate any free gold. The plus 5 μm pan tails of both samples were pulverised, screened at -5 μm and subjected to intensive double cyanidation for 48 hours. The leached residue was gold assayed.

Secondary ion mass spectrometry (SIMS) spot analysis was used to quantify gold concentrations in arsenopyrite and pyrite. A total of 50 sulphide grains using the external standardisation method as described by Chryssoulis et al. (1989) were analysed in order to obtain a sufficient data set for these potentially important carriers.

Four sulphide mineral grains were mapped by SIMS to establish the gold distribution within individual crystals following procedures described by Chryssoulis and Weisener (1991). SIMS analyses were carried out at the Advanced Mineral Technology Laboratory, University of Western Ontario, using an upgraded CAMECA IMS-3f ion probe with an integrated image analysis system, and using a primary beam of positive caesium ions. Gold was monitored as negative ions at 197 Dalton. Molecular interference was eliminated by voltage offsetting (Chrys-

soulis et al. 1989). The instrument was calibrated using gold-implanted pyrite and arsenopyrite. The results were standardised using mineral-specific calibration curves produced from the gold-implanted sulphides (Chryssoulis et al. 1989).

3. BULK ROCK CHEMICAL ANALYSES

Major element oxides and trace elements were analysed at the IGME's Chemical Laboratories in Athens by Inductively Coupled Plasma (ICP-AES). Au and Ag were analysed by Inductively Coupled Plasma (ICP-AES) at the CALEB BRETT Laboratories, Liverpool U.K, whilst Se, Te, Bi and Sb were analysed by Atomic Absorption Spectrophotometry (AAS) using hydrate generator at the OMAC Laboratories, Ireland. Detection limits of analysed elements are shown in Table 1.

Selective marble samples were analysed by XRF (pressed pellets) at IGME, Athens. The semiquantative estimation of dolomite and calcite has been estimated by X-Ray diffraction using the 104 peaks of both calcite and dolomite (Rouse et al., 1971). The stoichiometry of the dolomite and percentage of $MgCO_3$ into calcite lattice were determined by calculating the shift of the 104 peak of dolomite using quartz as an internal standard. Estimation of insoluble residue was made for the investigation of the relationship of the trace element concentration with the crystal lattice of the carbonate minerals and the determination of the purity of the carbonate rocks.

Table 1: Detection limits of analysed elements.

Element	Analytical ICP-AES	Method AAS	Element	Analytical ICP-AES	Method AAS
SiO_2	0.01%		Sb		0.2 ppm
TiO_2	0.01%		Bi		5 ppm
Al_2O_3	0.01%		Se		3 ppm
Fe_2O_3	0.01%		Te		0.1 ppm
MgO	0.01%				
MnO	0.01%		Cr	2 ppm	
CaO	0.01%		Ni	1 ppm	
K_2O	0.01%		Co	1 ppm	
Na_2O	0.01%		V	1 ppm	
P_2O_5	0.01%		Rb	2 ppm	
			Sr	2 ppm	
Au	5 ppb		Zr	2 ppm	
Ag	0.2 ppm		Y	2 ppm	
			Nb	2 ppm	
Pb	0.01%		Th	0.5 ppm	
Zn	0.01%		U	0.5 ppm	
Cu	0.01%		Ba	1 ppm	
			S	100 ppm	
As	1ppm				

4. FLUID INCLUSION STUDIES

Microthermometry

All samples studied were prepared for fluid inclusion microthermometry as doubly polished 100-150μm thick wafers. Microthermometric work was undertaken using a LINKAM THSM 600 Heating/Freezing stage. The stage was attached to a LEITZ ORTHOLUX microscope carrying a NIKON PLAN 40 long working distance objective. The operating procedures followed are described in Shepherd et al. (1985). Calibration of the stage was done by using the melting point of pure CO_2 (-56.6°C) in a natural sample where the CO_2 is known to be >99.96 pure CO_2. The data obtained from the 13 standards were used to construct the calibration curve, which is shown on Figure 3. The calibration curve relates a temperature correction factor ΔT, which is the difference between the actual temperature read from the digital read-out of the instrument, to the read temperature. Thus, any read temperature is simply converted to the actual temperature by the addition of the appropriate value for T. Accuracy is estimated at ~0.5 °C (between -100 and -20 °C), ~0.2 °C (between -20 and 30 °C), ~1 °C (between 30 and 200 °C) and ~5 °C (between 200 and 500 °C). Thus, analytical errors are insignificant with regard to any geological interpretation. Data reductions were undertaken using FLINCOR (Brown, 1989), software packages relating fluid inclusion microthermometry to fluid composition and P-T conditions of fluid trapping.

Bulk Volatile Analyses

Decrepitation-bulk volatile analyses of vein quartz provides a quantitative measure of the total fluid inclusion volatile content of a sample. For geologically and paragenetically well-constrained material, the analyses can be used to compare and contrast different generations of veins and identify temporal and spatial variations in volatile geochemistry. A total number of 9 samples were analysed at BGS, following

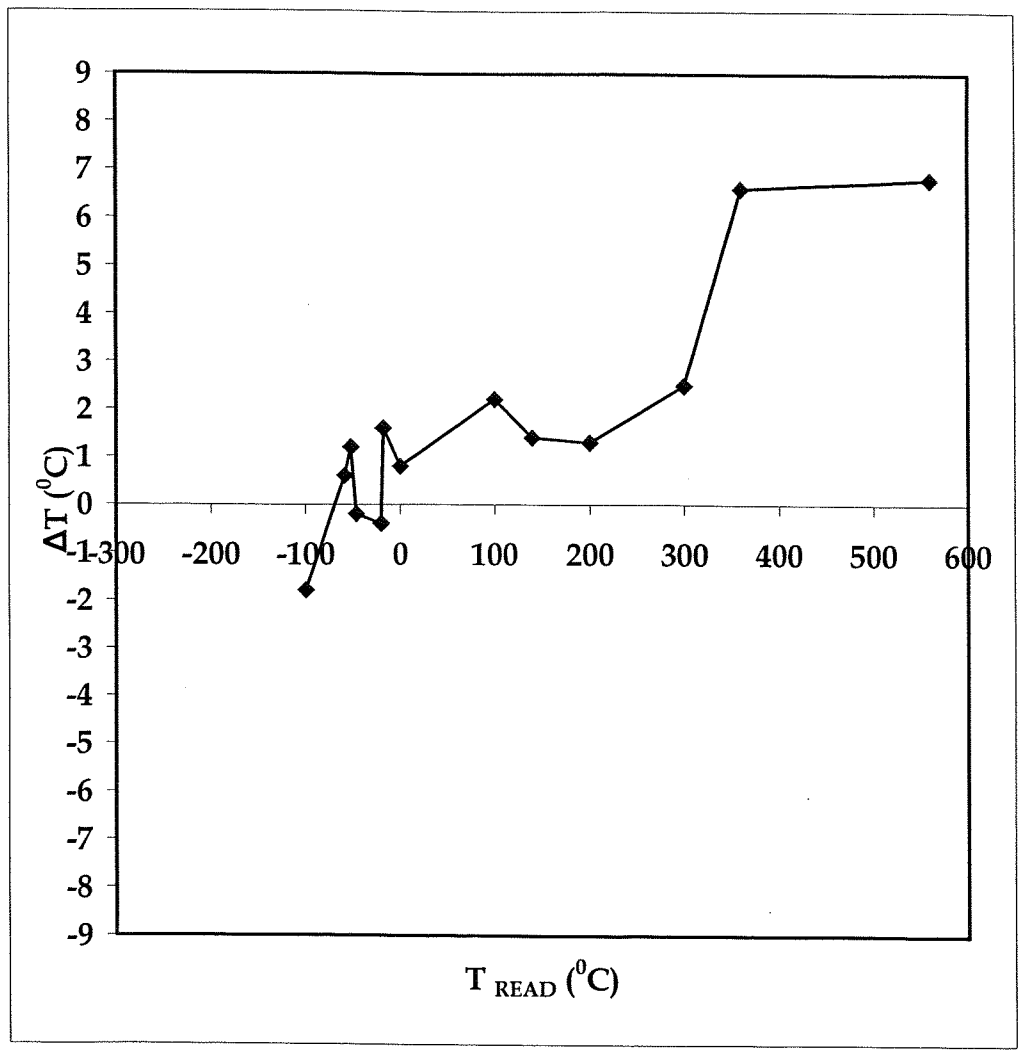

Figure 3: Calibration curve for Linkam TH 600 heating-cooling stage.
T_{READ} ^{0}C: Actual temperature read from the instrument.
□T ^{0}C: Correction factor

the method by Shepherd et al. (1991). The quartz samples were crushed, sieved and the 0.5-1.0 mm size fraction retained. The concentrates then were acid washed in hot 6m HCL to remove carbonate and sulphide impurities, rinsed several times in boiling de-ionised water and then dried under infrared lamps. Using hand-picked 0.5 gr sub-samples, the inclusion volatiles were released by thermal de-crepitation at 550 ^{0}C under vacuum. Bulk analysis of the inclusion volatiles was performed using a purposed built extraction line linked to a VG Micromass gas source quadrapole mass spectrometer (Shephered et al. 1985). By cryogenic trapping at -196 ^{0}C, H_2O and CO_2 were isolated from the "non-condensable" components: CH_4, N_2 and noble gases, together with any H_2 and CO. By measuring the pressure of the non-condensable gas fraction using a capacitance manometer, the total number of moles of gas in this fraction could be calculated. The mass spectrometer was then used to quantitatively identify the various individual gas species. After pumping away the non-condensable gas fraction, the trap temperature was raised to -78 ^{0}C, using a solid CO_2 / liquid nitrogen slush path. CO_2 was thus released and its pressure measured in a standard volume. For the determination of H_2O, a reduction furnace containing zinc at 400 ^{0}C was used to convert the water vapour to H_2, the pressure of which was subsequently recorded. Values for the volumes of CO_2 and H_2O released from replicate quantities of host mineral provided a valuable check of sub-sample homogeneity.

5. STABLE AND RADIOGENIC ISOTOPES

5.1 Stable Isotopes

Sulphur Isotopes

Ten representative sulphide samples from the 3K-D and 3K-H adits at Asimotrypes were collected for sulphur isotope analysis. The samples were crushed to a <0.5 mm grain size and subsequently pure sulphide concentrates (>97%) were produced by selection under a microscope. The sulphide separates were analysed

for their sulphur isotope signature relative to the Canyon Diablo troilite (CDT) standard, employing standard methods (mass spectrometer) at the Centre des Recherches Petrographic et Geochimiques, Nancy, France. Analytical uncertainties are ± 0.2 per mil for $\delta^{34}S$ and ± 0.4 per mil for the $\Delta\delta^{34}S$.

Carbon Isotopes

Fifteen representative calcite samples from the Asimotrypes area were collected along a profile away from the arsenopyrite-pyrite ore on the main thrust zone between gneisses and sheared marbles, at a distance from a few cm up to 50 m from the ore. These samples were analysed for their ^{13}C isotopic composition, at the University of Utrecht. XRD determinations were made on powdered carbonate samples prior to isotopic analyses to determine the relative percentages of calcite, dolomite and other carbonate types. No pure dolomite samples were found. Calcites were reacted with 100% phosphoric acid at 25 ^{0}C according to the method of McCrea (1950). Pure calcites, with less than 5% vol. dolomite, were reacted overnight, and mixtures of calcite and dolomite were reacted for about 2 hours after which calcite CO_2 was extracted. The carbon isotopes are related to the Peedee belemite (PDB) international standard. Both carbon and oxygen isotopes are measured with a precision of ± 0.2 per mil or better.

Oxygen Isotopes

Fifteen representative calcitic marble samples from the Asimotrypes area were collected along a profile away from the arsenopyrite-pyrite ore on the main thrust zone between gneisses and sheared marbles, at a distance from a few cm up to 50 m from the ore. These samples were analysed for their ^{18}O isotopic composition, at the University of Utrecht. The analytical method is described in the previous Section of Carbonate Isotopes.

Quartz and sericite mineral separates from ten representative samples from the

ore and rocks from the Transitional Zone were analysed for δ^{18} O SMOW at the CSIRO Petroleum Resources Laboratory in Australia. Sericite was obtained by griding to -100 mesh followed by repeat centrifuging in a heavy liquid to yield a concentrate of specific gravity > 2.76 and < 2.85 and taken to purification by magnetic methods. Silicates were reacted with BrF_5 to liberate oxygen and O_2 was converted to CO_2 before mass-spectrometric analysis, as described below, following the method of Clayton and Mayeda (1963).

Fifteen representative whole rock samples, more specifically six As-py-bearing quartzite samples, three amphibolite samples and six granite-granodiorite samples, were analysed for δ^{18} O SMOW at the CSIRO Petroleum Resources Laboratory in Australia. Carbon dioxide for whole rock oxygen isotope analysis was prepared using the method described by Clayton and Mayeda (1963). 8-10 mgs of powdered sample is weighed into delivery probes and loaded into nickel reaction vessels under a back flash of ultra-high purity argon. The bombs and manifold are evacuated, firstly by a rough pump, then by a high vacuum pump, an aliquot BrF_5 frozen into the bombs using liquid nitrogen and the bombs are heated to 550 ^{0}C for 14 hours. The resultant oxygen is pulsed over a hot carbon filament (30A, 50-70V, platinum electrodes to catalyse the reaction), the carbon dioxide collected as generated, the yield measured and gas collected for isotopic measurement in a mass spectrometer. For the NBS 26 international standard this technique gives δ^{18} O = 9.6 per mil. Replicate analyses of standards are generally better than ± 0.1. All oxygen isotopes are related to the Vienna-Standard Mean Ocean Water (SMOW) standard.

Hydrogen Isotopes

Hydrogen whole rock isotopic analysis was performed on eight representative samples from the main ore, the Transitional zone and the granite. The aim of these analyses is to use the D/H values combined with ^{18}O/ ^{16}O as indicators of the origin and history of the H_2O in the ore forming fluids. The D/H analyses

were done at the CSIRO Petroleum Resources Laboratory in Australia, following a modified method published by Bigeleisen et al. 1952. The samples were heated to > 1400 ^{0} C using an RF generator furnace. H_2 produced was converted to H_2O by contact with CuO_2 at 600 ^{0} C. All water was collected cryogenically and stores in sealed 6mm odd borosilicate glass tubes. The water was released from the sealed tubes in a vacuum line and circulated using a pump through depleted uranium at 800 ^{0} C. When conversion was complete the H_2 was pumped into the mass spectrometer via a stainless steel line and analysed immediately. Samples were analysed relative to an internal water standard prepared using the same circulation system. Standards were calibrated daily using laboratory and international standards. Replicate analyses of the standard waters are generally better than ± 1per mil. Analyses are reported in per mil relative to the SMOW standard.

5.2 Radiogenic Isotopes

Strontium Isotopes

Strontium isotope ratios (^{87}Sr / ^{86}Sr) from three representative impure calcitic marbles, at varying distances from the ore (0.5, 5 and 500 m respectively) were measured at the CSIRO Petroleum Resources Laboratory in Australia. Sr isotope ratios (^{87}Sr / ^{86}Sr) were determined in calcites which were dissolved in concentrated HCl and Sr was concentrated using conventional cation-exchange methods. Isotope ratios were measured in a mass-spectrometer. Replicate analyses of the NBS 987 international standard yielded a mean value of ^{87}Sr / ^{86}Sr = 0.710240 ± 20 (2σ). Strontium contents of marbles at Asimotrypes are in the 30 to 252 ppm range, and Rb contents are in the 1 to 10 ppm, yielding Rb/Sr ratios generally much less than 0.01. Accordingly, measured ^{87}Sr / ^{86}Sr ratios are assumed to be equivalent to the initial ^{87}Sr / ^{86}Sr ratio (Sr) at the time of mineralisation.

APPENDIX III

WHOLE ROCK ANALYSES

Table 1 :Abundances of major oxides and selected trace elements in marbles from the Asimotrypes Gold Deposit, Pangeon, N. Greece.

Sample	As-1	As-4	As-5	As-7	As-9	As-12	As-32
SiO_2	22.59	15.53	15.19	18.20	20.71	29.00	28.50
TiO_2	n.d	n.d	n.d	n.d	n.d	0.01	0.11
Al_2O_3	0.66	0.54	1.38	0.47	0.40	1.31	2.95
Fe_2O_3	1.99	0.45	1.55	0.32	0.22	1.01	1.83
MgO	1.17	1.02	1.23	1.40	0.88	1.28	1.32
MnO	1.04	0.08	0.05	0.02	0.03	0.04	0.05
CaO	39.08	45.30	44.40	43.50	42.00	37.20	34.95
K_2O	0.19	0.11	0.51	0.18	0.17	0.55	1.06
Na_2O	0.07	0.06	0.10	0.10	0.11	0.13	0.31
P_2O_5	0.04	0.03	0.02	0.03	0.03	0.04	0.05
L.O.I	31.90	37.00	36.10	35.50	35.10	27.80	25.50
Total	98.73	100.12	100.53	99.72	99.65	98.37	96.63
Au	0.17	0.07	0.09	0.06	0.16	0.67	0.04
Ag	17.00	26.00	12.50	8.60	9.00	8.30	6.20
Pb	3205	210	36	10	5	8	12
Zn	2465	85	72	11	5	20	27
Cu	n.d	n.d	n.d	n.d	n.d	n.d	n.d
As	1465	118	94	18	5	998	28
Sb	n.d	n.d	n.d	n.d	n.d	n.d	n.d
Bi	1	1	1	1	1	n.d	1
Se	1	1	1	1	1	n.d	1
Te	3	3	3	3	3	n.d	3
Cr	30	24	9	14	8	18	69
Ni	8	5	9	7	4	2	55
Co	62	56	50	50	59	67	48
V	6	1	6	n.d	1	7	15
Rb	n.d	2	11	1	n.d	10	40
Sr	247	244	188	280	212	171	248
Zr	13	13	24	11	13	20	43
Y	5	18	13	18	15	19	17
Nb	2	2	3	2	2	2	4
Th	n.d	n.d	n.d	1	n.d	2	6
U	n.d	1	n.d	1	n.d	1	4
Ba	12	1	14	9	4	16	102
S	6960	2280	5600	1100	980	3350	6450
H_2O	0.2	0.03	0.03	0.03	0.06	0.01	0.01

Major oxides in weight %, trace elements in ppm

Total iron is expressed as Fe_2O_3

Table 1: (cont'd)

Sample	As-18	As-22	As-23	As-24	As-26	As-27
SiO_2	0.70	1.81	6.00	3.50	3.68	2.00
TiO_2	n.d	n.d	0.03	n.d	n.d	n.d
Al_2O_3	0.08	0.46	1.05	1.00	0.75	0.55
Fe_2O_3	0.04	0.67	1.46	0.93	0.93	0.47
MgO	0.57	1.31	3.61	5.50	1.47	4.20
MnO	0.02	0.05	0.03	0.07	0.10	0.03
CaO	54.00	51.80	46.50	45.10	49.60	48.50
K_2O	0.04	0.09	0.15	0.22	0.13	0.10
Na_2O	0.11	0.07	0.24	0.09	0.04	0.05
P_2O_5	0.18	0.15	0.47	0.48	0.03	0.09
L.O.I	43.00	42.70	39.30	42.30	42.00	42.80
Total	98.74	99.11	98.84	99.19	98.73	98.79
Au	0.02	0.03	0.08	0.01	0.04	n.d
Ag	11.70	11.00	8.50	9.30	9.80	9.50
Pb	6	12	7	10	15	7
Zn	12	26	19	35	19	28
Cu	n.d	n.d	n.d	n.d	n.d	5
As	163	508	1364	203	331	72
Sb	n.d	n.d	n.d	n.d	n.d	n.d
Bi	n.d	1	1	1	n.d	n.d
Se	n.d	1	1	1	n.d	n.d
Te	n.d	3	3	3	n.d	n.d
Cr	1	7	50	11	29	8
Ni	1	10	27	21	20	13
Co	39	34	37	37	29	34
V	n.d	5	9	10	3	4
Rb	n.d	10	7	6	2	3
Sr	160	175	226	252	210	226
Zr	12	11	19	14	18	12
Y	11	11	7	10	4	6
Nb	1	1	2	2	1	1
Th	n.d	2	n.d	3	n.d	3
U	3	1	n.d	1	3	2
Ba	n.d	8	22	14	12	12
S	200	1575	3250	2270	2150	1175
H_2O	0.03	0.04	0.01	0.02	0.05	0.08

Major oxides in weight %, trace elements in ppm
Total iron is expressed as Fe_2O_3

Table 1: (cont' d)

Sample	As-30	As-50	As-51	As-52	As-53	As-54
SiO_2	1.20	1.20	0.70	0.30	21.50	0.50
TiO2	n.d	n.d	n.d	n.d	n.d	n.d
Al_2O_3	0.26	0.25	0.22	0.05	0.50	0.12
Fe_2O_3	0.19	0.13	0.25	0.00	0.41	1.11
MgO	15.50	0.64	20.50	1.20	0.78	20.20
MnO	0.04	0.02	0.05	0.01	0.06	0.32
CaO	36.30	53.00	31.20	54.70	42.00	31.50
K_2O	0.07	0.05	0.06	0.01	0.19	0.01
Na_2O	0.05	0.08	0.06	0.09	0.06	0.06
P_2O_5	0.02	0.01	0.02	0.02	0.02	0.01
L.O.I	45.20	43.00	46.50	43.20	33.80	46.50
Total	98.83	98.38	99.56	99.58	99.32	100.33
Au	0.15	0.08	0.01	0.01	0.01	0.06
Ag	7.00	9.70	6.00	9.00	7.60	5.80
Pb	8	6	10	5	5	24
Zn	34	9	30	11	7	24
Cu	n.d	n.d	n.d	n.d	n.d	n.d
As	28	46	22	7	7	25
Sb	n.d	n.d	n.d	n.d	n.d	n.d
Bi	1	1	n.d	1	1	1
Se	1	1	n.d	1	1	1
Te	3	3	n.d	3	3	3
Cr	2	1	n.d	n.d	10	3
Ni	5	5	4	4	6	2
Co	33	32	32	29	44	38
V	2	n.d	n.d	n.d	1	n.d
Rb	1	n.d	n.d	n.d	1	n.d
Sr	172	135	30	145	175	35
Zr	11	12	9	10	11	7
Y	5	6	5	6	11	3
Nb	1	1	1	2	1	1
Th	1	n.d	3	2	1	1
U	n.d	n.d	n.d	n.d	n.d	n.d
Ba	11	3	4	1	7	n.d
S	480	260	750	n.d	220	345
H_2O	0.04	0.06	0.10	0.24	0.13	0.08

Major oxides in weight %, trace elements in ppm
Total iron is expressed as Fe_2O_3

Table 2: Semiquantative calcite and dolomite estimation, insoluble residue and Sr, Fe and Mn contents in selective marbles from the Pangeon Mt.

Sample	$MgCO_3$ in calcite	$MgCO_3$ in dolomite	I.R %	Sr ppm	Fe ppm	Mn ppm
As-80			0.15	91	237	48
As-81			0	92	248	31
As-82			0	105	167	31
As-83			0.43	99	176	27
As-84	1.5	50.5	0.1	81	205	33
As-85	1	50	0.11	78	252	59
As-86	1.5	50	0	103	164	19
As-87			1.1	37	249	67
As-88	1.5	50	0.34	131	144	18
As-89	1.5	50	0	39	325	37
As-90			0.17	31	502	61
As-91	6.5	49	0.2	76	476	113
As-92			0	108	152	16
As-93	1.5	50.5	0.13	32	395	130
As-94	1	50	0	56	1038	615
As-95	6.5	50	0.67	49	830	320
As-96	6		0.29	173	765	122
As-97	5		0.43	232	828	132
As-98	2		0	152	304	35
As-99			0.15	29	318	82

Table 3: Abundances of major oxides and selected trace elements in marbles from the Avgo (Pilaf Tepe), Pangeon, N. Greece

Sample	As-55	As-56	As-58	As-76	As-77
SiO_2	0.40	1.80	6.30	1.85	3.85
TiO2	n.d	n.d	n.d	0.01	0.01
Al_2O_3	0.12	0.30	0.25	0.45	0.28
Fe_2O_3	0.22	24.93	10.10	0.62	13.10
MgO	1.07	1.17	14.47	1.29	14.97
MnO	0.01	5.72	5.22	0.07	5.12
CaO	54.50	34.51	23.60	52.8	28.10
K_2O	0.01	0.50	0.09	0.06	0.07
Na_2O	0.08	0.22	4.51	0.07	3.98
P_2O_5	n.d	0.03	0.04	0.15	0.02
L.O.I	42.50	31.50	34.50	41.9	30.45
Total	98.91	100.68	99.08	99.27	99.95
Au	n.d	0.35	0.03	0.10	0.03
Ag	9.00	50.00	26.60	13.50	22.60
Pb	2	10100	3095	35	2987
Zn	6	11920	359460	8	42760
Cu	n.d	n.d	n.d	n.d	n.d
As	9	3825	723	15	645
Sb	n.d	<2	<2	n.d	<2
Bi	n.d	1	1	n.d	1
Se	n.d	1	1	n.d	1
Te	n.d	3	3	n.d	3
Cr	n.d	6	21	4	19
Ni	4	14	54	2	48
Co	27	21	46	15	37
V	n.d	2	9	2	7
Rb	n.d	n.d	n.d	n.d	1
Sr	125	125	55	115	64
Zr	6	14	13	7	15
Y	2	n.d	n.d	2	n.d
Nb	1	2	2	n.d	2
Th	n.d	n.d	n.d	n.d	n.d
U	2	n.d	n.d	n.d	n.d
Ba	n.d	75	45	5	43
H_2O	0.12	n.d	n.d	0.1	0.15

Major oxides in weight %, trace elements in ppm
Total iron is expressed as Fe_2O_3

Table 4: Abundances of major oxides and selected trace elements in gneiss-schists from the Asimotrypes Gold Deposit, Pangeon, N. Greece.

Sample	As-6	As-8	As-10	As-15	As-17	As-62
SiO_2	43.12	49.00	50.80	46.50	47.00	52.50
TiO_2	0.61	0.73	0.51	0.61	0.60	0.71
Al_2O_3	10.10	15.30	10.80	13.60	10.50	14.80
Fe_2O_3	6.39	7.66	8.25	8.82	7.16	8.50
MgO	3.23	5.27	11.25	6.49	4.50	4.55
MnO	0.10	0.11	0.13	0.13	0.17	0.17
CaO	17.59	11.30	14.51	13.60	16.50	13.70
K_2O	2.81	2.50	1.25	1.65	1.52	2.04
Na_2O	2.15	3.60	2.55	3.00	2.30	2.19
P_2O_5	0.10	0.14	0.10	0.14	0.19	0.20
L.O.I.	10.10	1.00	0.40	5.80	4.70	1.20
Total	96.30	96.61	100.55	100.34	95.14	100.56
Au	0.08	0.06	0.44	0.14	0.01	0.01
Ag	1.80	1.20	0.70	1.70	1.10	1.30
Pb	20	15	10	39	15	18
Zn	85	90	87	115	64	106
Cu	n.d	n.d	n.d	55	n.d	52
As	334	46	15	2050	334	14
Sb	2	2	2	2	2	2
Bi	1	1	1	1	1	n.d
Se	1	1	1	1	1	n.d
Te	3	3	3	3	3	n.d
Cr	306	328	1233	234	295	566
Ni	139	172	572	113	153	186
Co	121	110	100	79	88	93
V	112	169	138	221	134	153
Rb	80	80	48	79	62	27
Sr	227	280	425	290	300	345
Zr	99	116	102	59	92	132
Y	20	23	19	16	21	30
Nb	10	10	9	5	6	12
Th	5	6	5	n.d	2	7
U	n.d	3	n.d	n.d	n.d	n.d
Ba	255	330	168	224	171	257

Major oxides in weight %, trace elements in ppm
Total iron expressed as Fe_2O_3

Table 5: Abundances of major oxides and selected trace elements in arsenopyrite-pyrite ore from the Asimotrypes Gold Deposit, Pangeon, N. Greece

Sample	As-11	As-14	As-16	As-19	As-21	As-31	As-37	As-44
SiO_2	22.54	9.50	46.50	4.30	6.40	18.84	16.40	26.40
TiO_2	n.d	n.d	n.d	n.d	0.01	n.d	0.01	n.d
Al_2O_3	0.59	0.31	0.63	0.84	1.83	0.32	4.65	0.90
Fe_2O_3	36.10	46.40	24.80	42.50	48.00	36.30	50.10	30.00
MgO	0.15	5.00	0.20	5.58	0.19	0.19	0.28	5.48
MnO	0.02	0.20	0.03	0.02	0.03	0.02	0.02	0.01
CaO	0.97	0.89	1.07	0.91	1.42	1.10	1.47	0.76
K_2O	0.12	0.07	0.20	0.18	0.29	0.07	1.45	0.10
Na_2O	0.10	0.08	0.30	0.07	0.11	0.07	0.12	0.09
P_2O_5	0.02	0.01	0.05	0.33	0.02	0.04	0.05	0.01
L.O.I	38.50	33.10	23.20	45.60	41.00	44.00	24.70	31.80
Total	99.11	95.56	96.98	100.33	99.30	100.95	99.25	95.55
Au	11.00	9.90	6.30	13.50	13.30	16.60	1.85	5.09
Ag	6.80	8.50	6.60	6.70	12.60	6.60	3.70	10.20
Pb	316	384	904	106	327	91	89	100
Zn	265	17065	115	45	317	24	14	70
Cu	n.d	n.d	n.d	n.d	3380	n.d	0	210
As	461965	323150	267450	496250	396850	347250	720	389290
Sb	60	55	90	70	100	2	2	60
Bi	42	67	35	44	58	9	103	65
Se	5	5	3	5	5	1	5	5
Te	3	3	3	3	3	3	33	3
Cr	128	66	263	62	228	167	160	130
Ni	82	70	51	95	116	19	54	80
Co	76	41	155	46	69	75	89	74
V	6	1	4	4	15	3	17	5
Rb	2	n.d	n.d	4	10	n.d	41	1
Sr	n.d	n.d	3	1	11	n.d	24	2
Zr	15	18	15	18	34	17	46	17
Y	1	n.d	n.d	n.d	n.d	n.d	5	1
Nb	1	2	1	1	1	1	5	n.d
Th	4	24	n.d	28	21	n.d	35	n.d
U	n.d	n.d	n.d	n.d	n.d	n.d	2	n.d
Ba	12	6	8	13	22	11	154	21
S	177600	219150	118350	215680	219750	193350	9750	192750

Major oxides in weight %, trace elements in ppm
Total iron is expressed as Fe_2O_3

Table 5: (Cont' d)

Sample	As-46	As-65	As-66	As-67	As-69	As-71	As-72	As-75
SiO_2	44.50	31.00	29.40	35.55	11.85	32.30	3.40	12.10
TiO_2	0.02	0.01	n.d	n.d	0.01	n.d	n.d	0.01
Al_2O_3	2.30	0.61	0.90	0.94	2.93	2.47	0.28	1.98
Fe_2O_3	22.60	26.90	30.70	25.40	45.20	33.90	54.65	44.10
MgO	0.77	4.48	5.28	1.93	1.29	0.18	5.48	1.30
MnO	0.01	0.10	0.25	0.49	0.19	0.06	0.15	0.12
CaO	0.07	0.86	0.97	0.81	0.90	0.71	0.93	0.90
K_2O	0.03	0.10	0.26	0.18	0.05	0.17	0.05	0.05
Na_2O	0.09	0.08	0.02	0.12	0.06	0.15	0.08	0.12
P_2O_5	0.08	0.04	0.07	0.02	0.01	0.04	0.02	0.02
L.O.I	25.50	35.10	31.20	32.80	35.50	28.70	33.20	38.20
Total	95.97	99.28	99.05	98.24	97.99	98.68	98.24	98.90
Au	0.22	5.85	4.20	4.80	5.30	3.30	6.30	5.30
Ag	320.00	18.40	16.00	17.30	22.10	173.00	14.60	104.00
Pb	5615	2390	3610	5250	310	80500	360	3250
Zn	450	1600	5600	1050	90	4250	255	1360
Cu	163675	1180	810	780	60	70	n.d	1440
As	6900	101150	72700	71850	268870	156750	441900	128750
Sb	2	65	52	51	90	58	20	86
Bi	107	68	35	48	65	42	25	63
Se	1	5	5	5	1	1	1	5
Te	3	3	3	1	3	3	3	1
Cr	445	140	138	126	225	154	67	213
Ni	57	88	96	75	45	67	26	54
Co	81	75	86	84	73	65	17	37
V	38	11	8	16	7	4	1	9
Rb	n.d	2	n.d	4	n.d	3	n.d	n.d
Sr	n.d	11	n.d	10	n.d	2	n.d	n.d
Zr	25	24	11	19	18	15	16	16
Y	n.d	1	n.d	n.d	n.d	1	1	n.d
Nb	2	1	2	2	1	1	2	4
Th	n.d	4	n.d	n.d	n.d	4	22	n.d
U	n.d	2	n.d	n.d	n.d	n.d	4	n.d
Ba	57	31	24	14	15	22	12	24
S	121690	124650	100950	126550	223540	163580	170200	211550

Major oxides in weight %, trace elements in ppm
Total iron is expressed as Fe_2O_3

Table 6: Abundances of major oxides and selected trace elements in oxidised ore from the Asimotrypes Gold Deposit, Pangeon, N. Greece

Sample	As-2	As-3	As-13	As-20	As-29	As-25	As-57	As-64
SiO_2	63.11	35.82	19.22	41.80	40.00	32.60	68.81	74.70
TiO_2	n.d	n.d	n.d	0.01	0.48	n.d	0.10	0.03
Al_2O_3	0.73	0.43	0.79	1.04	7.15	0.81	3.60	2.71
Fe_2O_3	7.66	38.60	37.30	13.82	8.37	15.00	12.14	18.44
MgO	0.31	0.14	0.36	1.84	2.31	0.75	2.20	0.27
MnO	3.66	0.17	0.29	0.25	4.56	0.14	0.32	0.01
CaO	9.98	0.93	1.86	12.60	9.00	10.90	5.07	0.85
K_2O	0.71	1.00	0.19	0.23	1.02	0.20	0.67	0.54
Na_2O	0.11	1.13	0.10	0.11	0.29	0.08	0.86	0.55
P_2O_5	0.06	0.04	0.03	0.02	2.28	0.04	0.11	0.14
L.O.I	7.50	21.20	37.00	27.50	26.30	40.00	4.50	2.00
Total	93.83	99.46	97.14	99.22	101.76	100.52	98.38	100.24
Au	0.10	3.24	6.77	1.25	0.2	0.60	n.d	0.02
Ag	42.50	8.50	5.60	3.30	16.20	4.10	4.10	1.20
Pb	20240	3790	2480	150	1647	125	286	37
Zn	4720	13530	17060	45	8537	30	15210	17
Cu	n.d	365	105	n.d	44	12	n.d	0
As	6900	9810	447970	7300	2461	10500	140	160
Sb	290	30	240	2	n.d	2	<2	2
Bi	28	1	1	4	n.d	3	9	16
Se	1	1	6	1	n.d	1	1	1
Te	3	3	3	3	n.d	3	3	5
Cr	202	166	70	107	85	28	592	437
Ni	23	20	70	31	127	20	63	13
Co	130	83	90	51	44	33	102	105
V	12	4	2	8	117	7	50	27
Rb	n.d	n.d	5	7	40	6	18	22
Sr	42	3	20	166	106	89	65	6
Zr	13	13	16	17	69	14	34	25
Y	n.d	n.d	n.d	5	30	3	13	18
Nb	1	1	3	2	6	1	4	4
Th	n.d	n.d	n.d	n.d	n.d	n.d	1	6
U	n.d	n.d	n.d	1	n.d	n.d	6	n.d
Ba	26	8	12	24	1337	79	105	73
S	35760	180650	190800	62400	5700	72350	64380	90350

Major oxides in weight %, trace elements in ppm

Total iron is expressed as Fe_2O_3

Table 7: Abundances of major oxides and selected trace elements in quartz veins with disseminated pyrite from the Asimotrypes Gold Deposit, Pangeon, N. Greece

Sample	As-34A	As-34B	As-35	As-36	As-41	As-45	As-61	As-63
SiO_2	75.00	75.80	73.00	73.00	89.00	94.00	65.50	76.50
TiO_2	0.01	0.07	0.05	0.08	0.02	0.01	0.02	0.11
Al_2O_5	8.08	12.52	9.28	13.28	3.26	0.80	9.40	4.75
Fe_2O_5	9.85	7.44	7.93	3.80	3.83	2.70	15.30	9.90
MgO	0.33	0.25	0.24	0.58	0.16	0.73	0.17	2.75
MnO	0.03	0.62	0.02	0.04	0.13	0.01	0.02	0.05
CaO	1.05	1.07	1.41	1.03	0.90	0.70	0.70	3.86
K_2O	3.80	0.67	3.45	5.80	0.94	0.10	4.20	0.52
Na_2O	0.26	0.45	2.25	0.46	0.69	0.09	1.47	0.50
P_2O_5	0.02	0.04	0.04	0.02	0.05	0.02	0.05	0.07
L.O.I.	1.30	1.40	1.30	0.90	0.50	0.10	3.00	1.50
Total	99.73	100.33	98.97	98.99	99.48	99.26	99.83	100.51
Au	0.15	0.18	0.05	0.12	0.07	0.15	0.06	0.01
Ag	1.60	1.50	0.90	0.70	0.70	9.80	4.00	1.20
Pb	69	22	30	23	9	15	210	21
Zn	n.d	6	n.d	n.d	n.d	n.d	25	47
Cu	n.d	n.d	n.d	n.d	n.d	n.d	n.d	n.d
As	895	20	227	44	92	580	140	39
Sb	2	2	2	2	2	2	2	2
Bi	22	22	2	25	1	1	103	7
Se	1	1	1	1	1	1	1	1
Te	7	7	3	9	3	3	58	3
Cr	268	144	333	144	413	286	235	866
Ni	5	17	7	6	5	25	9	133
Co	219	85	157	84	164	5	113	126
V	13	9	4	15	11	10	7	48
Rb	100	18	88	180	27	25	107	9
Sr	58	352	132	93	44	287	130	68
Zr	50	84	58	97	34	31	27	33
Y	6	22	15	9	5	5	11	11
Nb	5	12	10	10	3	5	9	4
Th	10	24	10	26	3	n.d	32	1
U	2	4	3	7	n.d	n.d	5	n.d
Ba	296	123	266	518	141	199	569	122

Major oxides in weight %, trace elements in ppm
Total iron expressed as Fe_2O_3

Table 8: Abundances of major oxides and selected trace elements in granites from the Asimotrypes Gold Deposit, Pangeon, N.Greece

Sample	As-33	As-36	As-38	As-39	As-40
SiO_2	71.50	73.00	68.00	69.00	60.00
TiO_2	0.07	0.08	0.13	0.18	0.23
Al_2O_3	13.40	13.28	16.08	14.80	9.33
Fe_2O_3	2.00	3.80	3.53	2.42	20.20
MgO	0.33	0.58	0.68	0.77	0.50
MnO	0.63	0.04	0.03	0.06	0.04
CaO	6.00	1.03	1.14	2.94	1.20
K_2O	0.68	5.80	7.30	3.70	3.10
Na_2O	4.90	0.46	1.52	4.70	0.50
P_2O_5	0.04	0.02	0.04	0.11	0.31
L.O.I.	0.30	0.90	1.40	1.30	5.25
Total	99.85	98.99	99.85	99.98	100.66
Au	0.02	0.12	0.01	0.03	0.53
Ag	0.70	0.70	1.40	1.00	3.30
Pb	21	23	105	38	188
Zn	17	n.d	43	15	17
Cu	n.d	n.d	n.d	n.d	n.d
As	25	44	99	16	5570
Sb	2	2	2	2	2
Bi	1	25	1	1	8
Se	1	1	1	1	1
Te	3	9	1	3	3
Cr	145	144	90	111	253
Ni	27	6	6	7	11
Co	83	84	92	89	123
V	8	15	19	24	92
Rb	18	180	194	136	117
Sr	355	93	219	682	88
Zr	85	97	134	108	175
Y	23	9	12	16	28
Nb	12	10	8	8	10
Th	27	26	25	24	22
U	10	7	2	10	11
Ba	125	518	1150	895	390

Major oxides in weight %, trace elements in ppm
Total iron is expressed as Fe_2O_3

Table 9: Abundances of major oxides and selected trace elements in quartz veins from the Asimotrypes Gold Deposit, Pangeon, N. Greece

Sample	As-42	As-43	As-60
SiO_2	81.50	89.00	90.50
TiO_2	0.06	0.05	n.d
Al_2O_3	2.40	2.00	3.00
Fe_2O_3	4.45	2.09	3.65
MgO	0.30	0.68	0.27
MnO	0.08	0.02	0.04
CaO	5.85	3.20	0.77
K_2O	0.25	0.39	0.69
Na_2O	0.07	0.17	0.75
P_2O_5	0.03	0.03	0.03
L.O.I.	4.90	1.30	0.10
Total	99.89	98.93	99.80
Au	0.02	n.d	n.d
Ag	1.20	1.10	1.90
Pb	11	3	75
Zn	11	n.d	656
Cu	n.d	n.d	492
As	198	31	58
Sb	n.d	n.d	2
Bi	n.d	n.d	n.d
Se	n.d	n.d	n.d
Te	n.d	n.d	n.d
Cr	612	573	338
Ni	76	23	5
Co	119	127	141
V	30	25	4
Rb	11	24	18
Sr	16	35	1
Zr	22	11	18
Y	10	6	7
Nb	3	2	3
Th	1	n.d	44
U	3	n.d	n.d
Ba	32	37	43

Major oxides in weight %, trace elements in ppm
Total iron is expressed as Fe_2O_3

Table 10: Abundances of major oxides and selected trace elements in skarn, from the Asimotrypes Gold Deposit, N. Greece.

Sample	As-47	As-48	As-49
SiO_2	35.50	15.50	35.00
TiO_2	0.28	0.23	0.93
Al_2O_3	4.35	3.84	13.50
Fe_2O_3	2.70	3.12	8.39
MgO	1.30	1.42	1.86
MnO	0.07	0.17	0.16
CaO	30.44	41.40	23.38
K_2O	1.36	0.81	2.90
Na_2O	0.44	0.46	0.31
P_2O_5	0.18	0.10	0.58
L.O.I.	23.80	33.50	13.80
Total	100.42	100.55	100.81
Au	0.05	0.06	0.07
Ag	6.60	8.80	4.00
Pb	22	32	29
Zn	28	49	142
Cu	0	205	17
As	108	88	82
Sb	n.d	n.d	n.d
Bi	1	1	1
Se	1	1	1
Te	3	3	3
Cr	67	57	327
Ni	27	61	88
Co	62	53	80
V	34	35	118
Rb	20	30	55
Sr	135	130	160
Zr	36	30	63
Y	22	13	36
Nb	3	3	3
Th	1	3	0
U	1	2	0
Ba	40	250	75

Major oxides in weight %, trace elements in ppm
Total iron is expressed as Fe_2O_3

REFERENCES

REFERENCES

Adams, J.E.., and Rhodes, M.L ., 1960: Dolomitization by seepage refluction:. *A.A.P.G. Bull., v. 44, p. 1912-1920.*

Al-Hashimi, W.S., 1976: Significance of strontium distribution in some carbonate rocks in the Carboniferous of Northumberland, England: *Jour. of Sed. Petrology, v. 46, p. 369-377.*

Amov, B.G., 1983: Evolution of uranogenic and thorogenic lead. 1. A dynamic model for continuous isotopic evolution: *Earth Planet. Sci. Letter, v. 65, p. 61-74.*

Amov, B.G., Arvanitides, N.D., and Constantinides, D.C., 1991: Isotopic composition of lead in galenas from some mineralizations in Greece and their interpretation: *Internal Report, IGME, Thessaloniki Branch, 10pp.*

Andrews, J.E., Hamilton, P.J., and Fallick, A.E., 1987: The geochemistry of early diagenetic dolostones from a low salinity Jurassic lagoon : *Jour. Geol. Soc. London, v. 144, p. 687-698.*

Arvanitides, N. D., 1993: Regional ore geological studies: Setting, Controls and Distribution of Metallic Deposit Types in the Serbomacedonian and Western Rhodope Zones: *EEC Project MA2M-CT90-0015, Final Internal Report, IGME, Athens, 99pp.*

Arvanitides, N. D., and Ashworth, K.L., 1993: Carbonate-hosted precious and base metal mineralizations in northern Greece: development of new exploration strategies. 3.1. Regional Geology: EEC *Project MA2M-CT90-0015, Final Report, IGME, Athens, p.7-12.*

Badiozamani, K., 1973: The Dorag dolomitization model application to the Middle Ordovician of Winsconcin: *Jour. Sed. Petrology, v. 43, p. 965-984.*

Baker, J.H., Eliopoulos, D.G., Arvanitides, N.D., and Chatzipanagis, J., 1993: Carbonate-hosted precious and base metal mineralizations in northern Greece: development of new exploration strategies. Fertile lineaments and regional variations of metallic elements. 3.4 The Pangeon - Symvolon regions: EEC *Project MA2M-CT90-0015, Final Report, IGME, Athens, p.42-*

48.

Baker, P.A., and Burns, S. J., 1985: Occurrence and formation of dolomite in organic-rich continental margin sediments: ***A.A.P.G. Bull., v.69, p. 1917-1930.***

Barton, P.B., 1979: Sulfide Petrology: ***Mineralogical Soc. Amer. Spec. Pap. 3, p. 187-198.***

Behrens, E.W., and Land, L.S., 1972: Subtidal Holocene dolomite, Baffin Bay, Texas: ***Jour. of Sedimentary Petrology, v. 42, p. 155-161.***

Belevantsev, V.I., Kolonin, G.R., Vasilyeva, N.G., Shironosova, G.P., Shamovskaya, G.I., and Peshchevitsky, B.I., 1982: Probable forms and solubility of gold in ore forming solutions. **In *Hydrothermal Low Temperature Ore Formation and Metasomatism. Akad. Nauk SSSR (Siberian Branch), 505: 83-117 (in Russian).***

Benning, L.G., and Seward, T.M., 1996: Hydrosulphide complexing of Au (I) in hydrothermal solutions from 150-400^0 C and 500-1500 bar: ***Geochim. and Cosmochim. Acta, v. 60, No 11, p. 1849-1996.***

Bigeleisen, J., Pearlman, M.L., and Prosser, A.C., 1952: Conversion of hydrogenic materials to hydrogen for isotopic analysis: ***Analytical Chemistry, v. 24, p. 1356-1357.***

Biscaye, P.E., and Dasch, J.E., 1971: The rubidium, strontium, strontium isotope system in deep-sea sediments: ***J. Geophys. Ress., V. 76, p. 5087-5096.***

Bodnar, R.J., 1983: A method of calculating fluid inclusion volumes based on vapor bubble diameters and P-V-T-X properties of inclusion fluids: ***Econ. Geol., v.78, p. 535-542.***

Bohlke, J.K., and Kistler, R.W., 1986: K-Ar and stable isotope evidence for the ages and sources of fluid components of gold bearing quartz veins in the northern Siera Nevada foothills metamorphic belt, California: ***Econ. Geol., v. 81, p. 296-322.***

Bottinga, Y., 1968: Calculation of fractionation factors for carbon and oxygen exchange in the system calcite-carbon dioxide-water: ***Jour. Phys. Chem., v. 72, p. 4338-4340.***

Boyle, R.W. , 1979: The geochemistry of gold and its deposits: *Geol. Surv. of Canada, Bull. 280, 584 pp.*

Bowers, T.S., and Helgeson, H. C., 1983a: Calculation of the thermodynamic and geochemical consequences of non ideal mixing in the system H_2O-CO_2-NaCl on phase relations in geologic systems: Equation of state for H_2O-CO_2-NaCl fluids at high pressures and temperatures: *Geochim. Cosmochim. Acta, v. 47, p. 1247-1275.*

Brace, W.F., 1980: Permeability of crystalline and argillaceous rocks: *Internat. Journal of Rock Mechanics Mining Sci., v. 17, p. 241-251.*

Brown, P.E., 1989: A microcomputer program for the reduction and investigation of fluid inclusion data: *Am. Mineral., v.74, p. 1390-1393.*

Brown, P.E ., and Lamp, W.M., 1989: P-V-T properties of fluids in the system H_2O-CO_2-NaCl: new graphical presentations and implications for fluid inclusion studies: *Geochim. Cosmochim. Acta, v. 53, p. 1209-1221.*

Budaj, J.M., Lohmann, K.C., and Owen, R.M., 1984: Burial dolomite in the Mississippian Madison limestone: *Jour. of Sed. Petrology, v. 54, p. 276-288.*

Burnham, C.W., Holloway, J.R., and Davis, N.F., 1969: Thermodynamic properties of water to 1000 ^{0}C and 10000 bars: *Geol. Soc. America, Spec. Paper 132, 96p.*

Burrows, D.R., Wood, P.C., and Spooner, E.T.C., 1986: Carbon isotope evidence for a magmatic origin for Archean gold-quartz vein ore deposits: *Nature 321, p. 851-854.*

Burrows, D.R., and Spooner, E.T.C., 1987: Generation of a magmatic H_2O-CO_2 fluid enriched in Mo, Au and W within an Archean sodic granodioritic stock, Mink lake, north-western Ontario: *Econ. Geol., v. 82, p. 1931-1957.*

Cameron, E.M., 1988: Archean gold: Relation to granulite formation and redox zoning in the crust: *Geology, v. 16, p. 109-112.*

Cameron, E.M., and Hatori, K., 1987: Archean gold mineralization and oxidized hydrothermal fluids: *Econ. Geol., v.82, p.1177-1191.*

Carter, O.F., 1948: Coniarum mine. Structural Geology of Canadian Ore Deposits, *v.I, Can. Inst. Min. Metall., Montreal, pp. 497-503.*

Chafetz, H.S., 1972: Surface diagenesis of limestone: *Jour. of Sed. Petrology, v. 42, p. 325-329.*

Chalkias, S., and Vavelidis, M., 1988: Interpretation of lead isotope data from Greek Pb-Zn deposits based on an empirical two-stage model: *Bull. of Geol. Soc. of Greece, Vol. XXIII/2, p.177-193.*

Changkakoti, A., Dimitrakopoulos, R., Gray, J., Krouse, H.R., Krstic, D., Kalogeropoulos, S.I., and Arvanitides, N.D., 1990: Sulphur and lead isotopic composition of sulphide minerals from Thermes and Essimi, Rhodope Massif, Greece: *N. Jb. Miner., Mh. Jg., H.9., p. 413-430.*

Channel, J.E .T., and Horvath, F., 1976: The African/Adriatic promotory as a paleogeographical premise for Alpine orogeny and plate movements in the Carpatho-Balkan region: *Tectonophysics, V.35, p.71-101*

Chatzipanagis, J., Companoni, R., and Sadrone, R., 1983: Studio geologico-petrographico del Bos-Dag settentrionale nella zona dei Rodopi (Macedonia Greca): *Soc. Ital. Min. Petr. Special Issue, 15p.*

Chatzipanagis, J., 1991: Geological evolution of the Falakron Mt. area: *Ph.D. Thesis, Athens Technical University, 179pp.*

Chatzipanagis, J., Evangelou, E., and Eliopoulos, D.G., 1992: Geology, Lithostratigraphy, Metamorphism, Tectonics, and Mineralizations of the Pangeon and Symvolon mountains: *EEC Project MA2M-CT90-0015, Internal Report, IGME, Athens, 18pp.*

Cheney, E.S., and Jensen, M.L., 1965: Stable carbon isotopic composition of biogenic carbonates: *Geochim. and Cosmochim. Acta, v. 29, p. 1331-1346.*

Chryssoulis, S.L., Cabri, L.J., and Lennard, W., 1989: Calibration of the ion probe for quantitative trace precious metal analyses of ore minerals:

Chryssoulis, S.L., and Weisener, C.G., 1991: Quantification and imaging of submicroscopic Au in ore minerals with the ion microprobe: *In: Int. Conf. on SIMS VIII., John Wiley, p. 517-520.*

Clayton, R.N., and Mayeda, T.K., 1963: The use of bromine pentafluoride in the

extraction of oxygen from oxides and silicates for isotopic analysis: *Geochim. and Cosmochim. Acta, v.27, p. 43-52.*

Collins, P.L.F., 1979: Gas hydrates in CO_2-bearing fluid inclusions and the use of freezing data for estimation of salinity: *Econ. Geol., v. 74, p. 1435-1444.*

Colvine, A .C., Andrews, A.J., Cherry, M.E., Durocher, M.E., Fyon, A.J., Lavigne, M.J.Jr., Macdonald, A.J., Marmont, S., Poulsen, K.H., Springer, J.S., and Troop, D.G, 1984: An integrated model for the origin of Archean lode gold deposits: *Ontario Geol. Surv., Open-File Report 5524, 85pp.*

Colvine, A.C ., Fyon, A.J., Heather, K.B., Marmont, S., Smith, P.M., and Troop, D.G., 1988: Archean Lode Gold Deposits in Ontario. *Ont. Geol. Survey, , Misc. Paper 139136pp.*

Connoly, J.A.D., and Thompson, A.B., 1989: Fluid enthalpy and production during regional metamorphism: *Contr. Mineralogy and Petrology, v.102, p.347-366.*

Craw, D., 1988: Shallow level metamorphic fluids in a high uplift rate metamorphic belt; Alpine schist, New Zealand: *Jour. Metamorphic Geology, v. 6, p. 1-16.*

Craw, D., and Coons, P.O., 1988: Tectonically induced gold mineralization adjacent to major fault zones: *Geol. Soc. Australia, Abstracts, v.22, p.338-343.*

Criss, R.E., and Taylor, H.P.,Jr., 1986: Meteoric-hydrothermal systems: *Reviews in Mineralogy, v.16, p. 373-424.*

Cumming, G.L., and Richards, J.R., 1975: Ore lead isotope ratios in a continuously changing earth: *Earth Plant. Sci. Letters, v. 28, p. 155-171.*

Deines, P., and Gold, D.P., 1973: The carbon isotopic composition of carbonitite and kimberlite carbonates and their bearing on the composition of deep-seated carbon: *Geochim. Cosmochim. Acta, v. 37, p. 1707-1733*

Deines, P., 1980: The carbon isotopic composition of diamonds, relationship to diamond shape, color, occurrence and vapor composition: *Geochim. Cosmochim. Acta, v. 44, p.943-961.*

Dewey, J.E., Pitman, W.C., Ryan, W.B.F. and Bonnin, J., 1973: Plate tectonics and the evolution of the Alpine System. *Geol. Soc. Am. Bull., v.84, 3137-3180.*

Diamond, L.W., 1990: Fluid inclusion evidence for P-V-T-X evolution of hydrothermal solutions in late-Alpine gold-quartz veins at Brusson, Val D' Ayas, NW Italian Alps: *Amer. Jour. Sci., v. 290, p. 912-958.*

Dimadis, E., and Zachos, S., 1986: Geological Map of the Rhodope massif, in 1:200 000. *IGME, Greece.*

Dimitrov, D.K., and Zidarov, N., 1969: On the stratigraphy of the Archaic metamorphic complex in the Rhodope massif. *Res. Bulgar. Geol. Soc. 303*

Dinder, D.A ., and Royden, L ., 1993: Late Cenozoic extension in northeastern Greece: Strymon Valley detachment system and Rhodope metamorphic core complex. *Geology, v.21, p. 45-48.*

Dinter, D.A., 1998: Late Cenozoic extension of the Alpine collisional orogen, northeastern Greece: Origin of the north Aegean basin: *Geol. Soc. America Bull., v.110, no 9, p. 1208-1230.*

Drever, J.I., 1982: The geochemistry of natural waters: *Englewood Cliffs, New Jersey, Pentice Hall, pp 388.*

Ellis, A.J., and Giggenbach, W., 1971: Hydrogen sulphide ionisation and sulphur hydrolysis in high temperature solution*: Geochim. and Cosmochim. Acta, v.35, p.247-260.*

Epitropou, N., and Chatzipanagis, J., 1989: Lithostratigraphic and tectonic controls of the iron-manganese, base and precious metal mineralizations in the West Rhodope. *Geol. Rhodopica, Sofia, v. 1, p. 381-388.*

Faure, G., 1986: Principles of isotope geology: *Wiley, 2nd edn., New York, pp 589.*

Ferguson, S.A., Buffan, B.S.W., Carter, O.F., Griffis, A .T., Holmes, T.C., Hurst, M.E., Jones, W.A., Lane, H.C., and Longley, C. S., 1968: Geology and ore deposits of the Tisdale township, district of Cochrane: *Ontario Dept. Mines Geol., Rept. 58, 177pp.*

Folk, R.L., Land, S.L., 1975: Mg/Ca ratio and salinity: two controls over crystallization of dolomite*: A.A.P.G., v. 59, p. 60-68.*

Frank, J.R., 1981: Dedolomitization in the Taum Sauk limestone (Upper Cambrian), southeast Missouri: *Jour. of Sed. Petrology, v.51, p.7-18.*

Frei, R., 1992: Isotope (Pb, Rb-Sr, S, O, C, U-Pb) geochemical investigation on Tertiary intrusives and related mineralizations in the Serbomacedonian Pb-Zn, Sb+Cu-Mo metallogenic province in N. Greece: *Ph. D Thesis, Swiss Federal Institute of Technology (ETH) Zurich, Switzerland, 321 p.*

Friedman, I., and O' Neil, J.R., 1977: Compilation of stable isotope fractionation factors of geochemical interest: In: Fleischer, M., (ed), *Data of Geochemistry, Sixth Edition: U.S. Geological Survey, Professional Paper 440-KK, p. KK1-KK12.*

Fripp, R.E.P., 1976a: Stratabound gold deposits in Archean banded iron-formation, Rhodesia: *Econ. Geol., v.71, p.58-75.*

Fyfe, W.S., and Henley, R.W., 1973: Some thoughts on chemical transport processes, with particular reference to gold: *Mineral. Sci. Eng., v.5, No 4, p. 295-303.*

Fyon, J.A., Schwarez, H.P., and Crocket, J.H., 1984: Carbonatization and gold mineralization in the Timmins area, Abitibi greenstone belt: Genetic links with Archean mantle CO_2 - degassing and lower crust granulitization (abs): *Geol. Assoc. Canada Program with Abstracts, v.9, p.65.*

Fytikas, M., Innocenti, F., Mannetti, P., Mazzuoli, R., Peccerillo, A., and Villari, L., 1980: Tertiary to Quaternary evolution of volcanism in the Aegean region: *Jour. Geol. Soc. London, Spec. Publ., 17, p. 687-699.*

Galanopoulos, V. P, Arvanitides, N.D., and Hellingwerf, R.W., 1992: Advanced Interdisciplinary Exploration Research for Base, Precious and Associated Metals in Polymetamorphic Terrains, N. Greece. *EEC Project MA1-0049-GR, Final Report, IGME, 32 pp.*

Gale, N.H., 1978: Lead isotopes and the Aegean metallurgy: *Thera and the Aegean World, v. 1, p.529-545.*

Gammon, C.H., and Williams-Jones, A.E., 1995: The solubility of Au-Ag alloy + AgCl in HCl/NaCl solutionsat 300 ^{0}C : New data on the stability of Au(I)

chloride complexes in hydrothermal solutions: *Geochim. and Cosmochim. Acta, v. 59, p. 3453-3468.*

Gehring, M., Lentz, H., and Franck, E.U., 1986: Concentrated aqueous sodium chloride solutions from 200 ^{0}C to 600 ^{0}C and 3000 bar-phase equilibria and PVT - data: *Ber. Bunsenges. Phys. Chem., v. 87, p. 597-600.*

German, K., Holzmann, G., and Winkler, J., 1980: Determination of marble provenance: limits of isotopic analysis: *Archeometry, v.22, p.96-106.*

Gibert, F., Pascal, M.L., and Pivachant, M., 1993: Solubility of gold in Kcl (0.5m) solution under hydrothermal conditions (350-450 ^{0}C, 500 bar) (abs): *In Proc. 4th International Symposium on hydrothermal reactions, Cuney, M., and Cathelineau, M., (eds), p. 65-68, Insitute Loraine des Geoscience.*

Giles, A .D., and Marshall, B., 1984: Fluid inclusion studies on a multiply deformed, metamorphosed volcanic-associated massive sulfide deposit, Joma mine, Norway: *Econ. Geol., vol. 89, p. 803-819.*

Goldberg, M., 1967: Supratidal dolomitization and dedolomitization in Jurassic rocks of Hamakhtesh Hagatan, Israel: *Jour. of Sed. Petrology, v.37, p.760-773.*

Goldfarb, R.J., Leach, D.L., and Pitchthorn, W.J., 1988: Application of fluid inclusion and stable isotope techniques to the study of Tertiary mesothermal gold deposits, Southern Alaska, U.S.A: In Bicentennial Gold 88, Goode, A.D.T., Smyth, E.L., Birch, W.D., and Bosma, L.I., (eds), *Geol. Soc. Australia, Abstracts, v.23, p. 439-441.*

Goldfarb, R.J., Leach, D.L., Rose, S.C., and Landis, G.P., 1989: Fluid inclusion geochemistry of gold-bearing quartz veins of the Juneau gold belt, southeastern Alaska: Implications for ore genesis: *Econ. Geol. Mon. 6, p. 363-375.*

Gregg, J. M., 1985: Regional epigenetic dolomitization in the Bonneterre Dolomite (Cambrian), southeastern Missouri: *Geology, v. 13, p.503-506.*

Groves, D.I., and Phillips, G.N., 1987: The genesis and tectonic control on Archean gold deposits of the Western Australian Shield: *Ore Geol. Reviews, v. 2, p.287-322.*

Groves, D.I., Phillips, G.N., Ho, S.E., Houstoun, S.M., and Standing, C. A., 1987:

Craton-scale distribution of Archean greenstone gold deposits. Predictive capacity of the metamorphic model: *Econ. Geol., v. 82, p. 2045-2058.*

Groves,D.I., Golding, S.D., Rock, N.M.S., Barley, M.E., and McNaughton, N.J., 1988: Archean carbon reservoirs and their relevance to the fluid source for gold deposits: *Nature, v. 331, p.254-257.*

Hardie, L.A., 1987: Dolomitization : A critical review of some current views: *Jour. of Sed. Petrology, v. 57, p. 166-183.*

Hatori, K., 1987: Magnetic felsic intrusions associated with Canadian Archean gold deposits: *Geology, v.15, p.1107-1111.*

Hayashi, K-I., and Ohmoto, H., 1991: Solubility of gold in NaCl- and H_2S bearing aqueous solutions at 250-350 ^{0}C: *Geochim. and Cosmochim. Acta, v.55, p. 2111-2126.*

Hellingwerf, R.W., Baker, J.H., Arvanitides, N.D., and Galanopoulos, V.P., 1991: Ore-forming processes, hydrothermal alteration and exploration for manganese, base and precious metals in W. Rhodope, Greece: *EEC Project MA1-0049-GR, Final Report, IGME, 28 pp.*

Hedenquist, J.W., and Henley, R.W., 1985: The importance of CO_2 freezing point measurements of fluid inclusions: evidence from geothermal systems and implications for epithermal ore deposition: *Econ. Geol., vol. 80, p.1379-1406.*

Hendel, E.M., and Hollister, L.,S., 1981: An empirical solvus for CO_2-H_2O -2.6 wt% salt: *Geochim. and Cosmochim. Acta, v.45, p. 225-228.*

Henley, R.W., 1973: Solubility of gold in hydrothermal chloride solutions: *Chem. Geology, v. 11, p. 73-87.*

Higgins, N., and Kerrich, R., 1982: Progressive ^{18}O depletion during CO_2 separation from a carbon dioxide rich hydrothermal fluid: evidence from the Gray River tungsten deposit: *Can. Journal of Earth Sci., v.19, p. 2247-2257.*

Hodgson, C .J., 1993: Mesothermal Lode-gold Deposits. In: Kirkham, R.V., Sinclair, W.D., Thorpe, R.I., and Duke, J.M., eds, Mineral Deposit Modeling:

Geological Association of Canada, Special Paper 40, p.635-678.

Hsu, K., Nachev, I., and Vuchev, T., 1977: Geologic evolution of Bulgaria in light of plate tectonics: *Tectonophysics, v. 40, p. 245-256.*

Hutchinson, R.W., 1987: Metallogeny of Precambrian gold deposits: Space and time relationships: *Econ. Geol., v. 82, p. 1993-2007.*

Hutchinson, R.W., and Burlington, J.L., 1984: Some broad characteristics of greenstone belt gold deposits. In: Foster, R.P., ed., Gold '82: The Geology, Geochemistry and Genesis of Gold Deposits: *Geological Survey of Zimbabwe, Special Publication 1, A.A Balkema, Rotterdam, The Netherlands, p. 339-372.*

Innocenti, F., Kolios, N., Mannetti, P., Mazzuoli, R., Peccerillo, A., Rita, L., and Villari, L.,1984: Evolution and geodynamic significance of the Tertiary orogenic volcanism in Northeastern Greece: *Bull. of Volcanology, v. 47, p. 25-37.*

Ivanov, R., 1989: The Mesta high metamorphic Supergroup in the Allocthone of the Mesta nappe [Abs]: *2nd Hellenic-Bulgarian Symposium on the Rhodope Massif, Aristotle University of Thessaloniki, Abstracts Volume, p.22.*

Kaziwara, Y., and Krouse, H.R., 1971: Sulphur isotope partitioning in metallic sulphide systems: *Can. Journal of Earth Sciences, v. 8, p. 1397-1408.*

Katz, A., 1971: Zoned dolomite crystals: *Jour. of Geology, v. 79, p. 38-51.*

Kastner, M., 1982: When does dolomitization occur and what controls it: *11th Intern. Congr. Sed. (Abst.), Hamilton, Ontario Canada, p. 124.*

Kerrich, R., 1976: Some effects of tectonic recrystallization on fluid inclusions in vein quartz: *Contributions to Mineralogy and Petrology, v. 59, p. 195-202.*

Kerrich, R., 1987: The stable isotope geochemistry of Au-Ag vein deposits in metamorphic rocks. In: Kyser, K.T., ed., Stable Isotope Geochemistry of Low Temperature Fluids. *Mineralogical Association of Canada, Short Course Handbook 13, p. 287-336.*

Kerrich, R., 1989: Geodynamic setting and hydraulic regimes: Shear zone hosted mesothermal gold deposits: *Geological Association of Canada, Short*

Course Notes, v. 6, p. 89-128.

Kerrich,R., 1989: Geochemical evidence for the sources of fluids and solutes for shear -zone hosted mesothermal gold deposits: In: Mineralization and shear zones. Barsnall, J.T. (ed), ***Ceol.Ass. Can. Short Course Notes 6, p. 129-198.***

Kerrich, R., 1990: Carbon isotopic systematics of Archean Au-Ag vein deposits in the Superior Province: ***Can. Journal of Earth Sciences, v.27, p. 40-56.***

Kerrich, R., and Fryer, B. J., 1979: Archean precious metal hydrothermal systems, Dome mine, Abitibi greenstone belt: REE and oxygen isotope relations: ***Can. Jour. of Earth Sci., v.16, p.440-458.***

Kerrich, R., and Fyfe, W.S., 1981: The gold-carbonate association: Source of CO_2 and CO_2-fixation reactions in Archean lode gold deposits: ***Chem. Geology, v. 33, p.265-294.***

Kilias, A., and Mountrakis, D., 1989: Kinematics of the crystalline sequences in the western Rhodope massif. 2nd Hellenic-Bulgarian Symposium on the Rhodope massif: ***Aristotle Univ. of Thessaloniki, Abstr. Vol., p. 28***

Kilias, S.P., 1990: Metallogeny of polymetallic sulphide and tungsten mineralizations in the Serbomacedonian massif, northern Greece: the examples of the Olympias Pb-Zn(Au,Ag) sulphide and the Metaggitsi scheelite deposits: ***Unpubl. Ph.D Thesis, Institute of Petrology, Univ. of Copenhagen, 221pp.***

Kilias, S.P., and Konnerup-Madsen, J., 1977: Fluid inclusion and stable isotope evidence for the genesis of quartz scheelite veins, Metaggitsi area, central Chalkidiki peninsula, N. Greece: ***Mineralium Deposita, v.32, p.581-595.***

Kockel, F., and Walther, H., 1965: Die Strymon-linie als Grenze zwinchen Serbomacedonischen und Rila-Rhodope-Massiv in Ost-Macedonien: ***Geol. Jb. 83, p. 575-602.***

Kokkinakis, A., 1977: Das intrusivgebiet des Symvolon-Gebriges von Kavala in Ostmakedonien, Griecheland: ***Diss. Univ. of Munchen, 255p.***

Kokkinakis, A., 1980: Altersbeziehungen swischen Metamorphosen, mechanismen, deformationen und intrusionen am Sudrand des Rhodope-Massives

(Macedonien, Griecheland): *Geol. Rundschau, v.69:3, p.726-744.*

Kretscchmar, V., and Scott, S.D., 1976: Phase relations involving arsenopyrite in the system Fe-As-S and their application: *Can. Mineral., v. 14, p. 364-386.*

Kreulen, R., 1980: CO_2 -rich fluids during regional metamorphism on Naxos, a study on fluid inclusions and stable isotopes: *Unpubl. Ph.D. Thesis, Univ. of Utrecht, pp. 85.*

Kretz, R., 1982: A model for the distribution of trace elements between calcite and dolomite: *Geochim. and Cosmochim. Acta, v. 46, p. 1979-1981.*

Kronberg, P., 1969: Gliederung, Petrographie und Tectonese des Rhodopen-Krystallins im Tsal-Dag, Symvolon und Ost- Pangeon (Griechsch-Makedonien): *Geotekt. Forsch., v.31, p.1-49.*

Kyriakopoulos, K., 1987: A geochronological, geochemical and mineralogical study of some Tertiary plutonic rocks of the Rhodope massif and their isotopic characteristics: *Ph.D. Thesis, Athens Univ., Greece, 343 p.*

Kyser, T.K., and O'Neil, J.R., 1984: Hydrogen isotope systematics of submarine basalts: *Geochim and Cosmochim. Acta, v. 48, p. 2123-2133.*

Kyser, T.K., and Kerrich, R., 1990: Geochemistry of fluids in tectonically active regions: *Mineralog. Assoc. of Canada Short Course, Handbook, v. 18, p.113-215.*

Lederer, C.M., Hollander, J.M., and Perlman, I., 1967: Table of isotopes: *Sixth ed. John Wiley, New York, pp 594.*

Liati, A., 1986: Regional metamorphism and overprinting contact metamorphism of the Rhodope zones, near Xanthi: Petrology, Geochemistry, Geochronology: *Ph.D. Thesis, Tech. Univ. Braunschweig, 186 p.*

Liati, A., and Mposkos, E., 1990: Evolution of the eclogites in the Rhodope Zone of northern Greece: *Lithos, v. 25, p.89-99.*

Liati, A., and Siedel, E., 1996: Metamorphic history of kyanite eclogites in Central Rhodope, northern Greece: *Contrib. Mineral. and Petrol., v. 123, p. 293-307.*

Lu, J., and Seccombe, P.K., 1993: Fluid evolution in a slate-belt gold deposit-a fluid inclusion study of the Hill End goldfield, NSW, Australia: *Minera-*

lium Deposita, v. 28, p. 310-323.

Lumsden, D.N., and Chimachuski, J.S., 1980: Relationship between dolomite nonstoichiometry and carbonate facies parameters: In: Zenger, D.H., Dunham, J.B., and Ethington, R.L., (eds), ***Concepts and Models of dolomitization-A reappraisal: Earth Science Reviews, V. 23, p. 175-222.***

Lusk, J., 1972: Examination of volcanic exhalative and biogenic origins for sulfur in the stratiform massive sulfide deposits of New Brunswick: ***Econ. Geol., v. 67, p. 169-183.***

Machel, H. G., and Anderson, J.H., 1989: Pervasive surface dolomitization of the Nisku Formation in Central Alberta: ***Jour. of Sed. Petrology, v. 59, p.891-911.***

Machel, H.G., and Moyntjoy, E.W., 1986: Chemistry and environments of dolomitization: A reappraisal: ***Earth Science Reviews, v. 23, p. 175-222.***

Madu, B.E., Nesbitt, B.E., and Muehlenbachs, K., 1990: A mesothermal gold-stibnite-quartz vein occurrence in the Canadian Cordillera: ***Econ. Geol., v. 85, p. 1260-1268.***

Magaritz , M., and Taylor, H.P., Jr., 1976: Oxygen, hydrogen and carbon isotope studies of the Franciscan formation, Cost Ranges, California: ***Geochim. and Cosmochim. Acta, v. 40, p. 215-234.***

Maheux, P.J., 1989: A fluid inclusion and light stable isotope study of antimony-associated gold mineralization in the Bridge River district, British Columbia, Canada: ***Unpub. M.Sc. Thesis, Univ. Alberta, 159pp.***

Mason, R., and Melnik, N., 1986: The anatomy of an Archean gold system- The McIntyre-Hollinger complex at Timmins, Ontario, Canada. In: Macdonald, A.J., ed., ***Proceedings of Gold '86 Conference. Toronto, Ont., p.40-55.***

Matsuhisa, Y., Goldsmith, J.R. and Clayton, R.N., 1979: Oxygen isotopic fractionation in the system quartz-albite-anorthite-water: ***Geochim. Cosmochim. Acta, v. 43, p. 1131-1140.***

Mattes B.W., and Moyntjoy, E.W., 1980: Burial dolomitization of the Upper Devonian Miette build up, Jasper National Park, Alberta: In: Zenger, D.H.,

Dunham, J.B., and Ethington, R.L., (eds): *Concepts and models of dolomitization, Spec. Publ. 28, p. 259-279.*

Mauger, R.L., 1972: A sulfur isotope study of the Ducktown, Tennessee district, U.S.A.: *Econ. Geol., v. 67, p. 497-510.*

McCrae, J. M., 1950: The isotopic chemistry of carbonates and a paleotemperature scale: *Jour. of Chemistry and Physics, v. 18, p. 849-857.*

Meyer, W., 1968: Zur Altersstellung des plutonismus im Sudteil der Rila-Rhodope masse (Nord Griechenland): *Geol. Paleontologica, p. 173-192.*

Milledge, H.J., Mendelssohn, M.J., Seal, M., Rouse, J.E., Swart, D.K., and Pillinger, C.T., 1983: Carbon isotope variation in spectral type II diamonds: *Nature, v. 303, p. 2084-2087.*

Moorbath, S., and Zagorzev, I., 1983: Rubidium-Strondium Isotopic data on the age of the first granitoid complex (Smilovene and Hisar plutons) in Sastinska Sredna Gora: *Geol. Balk., v. 13, p. 3-14.*

Morrow, D.W., 1982: Diagenesis 2. Dolomite, part 2: Dolomitization models and ancient dolostones: *Geoscience Canada, v. 9, p. 95-107.*

Mposkos, E., 1989a: High-pressure metamorphism in gneisses and pelitic schists in East Rhodope Zone: *Mineral. and Petrol., v.41, p.337-351.*

Mposkos, E., 1989c: Metamorphic evolution of the lower tectonic unit of east Rhodope, based on metabasite petrology: *Carpatho-Balkan Geol. Assoc., XIV Congress, v.1, p.317-320.*

Mposkos, E., 1991: Petrology of the metamorphic rocks of West Rhodope. In: MAIN- 0049-GR. Advanced interdisciplinary exploration research for base, precious and associated metals in polymetamorphic terrains. *IGME, Athens, pp.67.*

Mposkos, E., and Liati, A., 1993: Metamorphic evolution of metapelites in the high-pressure terrain of the Rhodope zone, northern Greece: *Can. Mineralogist, v.31, p. 401-424.*

Mposkos, E., Perdikatsis, V., and Eliades, A., 1994: Petrology of the metamorphosed ultramafic rocks of the upper tectonic unit in east Rhodope. Contribution to the metamorphic evolution of the Rhodope Zone: *Bull. Geol. Soc.*

Greece, v. XXX,v. 1, p. 241-254.

Mposkos, E., 1994: Interpretation of the metamorhic evolution of the lower and upper tectonic units in Rhodope: Similarities and differences: ***Bull. Geol. Soc. Greece, vol. XXX/1, p. 255-269.***

Mposkos, E., Chatzipanagis, J., and Papadopoulos, P.,1998: New data on the boundaring of the Pangeon and Sideronero tectonic units in the western Rhodope: ***Bull. Geol. Soc. Greece, v. XXXII, 1, p. 13-21***

Naden, J., and Shepherd, T., 1989: Role of methane and carbon dioxide in gold deposition: ***Nature, v. 342, p. 793-795.***

Neall, F.B., and Phillips, G.N., 1987: Fluid-wall rock interaction in the Archean hydrothermal gold deposits: A thermodynamic model for the Hunt mine Kambalda: ***Econ. Geol., v. 82, p. 1679-1694.***

Nebel, M.L., Hutchinson, R.W., and Zartman, R.E., 1991: Metamorphism and polygenesis of the Madem Lakkos polymetallic sulphide deposit, Chalkidiki, Greece: ***Econ. Geol., v. 86, p. 81-105.***

Nesbitt. B.E., 1988: The gold deposit continuum: A genetic model for lode gold mineralization in the continental crust: ***Geology, v. 16, p. 1044-1048.***

Nesbitt, B.E, 1990: Fluid flow and chemical evolution in the genesis of hydrothermal ore deposits: ***Mineralog. Assoc. of Canada, Short Course, Handbook, v. 18, p. 261-292.***

Nesbitt, B.E., 1993: Phanerozoic gold deposits in tectonically active continental margins:In Foster, R.P., (ed), ***Gold Metallogeny and Exploration: Glasgow, Blackie Sons, Ltd., P. 104-132.***

Nesbitt, B.E, Murowchick, J.B., and Muehlenbachs, K., 1986: Dual origin of lode gold deposits in Canadian Cordillera: ***Geology, v. 14, p. 506-509.***

Nesbitt, B.E, Murowchick, J.B., and Muehlenbachs, K., 1987: Reply to a comment on "Dual origins of lode gold deposits in the Canadian Cordillera: ***Geology, v. 15, p. 472-473.***

Nesbitt, B.E, and Muehlenbachs, K., 1989a: Geology, Geochemistry and Genesis

of Mesothermal Lode Gold Deposits of the Canadian Cordillera: Evidence for Ore Formation from Evolved Meteoric Water. In: Keays, R.R., Ramsay, W.R.H., and Groves, D.I., eds., The Geology of Gold Deposits: The Perspective in 1988: *Econ. Geol., Monograph 6, p. 553-563.*

Nesbitt, B.E, Muehlenbachs, K., and Murowchick, J.B., 1989: Genetic implications of stable isotope characteristics of mesothermal gold deposits and related Sb and Hg deposits in the Canadian Cordillera: *Econ. Geol., v. 84, p. 1489-1506.*

Nesbitt, R.W., Billet, M.F., Ashworth, K.L., Deniel, C., Constantinides, D., Demetriades, A., Katirtzoglou, K., Michael, K., Mposkos, E., Zachos, S., and Sanderson, D,. 1988: The geological setting of base metal mineralization in the Rhodope region, northern Greece: In Boissonas J., and Omenneto, P., (eds) Mineral deposits within the European Community: *Berlin, Heidelberg, Springer-Verlag, p. 499-514*

Norris R.J., and Henley, R.W., 1976: Dewatering of a metamorphic pile: *Geology, v. 4, p. 333-336.*

Oberthur, T., Weiser, T., Amanor, J.A., and Chryssoulis, S.L., 1997: Mineralogical siting and distribution of gold in quartz veins and sulphide ores of the Ashanti mine and other deposits in the Ashanti belt of Ghana*: Mineral. Deposita, v. 32, p. 2-15.*

Ogryzlo, S.P., 1935: Hydrothermal experiments with gold: *Econ. Geol., v.30, p. 400-424.*

Ohmoto, H., 1972: Systematics of sulphur and carbon isotopes in hydrothermal ore deposits: *Econ. Geol., v. 67, p. 551-578.*

Ohmoto, H., 1985: Thermodynamic and kinetik evaluation of the causes of metal-ratio regularities in low temperature hydrothermal deposits (abs): *Geol. Soc. Am. Abstracts with programs 17, p.680.*

Ohmoto, H., 1986: Stable isotope geochemistry of ore deposits: *Reviews in Mineralogy, v. 16, p. 491-560.*

Ohmoto, H., and Kerrick, D., 1977: Devolatilization equilibria in graphitic systems: *American Jour. of Science, v. 277, p. 1013-1044.*

Ohmoto,H., and Rye, 1979: Isotopes of sulphur and carbon: In: Barnes, H.L., (ed): Geochemistry of hydrothermal ore deposits: *Wiley Intersci., New York, p. 509-567.*

Omenneto, P., 1985: Report on Lead-Zinc ores of Thassos island: *Vol. I, II and III, Padova.*

Pan, P.,and Wood, S.A., 1994: The solubility of Pt and Pd sulphides and Au metal in bisulphide solutions. II. Results at 200-350 ^{0}C and at saturated vapor pressure: *Mineral. Deposita, v. 29, p. 373-390.*

Papadopoulos, P., 1980 : Geological map of Greece 1: 50000, Ferres Sheet: *IGME, Greece.*

Papanikolaou, D., and Panagopoulos, A., 1981: On the structure style of Southern Rhodope, Greece: *Geol. Balkanica, v.11, p.13-22.*

Patras, P., Kilias, A., Chatzidimitriadis, E., and Mountrakis, D., 1986: Study of the deformation phase of the Internal Hellenides in N. Greece: *Geol. Soc. Greece Bull., v. 20, p. 139-157.*

Patras, D., Kilias, A., Chatzidimitriadis, E., and Mountrakis, D., 1989: Structural analysis of deformation episodes and correlation with metamorphic events in the Rhodope massif and the phyllite series of Alexandroupolis area, N. Greece: *Geol. Rhodopica, v. 1, Kliment Ochridski Univ. Press, p. 131-144.*

Pavlidis, S., Mountrakis, D., Kilias, D., and Tranos, M., 1989: Transitional neo- and active tectonics in the vicinity of north Aegean trough: *2nd Hellenic-Bulgarian Symposium of the Rhodope massif, Aristotle Univ. of Thessaloniki, Abstr. Vol., p. 32.*

Peicheva, J.M., Bibikova, E.V., and Makarov, V., 1992: U-Pb isotope dating of zircons from two types of gneisses in southeastern Rhodope mountains (Bulgaria): *Comptes rendus de l' Academie Bulgare des Sciences, T.45, N8, p.71-74 (In Russian).*

Peterman, Z.E., Hedge, C.E., and Tourtelot, H.A., 1970: Isotopic composition of strontium in seawater throughout Phanerozoic time: *Geochim. and Cosmochim. Acta, v. 34, p. 105-120.*

Psilovikos, A., and Vavliakis, E., 1982: The problem of the planation surfaces in

the Serbomacedonian and the Rila-Rhodope massifs: ***Bull. Geol. Soc. Greece, v.16, p.182-195.***

Ramboz, C., Pichavant, M., Weisbrod, A., 1982: Fluid immiscibility in natural processes: use and misuse of fluid inclusion data in terms of immiscibility: ***Chem. Geol., v. 37, p. 29-48.***

Renders, P.J., and Seward, T.M., 1989: The stability of the hydrosulphido- and sulphido complexes of Au(I) andAg (I) at 25 ^{0}C: ***Geochim. and Cosmochim. Acta, v.53, p. 244-253.***

Richter, D.K., 1982: Origin and diagenesis of Devonian and Permotriassic dolomites in Eifel Mts (Germany). ***Contr. to Sedimentology, v. 2, p. 101.***

Ridler, R.H., 1976: Stratigraphic keys to the gold metallogeny of the Abitibi Belt: ***Can. Min. J., v.97, No 6, p.81-87.***

Roedder, E., 1984: Fluid inclusions: ***Reviews in Mineralogy, v. 12, pp. 644.***

Royse, C.R., 1971: X-Ray determination of calcite-dolomite: ***Jour. of Sed. Petrology, v. 41, p. 483-488.***

Rushton, R.W., Nesbitt, B.E., Muehlenbachs, K., and Mortensen, J., 1993: A fluid inclusion and stable isotope study of Au quartz veins in the Klondike district, Yukon Territory, Canada: A section through a mesothermal vein system: ***Econ. Geol., v. 88, p. 647- 678.***

Russel, M.J., 1983: Major sediment -hosted exhalative zinc+lead deposits: Formation from hydrothermal convection cells that deepen during crustal extension: ***Mineralog. Assoc. Canada Handbook, v.9, p. 251-282.***

Ryaskov, Ch., and Dobrev, T., 1989: Geophysical fields, internal structure and some geodynamic manifestations of the West Rhodope megablock : ***Geol. Rhodopica, v. 1, Kliment Ochridski Univ. Press, p. 56-65.***

Rye, D. M., and Rye, R. O., 1974: Homestake gold mine, South Dakota: I. Stable isotope studies: ***Econ. Geol., v. 68, p. 239-317.***

Rye, R.O., and Ohmoto, H., 1974: Sulpfur and Carbon Isotopes and Ore Genesis: A Review: ***Econ. Geol., v. 69, p. 826-842.***

Sakai, H., 1968: Isotopic properties of sulphur compounds in hydrothermal proc-

esses: *Geochemical Journal, v. 2, p. 29-49.*

Sakellariou, D.,1988: Deformation and metamorphism of the Serbomacedonian massif in northeast Chalkidiki, N. Greece: *Geol. Soc. Greece Bull., v.23, p. 47-61.*

Schidlowski, M., 1988: A 3,800 million year isotopic record of life from carbon in sedimentary rocks: *Nature, v. 333, p. 313-318.*

Scholle, P.A., 1971: Diagenesis of deep -water carbonate turbidites, Upper Cretaceous Monte Antola Flysch, northern Apennines, Italy: *Jour. of Sed. Petrology, v. 41, p. 233-250.*

Seward, T.M., 1973: Thio complexes of gold in hydrothermal ore solutions: *Geochim. and Cosmochim. Acta, v. 37, p. 379-399.*

Seward, T.M., 1982: The transport and deposition of gold in hydrothermal systems. In *Gold '82 (ed) Foster, Balkema, Rotterdam, 1984, p.165-181.*

Seward, T.M., 1991: The hydrothermal geochemistry of gold: In *Gold Metallogeny and Exploration (ed) Foster, R.P., Blackie, p. 37-62.*

Shanov, S., Ryazkov, Ch., and Boyanov, I., 1989: The Rhodope region in the light of some geophysical interpretations: *Geol. Rhodopica, v. 1, Kliment Ochridski Univ. Press, p. 51-55.*

Shaw, R.P., Morton, R.D., Gray, J., and Krouse, H.R., 1991: Origins of metamorphic gold deposits: Implications of stable isotope data from the central Rocky Mountains, Canada: *Mineralogy and Petrology, v. 43, p. 193-209.*

Shelton, K.L., and Rye, D.M., 1982: Sulphur isotopic compositions of ores from Mines Gaspe, Quebec: An example of sulphate-sulphide isotopic dissequilibria in ore forming fluids with application to other porphyry-type deposits: *Econ. Geol., v. 77, p. 1688-1709.*

Shelton, K.L., So, C.S., and Chang, J.S., 1988: Gold-rich mesothermal vein deposits of the republic of Korea: Geochemical studies of the Jungwon gold area: *Econ. Geol., v. 83, p. 1221-1237.*

Shenberger, D.M., and Barnes, H.L., 1989: Solubility of gold in aqueous sulphide solutions from 150 to 350 ^{0}C: *Geochim. and Cosmochim. Acta, v. 53, p. 269-278.*

Shepherd, T.J., Rankin, A.H., and Alderton, D.H.M., 1985: A practical quide to fluid inclusion studies: *Glasgow, Blackie and Son, pp. 239.*

Shepherd, T.J., Miller, M.F., Scrivener, R.C., and Darbyshire, D.P.F., 1985: Hydrothermal fluid evolution in relation to mineralization in southwest England with special reference to the Dartmoor-Bodmin area. In: High Heat Production (HHP) Granites, Hydrothermal Circulation and Ore Genesis. *Inst. Min. Metal. Symp. Proc., p. 345-364.*

Shepherd, T.J., Bottrell, S.H., and Miller, M.F., 1991: Fluid inclusion volatiles as an exploration guide to black shale-hosted gold deposits, Dolgellau gold belt, North Wales, U.K: *Jour. of Geochem. Exploration, v.42, p. 5-24.*

Shepherd, T.J., and Naden, J., 1993: Nestos basin brines: *EEC Project MA2M-CT90-0015, Internal Report, IGME, Athens, 18pp.*

Sheppard, S.M.F., 1986: Characterization and isotopic variations in natural waters: *Rev. Mineralogy, v.16, p. 165-183.*

Sibson, R.H., 1986: Earthquakes and lineament infrastructure: *Royal Soc. [London] Philos Trans., v. A317, p. 63-79.*

Sibson, R.H., 1990: Faulting and fluid flow: *Mineralog. Assoc.Canada, Short Course, Handbook, v. 18, p. 93-129.*

Sidiropoulos, P. 1991: Mineralogy, geology and geochemistry of the Vertiskos formation: *Ph. D. Thesis, Univ. of Thessaloniki, 210pp.*

Smith., J.W., Doolan, S., and McFarlane, E. F., 1977: A sulphur isotope geothermometer for the trisulphide system galena-sphalerite-pyrite: *Chem. Geology, v. 19, p. 83-98.*

Smith, J.W., Burns, M.S., and Croxford, N.J.W., 1978: Stable isotope studies of the origins of mineralization at Mount Isa: *Mineral. Deposita, v. 13, p. 369-381.*

Smith, T.J., and Kesler, S.E., 1985: Relation of fluid inclusion geochemistry to wallrock alteration and lithogeochemical zonation at the Hollinger-McIntyre gold deposit, Timmins, Ontario, Canada: *CIM Bulletin, v.78, p.35-46.*

So, C.S., and Yun T. Y., 1997: Jurassic mesothermal gold mineralization of the Samwanghak Mine, Youngdong Area, Republic of Korea: Constrains of

hydrothermal fluid geochemistry: *Econ. Geol., v. 92, p. 60-80.*

Sokoutis, D., Brun, J., Van Den Driessche, and Pavlidis, S., 1993 : A major Oligocene-Miocene detachment in southern Rhodope controlling north Aegean extension: *Jour. Geol. Soc. London, v. 150, p. 243-246.*

Soldatos, T., 1985: Petrology and Geochemistry of the Elatia pluton (Central Rhodope): *Ph. D. Thesis, Univ. of Thessaloniki, 262 p.*

Sorby, H.C., 1858: On the microscopical structure of crystals indicating the origin of rocks and minerals: *Q. J. Geol. Soc. London, v.14, p.453-500.*

Stacey, J.S., and Kramers, J.D., 1975: Approximation of terrestrial lead isotope evolution by a two-stage model: *Earth Planet. Sci. Letters, v. 26, p. 207-221.*

Steed, G.M., and Morris, J.H., 1997: Isotopic evidence for the origin of a Caledonian gold-arsenopyrite-pyrite deposit at Clontibret, Ireland: *Trans. Inst. Min. Metall., Section B: Appl. Earth Sci., v.106, B109-B118.*

Sterner,S.M., and Bodnar, R.J., 1991: Synthetic fluid inclusions: X: Experimental determination of P-V-T-X properties in the CO_2-H_2O system to 6 kb and 700 ^{0} C: *Amer. Journal of Science, v. 291, p. 1-54.*

Straus, J.M., and Schubert, G., 1977: Thermal convection of water in a porous medium: Effects of temperature and pressure dependent thermodynamic and transport properties: *Jour. Geophys. Research, v.82, p. 325-333.*

Suleimenov, O.M., and Krupp, R.E., 1994: Solubility of hydrogen sulphide in pure water and in NaCl solutions, from 20 to 320 ^{0}C and at saturation pressures: *Geochim. and Cosmochim. Acta, v. 58, p. 2433-2444.*

Taylor, B.E., 1986: Magmatic volatiles: isotopic variation of C, H, and S : In: Valley, J.W., Taylor, H.P. Jr., and O' Neil, J.R., (eds): Stable isotopes in high temperature geological processes, *Reviews in Mineralogy, v. 16, p. 185-225.*

Taylor, B.E., 1987: Stable isotope geochemistry of ore forming fluids: In: Stable isotope geochemistry of low temperature fluids, Kyser, T.K., (ed): *Mineral. Ass. Can. Short Course Handbook 13, p. 337-445.*

Theodorikas, S., 1983: The mineralogy, Petrology and Geochemistry of the Serres-Drama granitic complex, N. Greece: *Ph.D. Thesis, Univ. of Thessaloniki, 251 p.*

Touret, J., 1981: Fluid inclusions in high-grade metamorphic rocks: In: Hollister, L.S., and Crawford, M.L., (eds): Mineralogical Ass. of Can. Short Course In Fluid Inclusions: Applications to Petrology: ***Toronto, Mineralog. Ass. Can. Short Course Handbook, V.6, p. 182-208.***

Tsombos, P., and Karmis, P., 1988: Deep fracture pattern of the area between Axios and Strymon rivers N. Greece, as detected by Landsat TM images: ***Advances in Remote Sensing Conference, Thessaloniki.***

Tsombos, P., and Kalogeropoulos, S., 1990: Remote sensing as applied to mineral exploration in the Chalkidiki peninsula, northern Greece: ***ISPRS Jour. of Photogrammetry and Remote Sensing, v. 45, p.344-354.***

Tsombos, P., 1993: Identification of fertile lineaments using remote sensing data: ***EEC Project MA2M-CT90-0015, Final Report, IGME, Athens, p.29.***

Vahrekamp, V.C., and Swart, P.K., 1990: New distribution coefficient for the incorporation of strontium to dolomite and its implications for the formation of ancient dolomites: ***Geology, v. 18, p. 387-391.***

Valley, J.W., 1986: Stable isotope geochemistry of metamorphic rocks: In Valley, J.W., Taylor, H.P., Jr., and O'Neil, J.R., (eds), ***Stable isotopes in high temperature geological processes, Miner.Assoc. America Reviews in Mineralogy, v. 16, p. 445-490.***

Varti-Mataranga, M., and Eliopoulos, D.G., 1992: Petrological investigation of the Carbonate formations of the Pangeon area: ***EEC Project MA2M-CT90-0015, Internal Report, IGME, Athens, p.29.***

Varti-Mataranga, M., 1993: Petrological investigation of the Carbonate formations of the Myriophyton and Pangeon areas: ***EEC Project MA2M-CT90-0015, Final Report, IGME, Athens, p.53.***

Varti-Mataranga, M., and Eliopoulos, D.G., 1999: Petrological and Geochemical investigations of the Carbonate formations of the Pangeon: *(Submitted to Sedimentary Petrology)*

Vavelidis, M., Basiakos, I., Begeman, F., Patriarcheas, K., Pernicka, E., Schmitt-Strecker, S., and Wagner, G. A., 1985 : Geologie und Erzvorkommen del insel Sifnos. In: Wagner, G.A., and Weisgerber, G., (eds): Silber, Blei, und

Gold auf Sifnos; Praehistorische und antike Metallproduktion. *Der Anschnitt, Beiheft 3, S. 59-80; Bochum.*

Veizer, J., and Hoefs, J., 1976: The nature of $^{18}O/^{16}O$ and $^{13}C/^{12}C$ secular trends in sedimentary carbonate rocks: *Geochim. Cosmchim. Acta, v. 40, p. 1387-1395.*

Vilor, N.V., 1973: Laboratory and theoritical data on gold and silica in hydrochemical process: *Canditate Thesis, Inst. Zemoy Kory SO AN SSSR, Irkutsk.*

Wall, V.J., 1987: The Second Eastern Goldfields Geological Field Conference: *Abstracts and Excursion Guide, p. 8-23.*

Walsh, J.F., Kesler, S.E., Duff, D., and Cloke, P.L., 1988: Fluid inclusion geochemistry of high-grade, vein-hosted gold ore at the Pamour mine, Porcupine camp, Ontario: *Econ. Geol. , v. 83, p. 1347-1367.*

Walther, J.V., and Orville, P.M., 1982: Volatile production and transport in regional metamorphism: *Contr. Mineralogy and Petrology, v.89, p. 252-257.*

Wawrzenitz, N., Baummann, A., and Nollau, G., 1994: Miocene uplift of midcrustal rocks in the Rhodope metamorphic core complex, caused by late Alpine extension of previously thickened crust (Thassos island, Pangeon complex, northern Greece): *Bull. Geol. Soc. Greece, v.XXX/1, p. 147-157.*

Wawrzenitz, N., and Mposkos, E., 1997: First evidence for Lower Cretaceous HP/HT metamorphism in eastern Rhodope, north Aegean region, northeast Greece: *European Jour. of Mineralogy, v. 9, p.659-664.*

Weir, R.H., and Kerrick, D.M., 1987: Mineralogic, fluid inclusion, and stable isotope studies of several gold mines in the Mother Lode, Tuolumne and Mariposa Counties, California: *Econ. Geol., V.82, p. 328-344.*

Weissberg, B.G., 1970: Solubility of gold in hydrothermal alkaline sulphide solutions: *Econ.Geol., V.56, p. 551-556.*

Wilkins, R.W.T., and Barkas, J.P., 1978: Fluid inclusions, deformation and recrystallization in granite tectonites: *Contributions to Mineralogy and Pe-*

trology, v. 65, p. 293-299.

Woo, K.S., Anderson, T.F., Railsback, L.B., and Sandberg, P.A., 1992: Oxygen isotope evidence for high salinity surface seawater in the Mid-Cretaceous Gulf of Mexico: Implications for warm, saline deepwater formation: ***Paleoceanography, v.7, p. 673-685.***

Wood, P.C., Burrows, A.V., Thomas, A.V., and Spooner, E.T.C., 1986a: The Hollinger-McIntyre Au-quartz vein system, Timmins, Ontario, Canada: Geologic characteristics, fluid properties and light stable isotope geochemistry. In: Macdonald, A.J., ed., ***Proceedings of Gold '86 Conference. Toronto, Ont., p. 56-80.***

Wood, S.A., Crerar, D.A., and Borcsik, M.P., 1987: Solubility of the assemblage pyrite-pyrrhotite-magnetite-sphalerite-galena-Au-stibnite-bismuthinite-argentite-molybdenite in H_2O-NaCl-CO_2 solutions from 200 to 350 ^{0}C: ***Econ.Geol., v. 82, p. 1864-1887.***

Xidas, 1978: Geological Map of Greece, 1: 50 000, Rhodolivos Sheet: ***IGME, Greece.***

Zachos, S., and Dimadis, E., 1983: The geotectonic position of the Skaloti-Echinos granite and its relationship to the metamorphic formations of the Western and Central Greek Rhodopes: ***Geol. Balkanica, v. 13:5, p.17-24.***

Zagorcev, I., 1989: Pirin-Pangeon Unit: Metamorphic and igneous development: ***2nd Hellenic-Bulgarian Symposium on the Rhodope massif. Abstr. Vol., p.25***

Zenger, D.H., 1983: Burial dolomitization in the Lost Burro Formation (Devonian) east-central California and the significance of late diagenetic dolomitization: ***Geology, v. 11, p. 519-522.***

Zenger, D.H., and Dunham, J.B., 1988: Dolomitization of Siluro-Devonian limestones in a deep core (5350) southeastern New Mexico. In: Shukla, V. and Baker, P.A., (eds). ***Sedimentology and Geochemistry of dolostones: SEPM Spec. Publ. No 43, p. 160-173.***

Zotov, A.V., and Boranova, N.N., 1989: Thermodynamic features on the aurochloride solute complex, $AuCl_2^-$, at temperatures of from 350-500 ^{0}C and

under pressures of from 500 to 1500 bar: *Sci. Geol. Bull., v.42, p. 335-342.*

Zotov, A.V., and Boranova, N.N., 1995: The solubility of Au_2S and AuAgS in near-neutral sulphide solutions at temperatures of 25 and 80 ^0C and pressures of 1 and 500 bars: In *Water-Rock Interaction-8, Kharaka, Y.K., and Chudaev, O.V., (eds), Balkema Press, p. 773-776.*

Zviaginicev, O.E., and Paulsen, I.A., 1940: Contribution to the theory of formation of vein gold deposits: *Dokl. Akad. Nauk SSSr, v. 26, p. 647-651.*